Antioxidantes y nanoestructuras lipídicas para prevenir el daño solar en tejidos lipoqueratínicos

Estibalitz Fernández Pinto

Tesis doctoral

Antioxidantes y nanoestructuras lipídicas para prevenir el daño solar en tejidos lipoqueratínicos

Estibalitz Fernández Pinto

Barcelona, 2015

UNIVERSITAT DE BARCELONA

FACULTAD DE FARMACIA

UNIVERSITAT DE BARCELONA

CONSEJO SUPERIOR DE INVESTIGACIONES CIENTÍFICAS

INSTITUTO DE QUÍMICA AVANZADA DE CATALUÑA (IQAC-CSIC)

Departamento de Tecnología Química y Tensoactivos

Antioxidantes y nanoestructuras lipídicas para prevenir el daño solar en tejidos lipoqueratínicos

ESTIBALITZ FERNÁNDEZ PINTO

Barcelona, 2015

PROGRAMA DE DOCTORADO:

Investigación, Desarrollo y Control de Medicamentos

BIENNIO: 2012-2015

Antioxidantes y nanoestructuras lipídicas para prevenir el daño solar en tejidos lipoqueratínicos

Memoria presentada por ESTIBALITZ FERNÁNDEZ PINTO para optar al título de doctora por la Universidad de Barcelona.

Estibalitz Fernández Pinto

La presente Tesis Doctoral ha sido realizada en el Departamento de Tecnología Química y Tensoactivos del Instituto de Química Avanzada de Cataluña del Consejo Superior de Investigaciones Científicas (IQAC-CSIC) bajo la dirección de la Dra. Olga López Serrano y de la tutoría del Dr. Joan Estelrich Latras del Departamento de Fisicoquímica de la Universidad de Barcelona, que autorizan su presentación:

Dra. Olga López Serrano Dr. Joan Estelrich Latras

Barcelona, 2015

Para Aita y Ama

AGRADECIMIENTOS

Quiero agradecer en primer lugar a mi directora de tesis, la Dra. Olga López, su dedicación, sus buenas ideas y su paciencia a la hora de las correcciones. Gracias Olga por aceptarme como doctoranda y por enseñarme tanto.

Tampoco puedo olvidar a las Dras. Gelen Rodríguez, Mercedes Cócera y Lucyanna Barbosa-Barros, que siempre las he considerado mis segundas directoras. Gracias a las tres por vuestro constante apoyo y por tantas horas dedicadas a esta tesis. Gracias al Dr. Alfonso de la Maza, que también ha aportado su grano de arena en este trabajo.

Gracias a la Dra. Luisa Coderch y al Dr. José Luis Parra por confiar en mí y abrirme las puertas en la investigación de los tejidos lipoqueratínicos.

Al Dr. Joan Estelrich, por aceptar la tutoría de esta tesis y a la Dra. Marisa García por su ayuda en los trámites de ésta.

A todos mis compañeros de grupo: Rosana, Vero, Rafa, Montse y Santiago. Gracias a todos por vuestros ánimos y por vuestra amistad tanto fuera como dentro del trabajo.

A Isabel Yuste por su ayuda técnica y su amistad, y a mis compañeras de departamento Laia, Cris, Clara, y Meritxell por todos los buenos momentos en los laboratorios 315-316.

Al Dr. Lluis Fajarí, cuya colaboración ha sido fundamental en esta tesis. Gracias por saber trasmitir a la perfección todo lo relacionado con la técnica de EPR e incluso por la ayuda logística empleada en la creación de un nuevo accesorio para nuevos experimentos. Gracias también a Avencia Diez por toda la ayuda técnica recibida desde el servicio de Resonancia Paramagnética Electrónica del IQAC.

A la Dra. Carmen López-Iglesias por enseñarme muchísimo sobre técnicas microscópicas y al Dr. Tariq Jawhari por su ayuda en el tratamiento de los datos de la espectroscopia de Raman.

A todas las personas con las que he colaborado y han hecho posible mucho trabajo de esta tesis: Dr. Cristophe Sandt de la línea SMIS del Sincrotrón SOLEIL de Francia, Dra. Clotilde Policar y su equipo del École Normale Supérieure de París y Dra. Christina Kamma-Lorger de la línea NCD del Sincrotrón ALBA de Cerdañola.

A los que fueron mis compañeros de Microestructuras en Azti-Tecnalia por acompañarme en mis primeros pasos investigadores. Gracias Juan-Carlos y Esther por vuestra entrega y cercanía.

Gracias también a Itziar, Hiran, Nagore, Rubén y Marina, por su amistad y sus ánimos.

A mis amigas de Bilbao, por sus buenos consejos y por estar ahí siempre que lo he necesitado. Eskerrik asko Esther, Esti, Irene eta Irune.

A Mercé y Vicent por su apoyo incondicional desde el primer momento que pisé Barcelona, muchas gracias a los dos.

A mi familia: a mi hermana Elena, mi cuñado Joe y mi sobrino Jon. A mi hermano Patxi y mi cuñada Ester, que sin ellos esta tesis no hubiese sido posible y que siempre tienen palabras de ánimo. Y cómo no, a mis padres, eskerrik asko Aita eta Ama por todo vuestro amor y por creer en mí.

Y por supuesto, no podía olvidarme de la persona que ha estado desde principio a fin a mi lado apoyándome en todo y a quien también dedico este trabajo. Gracias Vicent por saber escucharme y ayudarme siempre a seguir adelante.

Eskerrik asko guztioi!!!

"La ciencia no es más que un refinamiento del pensamiento cotidiano"

Albert Einstein

ÍNDICE

ÍNDICE

ABREVIATURAS

ABREVIATURAS

CHOL Colesterol

CMC Complejo membranoso celular

Crio-TEM Criomiscroscopía electrónica de transmisión

DHPC Dihexanoilfosfatidilcolina

DMPO 2,2 dimetil- 1 oxido pirrolidina

DMSO Dimetilsulfoxido

DLS Dispersión dinámica de luz

DPPC Dipalmitoilfosfatidilcolina

EC Estrato córneo

Epi Epidermis

EPR Resonancia paramagnética electrónica

FSTEM Criosubstitución de microscopia de trasmisión electrónica

FTIR Espectroscopia infrarroja con transformada de Fourier

HD Diámetro hidrodinámico

IR Infrarrojo

MDA Maldonaldehido

MMP metaloproteasa de matriz-1

PC Fosfatidilcolina

q Relación molar entre fosfolípido de cadena larga y corta

ROS Especies reactivas de oxígeno

SAXS Dispersión de rayos X a ángulos pequeños

SEM Microscopía electrónica de barrido

TBA Ácido tiobarbitúrico

Trp Triptófano

UV Ultravioleta

VDW Van der Waals

VIS Visible

PLANTEAMIENTO GENERAL

PLANTEAMIENTO GENERAL

La radiación solar es, entre otros factores, responsable de la formación de radicales libres, que dependiendo de su concentración pueden desencadenar efectos negativos sobre la salud. El cabello y la piel son dos tejidos vulnerables a la formación de radicales libres por su continua exposición solar. Los efectos negativos de una excesiva exposición solar se asocian principalmente a la presencia de los rayos ultravioleta (UV), aunque la radiación infrarroja (IR) también puede desencadenar reacciones celulares que forman indirectamente radicales libres y dañan proteínas de la dermis como el colágeno.

La aplicación de antioxidantes sobre la piel y el cabello podría reforzar el sistema antioxidante natural de estos dos tejidos y como consecuencia, prevenir el daño causado por la radiación solar. Los antioxidantes son moléculas capaces de prevenir o retrasar la oxidación de otras moléculas, ya que pueden neutralizar los radicales libres oxidándose ellos mismos y así evitando la oxidación de tejidos como piel y cabello. Sin embargo, es necesaria la penetración de los antioxidantes en el tejido para poder esperar un efecto protector. En el caso de la piel, la penetración del tejido supone un reto debido a la potente función barrera que desempeña el estrato corneo (EC), la capa más superficial de la piel. Por otro lado, la inestabilidad química de los antioxidantes implica una dificultad adicional ya que estas moléculas son muy reactivas y consecuentemente pierden su eficacia rápidamente. Una de las estrategias utilizadas para resolver este problema es el uso de vehículos que promueven la penetración de activos en la piel y que retrasan la degradación de los antioxidantes.

Las bicelas son nanoestructuras discoidales de 15- 25 nm de diámetro formadas por fosfolípidos de cadena larga (generalmente dipalmitoilfosfatidilcolina, DPPC) y fosfolípido de cadena corta (generalmente dihexanoilfosfatidilcolina, DHPC) colocados en la zona plana y bordes de la estructura, respectivamente. Por otro lado los bicosomas surgen como una estrategia para proteger las bicelas en entornos de alta dilución en agua. Para ello, las bicelas son encapsuladas en vesículas esféricas formando los sistemas de bicosomas de diámetro alrededor de 200 nm. En trabajos anteriores se ha demostrado la efectividad de las bicelas como vehículos tópicos de diferentes moléculas con interés dermatológico. En el caso de los bicosomas, que

permiten un uso más amplio de las bicelas, las ventajas de su uso tópico no se habían demostrado hasta el momento, por lo que se convierten en el objeto de estudio de esta tesis.

Los objetivos de esta tesis han sido, por una parte, la optimización de las metodologías para evaluar la oxidación del cabello y la piel provocada por la radiación ultravioleta-visible (UV-VIS) e IR, y por otro lado, el estudio de la interacción de las bicelas y los bicosomas con la piel. Se ha evaluado la capacidad anti-radicalaria de ambos sistemas con y sin antioxidante incorporado, y se ha determinado la penetración de los bicosomas en piel normal y expuesta a radiación UV-VIS. Finalmente, se ha estudiado la estabilidad de los vehículos lipídicos frente a radiación UV-VIS, y con el fin de prolongar la eficacia de antioxidantes, se ha evaluado la capacidad de ambos sistemas lipídicos de conservar estas moléculas.

Los estudios del cabello, mostraron un incremento de radicales libres en las fibras expuestas a radiación UV-VIS. Además se observó una notable oxidación de la fracción proteica y lipídica del cabello. Las propiedades físicas como el brillo y el color del cabello también se vieron afectadas debido a la radiación UV-VIS. Estas propiedades físico-químicas del cabello se conservaron mediante la aplicación de diferentes formulaciones de antioxidantes provenientes de la alcachofa y del arroz.

La aplicación en la piel de bicelas y bicosomas con y sin el antioxidante β-caroteno mostró una capacidad anti-radicalaria frente a radiación UV-VIS, siendo el sistema más efectivo el bicosoma con β-caroteno incorporado. También se demostró una significativa penetración de los bicosomas en piel normal, mientras que la penetración de estos sistemas lipídicos en piel expuesta a radiación UV-VIS fue bastante menor. Se pudo comprobar que el alcance de penetración en la piel era también dependiente de las propiedades físico-químicas de la molécula incorporada en el bicosoma.
La degradación del β-caroteno debido a la radiación UV-VIS disminuye al incluir este antioxidante en las bicelas y los bicosomas, siendo el bicosoma el sistema lipídico que mejor protege al β-caroteno de su oxidación.

Gracias a un dispositivo de radiación IR que permite irradiar las muestras de piel controlando la temperatura, se evaluó la capacidad de la radiación IR de formar radicales libres en el cabello y la piel a temperaturas fisiológicas, algo que hasta el momento solo se había observado a temperaturas superiores a 40ºC. Adicionalmente,

también se observó un deterioro del colágeno cutáneo en piel expuesta a radiación IR, aunque en este caso fue necesario elevar la temperatura de la piel por encima de los 60ºC. Ambos daños causados por la radiación IR (creación de radicales libres y degradación del colágeno) fueron reducidos con un previo tratamiento de la piel con bicosomas incorporando β-caroteno.

1. INTRODUCCIÓN

1. INTRODUCCIÓN

1.1. RADICALES LIBRES Y ANTIOXIDANTES

1.1.1. Radicales libres

Los radicales libres son moléculas que en su estructura atómica presentan un electrón no apareado. Debido a la inestabilidad de su configuración electrónica, son generalmente muy reactivos. Esta reactividad es la base de su toxicidad y de su corta vida media [1]. La función de los radiales libres es dependiente de la concentración en la que se encuentran. Así, actúan como mediadores y reguladores a concentraciones fisiológicas [2, 3], mientras que a concentraciones elevadas pueden actuar como potentes oxidantes.

En los sistemas vivos se generan muchos tipos de radicales libres, siendo los más conocidos los radicales de oxígeno o las especies reactivas de oxígeno (ROS). Debido al funcionamiento del metabolismo aeróbico, las ROS se generan continuamente en el organismo en pequeñas cantidades, la mayoría a partir de las cadenas de transporte de electrones [4].

Nuestro organismo está expuesto a una gran variedad de ROS y otro tipo de radicales libres que pueden generarse a partir de fuentes endógenas, relacionadas con el metabolismo del oxígeno y con diversas reacciones de defensa de nuestro sistema inmunitario [5-7], o de fuentes exógenas, relacionadas principalmente con la contaminación y radiación solar, entre otros factores [8-10].

La radiación solar en la superficie de la tierra se divide de la siguiente manera: 6.8 % de radiación UV (0.5% UVB, 6.3% UVA), 3.8 % de radiación VIS y 54.3 % de radiación IR cercana [11]. Dentro de la radiación solar, las radiaciones UV son las principales causantes de radicales libres [10, 12, 13]. Sin embargo, recientemente también se ha demostrado la influencia que tienen las radiaciones VIS e IR (principalmente IR-A) en la formación de radicales libres [11, 14].

En los seres vivos existe un equilibrio entre la producción de radicales libres y antioxidantes. Cuando se genera un desequilibrio producido por un exceso de oxidación frente a la capacidad antioxidante de la célula, se desencadena un cuadro de

cambios fisiológicos y bioquímicos conocidos como estrés oxidativo. Este estrés oxidativo puede aparecer tanto por un exceso de producción de radicales libres como por la existencia de un problema o alteración en el sistema antioxidante [15]. El efecto oxidante tiene como diana todo tipo de moléculas biológicas, incluyendo lípidos, proteínas e hidratos de carbono y puede provocar procesos como la mutagénesis, carcinogénesis, y distintas lesiones en membranas celulares. Las consecuencias del estrés oxidativo así como los daños que ocasiona, pueden provocar el envejecimiento y enfermedades como el cáncer y enfermedades coronarias entre otras [5, 16, 17].

Una de las herramientas de las que se dispone para combatir el estrés oxidativo es la suplementación con antioxidantes. Sin embargo, esta suplementación se ha de diseñar y estudiar en profundidad para no acumular en el organismo y en las células un exceso de antioxidantes que podría alterar el equilibrio redox fisiológico.

1.1.2. Antioxidantes

Se define un antioxidante como cualquier sustancia o acción que retrasa, previene o elimina la oxidación de una molécula diana [18]. La oxidación es una reacción química de transferencia de electrones de una sustancia a un agente oxidante. Las reacciones de oxidación pueden producir radicales libres que comienzan reacciones en cadena que dañan las células. Los antioxidantes terminan estas reacciones destruyendo radicales libres intermedios e inhiben otras reacciones de oxidación oxidándose ellos mismos (Figura 1).

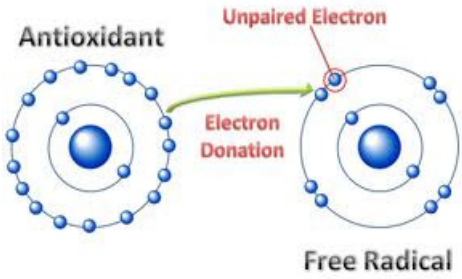

Figura 1. Mecanismo de acción de un antioxidante neutralizando un radical libre oxidándose él mismo.

Para prevenir y proteger los componentes celulares del daño inducido por los radicales libres, ROS y otras especies reactivas, los organismos aerobios han desarrollado un mecanismo de defensa antioxidante [19, 20]. Estos sistemas antioxidantes o mecanismos de defensa pueden clasificarse como sistemas antioxidantes endógenos (enzimáticos y no enzimáticos) [15, 20, 21], y exógenos (que se incluyen normalmente a través de la dieta) [19]. Estos mecanismos incluyen distintos modos de actuación tanto directos (interacción con las especies reactivas) como indirectos (reparación de moléculas dañadas, entre otros) [22].

En esta tesis se han utilizado dos formulaciones antioxidantes de activos provenientes de alcachofa (*Cynara scolymus L.*) y de arroz (*Oryza sativa L.*) en los experimentos con el cabello.

En el caso de la piel se ha empleado principalmente el β-caroteno, que además también es un antioxidante endógeno de este tejido [23-25]. Por otro lado también se ha utilizado un complejo de Mn que ha demostrado ser un potente antioxidante en células [26] y que no se había aplicado en piel hasta esta tesis (Figura 2).

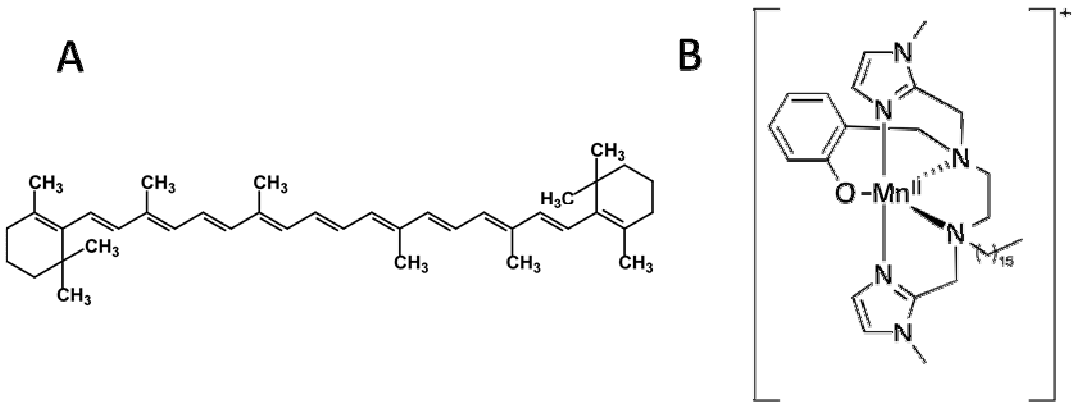

Figura 2. Estructura de los antioxidantes β-caroteno y complejo de Mn.

1.2. EL CABELLO

El pelo es un recubrimiento característico de la piel de los mamíferos, y probablemente, es una evolución de las escamas epidérmicas de los reptiles. Cada

fibra de cabello está formado por una masa de células queratinizadas, compactada y cementada, producida por un folículo piloso (Figura 3) [27].

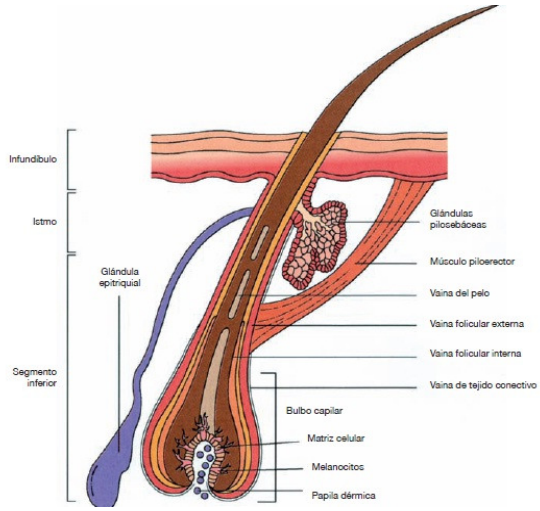

Figura 3. Morfologia del folículo del cabello.

1.2.1. Estructura morfológica

El cabello es un cilindro largo, muy organizado, formado por células inertes, la mayoría queratinizadas, que se han dispuesto siguiendo una orientación muy precisa y predeterminada, y forman una rígida estructura a nivel molecular capaz de aportar a la vez flexibilidad y gran resistencia mecánica.

La estructura del cabello contiene tres tipos de células: las cuticulares, formando un recubrimiento protector bastante grueso de las fibras, las corticales que comprenden la mayor parte de la masa de la fibra y las medulares situadas en el centro de la fibra. Además cada célula, tanto cuticular como cortical, está separada por el complejo membranoso celular (CMC) que tiene la función de unir las diferentes células (Figura 4) [27, 28].

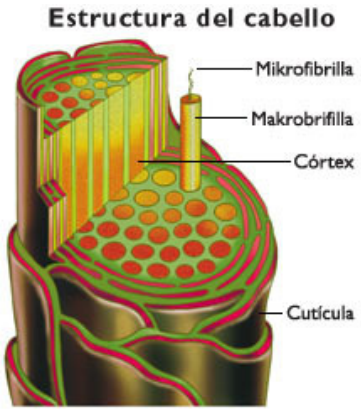

Figura 4. Estructura morfológica del cabello.

1.2.2. Composición química

Las fibras del cabello están formadas esencialmente por proteínas, entre un 75 y 85 %. Las proteínas son en su mayor parte queratina, y tienen un mayor contenido en azufre. Los aminoácidos que las componen son 18, pero los principales son: Cisteína, Histidina, Metionina y Triptófano. Siendo la cisteína el aminoácido que más abunda en la queratina. La constitución de las proteínas se define por su secuencia de aminoácidos o estructura primaria, así como por los modelos de organización espacial de las proteínas. En el caso del cabello se han detectado dos estructuras mediante difracción de rayos X: α-helicoidal y estructura β [27].

A pesar de la pequeña proporción de los lípidos en las fibras de cabello (2.3%) [29], estos lípidos tienen una importancia crucial en la cohesión estructural del cabello. Los lípidos que se forman durante el desarrollo del cabello en el folículo pueden localizarse en la superficie, íntimamente unidos a la cutícula, o estar situados en el interior de la fibra. Estos últimos, denominados lípidos internos, se supone que forman parte del CMC y están constituidos por colesterol, éster de colesterol, diglicéridos, triglicéridos, ácidos grasos libres y lípidos polares (principalmente ceramidas y glicolípidos).
Los lípidos del CMC parecen desempeñar un papel importante en las propiedades fisicoquímicas de las fibras del cabello; entre ellas, se pueden citar la barrera de la difusión química, la capacidad de retener agua y la cohesión celular [30, 31].

La estructura del cabello se forma a partir de diferentes enlaces: enlaces covalentes (formados por los grupos peptídicos), enlaces iónicos (existentes entre grupos ácidos y básicos de los restos de los laterales de los aminoácidos), enlaces disulfuro (del aminoácido cisteina), interacciones polares (debidas a enlaces por puentes de hidrogeno), interacciones hidrofóbicas y fuerzas de atracción de van der Waals [27].

1.2.3. Propiedades físico-químicas del cabello

El cabello posee ciertas propiedades físico-químicas que por su interés se mencionan a continuación [32] [27]:

- Resistencia al alargamiento
- Resistencia a la rotura
- Elasticidad
- Propiedades de superficie
- Propiedades de fricción
- Adsorción superficial
- Permeabilidad e hinchamiento de la fibra
- Brillo y color

1.2.4. La melanina como indicadora de la oxidación del cabello

La melanina es un pigmento que se encuentra en el cortex de las fibras del cabello y que es responsable del color de la fibra. Su función es actuar como un filtro para evitar daños causados por la radiación solar y es la principal defensa contra la formación de radicales libres. Un estrés oxidativo causaría la degradación de este pigmento formando radicales libres, y como consecuencia la oxidación de los componentes del cabello. Por lo tanto, este pigmento es un gran indicador de la oxidación de las fibras del cabello [33].

1.2.5. Exposición del cabello a radiación solar

En esta tesis la oxidación del cabello se ha llevado a cabo sometiendo el cabello a radiación UV-VIS con el equipo Suntest CPS+ (Atlas, Illinois, USA), del Instituto de Química Avanzada de Cataluña (IQAC-CSIC). Las muestras se han sometido a diferentes intensidades de irradiación y a diferentes tiempos de exposición dependiendo del experimento a realizar (Figura 5). El rango donde trabaja este simulador solar es de 310-800 nm (0,9% UVB, 17,3% UVA, 75.5% VIS y 8.1% IR-A).

Figura 5. Simulador solar Suntest CPS+.

1.2.6. Técnicas y ensayos utilizados en la evaluación del cabello

En este apartado se describen los ensayos y las técnicas utilizadas en esta tesis para evaluar la oxidación del cabello causada por la radiación UV-VIS.

1.2.6.1. Estudio de la formación de radicales libres mediante Resonancia Paramagnética Electrónica (EPR)

La Resonancia Paramagnética Electrónica (EPR) es una técnica espectroscópica sensible a electrones desapareados. Esto es, generalmente, un radical libre para moléculas orgánicas, o un ion de un metal de transición si es un compuesto inorgánico. El principio físico de esta técnica se basa en excitar espines electrónicos mediante la aplicación de un campo magnético [12, 34].

Como se ha mencionado anteriormente, la melanina presente en las fibras del cabello es la responsable de los radicales libres formados en el cabello [33]. Este pigmento puede degradarse a consecuencia de un exceso de radiación solar formando radicales libres. Por lo tanto, la cuantificación de los radicales libres de melanina formados en el cabello mediante la técnica de EPR, permite determinar el grado de oxidación de las fibras de cabello sometidas a un proceso de irradiación.

El espectrómetro de EPR utilizado para medir los radicales libres del cabello ha sido el EMX-Plus 10/12 de la casa Bruker BioSpin (Texas, USA) (Figura 6).

Figura 6. Imagen del equipo de Resonancia Paramagnética Electrónica (EPR).

Los experimentos han sido realizados en el servicio de Resonancia Paramagnética Electrónica del IQAC-CSIC en colaboración con el Dr. Lluís Fajarí y la Sra. Avencia Diez.

1.2.6.2. Evaluación de la degradación proteica

La determinación de la cantidad de proteína extraída del cabello sometido a irradiación permite demostrar la oxidación de esta fibra [35]. Por lo tanto, cuanto mayor sea la concentración de proteína extraída del cabello, el grado de oxidación de la fracción proteica es superior.

El Método de Bradford es un ensayo colorimétrico que permite medir la concentración de proteína total de una solución proteica desconocida. Se basa en la unión del colorante *azul brillante de Coomassie G 250* a las proteínas a través de grupos ionizados. Las proteínas se unen al colorante para formar un complejo proteína

colorante con un coeficiente de extinción mayor que el colorante libre, provocando un cambio en el espectro visible del colorante de manera tal que se produce una absorción máxima a 595 nm en lugar de la absorción de 465 nm del colorante en forma libre.

Para calcular la concentración de proteína degradada del cabello, primero se han de extraer las proteínas del cabello, y después se extrapolan los valores de absorbancia obtenidos en el ensayo de Bradford en una recta patrón con BSA (Bovine Serum Albumin) como estándar.

Los valores de absorbancia se miden mediante el espectrofotómetro de UV-VIS Cary 300 Bio UV-Visible (Varian, California, USA) del IQAC-CSIC.

1.2.6.3. Determinación de la descomposición del aminoácido Triptófano (Trp)

El Trp es un aminoácido esencial para el mantenimiento y desarrollo del cabello. Este aminoácido está presente en las fibras del cabello, y se excita mediante un haz de luz de 295 nm de longitud de onda. La energía que recoge de la luz, la emite con una longitud de onda mayor a la de la excitación (menor energía), y se produce la fluorescencia. La intensidad de la luz emitida es proporcional a la concentración de Trp, por lo que comparando intensidades de emisión de diferentes muestras podemos averiguar la concentración de Trp de cada muestra. El Trp del cabello tiene una gran tendencia a descomponerse por la luz del sol, por lo que midiendo la intensidad de luz de la fluorescencia producida por el Trp antes y después de la oxidación, podemos llegar a saber la cantidad de Trp descompuesto [36]. La detección del Trp del cabello por fluorescencia se lleva a cabo hidrolizando el cabello en una solución de NaOH 2M.

Los espectros de fluorescencia de cabello se han obtenido con el espectrofluorímetro RF-540 de Shimadzu (Kioto, Japón) del IQAC-CSIC.

1.2.6.4. Evaluación de la peroxidación de los lípidos

A bajos pHs y temperaturas elevadas, el reactivo malonaldehido (MDA), que es uno de los productos formados durante la peroxidación de los lípidos, participa en la adición

nucleofílica con el ácido tiobarbitúrico (TBA) formando el aducto 1:2 MDA: TBA (Figura 7), que es característico por su color rojo fluorescente y que se puede leer a 534 nm. La intensidad de la señal obtenida es proporcional al grado de oxidación de los lípidos [37].

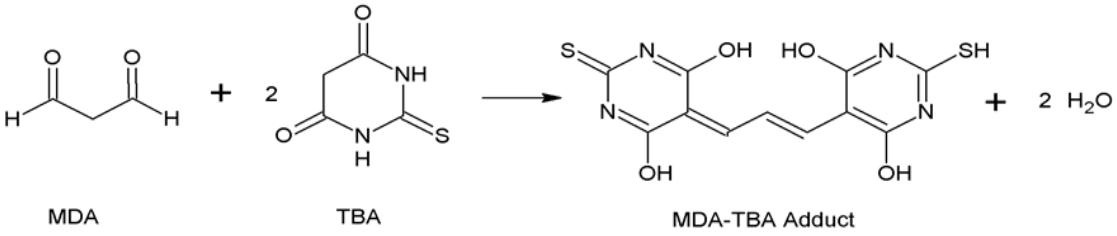

Figura 7. Reacción química entre el MDA y TBA formando el aducto MDA-TBA.

Para calcular la concentración de peróxidos de lípidos, primero se extraen los lípidos del cabello, y después se extrapolan los valores de absorbancia obtenidos en el ensayo del TBA en una recta patrón de MDA como estándar. Los valores de absorbancia se miden mediante el espectrofotómetro de UV-VIS Cary 300 Bio UV-Visible (Varian, California, USA) del IQAC-CSIC.

1.2.6.5. Trabajo de ruptura

El cabello es una fibra que posee una gran resistencia, requiriendo una carga de aproximadamente 12 kg/mm^2 (12X10^7) para romper una fibra de cabello natural y sana. La carga necesaria para la rotura de cabello es, aproximadamente, proporcional al diámetro de la fibra. Además varía con la edad, siendo más elevada a los 20 años y con la raza. El cabello de mujer parece más resistente a la rotura que el del hombre [27].

En este experimento el trabajo de ruptura de las fibras de cabello se ha medido con el dinamómetro Instron 5500R (Instron, Massachusetts, USA) del IQAC-CSIC bajo la asistencia técnica del Dr. Albert Manich.

1.2.6.6. Determinación del brillo del cabello

El brillo o luminosidad se refiere a la luz que emite o que está reflejando un objeto en concreto. Esta luminosidad estará relacionada con el número de partículas por unidad de superficie y por unidad de tiempo en un haz de luz.
Para medir el brillo del cabello, se ha utilizado el micro-TRI-gloss BYK-gardner GmbH (Geretsried, Alemania) del servicio de Adsorción Percutánea del IQAC-CSIC. Todas las medidas se han realizado en una sala acondicionada (23 ± 1ºC y 50 ± 5% RH).

1.2.6.7. Determinación del color del cabello

El color es la impresión producida por un tono de luz en los órganos visuales, o más exactamente, es una percepción visual que se genera en el cerebro de los humanos y otros animales al interpretar las señales nerviosas que le envían los foto-receptores en la retina del ojo, que a su vez interpretan y distinguen las distintas longitudes de onda que captan de la parte visible del espectro electromagnético.

Para la evaluación del color del cabello, se ha utilizado el espectrofotómetro Color-Eye 3000 (Macbeth, Altrincham, UK) del IQAC-CSIC.

Todas las medidas se han realizado en una habitación acondicionada (23 ± 1ºC y 60 ± 5% RH) y se han obtenido los valores de color CIELAB L, a y b. Los tres parámetros representan la luminosidad de color (L, L=0 negro y L=100 blanco), su posición entre magenta y verde (a, valores negativos indican verde mientras valores positivos indican magenta) y su posición entre amarillo y azul (b, valores negativos indican azul y valores positivos indican amarillo).

1.2.6.8. Visualización del cabello mediante microscopía electrónica de barrido

La microscopia electrónica de barrido (SEM) es una técnica de estudio de imágenes a gran aumento que, en vez de utilizar la luz para generarlas, usa haces de electrones que barren la superficie del tejido. Es una técnica muy potente para conocer la microestructura de los materiales. Los microscopios electrónicos disponen de un

cañón que emite electrones, que chocan contra la muestra, creando una imagen aumentada. Se utilizan lentes magnéticas para crear campos que dirigen y enfocan el haz de electrones, los cuales producen las imágenes. Esta técnica ha sido utilizada en diversos trabajos científicos con el fin de visualizar la superficie de la fibra del cabello. En nuestros experimentos, para la visualización de la superficie de las fibras de cabello se ha utilizado un microscopio electrónico de barrido de Quanta 6000 (FEI, Holanda) de los centros científicos y tecnológicos de la Universidad de Barcelona (CCiT-UB) [38].

1.3. LA PIEL

La piel es el órgano más grande del cuerpo humano, representa más del 10% de la masa corporal total [39]. Su principal función es actuar como barrera física evitando la pérdida de agua y protegiendo al organismo del medio que lo rodea. Además, controla la regulación térmica corporal a través del sistema vascular y de las glándulas sudoríparas, regula procesos endocrinos e inmunológicos y contiene una extensa red neurosensorial que nos mantiene en contacto con el entorno. Estas funciones son primordiales para la vida y requieren la específica composición y estructura que caracterizan a este importante órgano. Anatómicamente, este órgano está dividido en estrato córneo (EC), epidermis, dermis, e hipodermis (Figura 8).

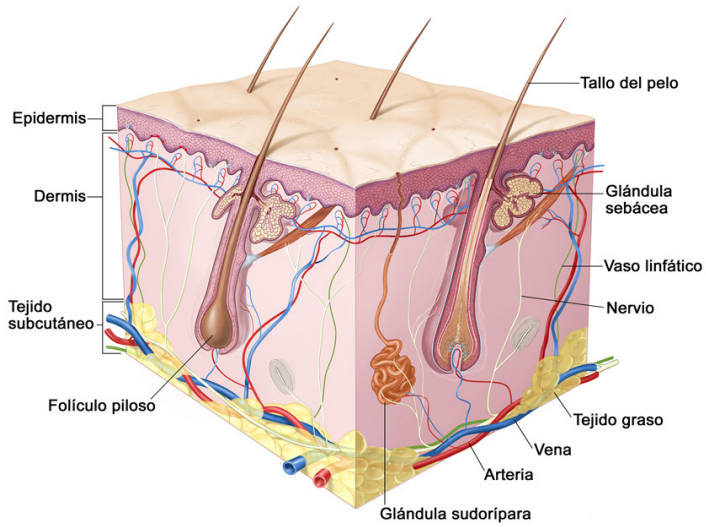

Figura 8. Esquema de la piel indicando las capas cutáneas.

El EC es la capa más externa de la piel de un espesor de 10-20 µm y está formado por células planas, anucleadas, y cornificadas (corneocitos) separadas por una matriz lipídica ordenada en láminas. Químicamente el EC se compone de un 15% de agua, un 70% de proteínas y un 15% de lípidos, aproximadamente. Esta composición es única respecto a las demás capas de la piel, por lo que le confiere al EC unas propiedades también únicas.

El EC es el principal responsable de la función barrera [40]. Hasta hace poco se le consideraba parte de la epidermis, sin embargo, actualmente se considera independiente de ésta debido a las características funcionales y estructurales específicas que presenta. La estructura del EC fue descrita por primera vez por Peter Elias [41] como un modelo de "ladrillos y cemento" donde los ladrillos son los cornecitos y el cemento que los rodea se refiere a la matriz lipídica ordenada en láminas (Figura 9).

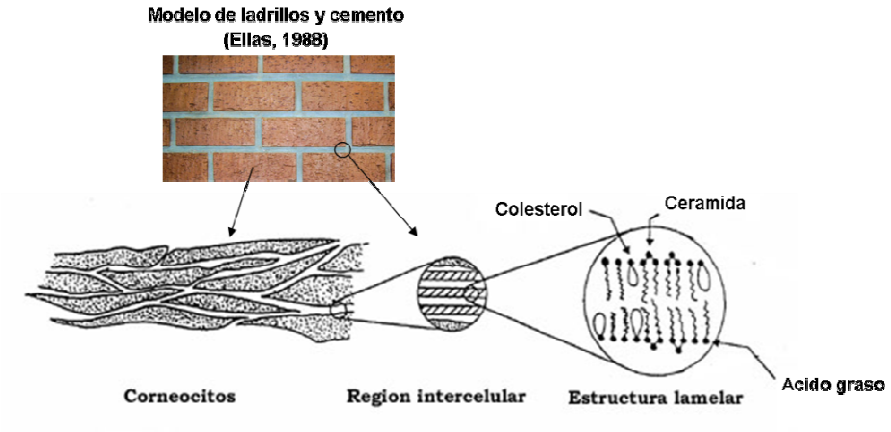

Figura 9. El modelo de "ladrillo y cemento" propuesto por Elias (1988), con un esquema representativo de la disposición de los corneocitos y de la estructura laminar lipídica de este tejido.

Los corneocitos son ricos en queratina y están interconectados entre sí por estructuras proteicas denominadas corneodesmosomas. La función barrera del EC se atribuye al contenido, la composición y, sobre todo, a la estructura organizada que adquiere la matriz lipídica intercelular que rodea a los corneocitos [40, 42].

Los lípidos del EC provienen, o bien de la diferenciación de los queratinocitos (células provenientes de la epidermis), o bien de la secreción sebácea. Los primeros se llaman lípidos intercelulares y tienen un papel muy importante en la función barrera. Su composición es aproximadamente: 40-50% de ceramidas, 25% de colesterol, 15-20% de ácidos grasos libres, 5% de sulfato de colesterol y 2% de ésteres de colesterol [39].

La epidermis (Epi) es una capa cuyo espesor depende de su localización anatómica oscilando entre los 0.04 mm en los parpados y los 1.5 mm en las palmas de las manos y pies (Figura 10). Es un tejido estratificado en tres capas de células vivas (queratinocitos) estrato basal, estrato espinoso y estrato granuloso [27].
A parte de los queratinocitos que se encuentran en un 80% en la epidermis, también están presentes otras células como los melanocitos (13%), las células de Langerhans (4%) y las células de Merkel (3%) [43-45].

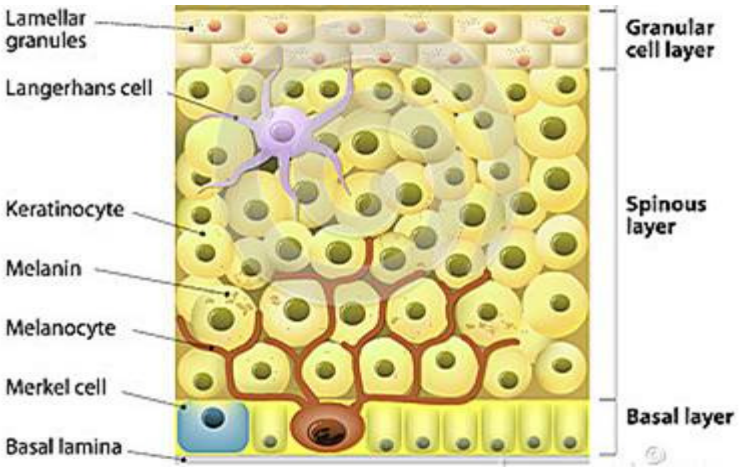

Figura 10. Esquema de la epidermis indicando los diferentes estratos.

La dermis es la capa más extensa de la piel y se trata de un tejido fibroelástico situado debajo de la epidermis que proporciona elasticidad y resistencia física. Por la dermis circulan vasos sanguíneos y linfáticos y asimismo también existen terminaciones nerviosas. Esta capa también contiene proteínas estructurales como el colágeno y la elastina [27]. El colágeno representa alrededor del 75% del peso de la piel y proporciona integridad a este tejido. Desde un punto de vista estructural, las moléculas de colágeno están formadas por tres cadenas polipeptídicas que se enrollan formando lo que constituye la hélice triple de colágeno. La unión de las triples hélices

por fuerzas intermoleculares forma lo que sería la fibrilla del colágeno, y a su vez, la unión de estas últimas forma la fibra de la proteína (Figura 11) [46].

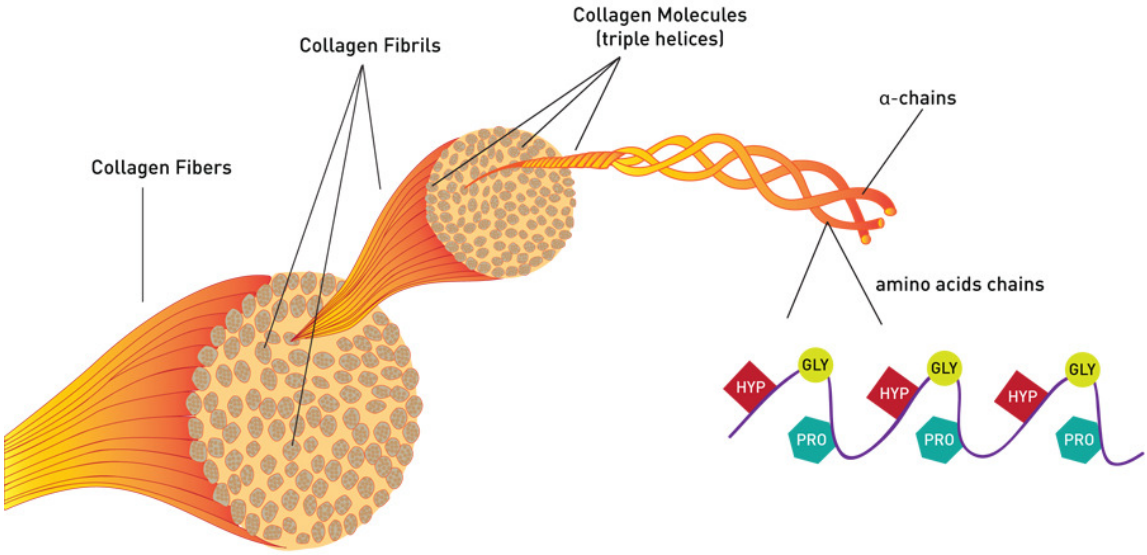

Figura 11. Estructura del colágeno. Hasta la fecha se han identificado más de 25 tipos de colágeno.

El colágeno muestra un ordenamiento característico en la piel, y cualquier cambio en el ordenamiento u organización de esta proteína conlleva alteraciones en el tejido como por ejemplo, la perdida de elasticidad, la aparición de arrugas, la descoloración o incluso desordenes de la función barrera [47].

La hipodermis es la capa cutánea más interna de la piel y está formada por tejido adiposo y fibras elásticas. El tejido adiposo sirve de almacén de energía, de aislante térmico y protege al tejido de agresiones externas [27].

1.3.1. Sistemas antioxidantes de la piel

La piel está directamente expuesta a un entorno oxidante, incluyendo la radiación solar y agentes contaminantes del aire [48]. Para neutralizar los efectos dañinos de los radicales libres, la piel está equipada de unos sistemas defensivos formados por una variedad de antioxidantes primarios (preventivos, como la vitamina C) y antioxidantes

secundarios (de intercepción, como la vitamina E). Este conjunto es denominado “red de antioxidantes”, y es responsable de mantener el equilibrio entre los prooxidantes y antioxidantes, con el fin de evitar el estrés oxidativo. Los datos de la cuantificación de los antioxidantes de la piel muestran una presencia superior en la epidermis frente a la dermis en concordancia con el hecho de que la epidermis está más directamente expuesta a fuentes externas de estrés oxidativo.

Además, el sistema antioxidante de la piel esta reforzado por el suplemento de antioxidantes exógenos, ya sea por administración oral o tópica. Esta ayuda permite la reducción de los ROS y otras especies en la fotocarcinogénesis y fotoenvejecimiento, por lo que su interés ha aumentado debido a su efecto fotoprotector en la piel [49]. De esta manera, la utilización de protectores solares para evitar la penetración de la radiación podría constituir una de las líneas y mecanismos preventivos para reducir el daño de la radiación en la piel. Por ello, el uso de antioxidantes se considera una medida necesaria para reforzar la barrera protectora de la piel frente a cualquier radiación solar.

1.3.2. Penetración transdérmica

El efecto de los activos aplicados tópicamente en la piel puede ser de dos tipos: *tópico y/o sistémico.* Así pues, tras la administración de un activo sobre la piel, éste puede ejercer su efecto solamente en los tejidos locales o capas más superficiales, y/o en cualquiera de los tejidos del cuerpo, como si su aplicación fuese por vía oral o parenteral. La administración transdérmica es una vía de administración alternativa más práctica, segura y menos invasiva que la vía parenteral. No obstante, se debe tener en cuenta que en la piel existe actividad metabólica [50], y aunque su carga metabólica es mucho menor que la hepática, ésta puede ser un inconveniente para la administración de determinados activos por esta vía.

Una molécula o fármaco puede utilizar dos vías de difusión para penetrar a través de la piel humana (Figura 12): a través del EC por la vía transepidérmica (flecha 1), o por los apéndices cutáneos (flechas 2 y 3).

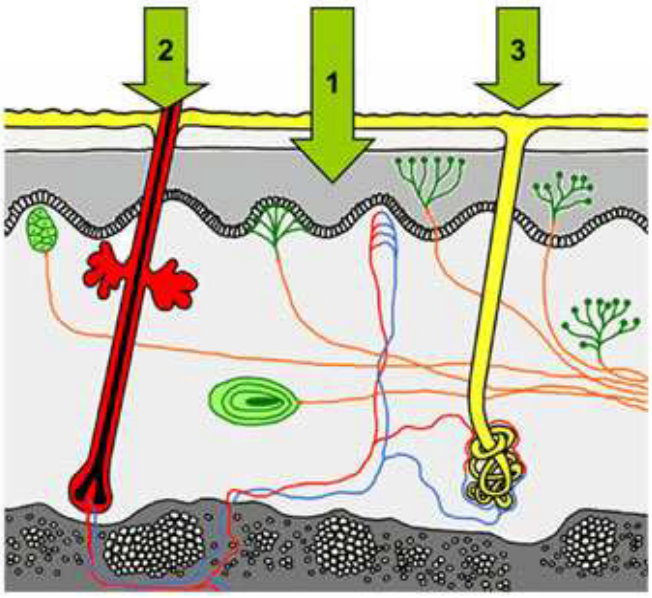

Figura 12. Posibles vías para la penetración a través de la epidermis. (1) a través del EC (transepidérmica), (2) a través de los folículos pilosos o (3) vía glándulas sudoríparas.

La vía de los apéndices cutáneos abarca el transporte por las glándulas sudoríparas y los folículos pilosos con sus glándulas sebáceas asociadas. La vía transepidérmica implica que las moléculas atraviesen la capa córnea intacta por difusión pasiva a través de dos rutas: la vía transcelular, donde las moléculas atraviesan la matriz lipoproteica de los corneocitos, o la vía intercelular, donde se produce el paso a través de los espacios intercelulares (Figura 13).

La posibilidad que tiene una molécula de atravesar las membranas depende de sus características: peso molecular, lipofilia, grado de ionización y su concentración en el vehículo. El itinerario principal seguido por una sustancia es determinado principalmente por el coeficiente de reparto, el cual está relacionado con su solubilidad en agua. Cuanto más lipofílico es el compuesto mayor es el coeficiente de reparto. Las moléculas hidrofílicas seguirán preferentemente el camino transcelular, mientras que las lipofílicas lo harán por la vía intercelular. La mayoría de las moléculas pasan a través del EC por ambas rutas [51].

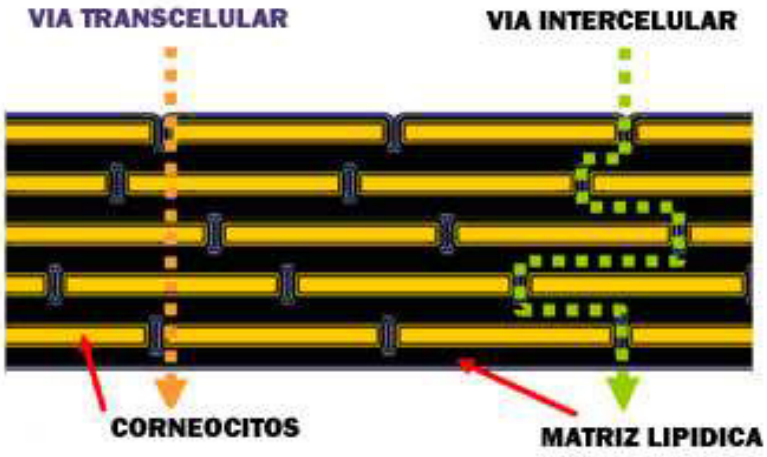

Figura 13. Diagrama esquemático de las vías de penetración transepidérmica.

1.4. SISTEMAS BICELARES Y BICOSOMAS

1.4.1. Bicelas

Los sistemas bicelares o bicelas son nanoagregados lipídicos formados por dos tipos de fosfolípidos, uno de cadenas alquílicas largas y otro de cadenas alquílicas cortas, dispersos en solución acuosa [52, 53]. Los fosfolípidos típicos utilizados para formar estos nanoagregados están compuestos por dos ácidos grasos cuyas cadenas alquílicas tienen enlaces saturados. En general, los fosfolípidos de cadena larga más usados son dipalmitoilfosfatidilcolina (DPPC) o dimiristoilfosfatidilcolina (DMPC). Como fosfolípido de cadena corta se utiliza dihexanoilfosfatidilcolina (DHPC). En esta tesis las bicelas utilizadas están formadas por DPPC y DHPC. Las estructuras moleculares de estos fosfolípidos se muestran en la figura 14.

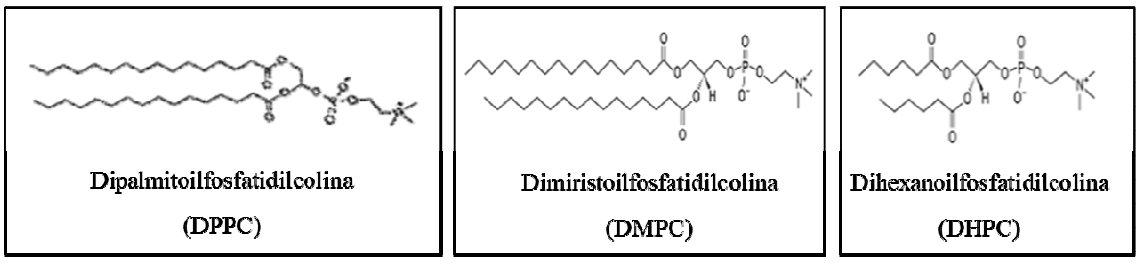

Figura 14. Estructura de los fosfolípidos típicos utilizados para formar sistemas bicelares.

La morfología más representativa de los sistemas bicelares es la discoidal. Los fosfolípidos de cadena larga se ensamblan formando una bicapa plana, mientras que los fosfolípidos de cadena corta se colocan en el borde estabilizando la estructura discoidal, como se muestra en la figura 15. Estas estructuras tienen un tamaño aproximado entre 10-50 nm de diámetro y entre 4-6 nm de grosor de la bicapa.

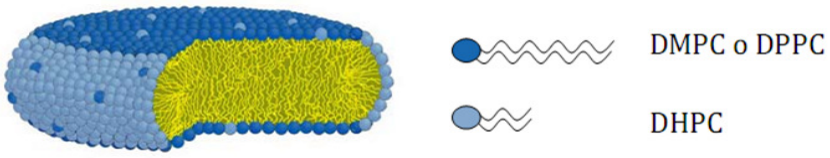

Figura 15. Representación de la estructura discoidal de las bicelas.

La composición de los sistemas y las condiciones del medio influyen directamente en las características morfológicas de las bicelas. El tamaño y morfología de los sistemas bicelares depende de la composición lipídica, de la relación molar entre el fosfolípido de cadena larga y el fosfolípido de cadena corta (q=DXPC/DHPC), de la concentración lipídica y de la temperatura [54, 55]. Dependiendo de estos factores, los sistemas bicelares pueden adoptar diferentes morfologías, siendo las micelas mixtas esféricas las estructuras más pequeñas, y las láminas o vesículas perforadas las estructuras más grandes. Entre las dos se encuentran morfologías intermedias como las bicelas discoidales, las micelas cilíndricas y las micelas cilíndricas ramificadas entre otras.

1.4.1.1. Aplicaciones de los sistemas bicelares

Una de las grandes ventajas de las bicelas frente a otros sistemas laminares es su capacidad de alinearse espontáneamente en un campo magnético, lo que las hace adecuadas para estudios estructurales y conformacionales de péptidos y proteínas usando resonancia magnética nuclear [56]. El alineamiento de las bicelas ocurre espontáneamente en campos magnéticos mayores de 1 tesla a temperatura igual o superior a la temperatura de transición del fosfolípido de cadena larga [57]. Las bicelas se orientan con la normal de la bicapa perpendicular a la dirección del campo magnético (B_0), como se muestra en la figura 16.

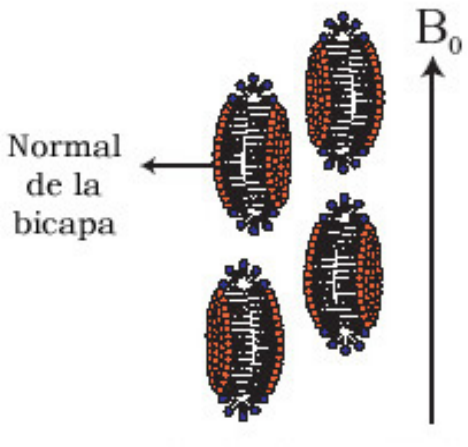

Figura 16. Representación de las bicelas discoidales alineadas en un campo magnético (B_0). Nótese que la normal de la bicapa se posiciona de forma perpendicular a la dirección del campo magnético.

Nuestro grupo de investigación es pionero en la novedosa aplicación de estos sistemas en estudios relacionados con la piel. Se ha observado que estos sistemas pueden modular la función barrera de la piel, aumentando o reforzando su permeabilidad en función de la composición del sistema [58]. Además, diferentes trabajos han demostrado el potencial de estos sistemas para encapsular sustancias de interés farmacológico y para liberarlas a través de la piel [59, 60]. Algunas de las sustancias que se han incorporado a las bicelas son ceramidas [61], diclofenaco sódico y ácido fluflenámico. Al incorporar estos dos últimos fármacos en las bicelas y aplicarlos en la piel se observó un efecto retardante en la absorción percutánea del fármaco. En cambio, un pretratamiento de bicelas sobre la piel y la posterior aplicación del fármaco promovió su absorción percutánea [60]. Por otro lado, se cambió la composición de las bicelas clásicas (DPPC/DHPC y DMPC/DHPC) y se observó una mejoraría en sus propiedades para la aplicación en la piel [62-65]. Además, se incorporaron un agente de contraste (gadodiamida) y un antifúngico (nistatina), para su posterior aplicación en otras vías diferentes a la tópica con mayor contenido en agua, como son la vía cerebrointraventricular y la transmucosa oral [66].

En esta tesis se ha evaluado la estabilidad morfológica y química de las bicelas frente a radiación UV-VIS y la capacidad anti-radicalaria de las mismas incorporando β-

caroteno. Adicionalmente también se ha estudiado la utilidad de las bicelas como transportador de un antioxidante de Mn^{II}.

1.4.1.2. Concentración lipídica de las bicelas: efecto de la dilución

El efecto de la dilución es un importante parámetro para controlar la estabilidad de los sistemas bicelares. Se sabe que las bicelas son estables en un rango de concentración lipídica entre 3 y 40% [55]. Cuando este porcentaje disminuye (dilución), las bicelas clásicas (DMPC/DHPC y DPPC/DHPC) se transforman en estructuras más grandes cambiando su morfología de discos a vesículas. Con la dilución, la concentración de DHPC en agua disminuye y para reestablecer la concentración monomérica de DHPC en agua, este fosfolípido tiende a dejar el borde de la bicela pasando al agua. Este fenómeno y la alta hidrofobicidad de los fosfolípidos de cadena larga, inducen un incremento de la relación molar en las estructuras, y un aumento en el diámetro del disco. Las condiciones de alta dilución llevan a la fusión de los discos para formar vesículas [67].

Diversos autores han diseñado varios métodos para estabilizar la morfología discoidal de las bicelas en condiciones de alta dilución, como el uso de bicelas formadas por fosfolípidos cargados [68] y mezclas de lípidos conjugados con polietilenglicol (lípido-PEG). Estos métodos de estabilización podrían limitar la funcionalidad conocida de las bicelas, que es detallada en la siguiente sección 1.4.2. Con el fin de evitar esta limitación y poder mantener la estructura de las bicelas en medios diluidos, se crearon los llamados “Bicosomas”, los cuales han sido objeto de estudio en esta tesis.

1.4.2. Bicosomas

Los bicosomas son nanoestructuras formadas por un grupo de bicelas encapsuladas por una vesícula esférica de alrededor de 150-250 nm (Figura 17) [66].

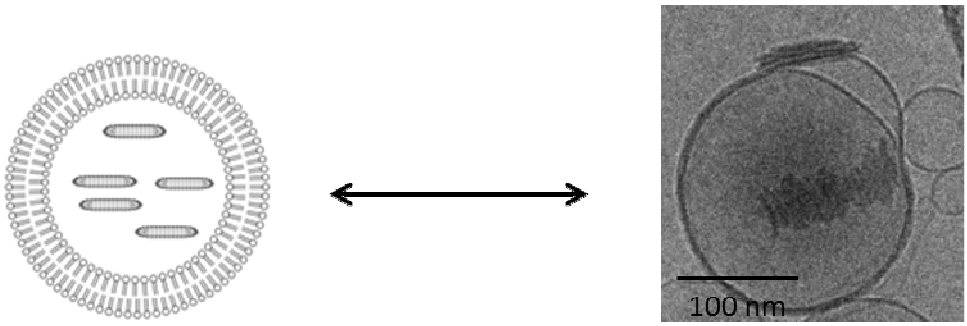

Figura 17. Estructura e imagen de microscopia por criotransmisión del bicosoma.

Los fosfolípidos típicos utilizados para formar estas estructuras son los ya mencionados fosfolípidos de las bicelas, y para la vesícula esférica exterior que encapsula las bicelas se utilizan fosfolípidos compuestos por dos ácidos grasos cuyas cadenas alquílicas pueden tener enlaces saturados o insaturados. En general estos fosfolípidos de la vesícula exterior suelen ser mezclas que contienen un 80-90% de fosfatidilcolinas (PC) formados mayoritariamente por ácido palmítico o ácido esteárico como acido saturado y principalmente ácido linoleico o linolénico como acido insaturado (Figura 18A). El 10-20% restante de la vesícula del exterior suele ser el colesterol (CHOL) (Figura 18B).

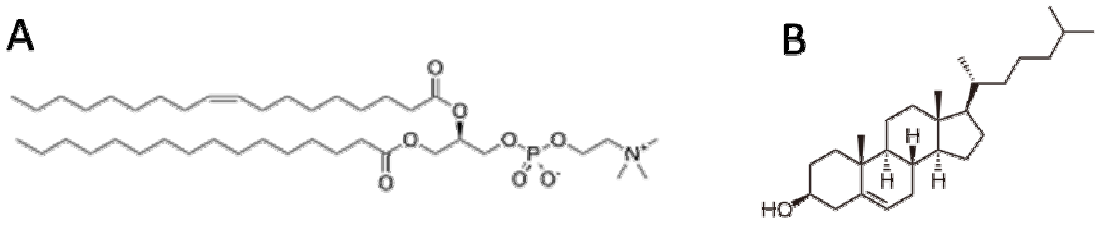

Figura 18. Estructura de los fosfolípidos típicos utilizados para formar la vesícula externa de los bicosomas, A) PC y B) CHOL.

Hasta el momento, los bicosomas se han aplicado junto con las bicelas en otras vías diferentes a la tópica con mayor contenido en agua, como son la vía cerebrointraventricular y la transmucosa oral [66]. Sin embargo, su aplicación en piel no se ha llevado a cabo hasta esta tesis.

Siguiendo la línea de investigación dermatológica, en esta tesis se propone aplicar los bicosomas en la piel y evaluar la interacción entre los sistemas lipídicos y el tejido. Primero se estudia el efecto anti-radicalario que pueden tener en la piel los sistemas de bicosomas con β-caroteno, y también se observa el efecto sobre la piel mediante microscopia (artículos, 2 y 3). Además, se incorporan los antioxidantes mostrados en la figura 2 y se estudia su penetración en piel normal y sometida a radiación UV-VIS (artículo 5 y 6). Por ultimo se estudia el efecto protector de los bicosomas con β-caroteno para prevenir la degradación del colágeno por radiación IR.

A lo largo de esta tesis se han utilizado un gran número de técnicas que han permitido caracterizar las bicelas y los bicosomas, y evaluar su interacción con los diferentes tejidos.

1.4.3. Técnicas de caracterización de las bicelas y los bicosomas

1.4.3.1. Dispersión dinámica de luz

La dispersión dinámica de luz (DLS) es una técnica utilizada para medir el tamaño y la polidispersidad de las partículas. Para ello, se detecta la intensidad de luz dispersada por las partículas en solución. Esta intensidad fluctúa con el tiempo, porque es debida al movimiento Browniano de las partículas de la muestra. Para evitar la dispersión múltiple en muestras muy concentradas se utiliza un tipo de detector no invasivo a gran ángulo (173º), denominado NIBS (del inglés "*Non Invasive Back Scatter*"), tal como muestra la figura 19.

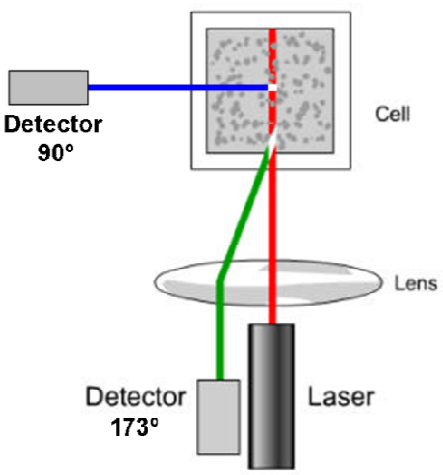

Figura 19. Esquema del equipo DLS utilizado con la posibilidad de detección de la luz dispersada a 90º y a 173º (tecnología NIBS del Zetasizer Nano ZS, Malvern Instruments).

Este equipo mide el diámetro hidrodinámico (HD) de una esfera que tiene el mismo coeficiente de difusión que la partícula a estudiar. Dado que las bicelas tienen estructura discoidal, el HD de la esfera determinada por DLS con el radio del disco de la bicela se calcula por medio de una ecuación matemática [69]. Una detallada descripción del cálculo del HD por DLS y del cálculo del radio del disco es ofrecida en el anexo I.

Las medidas de DLS se llevaron a cabo utilizando el Zetasizer Nano ZS (Malvern Instruments, Inglaterra) en el IQAC-CSIC.

1.4.3.2. Criomicroscopía electrónica de transmisión (Crio-TEM)

Con el método de Crio-TEM se pueden visualizar directamente las muestras vitrificadas a temperaturas muy bajas (-170 °C). La vitrificación es una técnica de criofijación basada en una congelación muy rápida que evita la formación de cristales de hielo que pueden generar daños en las estructuras que se quieren visualizar. Esta técnica permite obtener imágenes directas de agregados lipídicos en solución acuosa [70]. El proceso de vitrificación de las muestras se realiza de forma automatizada con el aparato Vitrobot (FEI Company, Eindhoven, Holanda), donde una pequeña cantidad de muestra se coloca en una rejilla de cobre recubierta con una película de carbono. Después se absorbe la muestra sobrante ("blotting") quedando una película fina de

muestra sobre la rejilla. A continuación, la muestra se vitrifica sumergiéndola inmediatamente en etano líquido (-180 ºC) y se almacena en nitrógeno líquido (-196 °C) hasta ser examinada por Crio-TEM a bajas temperaturas.

Esta técnica de microscopia permite estudiar la morfología y tamaño de estructuras pequeñas como pueden ser las bicelas y los bicosomas.

Figura 20. Imagen del Vitrorobot utilizado para la vitrificación de las muestras.

La preparación de las muestras y la posterior visualización por microscopía electrónica se han realizado en la unidad de Crio-Microscopía Electrónica del CCiT-UB, bajo la asistencia técnica de la Dra. Carmen López.

1.4.3.3. Oxidación de los lípidos de las bicelas y los bicosomas

El estudio de la degradación de los lípidos de las bicelas y los bicosomas fue realizado mediante el ensayo del TBA. Este procedimiento se ha explicado anteriormente en el apartado 1.2.6.4. relacionado con los ensayos de oxidación del cabello.

1.4.3.4. Espectroscopia Raman

El análisis mediante espectroscopía Raman se basa en el examen de la luz dispersada por un material al incidir sobre él un haz de luz monocromático. Una pequeña porción de la luz es dispersada inelásticamente experimentando ligeros cambios de frecuencia que son característicos del material analizado e independiente de la frecuencia de la luz incidente.

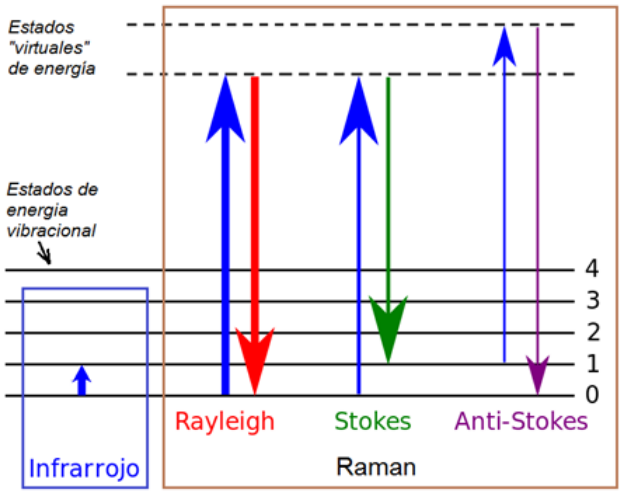

Figura 21. Esquema del fenómeno de trasmisión Raman.

La luz dispersada que mantiene la misma frecuencia que la luz incidente se conoce como dispersión Rayleigh y no aporta ninguna información sobre la composición de la muestra analizada. La luz dispersada que presenta frecuencias distintas a la de la radiación incidente, es la que proporciona información sobre la composición molecular de la muestra y es la que se conoce como dispersión Raman.

Una vez dispersada la luz, si la molécula vuelve a un estado de energía mayor al que tenía inicialmente, el fenómeno se denomina Raman Stokes (Figura 21). En cambio, si la molécula vuelve a un estado de energía menor al que tenía inicialmente, el fenómeno se denomina Raman Anti-Stokes (Figura 21) (esto significa que la molécula inicialmente no se encontraba en su estado vibracional fundamental sino en uno de mayor energía).

El β-caroteno es detectable por espectroscopia de Raman mediante el efecto Raman Stokes. Los picos característicos de este antioxidante en un espectro Raman se hallan a 1005, 1156 y 1523 cm^{-1} (Figura 22) [71].

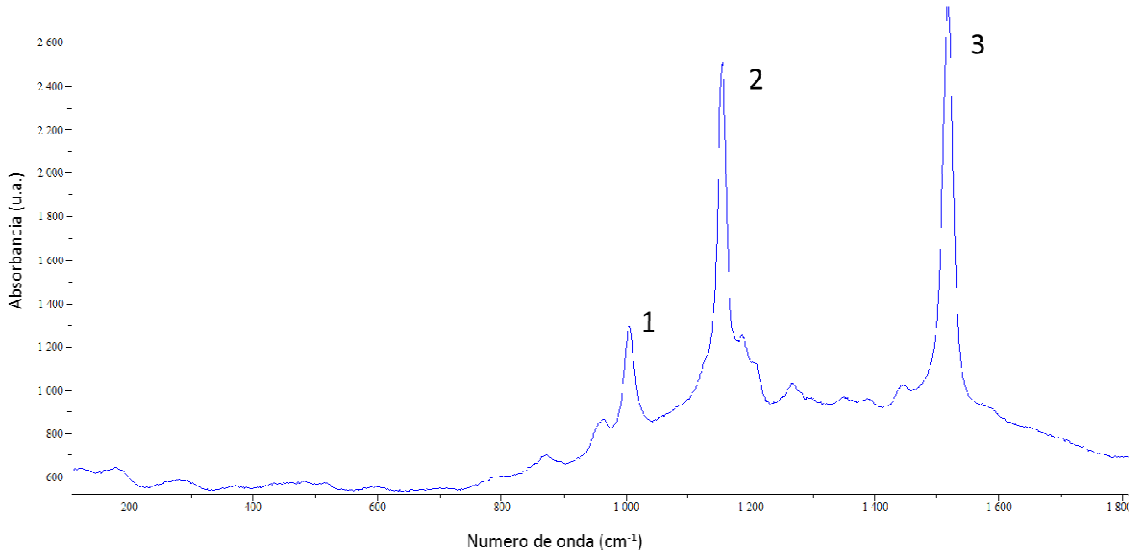

Figura 22. Espectro Raman del antioxidante β-caroteno con los picos característicos a 1005 (1), 1156 (2) y 1523 cm^{-1} (3).

Esta técnica se ha utilizado para evaluar la estabilidad frente a radiación UV-VIS del β-caroteno cuando es incorporado en las bicelas y los bicosomas.

Los espectros de Raman para las bicelas y los bicosomas con β-caroteno se llevaron a cabo utilizando el espectrómetro micro-Raman Labran HR 800 (Horiba, Jobin Yvon, France) de los CCiT-UB, en colaboración con el Dr. Tariq Jawhari.

1.4.4. Técnicas utilizadas para evaluar la interacción de las bicelas y/o los bicosomas con la piel

1.4.4.1. Estudio de la formación de radicales libres en la piel por efecto de la radiación UV, VIS e IR mediante EPR y el método "spin-trap"

En el caso de la piel, la detección de radicales libres por EPR no es tan sencillo como en el cabello. Los radicales formados en la piel son más inestables que los formados en el cabello, y no son detectables directamente mediante EPR. Para solucionar este problema se utiliza una molécula (un "spin-trap") que es la encargada de atrapar los

radicales formados en la piel para hacerlos más estables y así poder detectarlos por EPR [72]. En la figura 23 se muestra como un "spin-trap" común como el 5,5-Dimethyl-1-pyrroline-N-oxide (DMPO) se une a un radical hidroxilo para formar otro radical denominado aducto DMPO-OH. Este aducto es más estable que el radical hidroxilo y puede ser detectado por EPR.

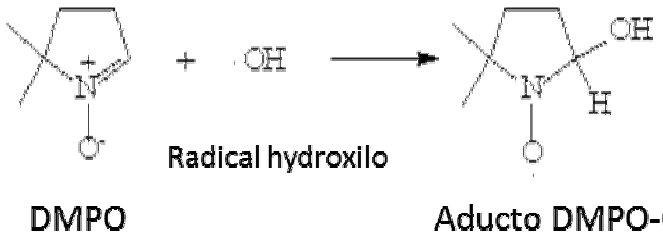

Figura 23. Esquema de unión del DMPO con un radical hidroxilo para formar el aducto DMPO-OH.

La radiación UV-VIS se lleva a cabo in situ en el equipo de EPR mediante una lámpara de mercurio de 500 W (Oriel) acoplada al equipo. La distancia entre la lámpara y la muestra es de 50 cm y la intensidad de irradiación a esa distancia es de 147.9 W/ m^2 (3.5 UVC, 5.9% UVB, 12.1% UVA, 39.9% VIS y 38.5% IR).

Por otro lado, la radiación IR se ha llevado a cabo mediante un accesorio hecho a mano acoplado al equipo de EPR (Figura 24). Este accesorio fue fabricado por el Dr. Lluís Fajarí y por el servicio de mantenimiento del IQAC-CSIC en colaboración con el grupo de Biofísica de Lípidos e Interfases del mismo instituto. El accesorio de IR consta de una lámpara infrarroja de 250 W (Philips BR I 25) cubierta de un bloque de aluminio (Figura 24, A) que permite direccionar la radiación a la zona de medición del EPR (Figura 24, B). Asimismo, el accesorio dispone de un ventilador que mantiene la temperatura de la muestra durante la irradiación entre los 25 y 30ºC (Figura 24, C). Gracias a este dispositivo, se ha podido evaluar la capacidad de la radiación IR de formar radicales libres en la piel a temperaturas fisiológicas, algo que hasta el momento solo se había observado a temperaturas superiores a 40ºC. La intensidad de irradiación esta distancia es de 0,108 W/cm^2.

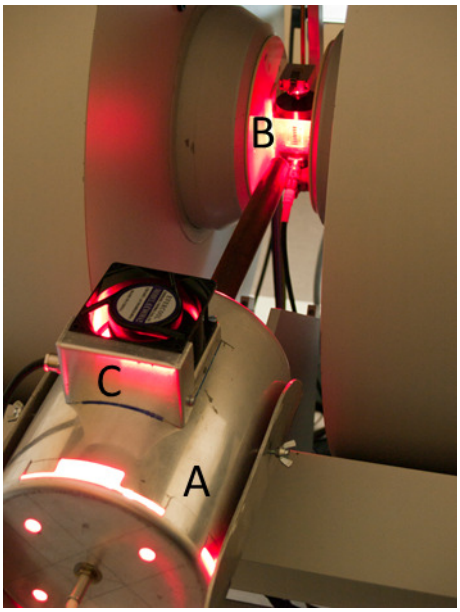

Figura 24. Accesorio construido en el IQAC para medir in situ los radicales libres en la piel mediante radiación IR a temperaturas entre 25 y 30ºC.

Igual que en el cabello, el espectrómetro de EPR utilizado fue el EMX-Plus 10/12 de la casa Bruker BioSpin (Figura 6) del servicio de Resonancia Paramagnética Electrónica del IQAC-CSIC en colaboración con el Dr. Lluís Fajarí y la Sra. Avencia Diez.

1.4.4.2. Criosustitución aplicada a la microscopia electrónica de transmisión (FSTEM)

Esta técnica se utiliza para visualizar la piel e incluye los siguientes procesos: fijación química (con glutaraldehído), post-fijación química donde se añaden los agentes de contraste, criofijación en nitrógeno líquido, y criosubstitución donde se intercambia el agua por metanol o acetona y se incluye el tejido en una resina (Lowicryl HM20 o Epon) que polimeriza bajo radiación UVA. Finalmente se hacen los cortes ultrafinos para ser visualizados en un TEM. La figura 25 resume el proceso de preparación de la muestra.

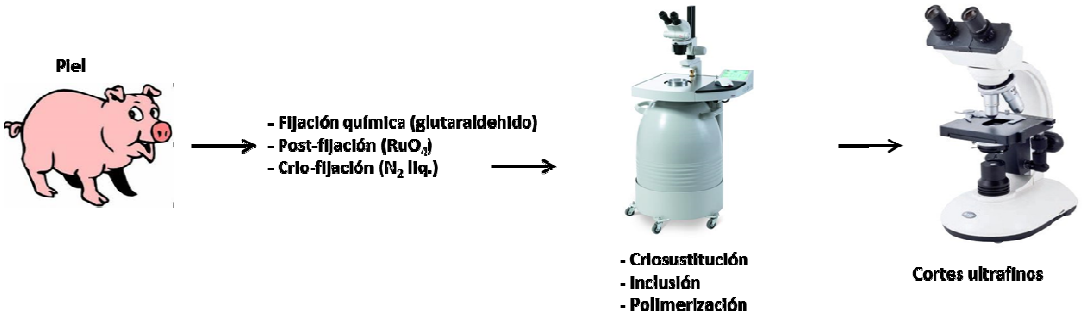

Figura 25. Esquema del proceso de preparación de la muestra para FSTEM.

Con esta técnica se visualizan los posibles cambios causados en la estructura de la piel debido a la radiación UV-VIS y debido al tratamiento con bicosomas.

La preparación de los tejidos y la posterior visualización de las muestras por microscopía electrónica se han realizado en la unidad de Crio-Microscopía Electrónica del CCiT-UB, bajo la asistencia técnica de la Dra. Carmen López.

1.4.4.3. Espectroscopia de infrarrojo con transformada de Fourier (FTIR) con fuente sincrotrón

La espectroscopia de infrarrojo con transformada de Fourier (FTIR) se basa en la interacción de la radiación IR media (4000 y 400 cm^{-1}) con la muestra. Esta técnica proporciona información sobre las vibraciones moleculares, ya que cada molécula o grupo funcional absorbe luz IR a una longitud de onda determinada.

Esta técnica se ha utilizado en estudios anteriores para evaluar la penetración de los sistemas bicelares en la piel utilizando lípidos deuterados para formar estos sistemas [65]. El enlace presente en las bicelas con lípidos deuterados (enlace C-D), muestra una vibración entre 2000-2300 cm^{-1} que puede diferenciarse fácilmente de la vibraciones de la piel debido a que este tejido no presenta ninguna vibración en este rango. Sin embargo, estos estudios no aportan información sobre la penetración de activos incorporados en las bicelas, únicamente permite seguir el sistema en la piel. Para poder obtener información sobre la distribución en la piel de activos incorporados en bicelas o bicosomas, es necesario detectar las vibraciones de la molécula, y no del

vehículo mediante el cual penetra en la piel. Además, se tiene que tener en cuenta que las vibraciones de la molécula no tienen que interferir con las vibraciones de la piel.

El derivado de Re que se muestra en la figura 26 presenta dos vibraciones a 1920 cm^{-1} (vibración E) y en 2020 cm^{-1} (vibración A_1). Estas dos frecuencias de vibración no interfieren con las vibraciones infrarrojas de la piel (Figura 30) [73].

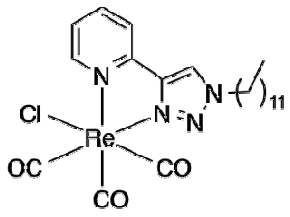

Figura 26. Derivado de Re acoplado a los bicosomas ($C_{12}Re(CO)_3$: (fac-[$Re(CO)_3Cl$(2-(1-dodecyl-1H-1,2,3,triazol-4-yl)-pyridine)]).

Acoplando este derivado de Re en las bicelas o bicosomas, es posible distinguir las vibraciones de esta molécula de las vibraciones de la piel, tal y cómo se muestra en el espectro de la figura 27, y por lo tanto, se puede obtener información relacionada con la distribución de esta molécula en la piel por medio de ambos sistemas lipídicos.

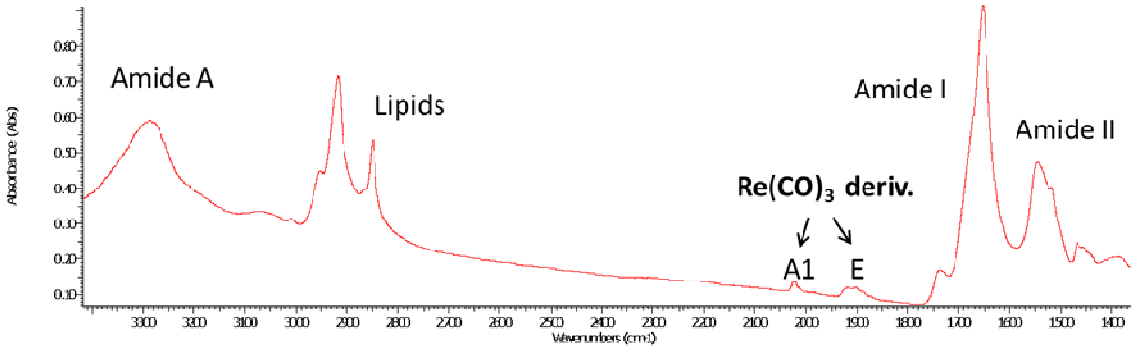

Figura 27. Espectro infrarrojo de la piel tratada con bicosomas incorporando el derivado de Re. De izda. A dcha: amida A (enlace NH), lípidos de la piel y de bicosomas (enlace CH), vibraciones A1 y E del derivado de Re, amida I (enlace CO), y amida II (enlace CN).

Por otro lado, acoplando un microscopio a la espectroscopia de IR y radiación sincrotrón, es posible obtener imágenes de la distribución del derivado de Re en la piel a altas resoluciones tal y como se muestra en la figura 28.

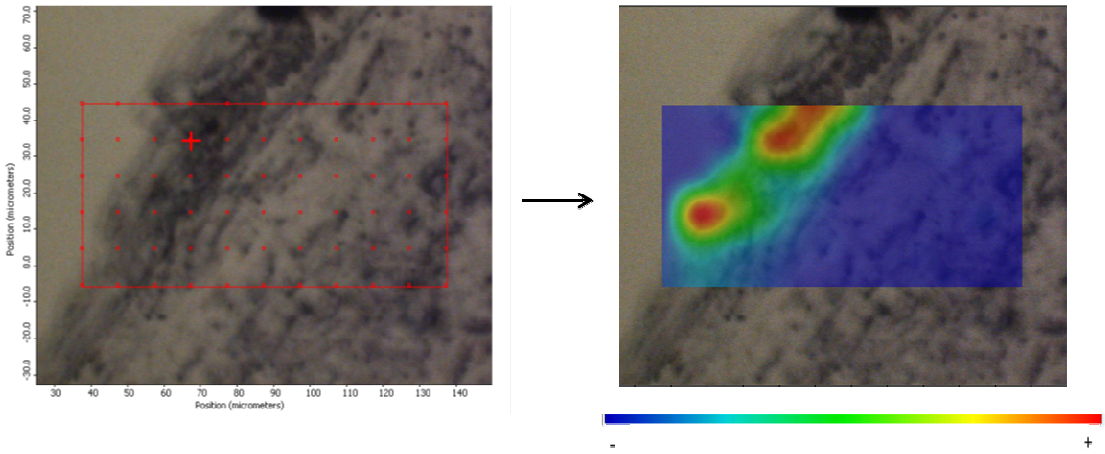

Figura 28. Distribución en una sección de piel del derivado de Re incorporado en bicosomas. La escala de colores desde el azul al rojo indica la concentración del derivado de Re en cada sección de piel o zona analizada. El color rojo indica una máxima concentración y el azul indica ausencia del derivado. El verde y amarillo representan concentraciones intermedias de esta molécula.

En esta tesis la técnica FTIR se ha utilizado para estudiar la capacidad de los bicosomas en incorporar el derivado de Re en la piel. Adicionalmente, el derivado de Re se ha empleado como marcador de los bicosomas para evaluar la penetración de estos sistemas en la piel incorporando los antioxidantes de la figura 2. Asimismo, el estudio de la penetración de los bicosomas también se ha llevado a cabo en piel expuesta a radiación UV-VIS para ver el efecto que puede causar la irradiación en la penetración de estos sistemas.

El equipo utilizado en esta investigación ha sido el microscopio de IR Thermo Continuum XL acoplado a un espectrómetro FTIR Nicolet Nexus 5700 (Madison, Wisconsin, USA). Los experimentos se han realizado en la línea SMIS del Sincrotrón SOLEIL (Francia), en colaboración con el Dr. Christophe Sandt y la Dra. Clotilde Policar y su equipo del Ecole Normale Supérieure de París.

1.4.4.4. Dispersión de rayos X a ángulos pequeños (SAXS) con fuente Sincrotrón

La dispersión de rayos X es una técnica en la que se hace incidir un rayo de radiación monocromática sobre la muestra, dando como resultado un patrón de dispersión. Este patrón muestra las diferentes intensidades de rayos X dispersados a diferentes ángulos, pequeño (SAXS) o grande (WAXS), lo que permite calcular las dimensiones, la forma y la organización de la estructura.

La técnica de SAXS con radiación sincrotrón es excelente para estudiar la organización del colágeno de la piel. La radiación sincrotrón se produce aplicando una aceleración centrípeta, con velocidad constante, a un haz de electrones. Tiene un rango espectral muy amplio (del infrarrojo a rayos X). Una de las ventajas de la luz sincrotrón es que produce un haz de rayos X de alta intensidad permitiendo realizar experimentos en tiempos muy cortos, con una extraordinaria relación señal/ruido y con una alta resolución en energía. El considerable aumento de la relación señal/ruido permite resolver estructuras que antes quedaban ocultas por su baja intensidad como es el caso de la estructura del colágeno.

En esta tesis la técnica de SAXS se ha utilizado para evaluar la degradación del colágeno de la piel mediante radiación IR. El colágeno es una proteína de la dermis que tiene una determinada organización (Figura 11) que puede ser estudiada por rayos X [74]. Esta proteína muestra un perfil de dispersión de rayos X característica de su organización. El perfil de rayos X característico del colágeno muestra reflexiones periódicas de densidad electrónica. La figura 29, representa la disposición de la muestra y del detector, y los perfiles de dispersión que se pueden obtener a ángulo pequeño (SAXS) del colágeno de la piel.

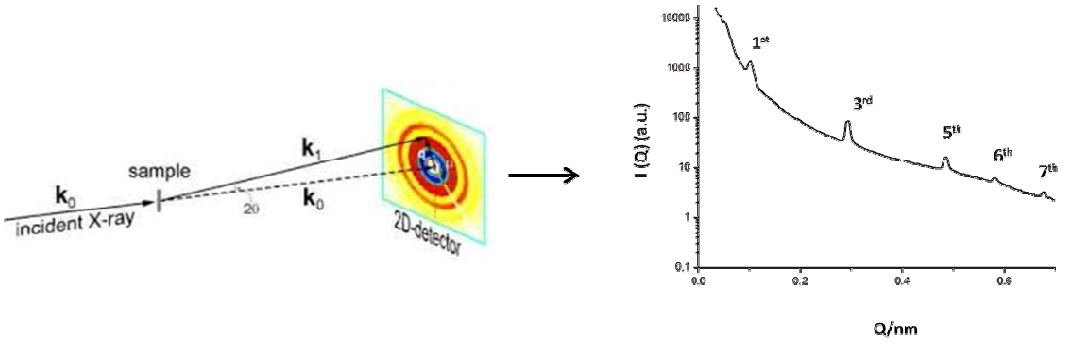

Figura 29. Representación esquemática de una medida de SAXS dando lugar al perfil de dispersión característico del colágeno de la piel (reflexiones periódicas de densidad electrónica del colágeno).

La intensidad de dispersión I(*Q*) se mide en función del módulo del vector de dispersión, *Q* . Éste último está definido como:

$$|Q| = \frac{(4\pi \sin\theta)}{\lambda} \qquad \text{(Ec. 1)}$$

Donde θ es el ángulo de dispersión y λ es la longitud de onda de la radiación (1.542 Å).

Para estructuras laminares apiladas, los picos están posicionados a distancias equidistantes, de esta forma,

$$Q_n = \frac{2\pi n}{d} \qquad \text{(Ec. 2)}$$

donde Q_n es la posición del orden de difracción, n es el orden de difracción y d es la distancia de repetición.

La degradación del colágeno de la piel se ha realizó exponiendo la piel a radiación IR con una lámpara infrarroja de 250 W (Philips BR I 25) tal y como se muestra en la figura 30.

Figura 30. Procedimiento de irradiación para evaluar la deterioración del colágeno en la piel por luz IR.

Las muestras de piel se colocaron a 10 cm de la lámpara de IR consiguiendo una intensidad de irradiación de 0,91 W/cm^2. Esta intensidad de irradiación fue la mínima necesaria para poder observar el deterioro del colágeno.

Las medidas de SAXS se llevaron a cabo utilizando un detector de SAXS 2D ADSC 210r (ADSC, Poway, CA, USA) y se realizaron en la línea BL11-NCD del sincrotrón ALBA en Cerdañola del Valles (Barcelona) bajo la asistencia técnica de la Dra. Christina Kamma-Lorger.

2. OBJETIVOS

2. OBJETIVOS

El objetivo principal de la investigación realizada en esta tesis ha sido evaluar *in vitro* los efectos producidos por la radiación solar en el cabello y en la piel, y determinar una posible prevención de daños en ambos tejidos mediante la aplicación de formulaciones antioxidantes y antioxidantes vehiculizados mediante bicelas y bicosomas. También se ha evaluado la interacción de ambos sistemas lipídicos con la piel y la estabilidad de los sistemas frente a radiación UV-VIS.

Con este fin se han establecido unos objetivos más específicos:

- Optimizar las diferentes metodologías para poder establecer la oxidación del cabello y de la piel mediante radiación UV-VIS e IR.
- Evaluar la acción protectora de dos formulaciones antioxidantes en el cabello.
- Evaluar la actividad anti-radicalaria en la piel de las bicelas y los bicosomas frente a radiación UV-VIS y determinar el efecto de incluir el antioxidante β-caroteno en ambos sistemas lipídicos.
- Evaluar los efectos causados por la radiación IR en la piel manteniendo la temperatura de este tejido entre los 25-30ºC. Estudiar el posible efecto protector del sistema de bicosomas con β-caroteno para prevenir los efectos causados por radiación IR en la piel.
- Determinar la capacidad de los bicosomas en promover la penetración de activos en la piel.
- Determinar la diferencia de penetración de los bicosomas en una piel normal y en una piel expuesta a radiación UV-VIS.
- Evaluar la estabilidad morfológica y química de las bicelas y los bicosomas expuestos a radiación UV-VIS, y de la misma manera evaluar también la estabilidad del β-caroteno en estos sistemas bajo la misma dosis de irradiación.

Los objetivos propuestos en esta tesis han dado lugar a unos resultados que se han publicado en los artículos detallados en la siguiente sección.

En los artículos 1 y 2 se ha estudiado el efecto oxidativo de la radiación UV-VIS en el cabello y la prevención de esta oxidación mediante tratamiento con formulaciones antioxidantes.

En el artículo 3 se ha evaluado la efectividad anti-radicalaria en la piel de las bicelas y los bicosomas que incorporan el antioxidante β-caroteno. Asimismo se hace una simulación de los diferentes tipos de radicales que se pueden formar en la piel y se cuantifica la concentración de cada tipo de radical.

En el artículo 4 se ha estudiado la estabilidad morfológica de las bicelas y bicosomas con β-caroteno expuestos a radiación UV-VIS, y se estudia la estabilidad de este antioxidante frente a la misma dosis de irradiación cuando se incorpora en bicelas y bicosomas. Posteriormente se observan por microscopia muestras de piel tratadas con bicosomas incorporando β-caroteno.

En los artículos 5 y 6 se estudia principalmente la capacidad de los bicosomas como vehículo para promover la penetración de activos en la piel. Con el fin de determinar cómo influye la penetración de los bicosomas en piel sometida a radiación UV-VIS, también se estudia la penetración de este sistema lipídico en piel previamente expuesta a radiación UV-VIS.

Finalmente, en el artículo 7 se estudian los daños causados por radiación IR en la piel. Para determinar si los efectos causados por esta radiación dependen del aumento de temperatura producido en la piel, se estudia la formación de radicales libres en este tejido a temperaturas entre 25-30ºC. Adicionalmente se determinan las condiciones necesarias para dañar el colágeno cutáneo mediante exposición a luz IR.

En la sección de resultados se adjuntan dichos artículos con un breve resumen.

3. RESULTADOS

3. RESULTADOS

Los resultados de la presente tesis doctoral están reflejados en los siguientes artículos científicos presentados a continuación acompañados con un breve resumen.

Artículo 1: Photodamage determination of human hair. E. Fernández, C. Barba, C. Alonso, M. Marti, J.L. Parra, L. Coderch. *Journal of Photochemistry and Photobiology B: Biology,* 2012, **106**, 101-106.

Artículo 2: Efficacy of antioxidants in human hair. E. Fernández, B. Martinez-Teipel, R. Armengol, C. Barba, L. Coderch. *Journal of Photochemistry and Photobiology B: Biology,* 2012, **117**, 146-156.

Artículo 3: Bicelles and bicosomes as free radical scavengers in the skin.
E. Fernández, L. Fajarí, G. Rodriguez, C. López-Iglesias, M. Cócera, L. Barbosa-Barros, A. de la Maza, O. López. *RCS Advances*, 2014, **4**, 53109-53121.

Artículo 4: Advanced lipid systems containing ß-carotene: stability under UV-VIS radiation and application on porcine skin *in vitro.* E. Fernández, G. Rodriguez, M. Cócera, L. Barbosa-Barros, C. Alonso, C. López-Iglesias, T. Jawhari, A. de la Maza, O. López. *Physical Chemistry Chemical Physics,* 2015, **17**, 18710-18721.

Artículo 5: A rhenium tris-carbonyl derivative as a model molecule for incorporation into phospholipid assemblies for skin applications. E. Fernández, G. Rodriguez, S. Hostachy, S. Clède, M. Cócera, C. Sandt, F. Lambert, A. de la Maza, C. Policar, O. López. *Colloid and surfaces B: Biointerfaces*, 2015, **131**, 102-107.

Artículo 6: Conditional factors in skin permeation of antioxidants using bicosomes.
E. Fernández, S. Hostachy, G. Rodriguez, S. Clède, M. Cócera, C. Sandt, F. Lambert, H.C. Bertrand, A. de la Maza, C. Policar, O. López. *Expert Opinion on Drug Delivery,* en revisión.

Artículo 7: Reducing the harmful effects of IR radiation on the skin using bicosomes
E. Fernández, L. Fajarí, G. Rodriguez, M. Cócera, C. Kamma-Lorger, L. Barbosa-Barros, A. de la Maza, O. López. *Journal of Dermatological Science,* en revisión.

ARTÍCULO 1

Photodamage determination of human hair

Journal of Photochemistry and Photobiology B: Biology, 2012, **106**, 101-106

La radiación UV deteriora el cabello causando la creación de radicales libres, la oxidación de proteínas y lípidos y la degradación del aminoácido Trp, también presente en esta fibra. En este estudio se han optimizado las condiciones de diferentes metodologías para evaluar estas consecuencias de la irradiación en fibras de cabello. La radiación es aplicada mediante un simulador solar (Suntest CPS+) en un rango entre 310 y 800 nm.

La formación de radicales libres en el cabello se lleva a cabo sometiendo diferentes masas de cabello a diferentes intensidades de irradiación y a diferentes tiempos de exposición. La concentración de radicales libres formados se determina mediante la técnica de EPR.

La oxidación de proteínas del cabello se determina de la fracción proteica extraída de fibras sometidas a una intensidad de irradiación de 500 W/m^2 durante diferentes tiempos. La extracción de proteína del cabello se realiza en diferentes masas y a diferentes temperaturas. Finalmente, la fracción de proteína oxidada se determina mediante el ensayo de Bradford.

La oxidación de los lípidos del cabello se determina de la fracción de peróxidos formados en fibras sometidas a una intensidad de irradiación de 500 W/m^2 durante diferentes tiempos. La extracción de peróxidos del cabello se realiza en diferentes masas de cabello y se determina mediante el ensayo del TBA.

Por último, la degradación del Trp se determina mediante espectroscopia de fluorescencia en cabellos sometidos a una intensidad de irradiación de 500 W/m^2 durante diferentes tiempos. La detección del Trp del cabello por fluorescencia se lleva a cabo hidrolizando el cabello en una solución de NaOH 2M.

Los resultados de EPR mostraron una mayor concentración de radicales libres en el cabello expuesto a 500 W/m^2 durante 24 h. Sin embargo, una vez interrumpida la irradiación, la concentración de radicales incrementó, algo que no es común en el

comportamiento de los radicales libres, que sin irradiación tienden a bajar su concentración. Los cabellos sometidos a 283 W/m^2 durante 45 y 90 min mostraron también un incremento de radicales libres, y una vez cesada la irradiación, la concentración de radicales decae. Por lo tanto, se estableció una intensidad de irradiación de 283 W/m^2 como mejor opción para determinar la formación de radicales libres en el cabello mediante esta técnica.

Las condiciones para una extracción óptima de proteínas en cabello se establecieron en una masa de 100 mg y en una temperatura de extracción de 45ºC durante 5 h. La fracción de proteína degradada aumentó a medida que incrementaba el tiempo de exposición a radiación UV-VIS.

Para una extracción óptima de peróxidos en el cabello se estableció una masa de cabello de 500 mg, y se observó que la fracción de peróxidos formados aumenta a medida que incrementaba el tiempo de exposición a la radiación UV-VIS.

Por último, la detección del Trp mediante fluorescencia hidrolizando el cabello con una solución de NaOH demostró ser útil para poder cuantificar este aminoácido en el cabello. En este caso, la degradación de este aminoácido también incrementó a medida que aumentaba el tiempo de exposición a la luz UV-VIS.

Por lo tanto, quedan establecidas las condiciones óptimas de cada estudio para poder evaluar la oxidación del cabello sometido a radiación UV-VIS. Estas metodologías resultan ser útiles para estudiar la eficacia de formulaciones antioxidantes para el cabello (artículo 2).

Journal of Photochemistry and Photobiology B: Biology 106 (2012) 101–106

Contents lists available at SciVerse ScienceDirect

Journal of Photochemistry and Photobiology B: Biology

journal homepage: www.elsevier.com/locate/jphotobiol

Photodamage determination of human hair

Estibalitz Fernández *, Clara Barba, Cristina Alonso, Meritxell Martí, José Luis Parra, Luisa Coderch

Department of Chemical and Surfactants Technology, Institute of Advanced Chemistry of Catalonia IQAC-CSIC, Barcelona, Spain

ARTICLE INFO

Article history:
Received 18 July 2011
Received in revised form 17 October 2011
Accepted 27 October 2011
Available online 7 November 2011

Keywords:
Photo-degradation
Hair
Lipid peroxides
Free radicals
ESR
Tryptophan

ABSTRACT

Sunlight on human hair causes photo-degradation. This results in bleaching due to melanin oxidation through free radicals, and induces keratin impairment. Protein degradation, tryptophan degradation, lipidic peroxidation and electron paramagnetic resonance can be used to evaluate proteic and lipidic photodecomposition and free radical formation in hair fibres subjected to antioxidant action and different UV intensities. All these methodologies have been optimised to determine protein, lipid and melanin degradation in hair subjected to different UV intensities.

1. Introduction

Hair fibres are made up of fibrous proteins of the keratin family. A minor contribution to the total hair mass derives from melanin pigment and lipids [1]. The greatest mass of the hair shaft is the cortex, which contributes to the mechanical properties of hair. The melanin granules are located inside the cortex (about 3% by weight). These are the hair pigments, whose type, size and quantity establish hair colour [2,3]. The disulphide bonds, each connecting two sulphur-containing amino acids (mostly cysteine), form an extensive cross-linked network within the hair fibre, which is believed to contribute significantly to the mechanical stability and chemical resistance of the fibre [4].

Sunlight on human hair causes photo-degradation. This results in bleaching due to melanin oxidation through free radicals, and induces keratin impairment. The worst effect of sunlight on hair is cystine oxidation to cysteic acid, which modifies its mechanical properties (long UV exposure) [5–9]. Shorter radiations induce undesirable effects such as a decrease in hydration, increases permeability, leading to a loss of shine and colour to an increase in combing resistance [10,11]. Thus, UV irradiation weakens the structural integrity of fibre as is evident from the diminished wet tensile properties [5], and increased transverse swelling in solvents [12].

UV exposure involves considerable changes in the structure of keratin including the photo-oxidation of aminoacids, sterol and fatty acids, resulting in rupture of sulphur bridges, decomposition of lipids, decrease in melanin as well as numerous micro-molecular lesions [13,14]. Both UV-A (400–315 nm) and UV-B (315–280 nm) are very harmful to hair. The effects of UV-B radiation can be severe, resulting in the breakdown of disulphide bonds inside the hair fibre and on the surface of the cuticle. However, UV-A radiation mainly produces free radical/reactive oxygen species (ROS) through the interaction with endogenous photosensitizers.

Studies show that an acceptable photo-oxidation of hair fibre is the fracture of C–S linkages from proteins [15], oxidation of internal lipids [16], and melanin granules [17] and tryptophan degradation of keratin [18]. Melanin is a homogeneous biological polymer containing a population of intrinsic, semiquinone-like radicals. There are two types of melanin, the brown–black pigments (eumelanins) and the less prevalent red pigments (pheomelanins) [2,3]. Exposure to sunlight leads to hair decoloration due to melanin oxidation via free radicals [7,8]. Additional extrinsic free radicals are reversibly photo-generated by UV and visible light. Melanin photochemistry, particularly the formation and decay of extrinsic radicals has been the subject of numerous electron spin resonance (ESR) spectroscopy studies [19–21]. The present study seeks to investigate the suitability of melanin as a detector of UV-generated free radicals in hair.

On the other hand, keratin fibre impairment of the proteic and lipidic fraction [6] and the degradation of amino acids susceptible to photo-degradation such as tryptophan [18,22,23], can determine the decomposition of hair fibre. The lipid and protein fraction plays an important role in the structure and integrity of hair fibre,

* Corresponding author. Address: IQAC-CSIC, Jordi Girona 18-26, 08034 Barcelona, Spain. Tel.: +34 934 006 100; fax: +34 932 045 904.
E-mail address: efptqt@cid.csic.es (E. Fernández).

1011-1344/$ - see front matter © 2011 Elsevier B.V. All rights reserved.
doi:10.1016/j.jphotobiol.2011.10.011

protecting against of external agents. In contrast to fibre damage, pigment decomposition can be readily observed.

Protein degradation, lipidic peroxidation, electron paramagnetic resonance and tryptophan degradation can be used to evaluate proteic and lipidic photodecomposition and free radical formation in hair fibres subjected to antioxidant action. Antioxidants are compounds that at low concentrations delay or prevent substrate oxidation. Different evaluation protocols to evaluate hair fibre decomposition were optimised to determine the efficacy of formulations with antioxidant active agents.

Accordingly, protein degradation was evaluated by protein solubilisation in SDS extracts. Lipid peroxidation was performed by the malondialdehyde (MDA) with the thiobarbituric acid test (TBA) [24,25]. Free radicals/ROS were detected by the amount of melanin found by ESR spectroscopy [8] and tryptophan decomposition was determined through comparative fluorescence intensities of alkaline hydrolised hair tresses using a spectrofluorometer [22].

2. Materials and methods

2.1. Materials

Methanol, trichloroacetic acid (TCA) and sodium dodecyl sulphate (SDS) were supplied by Merck (Darmstadt, Germany) and Bovine Serum Albumin (BSA), brilliant blue Gmalondialdehyde (MDA) and thiobarbituric acid (TBA) by Sigma (St. Louis, MO, USA). Natural red hair tresses (20 cm in length) were purchased from De Meo Brothers Inc. (New York). All the methodologies were carried out at 50% ± 5 of relative humidity.

2.2. Hair UV exposure

The hair tresses were subjected to electromagnetic radiation spectra from 310 nm to 800 nm (UV-A and visible light). Human hair was irradiated using a light source simulating UV solar radiation (283 W/m^2 equivalent to 1.77 J/min cm^2 or 500 W/m^2 equivalent to 3.0 J/min cm^2, Suntest CPS, Atlas, USA). The radiation of 283 W/m^2 is similar to that of the radiation of 1 day in June in Catalonia (1.50–1.84 J/min cm^2 equivalent to 21–26.5 MJ/m^2 per day [26]). As for the radiation of 500 W/m^2, the radiation is double. Moreover, the UV radiation intensity was modified at different exposure times depending on the test applied: 283 W/m^2 for 45 min (79.65 J/cm^2), 283 W/m^2 for 90 min (159.3 J/cm^2), 500 W/m^2 for 9 h (1600 J/cm^2), 500 W/m^2 for 18 h (3240 J/cm^2), 500 W/m^2 for 36 h (6480 J/cm^2), 500 W/m^2 for 24 h (J/cm^2) and 500 W/m^2 for 48 h (J/cm^2).

2.3. Electron paramagnetic resonance (EPR)

Two different experimental procedures were followed:

Procedure A: different amount of red hair (10, 40 and 70 mg) was introduced in a quartz tube and the melanin signal intensities were measured using a EMX-Plus 10/12 Brucker BioSpin spectrometer (Table 1). The same tube with the human hair was exposed to UV light (Suntest CPS) at different times, 45 min and 24 h at 500 W/m^2. Free radical formation due to UV irradiation and their dependence on the recovery time were evaluated.

Table 1
Spectrometer parameters.

Magnetic field	3485 Gauss
Sweep width	100 Gauss
Microwave frequency	9.73 GHz
Microwave power	20.00 mW
Modulation frequency	100 kHz
Modulation amplitude	2 Gauss
Time constant	20.48 ms
Sweep time	41 s

Procedure B: 10 mg of hair, previously cut into pieces of 1.5 cm, was fixed into a special ESR flat cell and the melanin signal intensities were measured using an EMX-Plus 10/12 Brucker BioSpin spectrometer (Table 1). The special ESR flat cell with the hair was then exposed to UV light (Suntest CPS) at times of 45 min (283 W/m^2) and 90 min (283 W/m^2). The intensity of the melanin ESR signal was measured before and after the irradiations. Furthermore, the dependence of the melanin signal on the recovery time was also evaluated.

2.4. Protein degradation

A total of 100 mg of hair was exposed to UV radiation (500 W/m^2) at different times (9, 18 and 36 h). Hair proteins and peptide solubilisation were carried out with the 100 mg of hair subjected to UV radiation, diluted in 1 ml of 2% SDS aqueous solution and sonicated using a Labsonic 1510 device (B. Braun, Melsungen, Germany) for 5 h and at 45 °C. Hair extracts were then diluted to 0.01% SDS concentration and the Bradford colorimetric assay was used to quantify the proteins and peptides solubilised This assay is based on the formation of a complex between the dye, Brilliant Blue G and the proteins in solution, which leads to an increase in absorption at 595 nm and is proportional to the amount of protein in the solution [27]. Bovine Serum Albumin (BSA) was used as a standard to calculate the amount of protein. This procedure was also performed for non-irradiated hair as a control.

2.5. Tryptophan decomposition

Hair tresses were exposed to UV radiation (500 W/m^2) at different times (24 and 48 h). Solutions were prepared dissolving 50 mg of irradiated or non-irradiated hair tresses in 50 ml of 2 M NaOH solution. The solution was allowed to stand for 24 h at room temperature without stirring. Thereafter, the solution was filtered and was used for fluorescence experiments [18,22,23]. Fluorescence spectra were obtained in a Shimadzu RF-540 spectrofluorimeter using 1 cm quartz cell. The excitation and emission wavelength were 290 nm and 345 nm, respectively. Measurements were made with the excitation and the emission slits set at 2 nm band passes. The intensity of samples was measured in arbitrary units, which were proportional to the amount of tryptophan in each hair sample.

2.6. Lipid peroxidation measurements

Lipids from human hair exposed to UV radiation (500 W/m^2) at different times (9, 18 and 36 h) were extracted with methanol (500 mg hair/10 ml methanol) in a sonicated device Labsonic 1510 (B. Braun, Melsungen, Germany) for 15 min. Next, the hair extracts were dried under a N_2 current and diluted again in 1.5 ml of methanol.

Lipid peroxides (LPO species) were measured by thiobarbituric acid (TBA) assay [21]. The thiobarbituric acid-reactive species (TBARS) were quantified by spectrophotometry at 534 nm (Cary 300 Bio UV–Visible Spectrophotometer, Varian, USA). At low pH and elevated temperature, MDA readily participates in nucleophilic addition reaction with TBA, generating a red, fluorescent 1:2 MDA: TBA adduct according to the reaction shown in Fig. 1.

The results were expressed as malonaldehyde bis(dimethylacetal) equivalents (μM MDA) using a standard curve for pure MDA–TBA complex. The calibration curve was obtained by using MDA at different concentrations (0.5–30 μM). Negative and

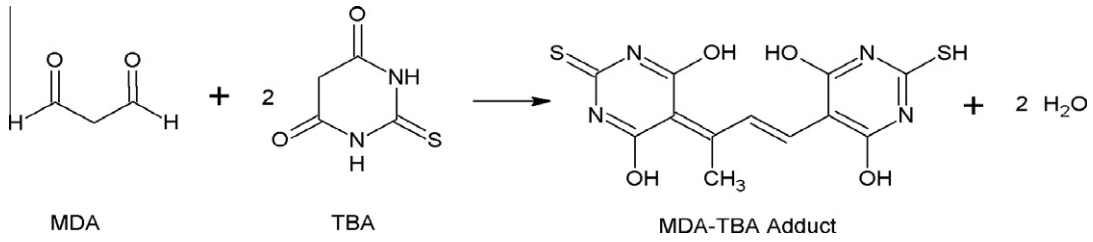

Fig. 1. Reaction proposed for the detection of MDA after lipid peroxidation.

Table 2
Free radical detection of non-irradiated and irradiated hair at different times, and measured at 0 and 60 min. ROS integration and percentage of ROS with respect to the non-irradiated sample (Procedure A and B).

	Irradiation, time	**Non Irradiated** ROS Integration ($x10^{10}$)	**Irradiated** ROS Integration at 0min decay ($x10^{10}$)	**Irradiated** ROS Integration at 60min decay ($x10^{10}$)
Procedure A 70mg of hair **M+SD**	500W/m^2, 24h	**12.521**	**1.764**	**2.661**
Decrease of ROS (%)			**14%**	**21%**
Procedure B 10mg of hair **M+SD**	283W/m^2, 45min	5.323	8.764 (164%)	8.075 (152%)
		4.594	6.466 (141%)	5.801 (126%)
		7.748	9.217 (119%)	8.529 (110%)
		5.888 ± 1.65	**8.149 ± 1.48**	**7.468 ± 1.46**
Increase of ROS (%)			**38%**	**27%**
Procedure B 10mg of hair **M+SD**	283W/m^2, 90min	6.548	9.810 (150%)	8.744 (134%)
		5.201	8.521 (164%)	7.549 (145%)
		4.162	7.525 (181%)	6.620 (160%)
		5,304 ± 1.20	**8.619 ± 1.15**	**7.638 ± 1.06**
Increase of ROS(%)			**63%**	**44%**

positive controls were also quantified using 0 and 100 μM of MDA. The calibration curve was prepared on each day of the experimental study. Briefly, the LPO species present in the samples (0.5 mL) were added to aliquots (1 mL) of a solution made up of 0.4% of TBA and 15% of trichloroacetic acid (TCA) in 100 mL of HCl solution (0.25 M). The mixture was incubated in a bath of boiling water for 1 h. Fresh TBA/TCA stock solution was prepared on each day of analysis. This procedure was also performed for non-irradiated hair as a control.

2.7. Statistics

Standard deviations were calculated for all mean values. Analysis of variance (ANOVA) with a one-way layout was applied for group comparisons. The software used was the STATGRAPHICS plus 5. Significant differences in the mean values were evaluated by the *F*-test. A *p* value below 0.05 was considered significant.

3. Results and discussion

Four tests to determine the oxidation of different hair compounds before and after exposure to UV were optimised. As stated, the free radicals (ROS) created were calculated by the amount of melanin detected by ESR spectroscopy; the protein degradation was evaluated by protein solubilisation in SDS extracts; the study of tryptophan decomposition was undertaken by the hydrolysed NaOH 2 M solution of irradiated and non-irradiated hair fibres and the lipid peroxidation was assessed the malondialdehyde (MDA) with the thiobarbituric acid test (TBA). Details of the experimental procedures assayed and the results for each test are described below.

3.1. Free radicals

Free radicals creation in hair after UV exposure was evaluated by antioxidant effectiveness studies. Melanin is known by its

intrinsic content of semiquinone-like radicals that can be detected by ESR spectroscopy. Moreover, extrinsic free radicals can be photo-generated by UV and visible light. Melanin photochemistry, especially the formation and the decay of extrinsic radicals, has been the subject of numerous electron spin resonance (ESR) spectroscopy studies [7,8,16].

The melanin granules are the hair pigments, whose type, size and quantity establish hair colour [2,3]. As stated in Section 1, there are two types of melanin, the brown–black pigments (eumelanins) and the less prevalent red pigments (pheomelanins) [2,3]. In this study red hair is used with higher percentage of pheomelanin. Hair melanins provide some photochemical protection to hair proteins, especially at lower wavelengths, where both the pigments and the proteins absorb light [4].

Following procedure A, 70 mg were introduced into an EPR tube and intrinsic radicals of melanin were quantified. Next, the tube was irradiated at 500 W/m^2 for 24 h and ROS quantification was carried out immediately and after 60 min (Table 2). ROS quantification indicates that the melanin was partially destroyed by the strong irradiation at 0 min the free radicals fell to about 14% instead of increasing, and then rose to 21% after 1 h. The experimental procedure was therefore replaced by procedure B with much less irradiation.

Following procedure B, 10 mg of hair were fixed onto a special flat cell for EPR evaluation. Next, the cell was irradiated at 283 W/m^2 for 45 or 90 min and again ROS quantification was carried out immediately and after 60 min. At 0 min this radiation time led to an increase of 138% in free radicals after radiation for 45 min (Table 2), and to an increase of 163% after radiation for 90 min. At 60 min the free radicals decreased to 127% after radiation for 45 min, and to 144% after radiation for 90 min (Table 2).

A marked increase in ROS was found for the two irradiations assayed. However, the ROS fall of about 10–20% only after 1 h of irradiation should be borne in mind. The variations in the measurements yielded an important standard deviation and only significant differences were found between untreated and 90 min UV treated hair, measured immediately after irradiation. The ROS decay with time should be noted.

The variations in the ROS (Table 2 and Fig. 2) quantification for the untreated, non-irradiated hair samples are attributed to different melanin content, the amount of hair, the area in which the hair is evaluated, the alignment of the hair, etc. Therefore the ROS quantification after UV radiation must be performed with the same sample without removing it from the flat cell. At least three evaluations for each sample should be performed. With these results, free radicals detection of melanin in hair should be used to evaluate the efficacy of hair care products.

3.2. Protein degradation

A protocol for hair protein degradation determination after UV exposure was optimised. Hair was first exposed to UV radiation (500 W/m^2) at different times (9, 18 and 36 h).

Hair proteins and peptide solubilisation was carried out using different amounts of hair (20, 50, 100 and 500 mg). They were treated in 1 ml of 2% SDS aqueous solution and sonicated using a Labsonic 1510 device (B. Braun, Melsungen, Germany) for different times (3 and 5 h) and at different temperatures (40 and 45 °C). Since surfactant agents are known to interfere in the Bradford colorimetric assay [27], the extraction solutions were diluted to 0.005% or 0.01% of SDS. This procedure was also performed for non-irradiated hair as a control.

The radiation power and time were suitable for detecting differences in protein and peptide solubilisation. The amount of hair should be at least 100 mg to ensure reliable results of extracted protein and the best extraction procedure was achieved at 45 °C for 5 h. On the other hand, dilution to 0.01% was enough to obtain reliable results for protein quantification. Therefore, the optimised conditions, detailed in the experimental section.

Following this methodology, non-irradiated samples present a protein or peptide solubilisation ranging between 11 and 12.5 μg protein/mg hair (Table 3). Irradiation of 500 W/m^2 at 9, 18 and 36 h shows an increase in protein solubilisation from 160% up to 228% (Table 3 and Fig. 3). The values obtained for protein solubilisation and their standard deviations at the three UV-radiations indicate that this protocol can be used to determine fibre damage, highlighting the significant differences in all the hair samples. This could therefore be a good assay for evaluating the effectiveness of antioxidant treatments on human hair.

Table 3
Protein hair solubilisation with 2% SDS of non-irradiated and irradiated hair at 500 W/m^2 for 9, 18 and 36 h. Percentage of increase of protein degradation with respect to the non-irradiated sample.

Samples	Non-irradiated (μg prot/mg hair)	9 h UV (μg prot/mg hair)	18 h UV (μg prot/mg hair)	36 h UV (μg prot/mg hair)
1	12.46	21.26	18.59	27.89
2	11.00	16.82	22.40	26.87
3	12.62	19.70	19.79	27.52
M + SD	**12.03 ± 0.89**	**19.26 ± 2.25**	**20.26 ± 1.95**	**27.43 ± 0.52**
Increase of protein degradation (%)		**60.1**	**68.5**	**128.0**

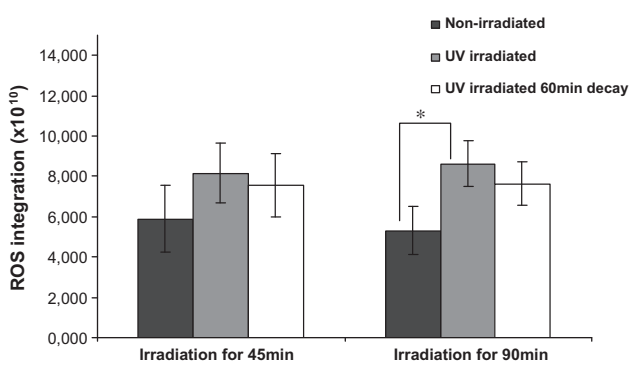

Fig. 2. Free radicals obtained for non-irradiated and irradiated hair measured at 0 and 60 min at 283 W/m^2 UV radiation during 45 and 90 min (*$p < 0.05$).

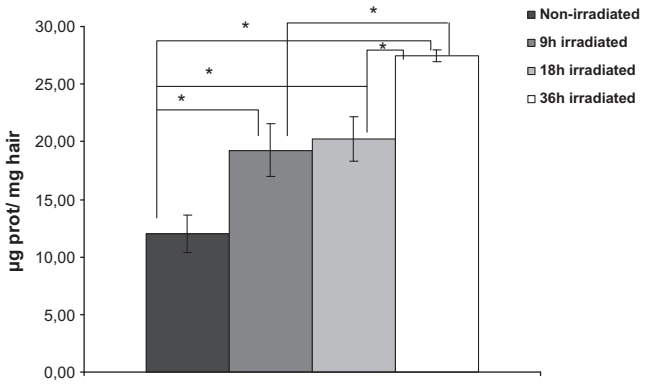

Fig. 3. Protein degradation obtained for non-irradiated and irradiated hair at 500 W/m^2 during 9, 18 and 36 h (*$p < 0.05$).

Table 4
Fluorescence intensity at 355 nm of 50 mg non-irradiated and irradiated hair at 500 W/m^2 for 24, and 48 h. Percentage of trp degradation with respect to the non-irradiated sample.

Samples	Non-irradiated fluoresc. int. (a.u.)	24 h UV fluoresc. int. (a.u.)	48 h UV fluoresc. int. (a.u.)
1	23.47	21.15	19.29
2	23.47	21.77	21.60
3	23.80	21.08	20.37
M + SD	**23.56 ± 0.21**	**21.33 ± 0.38**	**20.41 ± 1.71**
trp degradation (%)		**9.45**	**13.36**

3.3. Tryptophan degradation

A protocol for decomposition of a particular aminoacid such as tryptophan after UV exposure was also optimised. Tryptophan measurement was carried out on hair exposed to UV radiation (500 W/m^2) at different times (24 and 48 h). Tryptophan from hair is usually measured directly as a solid spectrofluorimetrically [18,23]. A protocol to hydrolyse the fibre was followed to measure the tryptophan in the alkaline solution spectrofluorimetrically [22]. A total of 50 mg of irradiated and non-irradiated hair was chopped from hair tresses and then dissolved in 50 ml of 2 M NaOH solution for 24 h. This enabled a complete release of tryptophan from hair and a quantification of tryptophan in order to correlate the variations in hair at different UV exposure times [22]. The measures of tryptophan intensity at different UV exposure times were obtained at 355 nm in the fluorescence spectrum, which is the emission wavelength of tryptophan in solution.

Following this methodology, the fluorescence intensity of non-irradiated samples presents an intensity of about 23.6 (a.u). Irradiation of 500 W/m^2 at 24, and 48 h shows a significant tryptophan decomposition from 9.45% up to 13.36%. The values for the amount of tryptophan in hair and their standard deviations (Table 4 and Fig. 4) indicate that they were significantly different despite their similarities. Consequently, this protocol can be used to determine degradation of this aminoacid in hair.

3.4. Lipid peroxidation

A protocol for the hair lipid peroxide formation after UV exposure was also optimised. After UV radiations, different amounts of hair were extracted with methanol to evaluate the presence of lipid peroxides in the lipid extract. Hair was extracted (200 mg and 500 mg) with 10 mL of methanol. An aliquot, 0.5 mL of these extracts was added to the TBA/TCA solution to determine the amount of lipid peroxides as detailed in the experimental section. Because of the small amount of peroxides detected, we chose the amount of 500 mg of hair to be extracted in the 10 mL of methanol. Quantification of LPO was performed by spectrophotometry and the results were expressed as malonaldehyde bis(dimethylacetal) equivalents (μM MDA) using a standard curve for pure MDA–TBA complex.

Table 5
Lipid peroxides present in non-irradiated and irradiated hair at 500 W/m^2 for 9, 18 and 36 h. Percentage of increment of LPO formation with respect to the non-irradiated sample.

Samples	Non-irradiated (nM MDA/mg hair)	9 h UV (nM MDA/mg hair)	18 h UV (nM MDA/mg hair)	36 h UV (nM MDA/mg hair)
1	3.582	4.463	7.203	6.826
2	2.693	4.595	6.125	7.048
3	2.834	4.696	6.191	7.046
M + SD	3.04 ± 0.48	4.58 ± 0.12	6.51 ± 0.60	6.97 ± 0.13
Increase of LPO (%)		54.6	116.6	132.5

Therefore the optimised experimental conditions, detailed in the experimental section, were carried out to determine the lipid peroxide formation of hair fibre subjected to 500 W/m^2 at 9, 18 and 36 h.

Following this methodology, non-irradiated samples present a similar amount of MDA equivalent to 3.004 ± 0.50 nM MDA/mg hair. Radiation of 500 W/m^2 at 9, 18 and 36 h shows an increase of LPO formation ranging from the 155% up to the 233% (Table 5 and Fig. 5). This increase in LPO formation at the three radiations studied is very similar to the increase in protein solubilisation at the same radiations. This indicates that proteins and lipids from the hair fibre are affected in a similar way when subjected to UV radiation.

The values obtained for the amount of MDA equivalent to lipid peroxides and the standard deviations at the three UV-irradiations indicate that this protocol yields significant differences between non-irradiated and all irradiated hair samples. There are a number of methodologies that are used to determine protein damage to hair fibres [28–30]. However, it is not easy to evaluate lipid extraction because of the low amount of lipids in the hair fibres (2.3%) [31]. This test therefore seeks to determine the effectiveness of antioxidant treatments directly performed on human hair by evaluating the peroxide formation in the lipid fraction.

All these methodologies were optimised to determine protein, lipid, melanin and tryptophan degradation in hair subjected to different UV intensities. Results indicate that free radical creation is very sensitive to time decay. However, all the protocols based on protein or tryptophan degradation as well as those based on lipid peroxide yield reliable results for irradiated fibres. Further work will be

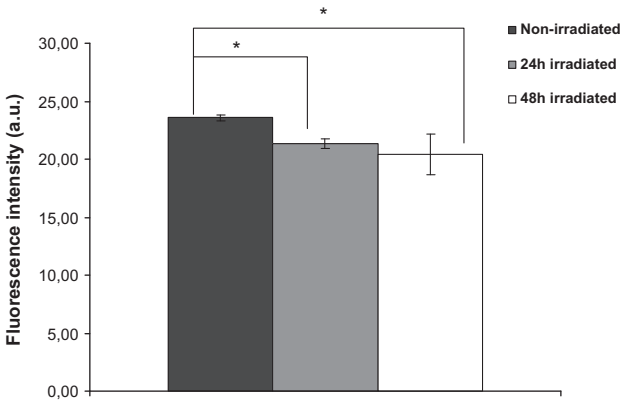

Fig. 4. Fluorescence intensity values obtained for 50 mg of non-irradiated and irradiated hair at 500 W/m^2 during 24 and 48 h (*$p < 0.05$).

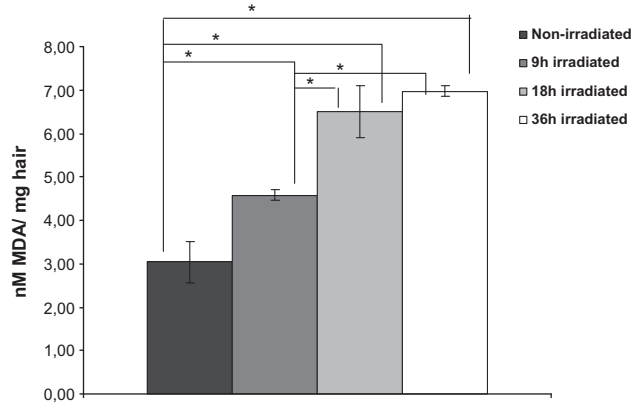

Fig. 5. Lipid peroxidation obtained for non-irradiated and irradiated hair at 500 W/m^2 during 9, 18 and 36 h (*$p < 0.05$).

performed with these methodologies to determine the efficacy of the antioxidants on the protection of hair fibres against UV light.

4. Conclusions

Methodologies to determine protein, lipid, melanin and tryptophan decomposition of hair fibres subjected to different UV intensities were optimised. Free radical formation in hair after UV exposure was evaluated by ESR spectroscopy and significant increases in ROS were found for the radiations assayed. Radiation of hair fibres shows an increase in protein solubilisation and tryptophan degradation. The values obtained for protein solubilisation at different UV-radiations indicate that the protocol can be followed to determine fibre damage. Moreover, the values obtained for fluorescence intensity of tryptophan suggest that the study of degradation of this aminoacid can help to determine hair damage. Furthermore, radiation of hair fibres showed an increase in LPO formation and a test is proposed to determine photo-degradation of hair evaluating the peroxide formation in the lipid fraction.

In the light of our findings, different methodologies were optimised to study the integrity of human hair. The study of the stability of proteins or aminoacids, free radical formation of melanin and lipid peroxidation could help to evaluate the degree of damage in the fibre subjected to UV radiation and the effectiveness of antioxidants on human hair.

Acknowledgements

We wish to thank L. Juliá and I. Yuste for their expert technical assistance. The authors would like to thank Provital SL for cooperation and financial support. Thanks are also due to the TRACE Program (TRA2009_0282) and the Spanish National Project CTQ-PPQ2009-13967-C03-01 for financial support.

References

[1] Z.D. Draelos, The biology of hair care, Dermatol. Clin. 18 (2000) 651–658.
[2] N.A. Barnicot, M.S.C. Birbeck, The electron microscopy of human melanocytes and melanin granules, in: W. Montagna, R.A. Ellis (Eds.), The Biology of Hair Growth, Academic Press, New York, 1958, pp. 239–252.
[3] I.A.F. van der Mei, L. Blizzard, J. Stankovich, A.L. Ponsonby, T. Dwyer, Misclassification due to body hair and seasonal variation melanin density estimates for skin type using spectrophotometry, J. Photochem. Photobiol. B: Biol. 68 (2002) 45–52.
[4] C.R. Robbins, Chemical and Physical Behaviour of Human Hair, fourth ed., Springer-Verlag, New York, 2002.
[5] R. Beyak, G.S. Kass, C.F. Meyer, Elasticity and tensile properties of human hair II: light radiation effects, J. Soc. Cosmet. Chem. 22 (1971) 667–678.
[6] L. Wolfram, The Reactivity of Human Hair: A Review, Springer-Verlag, New York, 1981. pp. 479–500.
[7] P.M. Plonka, Electron paramagnetic resonance as a unique tool for skin and hair research, Exp. Dermatol. 18 (2009) 472–484.
[8] T. Herrling, K. Jung, J. Fuchs, The role of melanin as protector against free radicals in skin and its role as free radical indicator in hair, Spectrochim. Acta Part A Mol. Biomol. Spectrosc. 69 (2007) 1429–1435.
[9] C. Dubief, Experiments in hair degradation, Cosmet. Toiletries 107 (1992) 95–102.
[10] A.C. Santos Nogueira, I.J. Joekes, Hair color changes and protein damage caused by ultraviolet radiation, J. Photochem. Photobiol. B: Biol. 74 (2004) 109–117.
[11] E. Tolgyesi, Weathering of hair, Cosmet. Toiletries 98 (1983) 29–33.
[12] C.R. Robbins, M.J. Bahl, Analysis of hair by electron spectroscopy for chemical analysis, J. Soc. Cosmet. Chem. 35 (1984) 379–390.
[13] A. Roddick-Lanzilotta, R. Kelly, Measurement and prevention and of hair photoaging, J. Cosmet. Sci. 55 (Suppl) (2004) S113–S121.
[14] Z.D. Draelos, Sunscreens and hair photoprotection, Dermatol. Clin. 24 (2006) 81–84.
[15] E. Hoting, M. Zimmerman, B. Hilterhaus, Photochemical alterations on human hair. Part I: artificial irradiation and investigations of hair proteins, Soc. Cosmet. Chem. 46 (1995) 85–99.
[16] E. Hoting, M. Zimmerman, H. Hocker, Photochemical alterations on human hair. Part II: analysis of melanin, J. Soc. Cosmet. Chem. 46 (1995) 181–190.
[17] E. Hoting, M. Zimmerman, Photochemical alterations on human hair. Part III: investigations of internal lipids, J. Soc. Cosmet. Chem. 47 (1996) 201–211.
[18] M.P. Chandra, J. Janus, Hairphotodamage-measurements and prevention, J. Soc. Cosmet. Chem. 44 (1993) 109–122.
[19] A. Valavanidis, M. Rallis, G. Papaioannou, K. Xenos, A. Katsarou, Studies in vivo by electron spin resonance of free radical mechanism implicated in UV-induced skin photocardiogenesis, Int. J. Cosmet. Sci. 17 (1995) 157–163.
[20] L.J. Kirschenbaum, X. Qu, E.T. Borish, Oxygen radicals from photoirradiated human hair: an ESR and fluorescence study, J. Cosmet. Sci. 51 (2000) 169–182.
[21] X. Qu, L.J. Kirschenbaum, E.T. Borish, Hydroxyterephtalate as a fluorescent probe of hydroxyl radicals: application to hair melanin, Photochem. Photobiol. 71 (2000) 307–313.
[22] A.C.S. Nogueira, M. Richena, L.E. Dicelio, I. Joekes, Photo yellowing of human hair, J. Photochem. Photobiol. B: Biol. 88 (2007) 119–125.
[23] T. Gao PhD, J.M. Tien, A. Bidaye, S. Cardinali, J. Kinney, A diester to protect hair from color fade and sun damage, Cosmet. Toiletries 124 (2009) 70–78.
[24] L.J. Marnett, Lipid peroxidation-DNA damage by malonaldehide, Mutat. Res. 424 (1999) 83–95.
[25] C. Alonso, C. Barba, L. Rubio, S. Scott, A. Kilimnik, L. Coderch, J. Notario, J.L. Parra, An ex vivo methodology to asses the lipid peroxidation in stratum corneum, J. Photochem. Photobiol. B: Biol. 97 (2009) 71–76.
[26] J.M. Baldasano, C. Soriano, H. Flores, J. Esteve, A. Mitjà, Atlas de Radiació solar a Catalunya, first ed., Institut Català d' Energia, Barcelona, 2001. <http://www20.gencat.cat/docs/icaen/02_Energies%20Renovables/Documents/Arxius/Atlas%20de%20radiacio%20solar.pdf>.
[27] M.M. Bradford, A rapid and sensitive method for the quantization of microgram quantities of protein utilizing the principle of protein-dye binding, Anal. Biochem. 72 (1976) 248–254.
[28] A. Valenzuela, The biological significance of Malondialdehyde determination in the assessment of tissue oxidative stress, Life Sci. 48 (1991) 301–309.
[29] A.C.S. Nogueira, C. Scanavez, I. Joekes, Degradation of human hair caused by ultraviolet radiation: measurement of protein loss and color changes, XV Congreso Lationoamericano e Ibérico de Químicos Cosméticos (2001) 485–490.
[30] C.M. Pande, J. Jachowicz, Hair photodamage. Measurement and prevention, J. Soc. Cosmet. Chem. 44 (1993) 109–122.
[31] Y. Masukawa, N. Hirofumi, G. Imokawa, Characterization of the lipid composition at the proximal root regions of human hair, J. Cosmet. Sci. 56 (2005) 1–16.

ARTÍCULO 2

Efficacy of antioxidants in human hair

Journal of Photochemistry and Photobiology B: Biology, 2012, **17**, 146-156

En este trabajo se evalúa el potencial antioxidante de dos formulaciones basadas en activos procedentes de alcachofa y arroz en cabellos expuestos a radiación UV-VIS. La irradiación del cabello se lleva cabo con las condiciones optimizadas en el artículo 1. El cabello es expuesto a la irradiación después de la aplicación de las formulaciones antioxidantes. La irradiación es aplicada mediante un simulador solar (Suntest CPS+) en un rango entre 310 y 800 nm.

Los ensayos utilizados para la evaluación de oxidación del cabello normal y tratado con formulación antioxidante son el trabajo de ruptura, la oxidación de proteínas del cabello mediante el ensayo de Bradford, la evaluación de la degradación del Trp mediante fluorescencia y la oxidación de lípidos mediante el ensayo del TBA. La superficie del cabello también se visualiza mediante SEM. Adicionalmente, para evaluar el efecto de la irradiación en el aspecto físico del cabello, se realiza la medición del brillo y del color en cabellos teñidos e irradiados y tratados con ambas formulaciones antioxidantes. La determinación del brillo y del color se realiza con un medidor de brillo y un colorímetro, respectivamente.

Los resultados mostraron que el trabajo de ruptura en los cabellos tratados con ambas formulaciones antioxidantes incrementa, lo que significa que la fibra de cabello es más resistente a la rotura. El incremento más alto del trabajo de ruptura se observó en los cabellos tratados con la formulación de activos de arroz.

La conservación de proteínas, lípidos y Trp fue mayor en las muestras de cabello tratado con ambas formulaciones que en los cabellos no tratados con formulaciones. La formulación antioxidante más efectiva en el caso de las proteínas y los lípidos fue la proveniente de activos de alcachofa, y en el caso del Trp la proveniente de los activos de arroz.

Las fotos de microscopia mostraron un daño en la cutícula del cabello debido a la radiación UV-VIS, mientras que las fibras irradiadas y tratadas con las formulaciones antioxidantes mantuvieron la superficie de la cutícula del cabello en perfecto estado.
Por último, el brillo y el color de los cabellos teñidos también se conservaron mejor con ambas formulaciones antioxidantes, siendo la formulación de antioxidantes de arroz la más efectiva.

Journal of Photochemistry and Photobiology B: Biology 117 (2012) 146–156

Contents lists available at SciVerse ScienceDirect

Journal of Photochemistry and Photobiology B: Biology

journal homepage: www.elsevier.com/locate/jphotobiol

Efficacy of antioxidants in human hair

Estibalitz Fernández [a,*], Blanca Martínez-Teipel [b], Ricard Armengol [b], Clara Barba [a], Luisa Coderch [a]

[a] Institute of Advanced Chemistry of Catalonia (IQAC-CSIC), Jordi Girona 18-26, 08034 Barcelona, Spain
[b] Provital, Barberá del Vallés, Barcelona, Spain

ARTICLE INFO

Article history:
Received 11 June 2012
Received in revised form 14 September 2012
Accepted 25 September 2012
Available online 13 October 2012

Keywords:
Antioxidants
Hair
Efficacy
Strength
Lipid peroxides
Tryptophan

ABSTRACT

Hair is exposed every day to a range of harmful effects such as sunlight, pollution, cosmetic treatments, grooming practices and cleansing. The UV components of sunlight damage human hair, causing fibre degradation. UV-B attacks the melanin pigments and the protein fractions (keratin) of hair and UV-A produces free radical/reactive oxygen species (ROS) through the interaction of endogenous photosensitizers. Hair was dyed and the efficacy of two antioxidant formulations was demonstrated after UV exposure by evaluating, surface morphology, protein and amino acid degradation, lipidic peroxidation, colour and shine changes and strength/relaxation properties. UV treatment resulted in an increase in protein and lipid degradation, changes in colour and shine and in adverse consequences for the mechanical properties. Natural antioxidants obtained from artichoke and rice applied to pretreated hair improved mechanical properties and preserved colour and shine of fibres, coating them and protecting them against UV. Furthermore, the lipidic peroxidation of the protein degradation caused by UV was reduced for some treated fibres, suggesting an improvement in fibre integrity. This was more marked in the case of the fibres treated using the artichoke extract, whereas the rice extract was better preserving shine and colour of hair fibres.

1. Introduction

It is well known that the UV components of sunlight damage human hair. This observation has been reported using a laboratory simulation of sunlight [1]. UV irradiation (mainly UV-B) attacks both the melanin pigments and the protein fractions (keratin) of hair [2]. The effects of UV-B irradiation can be severe, resulting in the breakdown of disulfide bonds inside the hair fibre and on the surface of the cuticle. However, UV-A irradiation mainly produces free radical/reactive oxygen species (ROS) through interaction with endogenous photosensitizers. Studies have shown that photo-oxidation of hair fibre involves the fracture of C–S linkages from proteins [3], oxidation of internal lipids, [4] and melanin granules [5] and tryptophan degradation of keratin [6]. Moreover, exposure to sunlight leads to hair decoloration due to melanin oxidation via free radicals, [7,8]. Melanin is a homogeneous biological polymer containing a population of intrinsic, semiquinone-like radicals. There are two types of melanin, the brown–black pigments (eumelanins) and the less prevalent red pigments (pheomelanins) [9]. Melanin granules selectively absorb radiation and offer photoprotection but become degraded or bleached in the process [10].

The lipid and protein fractions play a major role in the structure and integrity of the hair fibre, protecting it against external agents. Therefore, aggressions to the proteic and lipidic fraction [3,4] and the degradation of amino acids susceptible to photodegradation such as tryptophan, [6,9,11] can help us to evaluate the decomposition of hair fibre [12].

The most harmful effect of sunlight on hair is cystine oxidation to cisteic acid, which alters its mechanical properties (long UV exposure) [13]. Shorter irradiations cause unwanted effects such as a decrease in hydration, increased permeability, leading to a loss of colour and shine and to an increase in combing resistance [10,14].

The rapid increase in hair treatments (bleaching, dyeing, etc.) has led to a proliferation of hair cosmetics that facilitate repair and prevent adverse effects on the capillary structure. Vitamins and antioxidants have been included in cosmetic formulations specially designed to reduce the adverse effects on hair fibre. The most effective ingredients are antioxidants that can interrupt radical-chain processes, help to repair skin/hair systems, protect against oxidative damage and are frequently used in food and cosmetics [15]. For instance, vitamin B5 has been used for many years in hair care products because it functions as humectant, increases the water content and improves the elasticity of hair [15]. Incorporation of antioxidants, at low concentrations, in cosmetics can better protect and possibly correct the damage by neutralising free radicals and retard lipid oxidation.

The aim of this work is to study the efficacy of different antioxidant formulations after application on hair subjected to UV radiation and to the most common capillary treatments (dyeing). Two

* Corresponding author. Tel.: +34 934 006 100; fax: +34 932 045 904.
E-mail address: efptqt@cid.csic.es (E. Fernández).

1011-1344/$ - see front matter © 2012 Elsevier B.V. All rights reserved.
http://dx.doi.org/10.1016/j.jphotobiol.2012.09.009

natural antioxidant active ingredients were selected to evaluate their effect on hair fibres; a *Cynara scolymus* L. extract obtained from the leaves of artichoke (KERACYN tm) and an *Oryza sativa* L. extract obtained from rice grain (KERARICE tm).

The leaves of artichoke (*C. scolymus* L.) contain the greatest concentration of active principles. Hydroxycinnamic acids (Fig. 1) in artichoke have the general C6–C3 structure with the same aromatic ring and hydroxyl group as phenolic compounds, and a carboxylic function. These hydroxycinnamic acids are rarely free. They are usually found in the form of derivatives, e.g., caffeic acid is esterified with quinic acid, resulting in chlorogenic acid, isochlorogenic acid and neochlorogenic acid. Shahidi and Chandrasekara conducted an extensive review of the antioxidant activity [16], both in vitro and in vivo, of hydroxycinnamic acids (ferulic, caffeic, coumaric, sinapic and derivatives). Flavonoids, which are other molecules present in Artichoke leaves, act as antioxidant agents by inactivating free radicals generated by irradiation.

Rice can grow in diverse media. It will grow faster and more vigorously in hot and humid environments. The chemical composition of the active ingredient is characterised by the presence of biofunctional peptides and amino acids, polysaccharides and phytic acid.

The amino acid composition of the peptides present in the active ingredient is characterised by a high concentration of glutamic acid (up to 17%) and large amounts of aspartic acid, arginine, leucine, phenylalanine, serine, valine and tyrosine (up to 10%). Approximately 80% of the protein hydrolyzate has a molecular weight between 500 and 3000 Da. The molecular weight of the peptides present is directly related to its function in the hair. Low molecular weight peptides (<1000 Da) can penetrate and repair hair fibres from the inside. Medium molecular weight peptides (1000–3000 Da) can repair the cuticle [17,18], and account for 42% of the extract.

The main polysaccharide present in the rice active ingredient is amylopectin (Fig. 2a).This is a water-soluble branched polymer composed of glucose units connected linearly by bonds α $(1 \rightarrow 4)$. Each molecule of amylopectin can contain between 100.000 and 200.000 glucose units, and each branch is formed by 20–30 glucose units in length. This type of three-dimensional structure prevents an excessive accumulation of the active ingredient and hair matting, compared with normally used linear polymers.

Phytic acid (myo-inositol hexaphosphoric acid, abundant in edible legumes, cereals and seeds) (Fig. 2b) is another key component of rice and acts as an antioxidant agent by inactivating free radicals generated by irradiation. Phytic acid is capable of chelating metals, especially divalent metals. It forms an iron chelate which greatly accelerates Fe^{2+}mediated oxygen reduction yet blocks iron-driven hydroxyl radical generation and suppresses lipid peroxidation [19].

Protein and amino acid degradation, lipid peroxidation, strength, shine and colour measurements were used to evaluate proteic and lipidic photodecomposition in hair fibres subjected to antioxidant action.

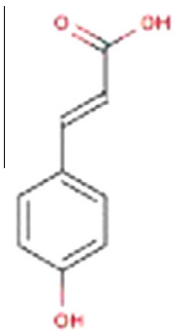

Fig. 1. Hydroxycinnamic acid.

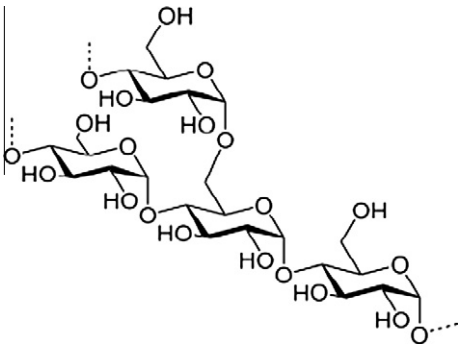

Fig. 2a. Amilopectin.

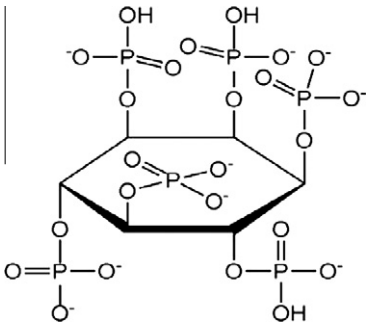

Fig. 2b. Phytic acid.

A Scanning Electron Microscopy (SEM) study was also performed with all hair samples to evaluate the possible changes in the surface morphology of the hair fibres due to the different treatments [20].

All these methodologies were applied to virgin or dyed hair tresses subjected to UV radiation and pre-treated with the two antioxidant formulations in order to achieve a possible protection of hair properties.

2. Materials and methods

2.1. Chemicals

Revlon 7.45 dye was provided by The Colomer Group (Barcelona, Spain). Natural dark brown hair tresses (20 cm in length) were purchased from De Meo Brothers Inc (New York). Hair tresses were treated with a shampoo base formulation (Table 1), placebo and a protective serum which contained *C. scolymus* antioxidant active (Cyn) and *O. sativa* antioxidant active (Rice) (Table 2).

2.2. Hair Treatments

Hair was chemically treated by dyeing and also subjected to antioxidant treatments:

2.2.1. Dyeing procedures

Untreated hair (32 g) was dyed with 70 ml of dye solution containing 50 ml of Revlon 7.45 dye and 20 ml of H_2O_2 (20 vol.%). The hair was covered and maintained for 30 minutes at 25–29 °C. Finally, the hair was washed with neutral shampoo and was dried at 30–40 °C.

2.2.2. Antioxidant treatments

Four dyed (D) hair tresses of 8 g each were prepared. For comparison, four tresses of 10 g untreated (UT) hair (virgin hair) were

Table 1
Shampoo base formulation.

Ingredient	% (w/w)
Aqua (water)	73.16
Acrylates/C10-30 alkyl acrylate crosspolymer	1.00
Propanediol	5.00
Sodium laureth sulfate, aqua (Water), sodium chloride	12.00
Cocamidopropyl betaine	6.00
Sodium hydroxide, aqua (Water)	2.14
Phenoxyethanol, propylparaben, ethylparaben, methylparaben, butylparaben, isobutylparaben	0.60
Maris sal (Sea Salt)	0.10

also prepared as control. All tresses were washed daily with a neutral shampoo for two minutes and then rinsed with water. Then, three tresses of each kind of hair (UT, D) were treated with the protective serums: placebo (P) and Cyn and Rice antioxidant agents, respectively. The treatment of approximately 0.5 g of each formulation for 8 g of dyed tresses, and 0.6 g for 10 g of untreated hair was repeated everyday for 10 days. The formulations were applied to the hair tresses for 24 h. Next, all the tresses were washed and the formulations were applied again. The other UT, D tresses were only washed but not post treated.

All hair tresses are described below:

- Untreated hair (UT).
- Untreated hair post treated with placebo (UTP).
- Untreated hair post treated with Cyn (UTC).
- Untreated hair post treated with Rice (UTR).
- Dyed hair (D).
- Dyed hair post treated with placebo (DP).
- Dyed hair post treated with Cyn (DC).
- Dyed hair post treated with Rice (DR).

2.3. Hair UV exposure

Human hair was irradiated using a light source simulating UV solar irradiation (500 W/m^2 equivalent to 3.0 J/min cm^2, Suntest CPS, Atlas, USA). The irradiation of 500 W/m^2 is equivalent to 2 days in June in Catalonia (1.50–1.84 J/min cm^2 equivalent to 21–26.5 MJ/m^2 per day [21]). Moreover, the UV radiation intensity was modified by different exposure times depending on the test applied: 500 W/m^2 during 18, 24, 36 and 48 h.

2.4. Tensile properties of the hair fibres

A stress–strain test was performed with 25 irradiated (at 500 W/m^2 during 36 h), and non-irradiated UT, UTP, UTC and UTR fibres, which were randomly taken from the hair samples previously conditioned for 48 h in a standard atmosphere (20 °C and 65% relative humidity) and centrally attached to a pair of cardboard frames with an internal rectangular cut frame of 50 × 25 mm^2 following the longest length.

Samples on the cardboard were attached to an Instron 5500R dynamometer with a gauge length of 50 mm. The two sides of the cardboard were cut before the beginning of the stress–strain test to enable just the fibre under testing to be stressed. The test was performed according to the ASTM Standard D 3822 methodology. A gauge length of 50 mm, a rate of strain of 30 mm/min, and the breaking stress (MPa) and strain (%) were recorded. The multiplication of breaking stress and percentage strain gave rise to breakage work, which evaluated fibre conditions [22].

2.5. Protein degradation

A total of 100 mg of UT, UTP, UTC and UTR hair was exposed to UV radiation (500 W/m^2) at different times (18 and 36 h). Proteins and peptide solubilisation was carried out with 100 mg of hair subjected to UV radiation, diluted in 1 ml of 2% SDS aqueous solution and sonicated using a Labsonic 1510 device (B. Braun, Melsungen, Germany) for 5 h at 45 °C. Hair extracts were then diluted to 0.01% SDS concentration and the Bradford colorimetric assay was used to quantify the proteins and peptides solubilised [12]. This assay is based on the formation of a complex between the dye, Brilliant Blue G, and the proteins in solution, which leads to an increase in absorption at 595 nm and is proportional to the amount of protein in the solution [23]. Bovine Serum Albumin (BSA) was used as a standard to calculate the amount of protein. This procedure was also performed for non irradiated hair as a control.

2.6. Tryptophan decomposition

Tryptophan measurements were carried out with UT, UTP, UTC and UTR hair unexposed and exposed to UV radiation (500 W/m^2) at different times (24 and 48 h).

A protocol to hydrolyse the fibre was followed to measure the tryptophan in the alkaline solution with a spectrofluorimeter [9]. A total of 50 mg of irradiated and non-irradiated hair was chopped from hair tresses and then dissolved in 50 ml of 2 M NaOH solution for 24 h. This led to a release of tryptophan from hair and enabled us to quantify tryptophan in order to correlate the variations in hair at different UV exposure times [9]. The measurements of tryptophan intensity were obtained at 345 nm in the fluorescence spectrum, which is the emission wavelength of tryptophan in solution [12].

Table 2
Protective serum formulations.

Ingredients	Cyn	Rice	Placebo
Aqua (Water)	76.90	76.90	81.90
Glycerin	2.00	2.00	2.00
Tetrasodium glutamate diacetate, sodium hydroxide, aqua (Water)	0.20	0.20	0.20
Hydroxypropyl starch phosphate	5.50	5.50	5.50
Sucrose laurate, aqua (water), alcohol denat.	5.00	5.00	5.00
Prunus amygdalus dulcis (Sweet Almond) oil	4.00	4.00	4.00
Phenoxyethanol, methylparaben, ethylparaben, butylparaben, propylparaben, isobutylparaben	0.60	0.60	0.60
Parfum (Fragrance)	0.30	0.30	0.30
C. scolymus active (*Cyn*)	5.00	–	–
O. sativa active (*Rice*)	–	5.00	–
Aqua (Water), lactic acid	0.50	0.50	0.50

2.7. Lipid peroxidation measurements

Lipids from UT, UTP, UTC and UTR human hair unexposed and exposed to UV radiation (500 W/m^2) at different times (18 and 36 h) were extracted with methanol (500 mg hair/10 ml methanol) in a sonicating device Labsonic 1510 (B. Braun, Melsungen, Germany) for 15 min. Next, the hair extracts were dried under a N_2 flow and diluted again in 1.5 ml of methanol. Lipid peroxides (LPO species) were measured by thiobarbituric acid (TBA) assay [24,25]. The thiobarbituric acid-reactive species (TBARS) were quantified by spectrophotometry at 534 nm (Cary 300 Bio UV–Visible Spectrophotometer, Varian, USA). At low pH and at a high temperature, MDA readily participates in nucleophilic addition reaction with TBA, generating a red, fluorescent 1:2 MDA: TBA adduct according to the reaction shown in Fig. 3.

The results were expressed as malonaldehyde bis(dimethylacetal) equivalents (μM MDA) using a standard curve for the pure MDA–TBA complex. The calibration curve was obtained by using MDA at different concentrations (0.5–30 μM). Negative and positive controls were also quantified using 0 and 100 μM of MDA. The calibration curve was prepared on each day of the study. Briefly, the LPO species present in the samples (0.5 mL) were added to aliquots (1 mL) of a solution made up of 0.4% of TBA and 15% of trichloroacetic acid (TCA) in 100 mL of the HCl solution (0.25 M). The mixture was incubated in a bath of boiling water for 1 h. Fresh TBA/TCA stock solution was prepared on each day of the analysis. This procedure was also performed for non irradiated hair as a control.

2.8. Scanning electron microscopy (SEM)

A SEM study was performed with non-irradiated and irradiated (at 500 W/m^2 during 36 h) UT, UTP, UTC and UTR hair samples to evaluate the possible changes in the surface morphology of the hair fibres due to the different treatments. To this end, the samples were studied with a TM-1000 Tabletop scanning electron microscope (Hiatchi). The microscope was operated at 15.0 kV. Several fibres from each hair sample were viewed, and representative images were taken.

2.9. Shine measurements

Shine measurements of irradiated (at 500 W/m^2 during 36 h), and non-irradiated UT, UTP, UTC and UTR; D, DP, DC and DR hair tresses were obtained using a micro-TRI-gloss BYK-Gardner GmbH (Geretsried, Germany) with standard geometries of 20°, 60° or 85°. Hair tresses were aligned by combing and the measurement at the three angles was performed through a plate glass (slide) pressed over the tresses. The alignment of fibres showed to be more important than roughening or hair surface on brightness [26]. The measurements were performed under controlled conditions (23 °C and 50% relative humidity). Mean values were obtained for the 15 values of 85° incidence angle of the 24 strands [27].

2.10. Colour measurements

Changes in hair colour of irradiated (at 500 W/m^2 during 36 h), and non-irradiated UT, UTP, UTC and UTR; D, DP, DC and DR hair tresses were measured using a spectrophotometer (Macbeth Color-eye 3000, Neurtek Instruments, Spain). The colour measurements were obtained using The CIE L^*a^*b model, developed by the Commission Internationale de l'Eclairage. Colour on three axes corresponds to trichromatic human perception and reflects the degree of change in colour that humans can perceive [28]. This model has the advantage of corresponding to the human perception of colour and has the additional benefit of giving a grid point for each specific colour.

The lightness or intensity of a colour is measured on the 'L^*' axis on a scale from 0 (black) to 100 (white). The colour is also measured on the 'a^*' axis that gives a value from −100 (green) to +100 (red). The 'b^*' axis measures colour from −100 (blue) to +100 (yellow). One unit on the L^*, a^* or b^* axes is considered to be the smallest difference that the human eye can perceive [29]. This grid point allows the mathematical comparison of colour and also enables colours to be corrected for different conditions. It should be noted that, theoretically, the a^* and b^* axes have no maximum or minimum values. Our research has used the cut off point of +/−100 because this is the practical limit of the instrument used to measure colour [30].

On the order hand, the total colour loss (ΔE) was calculated by assessing the changes in L^*, a^*, b^* readings on the treated tresses using a spectrocolorimeter.

The equation used to calculate the total colour loss was [11]:

$$\Delta E = [(\Delta L)^2 + (\Delta a)^2 + (\Delta b)^2]^{1/2}$$

2.11. Statistics

Standard deviations were calculated for all mean values. Analysis of variance (ANOVA) with a one-way layout was applied to group comparisons. The software used was the STATGRAPHICS plus 5. Significant differences in the mean values were evaluated by the F-test. A p value below 0.05 was considered significant.

3. Results and discussion

3.1. Tensile properties of the hair fibres

There is a long-standing hypothesis, that the cortex is primarily responsible for the tensile properties of human hair [31] and that the cuticle has little involvement. Then, the tensile properties are primarily an index of cortical damage [32]. Moreover, the mechanical properties of hair depend on the condition of the hair fibre, primarily of keratin and its three-dimensional arrangement [32]. In this study a stress–strain test was performed on untreated (UT) and treated fibres with placebo (UTP) and the two antioxidant formulations (UTC and UTR) with and without UV radiation. Mean values of breaking stress and deformation at break for the different hair samples are given in Table 3.

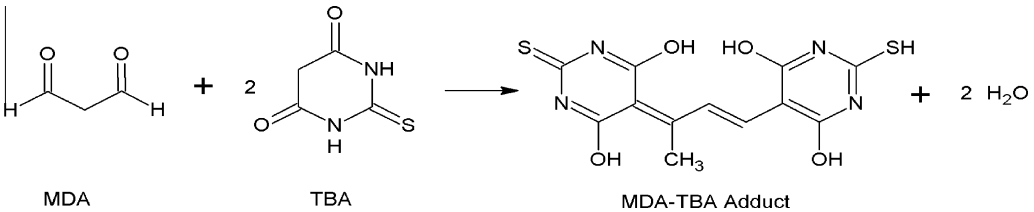

Fig. 3. Reaction proposed for the detection of MDA after lipid peroxidation.

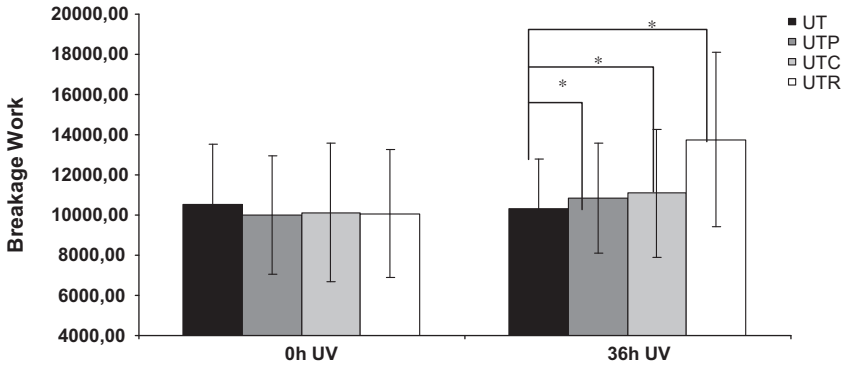

Fig. 4. Breakage work of UT, UTP, UTC and UTR samples with and without UV irradiation (* $p < 0.05$).

Table 3
Breaking Stress, deformation at break and breakage work of untreated (UT) and treated fibres (UTP, UTC and UTR) with and without irradiation at 500 W/m^2 for 36 h.(Mean ± SD) (* $p < 0.05$).

	Breaking stress (Mpa)	Deformation at break (%)	Breakage work
UT	239.63 ± 72.10	44.12 ± 4.28	10525.78 ± 2999.71
UTP	226.23 ± 52.51	44.19 ± 4.81	10001.14 ± 2948.61
UTC (Cyn)	227.74 ± 74.27	44.11 ± 4.18	10129.30 ± 3442.29
UTR (Rice)	217.61 ± 60.93	45.90 ± 3.21	10076.21 ± 3165.84
UT 36 h UV	230.32 ± 52.26	45.11 ± 4.51	10315.38 ± 2476.73
UTP 36 h UV	235.58 ± 59.71	45.75 ± 2.95	10844.38 ± 2721.67
UTC (Cyn) 36 h UV	237.57 ± 75.70	45.77 ± 3.44	11084.64 ± 3187.65
UTR (Rice) 36 h UV	303.88* ± 101.67	46.80* ± 2.75	13761.58* ± 4356.56

Breaking stress evaluates fibre integrity. Therefore, higher values of this parameter indicate a larger amount of bonds present in the fibre structure. First results showed that the UV irradiation leads to a modification of the hair fibre integrity with a decrease in the values of stress at break from 239.62 to 230.32 Mpa for UT fibres. When evaluating the different hair treatments (placebo and the two antioxidant formulations), an increase in the breaking stress after 36 h of UV irradiation was observed, suggesting an improvement in fibre integrity. This increase was statistically significant for the fibres treated with the Rice formulation.

Moreover, results of deformation at break indicated a significant increase in irradiated fibres treated with the Rice formulation (Fig. 4). An increase in the deformation at break indicates an increase in fibre plasticity. This increase may be attributed to (1) an increase in the water content of the fibres due to the antioxidant formulations; the higher the moisture content, the greater the ability of the fibre to be deformed; and to (2) a binding of some functional groups in the formulations to cystine in the hair fibre, which restores some of the disulfide bonds broken upon UV radiation. This could also confer greater elasticity onto the fibre. When deformability is increased, the resulting hair fibres are softer and more resistant to breakage.

As stated in the experimental part, considering stress and deformation at break values, breakage work can be calculated. The results of the different hair fibres are detailed in irradiated samples showed a significant increase in breakage work for the samples treated with the placebo and the two antioxidants. Again, this improvement was more marked for the hair fibres treated with the *Rice* antioxidant formulation, reaching values higher than those obtained for untreated fibres. The mechanism for protection of the fibre strength could arise from the low molecular weight components of the active. The *Rice* extract has biofunctional peptides with high substantively for keratin. More than 45% of the peptides in this extract have molecular weights lower than 1000 Da. According to Stern and Johnson, peptides with a molecular weight lower than 1000 Da, can penetrate and perform a repairing action of the hair fibres from the inside [17]. The effects of these peptides on hair have been described in numerous studies which demonstrate protection of hair against alkali and oxidizers [33] or improvement of esthetic characteristics of hair (elasticity, body) [34,35]. Furthermore, these peptides provide protection from radical mediated damaged due to UV insult through the radical scavenging ability associated, as in other works [17,18,36], with the cystine residues present within the peptides.

3.2. Protein degradation

Hair is composed primarily of *proteins* (88%). These proteins are of a hard fibrous type known as keratin. Loss of protein due to UV radiation will lead to damaged hair structure. The decrease of cystine due to photodamage of hair does not necessarily imply large protein solubilisation. Breaking disulphide bridges with formation of cysteic acid and by main chain scission causes a formation of secondary crosslinks between protein residues such as lanthionine and dityrosine which limit the extractability of the protein [37]. However the amount of protein solubilisation due to UV radiation could be enough to demonstrate antioxidant protection.

Protein degradation from hair was measured using the Bradford assay. This assay is based on the formation of a complex between the Brilliant Blue G dye and the proteins in solution, which leads to an increase in absorption at 595 nm and is proportional to the amount of protein in the solution [23]. Bovine Serum Albumin (BSA) was used as a standard to calculate the amount of protein. The Bradford assay was performed on UT and on treated fibres with placebo (UTP) and the two antioxidant formulations (UTC and UTR) with and without UV radiation. The results for the different hair fibres are detailed in Table 4 and Fig. 5.

Non-irradiated samples presented protein solubilisation ranging between 8.42 and 13.29 μg protein/mg hair. However, it should be pointed out that hair treated with the *Cyn* and *Rice* extracts showed significantly lower values of protein solubilisation with respect to untreated hair, suggesting protection of the fibres due to these

Table 4
Protein hair solubilisation with 2% SDS of untreated (UT) and treated fibres (UTP, UTC and UTR) with and without irradiation at 500 W/m^2 for 36 h (Mean ± SD). Percentage of increase in protein degradation with respect to UT sample.

	μg Protein/mg hair	Increase in protein degradation (%)
UT	12.38 ± 1.35	
UTP	13.29 ± 1.63	107.35
UTC (Cyn)	9.23 ± 0.78	74.58
UTR (Rice)	8.42 ± 0.45	68.01
UT 18 h UV	21.78 ± 1.72	175.93
UTP 18 h UV	19.58 ± 1.21	158.16
UTC (Cyn) 18 h UV	14.04 ± 0.45	113.41
UTR (Rice) 18 h UV	14.55 ± 0.30	117.53
UT 36 h UV	25.38 ± 0.63	205.00
UTP 36 h UV	20.18 ± 0.27	163.00
UTC (Cyn) 36 h UV	13.62 ± 0.16	110.02
UTR (Rice) 36 h UV	16.77 ± 0.30	135.46

Table 5
Fluorescence intensity values obtained at 355 nm of untreated (UT) and treated fibres (UTP, UTC and UTR) with and without irradiation at 500 W/m^2 for 36 h (Mean ± SD). Percentage of conservation of trp with respect to UT sample.

	Fluorescence intensity at 355 nm (50 mg hair)	Conservation of trp %
UT	66.45 ± 4.40	
UTP	66.75 ± 4.11	100.45
UTC (Cyn)	67.77 ± 4.39	101.98
UTR (Rice)	67.23 ± 2.64	101.18
UT 24 h UV	47.13 ± 1.61	70.93
UTP 24 h UV	49.82 ± 1.07	74.93
UTC (Cyn) 24 h UV	56.80 ± 0.63	83.82
UTR (Rice) 24 h UV	60.80 ± 0.56	90.43
UT 48 h UV	48.78 ± 3.48	73.41
UTP 48 h UV	48.57 ± 4.93	72.76
UTC (Cyn) 48 h UV	50.12 ± 2.64	73.95
UTR (Rice)48 h UV	57.07 ± 3.88	84.88

formulations. Irradiated and non treated samples showed an increase in protein solubilisation ranging between 21.78 and 25.38 μg protein/mg hair for 18 h and 36 h UV, respectively. When evaluating the protective capacity of the different hair treatments, a significant decrease in protein degradation for the hair fibres treated with the Cyn and Rice extracts after 18 h of UV radiation was observed. Furthermore, after 36 h of irradiation, fibre improvement was also significant for the fibres treated with the placebo and the two antioxidant treatments, suggesting a conservation of the fibres.

The protection of hair with the *Cyn* and *Rice* extracts was clearly demonstrated even with the non-irradiated fibres. Moreover, after 18 h irradiation and at 36 h irradiation, protection of protein degradation is significant in the two treatments (Fig. 5). The percentage of increase in protein degradation with respect to the UT sample is shown in Table 4. UT and UTP irradiated samples showed an increase of 160 and 200% in protein degradation, whereas samples treated with the *Rice* and *Cyn* range between 110 and 135% after irradiation. Other strong antioxidants based on procyanidins together with tocopherols also preserve protein degradation but to a lower extent [38]. Comparison of the two antioxidants showed a higher protection of protein degradation of the Cyn extract. This is probably due to the strong antioxidants such as hydroxycinnamic derivatives in the extract. These derivates could promote the protection of the fibre.

3.3. Tryptophan degradation

The aromatic amino acids, tyrosine phenylalanine and mainly tryptophan, which are associated with photo-yellowing of hairs, are easily degraded by light [39]. Of all the amino acids present on the fibre surface, tryptophan is the most sensitive to UVB radiation. Therefore, it is commonly used to evaluate the protective effect of cosmetic active ingredients for hair. Tryptophan from hair is usually measured as a solid using a spectrofluorimeter [6,11]. A protocol to hydrolyse the fibre was followed to measure the tryptophan in the alkaline solution [9]. A total of 50 mg of hair was chopped from hair tresses and then dissolved in 50 ml of 2 M NaOH solution for 24 h. This led to a release of tryptophan from hair and enabled us to quantify it in order to correlate the variations in hair at different UV exposure times. The measures of fluorescence intensity at different UV exposure times were obtained at 355 nm in the fluorescence spectrum, which is the emission wavelength of tryptophan in solution. Tryptophan fluorescence measurements were performed on UT and treated fibres with placebo (UTP) and the two antioxidant formulations (UTC and UTR) with and without UV radiation. The decrease in tryptophan degradation for irradiated hair fibres treated with the antioxidant formulations is shown in Table 5 and Fig. 6.

Non-irradiated samples presented a fluorescence intensity of about 66–67 (a.u), whereas irradiated samples (at 500 W/m^2 at 24, and 48 h) showed a decrease in fluorescence intensity between 47 and 60 (a.u). When evaluating tryptophan on hair subjected to the extracts, higher values in fluorescence intensity were observed for the hair fibres treated with the Cyn and Rice extracts after 24 and 48 h of UV radiation. However, comparison of the behaviour of the two formulations after 48 h of radiation showed that the improvement was more marked in the fibres treated with the Rice formulation (Fig. 6).

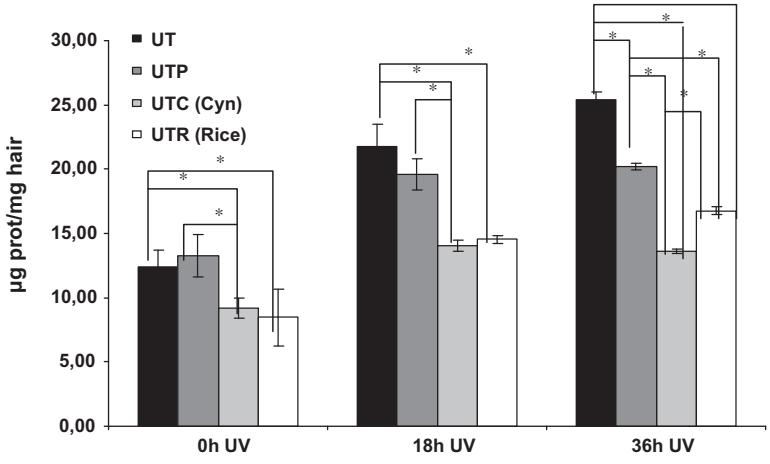

Fig. 5. Degradation of hair proteins of UT, UTP, UTC and UTR samples with and without UV irradiation ($^*p < 0.05$).

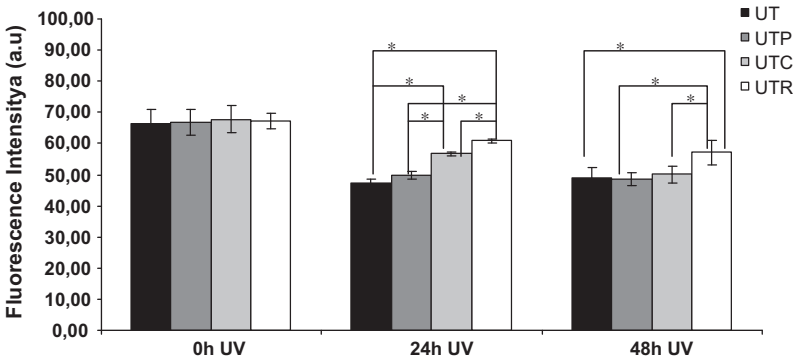

Fig. 6. Fluorescence intensity of UT, UTP, UTC and UTR samples with and without UV irradiation (Mean ± SD) (*$p < 0.05$).

Table 6
Lipid peroxides of untreated (UT) and treated fibres (UTP, UTC and UTR) with and without irradiation at 500 W/m^2 for 36 h (Mean ± SD). Percentage of increase in lipid peroxidation with respect to UT sample.

	μM MDA/mg hair	Increase in lipidic peroxidation (%)
UT	0.0019 ± 0.0000	
UTP	0.0022 ± 0.0002	115.79
UTC (Cyn)	0.0022 ± 0.0003	115.79
UTR (Rice)	0.0024 ± 0.0005	126.31
UT 18 h UV	0.0039 ± 0.0003	205.26
UTP 18 h UV	0.0026 ± 0.0001	136.84
UTC (Cyn) 18 h UV	0.0021 ± 0.0002	110.52
UTR (Rice) 18 h UV	0.0023 ± 0.0003	121.05
UT 36 h UV	0.0061 ± 0.0000	321.05
UTP 36 h UV	0.0064 ± 0.0001	336.84
UTC (Cyn) 36 h UV	0.0035 ± 0.0000	184.21
UTR (Rice) 36 h UV	0.0043 ± 0.0005	226.31

The percentages of tryptophan conservation with respect to the UT sample are shown in Table 5. UT and UTP irradiated samples presented a trp conservation of about 70% and 73% after 24 and 48 h of irradiation, respectively. By contrast, samples treated with the *Rice* extract reached 90% and 85% after 24 and 48 h UV. The results obtained using this formulation could indicate a higher fibre UV protection due to the composition of the Rice extract. The presence of phytic acid antioxidant and moreover the medium molecular weight peptides (1000–3000 Da) may form a protective layer on the fibre surface. Similarly to other protein and peptides [17,18,36] the UV damage should occur preferentially to the active rather than the fibre beneath.

3.4. Lipid peroxidation

Human hair contains 1.9-5% of internal lipids [40] but despite this low amount, the cell membrane lipids are very important as they make possible a continuous pathway of diffusion into the fibre [41]. Furthermore, according to recent studies on human hair, a correlation has been found between the amount of internal lipids and the moisture content in the hair fibre [42]. Integral lipids of hair fibre are degraded by UV light as well as visible light, cause weakening of the cell membrane complex exposed to light radiation [43].

Lipid peroxides (LPO species) were measured by thiobarbituric acid (TBA) assay [27,28]. The thiobarbituric acid-reactive species (TBARS) were quantified by spectrophotometry at 534 nm (Cary 300 Bio UV–Visible Spectrophotometer, Varian, USA). Lipid peroxidation measurements were performed on UT and treated fibres with placebo (UTP) and the two antioxidant formulations (UTC and UTR) with and without UV irradiation.

Non-irradiated samples presented lipidic peroxidation ranging between 0.0019 and 0.0024 μM MDA /mg hair (Table 6 and Fig. 7). Irradiated samples (at 500 W/m^2, during 18 and 36 h) showed an increase in lipidic peroxidation ranging between 0.0021 and 0.0060 μM MDA/mg hair. Evaluation of the antioxidant ability of the different hair treatments showed a significant decrease in lipidic peroxidation for the hair fibres treated with the placebo and the Cyn and Rice extracts after 18 h of UV radiation (Fig. 7). However, after 36 h of irradiation, the improvement was only significant for the fibres treated with the two antioxidant formulations.

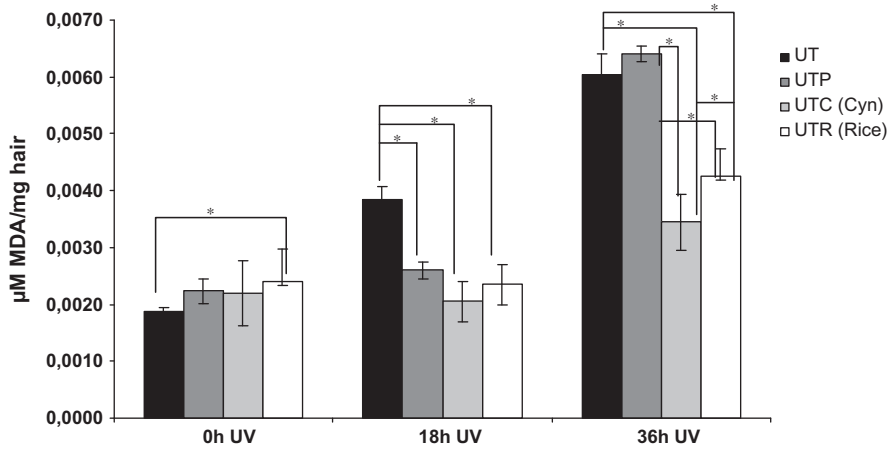

Fig. 7. Lipid peroxidation of UT, UTP, UTC and UTR samples with and without UV irradiation (Mean ± SD) (*$p < 0.05$).

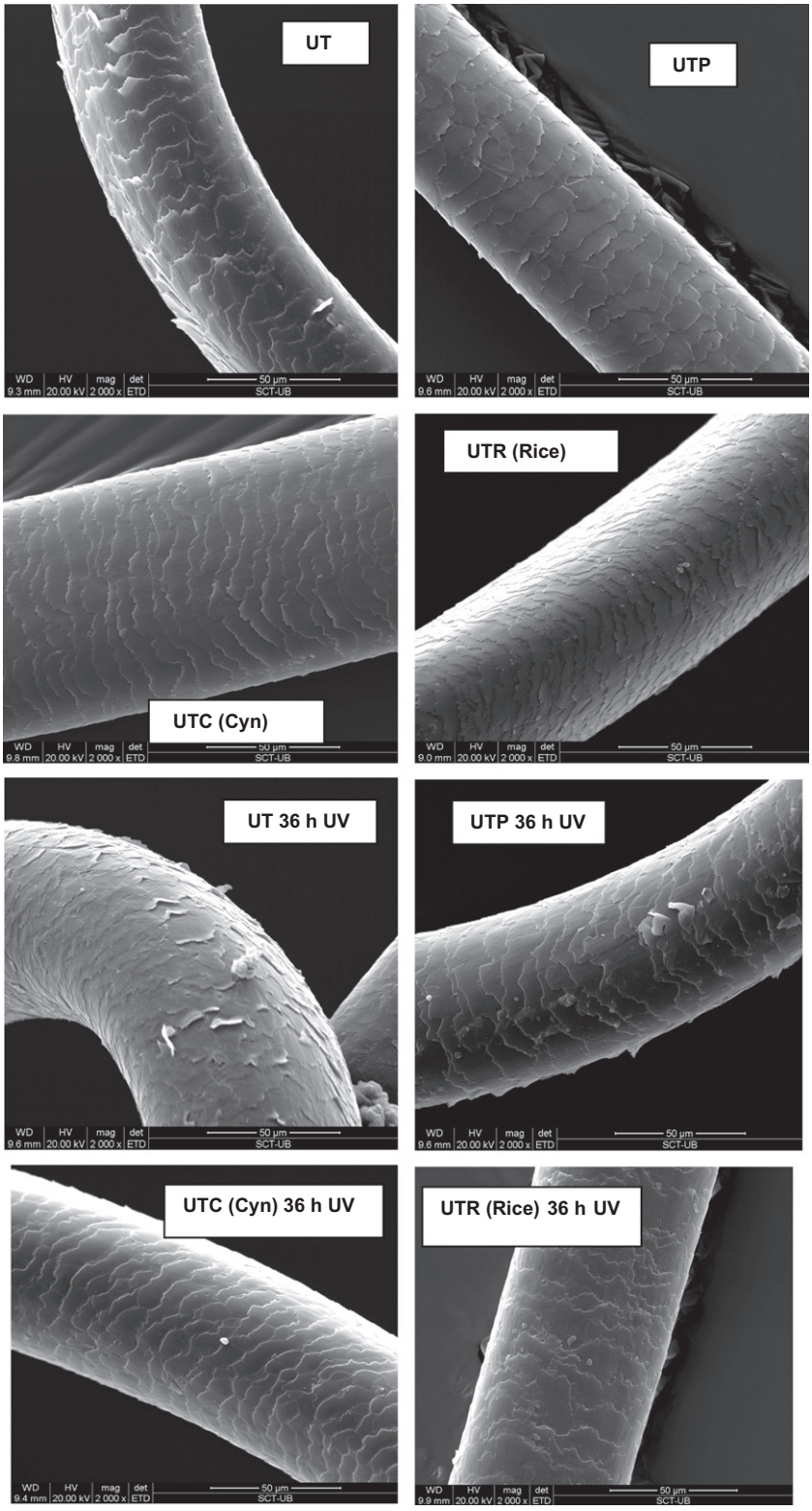

Fig. 8. Representative SEM micrographs of UT, UTP, UTC and UTR samples with and without UV irradiation.

The percentages of lipidic peroxidation with respect to the UT sample are shown in Table 6. UT samples presented an increase in lipidic peroxidation of about 205–321% after 18 and 36 h, respectively. In contrast, the samples treated with *Rice* attained only 121 and 226% after 18 and 36 h UV, respectively. Moreover, samples treated with *Cyn* only increased lipid peroxidation to 110% and 184% after 18 and 36 h UV, respectively. The similarity between Fig. 5 (protein degradation) and Fig. 7 (LPO formation) indicates that proteins and lipids from the hair fibre are affected similarly when subjected to UV irradiation. This similarity could be used to determine the efficacy of antioxidant treatments on human hair. As in the case of protein degradation, the antioxidant

behaviour of the Cyn extract is more marked than the behaviour of the Rice extract. Phytic acid in Rice was demonstrated to inactivate free radicals generated by radiation and be capable of chelating metals and inhibit lipid peroxidation [19] However, the presence of strong antioxidants such as hydroxycinnamic derivatives and flavonoids in Cyn, provides better protection in this extract, preserving the inner substance of the hair (proteins and lipids).

3.5. Surface changes

SEM images revealed some differences in the conditions of the surface morphology of the hair samples due to the treatments. Some hair fibres were evaluated and images of UT fibres and those treated with the placebo and the two antioxidant formulations UTP, UTC and UTR were obtained (Fig. 8). Images of irradiated fibres (at 500 W/m^2 during 36 h) were also obtained and the restorative capacities were compared. Irradiation of UT hair (UT 36 h) showed the largest differences as clearly lifted cuticles when compared with the non-irradiated hair sample (UT). The application of the placebo and the Cyn and Rice formulations led to a slight improvement in the hair surface without open cuticles when subjected to UV radiation.

The improvement in hair surface of the two formulations could be attributed to the antioxidant role of hydroxycinnamic derivates of the *Cyn* and phytic acid in the *Rice* extracts. These molecules help to prevent the oxidation of hair fibres subjected to UV, repairing the cuticle and protecting the hair.

3.6. Shine measurements

Shine is one of the most valued hair properties, as it implies hair health and beauty. This property is closely linked to the structure of the hair fibre and, in particular, it depends on the condition of the cuticle. Antioxidants are usually applied to protect shine and colour not only in natural hair but especially in dyed hair [44]. Untreated and dyed fibres (D, DP, DC and DR) were also evaluated. Shine measurements were performed on UT and D fibres treated with placebo (UTP and DP) and the two antioxidant formulations (UTC, UTR, DC and DR) with and without UV radiation. As described in the experimental part, shine measurements were performed using a micro-TRI-gloss BYK-Gardner GmbH with standard geometries of 20°, 60° or 85°. The measurements were carried out under controlled conditions (23 °C and 50% relative humidity) and mean values were obtained for the 15 evaluations for each incidence angle. The results for shine for the three different incident angles are shown in Table 7.

Non-irradiated (D) fibres showed a small but significant increase in shine values when treated with the two antioxidant formulations. As expected, the UV irradiation leads to a reduction in shine. This is evidenced by comparing UT and D fibres with irradiated samples (UT 36 h UV and D 36 h UV).

Fig. 9 shows the values of shine for the 60° incidence angle for UT and D fibres and those treated with the placebo and the two antioxidant formulations before and after 36 h of UV radiation (UTP, UTC, UTR, DP, DPC and DPR). The graph shows a significant increase in shine values in the antioxidant treated fibres UTC, UTR, DPC, and DPR after irradiation. This improvement in shine is significant for both fibres treated with Cyn and Rice formulations. This suggests that the presence of actives in the formulations preserves the shine of the fibres. The irradiated samples (DR 36 h UV) attained the same values as the non-irradiated ones. Moreover, a higher increase is observed in both irradiated fibres using the Rice extract. The Rice formulation probably contributes to the higher protective effect due to the presence of phytic acid and moreover the peptides with restorative properties preserving hair brightness of natural and dyed hair.

Table 7
Shine values of untreated and dyed (UT, D) and treated fibres (UTP, UTC, UTR, DP, DC,DR) with and without irradiation at 500 W/m^2 for 36 h (Mean ± SD).

HAIR	20°	60°	85°
UT	128.67 ± 1.75	142.00 ± 0.00	118.07 ± 1.69
UTP	127.33 ± 2.44	141.00 ± 0.55	115.27 ± 3.33
UTC (Cyn)	117.87 ± 7.71	141.69 ± 0.48	115.87 ± 4.02
UTR (Rice)	126.93 ± 2.37	140.80 ± 1.01	115.00 ± 3.23
UT 36 h UV	117.73 ± 3.24	133.47 ± 2.47	113.40 ± 2.16
UTP 36 h UV	119.80 ± 2.54	133.93 ± 1.75	112.00 ± 2.54
UTC (Cyn) 36 h UV	121.60 ± 6.00	135.27 ± 4.44	107.93 ± 4.04
UTR (Rice) 36 h UV	120.60 ± 1.01	136.67 ± 0.90	114.23 ± 2.13
D	122.52 ± 4.05	137.24 ± 2.20	113.52 ± 2.16
DP	122.96 ± 3.60	136.86 ± 1.40	113.03 ± 3.60
DC (Cyn)	123.77 ± 2.80	137.90 ± 1.74	113.83 ± 1.92
DR (Rice)	124.36 ± 2.16	138.11 ± 0.99	113.90 ± 1.95
D 36 h UV	124,14 ± 2.50	135.20 ± 1.71	108.37 ± 2.87
DP 36 h UV	120.37 ± 2.59	134.46 ± 1.64	109.30 ± 4.43
DC (Cyn) 36 h UV	124.57 ± 3.01	136.57 ± 1.38	113.67 ± 2.37
DR (Rice) 36 h UV	124.90 ± 1.90	137.60 ± 1.30	114.60 ± 1.22

3.7. Colour measurements

Hair melanins provide some photoprotection to hair proteins by absorbing and filtering the impinging radiation and subsequently dissipating this energy as heat. However, red and dark-brown hairs photo-yellow when exposed to near ultraviolet plus visible radiation [9]. Hair colour resulting from a cosmetic treatment (artificial colour) is very sensitive to sunlight. UVA radiation resulted in a significant and perceivable change in the dye red hair colour as the one assayed in this work. The red pigment introduced into the hair fibre by the dyeing process acts as a photoreceptor, absorbing photons and photochemically degrading after UVA and visible light irradiation [11].

It is therefore essential to evaluate colour changes in dyed fibres subjected to UV radiation [10,45]. Colour measurements were performed on UT and D fibres treated with placebo (UTP and DP) and the two antioxidant formulations (UTC, UTR, DC and DR) with and without UV irradiation. As described in the experimental part, colour measurements were performed using a spectrophotometer (Macbeth Color-eye 3000). The colour measurements were obtained using The CIE L^*a^*b model, in which colour on the three axes correspond to trichromatic human perception. This model has the advantage of corresponding to the human perception of colour and has the additional benefit of giving a grid point for each specific colour. Then the total colour loss (ΔE) parameter was calculated using the following equation:

$$\Delta E = [(\Delta L)^2 + (\Delta a)^2 + (\Delta b)^2]^{1/2}$$

The results of total the colour loss parameter for hair fibres before and after 36 h UV irradiation are shown in Table 8 and Fig. 10.

The results showed a significant decrease in the colour loss parameter in the UT and D fibres when placebo and the two antioxidants were applied, indicating a good colour conservation of the fibres. As in the case of shine measurements, this effect is more marked in the case of the Rice extract, which probably protects the colour of fibres better than the Cyn extract.

Melanins, mainly located in the cortex, provide some photochemical protection to hair proteins, however in the process of protecting the hair proteins from light; the pigments are degraded or bleached. The main result of this process is hair colour changes [9,10]. Besides, tryptophan associated with photo-yellowing, of hair is one of the most degraded amino acid after exposure to UV [9,10]. This amino acid of the cuticle is altered to a greater extent than those of the cortex. Therefore the results of color loss prevention could be related to the ones obtained for thryptophan evaluation. The higher oxidation prevention of Rice extract could be

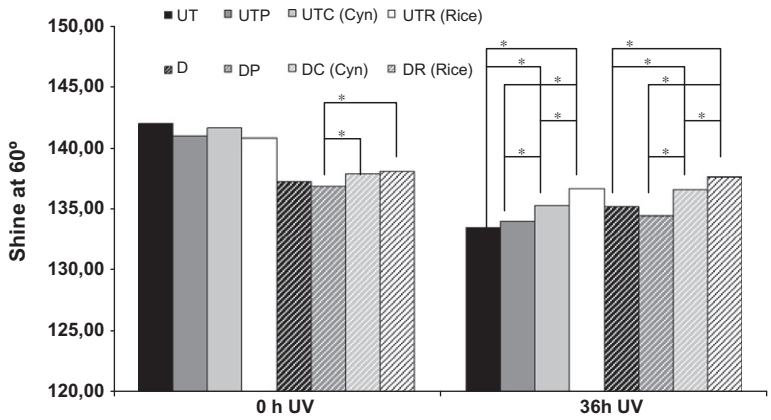

Fig. 9. Shine at 60° of UT, UTP, UTC, UTR, D, DP, DC and DR samples with UV irradiation at 500 w/m^2 for 36 h (Mean ± SD) ($^*p < 0.05$).

Table 8
CIE L^*a^*b parameters of UT, UTP, UTC, UTR, D, DP,DC and DR samples with and without UV irradiation (Mean ± SD). Total colour loss parameter for untreated fibres treated with the placebo (UT, UTP, D, and DP) and the two antioxidant formulations (UTC, UTR, DC and DR) irradiated for 36 h UV.

	L	*a*	*b*	Δ*E*
UT	20,74	4,80	6,61	
UT 36 h UV	23,37	4,84	6,58	2,63 (36 h UV)
UTP	22,36	5,17	7,33	
UTP 36 h UV	21,32	4,86	6,71	1,25 (36 h UV)
UTC (Cyn)	22,75	5,30	7,24	
UTC (Cyn)36 h UV	21,56	4,60	6,13	1,78 (36 h UV)
UTR (Rice)	22,74	5,31	7,79	
UTR (Rice)36 h UV	21,94	5,15	7,42	0,89 (36 h UV)
D	24,33	8,64	9,31	
D 36 h UV	22,09	7,90	8,76	2,42 (36 h UV)
DP	23,59	8,79	9,54	
DP 36 h UV	22,96	8,93	9,75	0,68 (36 h UV)
DC (Cyn)	23,36	7,99	9,42	
DC (Cyn)36 h UV	21,90	7,50	8,85	1,35 (36 h UV)
DR (Rice)	23,15	8,74	9,81	
DR (Rice)36 h UV	23,24	8,52	9,56	0,34 (36 h UV)

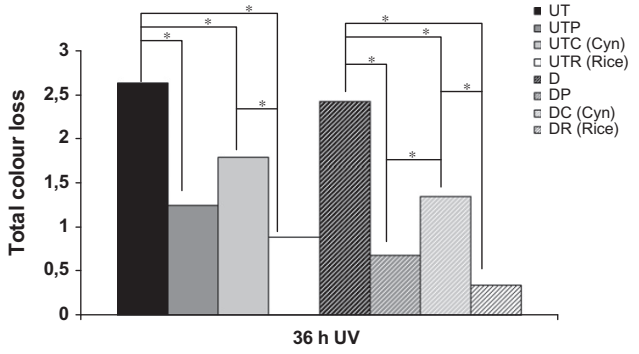

Fig. 10. Total colour loss (ΔE) of UT, UTP, UTC, UTR, D, DP, DC and DR samples with and without UV irradiation (Mean ± SD) ($^*p < 0.05$).

ascribed to the phytic acid antioxidant and moreover to the peptides that as in the case of triptophan evaluation were supposed to be the reason of a stronger protection effect at the fibre surface.

4. Conclusions

Irradiated hair samples were observed to be damaged chemically and mechanically with a decrease in breakage work and adverse consequences for the mechanical properties. Furthermore, the physical appearance of hair showed a decrease in shine and loss of colour. Treatments with antioxidants improved the mechanical properties of irradiated hair especially in the case of the Rice extract. Low molecular weight peptides of the rice formulation probably penetrate hair and improve the mechanical properties at the cortex level and higher molecular weight peptides may form a protective layer preventing tryptophan degradation and color loss.

Moreover, lipidic peroxidation and protein degradation of hair are significantly reduced in the antioxidant treated samples, suggesting an improved integrity of the fibre. This is more marked in the case of the Artichoke extract, indicating higher antioxidant properties for hydroxycinnamic derivates contained in this formulation. SEM images showed that the application of antioxidants to hair fibres leads to an improvement in the cuticle scale with a smoothing of the scale edge. These images coincide with the conservation of colour and shine in the dyed tresses.

The two formulations provided protection against UV irradiation and corroborated a significant protection capacity; the Cyn formulation proved to be more effective in preventing protein degradation and lipid peroxidation. The Rice extract led to higher breakage work, and a lower degradation of colour and shine. The different methodologies assayed help to evaluate the degree of damage in the fibre subjected to UV radiation. Moreover they determine the effectiveness and the action mechanism of the different antioxidant formulations applied to human hair.

Acknowledgements

Thanks are due to the TRACE Program (TRA 2009-0282) for finacial support.

References

[1] V. Signori, Review of the current understanding of the effect of ultraviolet and visible radiation on hair structure and options for photoprotection, Cosmet. Sci. 55 (2004) 95–113.
[2] A.C.S. Nogueira, L.E. Dicelio, I. Joekes, About photo-damage of human hair, Photochem. Photobiol. Sci. 5 (2006) 165–169.
[3] E. Hoting, M. Zimmerman, B. Hilterhaus, Photochemical alterations on human hair. Part I: Artificial irradiation and investigations of hair proteins, J. Soc. Cosmet. Chem. 46 (1995) 85–99.
[4] E. Hoting, M. Zimmerman, Photochemical alterations on human hair. Part III: Investigations of internal lipids, J. Soc. Cosmet. Chem. 47 (1996) 201–211.
[5] E. Hoting, M. Zimmerman, H. Hocker, Photochemical alterations on human hair. Part II: Analysis of melanin, J. Soc. Cosmet. Chem. 46 (1995) 181–190.
[6] M.P. Chandra, J. Janus, Hair photodamage-Measurements and prevention, J. Soc. Cosmet. Chem. 44 (1993) 109–122.
[7] P.M. Plonka, Electron paramagnetic resonance as a unique tool for skin and hair research, Exp. Dermatol. 18 (2009) 472–484.

[8] T. Herrling, K. Jung, J. Fuchs, The role of melanin as protector against free radicals in skin and its role as free radical indicator in hair, Spectrochim, Acta. Part A. Mol. Biomol. Spectrosc. 69 (2007) 1429–1435.
[9] A.C.S. Nogueira, M. Richena, L.E. Dicelio, I. Joekes, Photo yellowing of human hair, J. Photochem. Photobiol. B: Biol. 88 (2007) 119–125.
[10] A.C.S. Nogueira, I. Joekes, Hair color changes and protein damage caused by ultraviolet radiation, J. Photochem. Photobiol. B: Biol. 74 (2004) 109–117.
[11] T. Gao, J.M. Tien, A. Bidaye, S. Cardinali, J. Kinney, A diester to Protect Hair from Color Fade and Sun Damage, Cosmet. Toiletr. 124 (2009) 70–78.
[12] E. Fernandez, C. Barba, C. Alonso, M. Marti, L. Coderch, J.L. Parra, Photodamage determination of human hair, J. Photochem. Photobiol.B. 106 (2012) 101–106.
[13] R. Beyak, G.S. Kass, C.F. Meyer, Elasticity and tensile properties of human hair II: Light radiation effects, J. Soc. Cosmet. Chem. 22 (1971) 667–678.
[14] E. Tolgyesi, Wheatering of hair, Cosmet. Toiletr. 98 (1983) 29–33.
[15] P. Mary, M.D. Lupo, Antioxidants and Vitamins in cosmetics, Clin. Dermatol. 19 (2001) 467–473.
[16] A. Chandrasekara, F. Shahidi, Content of insoluble bound phenolics in millets and their contribution to antioxidant capacity, J. Agri. Food Chem. 58 (2010) 8842–8847.
[17] E.S. Stern, V.L. Johnson, Studies of the molecular weight distribution of cosmetic protein hydrolysates, J. Soc. Cosmet. Chem. 28 (1977) 447–455.
[18] A. Teglia, G. Mazzola, G. Secchi, Chemical characteristics and cosmetic properties of protein hydrolysates, Cosmet. Toiletr. 108 (1993) 56–65.
[19] E. Graf, K.L. Empson, J.W. Eaton, Phytic acid: a natural antioxidant, J. Biol. Chem. 262 (1987) 11647–11650.
[20] R. De Cassia Comis Wagner, P. Kunihiko Kiyohara, M. Silveira, I. Joekes, Electron microscopic observations of human hair medulla, J. of Micros. 226 (2007) 54–63.
[21] J.M. Baldasano, C. Soriano, H. Flores, J. Esteve, A. Mitjà, Atlas de Radiació solar a Catalunya. (Edited by Institut Català d' Energia, Barcelona 2001) http://www20.gencat.cat/docs/icaen/02_Energies%20Renovables/Documents/Arxius/Atlas%20de%20radiacio%20solar.pdf.
[22] C. Barba, S. Scott, R. Kelly, J.L. Parra, L. Coderch, New Anionic Surface- Active Agent Derived from Wool Proteins for Hair Treatment, J. Appl. Polym. Sci. 115 (2010) 1461–1467.
[23] M.M. Bradford, A Rapid and Sensitive Method for the quantization of microgram quantities of protein utilizing the principle of protein-dye binding, Anal. Biochem. 72 (1976) 248–254.
[24] L.J. Marnett, Lipid peroxidation-DNA damage by malonaldehide, Mutat. Res. 424 (1999) 83–95.
[25] C. Alonso, C. Barba, L. Rubio, S. Scott, A. Kilimnik, L. Coderch, J. Notario, J.L. Parra, An Ex Vivo Metholdology to Asses the Lipid Peroxidation in Stratum Corneum, J. Photochem. Photobiol. B: Biol. 97 (2009) 71–76.
[26] J.H. S Rennie, S.E. Bedford, J.D. Hague, A model for the shine of hair arrays, Int. J. Cosmet. Sci. 19 (1997) 131–140.
[27] A. Benaiges, E. Fernandez, B. Martinez-Teipel, R. Armengol, C. Barba, L. Coderch, Hair efficacy of botanical extracts, J. Appl. Poly. Sci. (2012), http://dx.doi.org/10.1002/APP.38244.
[28] A. Ford, A. Roberts, Colour Space Conversions (1998).
[29] TASI, Colour theory: understanding and modelling colour, Technical Advisory Service for Images. (Bristol, UK: University of Bristol 2004).
[30] S. Napier, Personal communication, Biolab Group Australia 2007.
[31] C.R. Robbins, Chemical and Physical Behavior of Human Hair, second ed., Springer-Verlag, NewYork, 1988. p. 226.
[32] C.R. Robbins, R.J. Crawford, Cuticle damage and the tensile properties of human hair, J. Soc. Cosmet. Chem. 42 (1991) 59–67.
[33] R.J. Bouthilet, A. Karler, Cosmetic effects of substantive protein, Proc. Sci. Sect. Toilet. Goods. Assn. 44 (1965) 27–31.
[34] R.R. Riso, Proteins, some new derivates, Proc. Sci. Sect. Toilet. Goods. Assn. 42 (1964) 36–39.
[35] R.R. Riso, Protein derived detergents, Soap. Cosm. Chem. Spec. Goods. Assn. 39 (1963) 82–84.
[36] A. Roddick- Lanzilotta, R. Kelly, S. Scott, S. Chahal, N. Challoner, Anti-ageing efficacy in hair care products, SÖFW Journal 130 (2004) 3–9.
[37] C.W.M. Yuen, C.W. Kan, S.Y. Cheng, Evaluation of Keratin Fibre Damages, Fibers and Polymers 8 (2007) 414–420.
[38] F. Zülli, E. Belser, M. Neuenschwander, R. Muggli, Antioxidants from grape seeds protect hair against reactive oxygen species, Personal Care (2001) 65–67.
[39] S.Y. Jeon, L.Q. Pi, W.S. Lee, Comparison of hair shaft damage after UVA and UVB irradiation, J. Cosmet Sci. 59 (2008) 151–156.
[40] D.A. Shaw, The extraction and quantification and nature of hair lipids, J. Cosmet. Sci. 1 (1979) 291–302.
[41] J. D. Leeder, J. A. Rippon, F. E. Rothery, I. W. Stapleton, Use of the transmission electron microscope to study dyeing and diffusion processes, Proc. 7th Int. Wool. Text. Res. Conf. 5 (1985) 89-99.
[42] K. Nishimura, M. Nishino, Y. Inaoka, Y. Kitada, M. Fukushima, Interrelationship between the hair lipids and the hair moisture, Nippon. Koshohin. Kagakkaishi. 13 (1989) 134–139.
[43] L. Won-Soo, Photoaggravation of hair aging, Int. J. Trichology. 1 (2009) 94–99.
[44] P. Maillan, UV protection of artificially coloured hair using a leave-on formulation, Int. Jour. of Cosmet. Sci. 24 (2002) 117–122.
[45] J.T. Guthrie, A.L. Rongong, S. Rush, The characterisation of treated and dyed hair, Dyesand. Pigm. 29 (1995) 23–44.

ARTÍCULO 3

Bicelles and bicosomes as free radical scavengers in the skin

RSC Advances, 2014, **4**, 53109-53121

La radiación UV forma radicales libres en la piel. En este estudio se evalúa mediante EPR la actividad anti-radicalaria de las bicelas y los bicosomas en una piel sometida a radiación UV-VIS, y se determina el efecto de incluir el antioxidante β-caroteno en ambos sistemas lipídicos. La radiación UV-VIS se aplica simultáneamente a la medición de radicales libres mediante una lámpara acoplada al equipo de EPR. La intensidad de irradiación es de 147.9 W/m^2 y el tiempo de exposición es de 30 min. Además, se lleva a cabo la simulación de los espectros de EPR para identificar y cuantificar los diferentes radicales producidos en la piel por radiación UV-VIS. Por otro lado también se caracterizan las bicelas y los bicosomas con β-caroteno mediante DLS y Crio-TEM.

Los radicales libres de la piel son más inestables que los del cabello y no son detectables por EPR. Por esa razón es necesario utilizar una molécula "spin-trap" que es capaz atrapar los radicales formados en la piel formando otros radicales más estables que pueden ser detectados por EPR. En este estudio el "spin-trap" utilizado es el DMPO.

Los resultados mostraron una ligera modificación en el tamaño de los sistemas lipídicos con la incorporación de β-caroteno incrementando el diámetro más notablemente en los bicosomas.

Los resultados de EPR mostraron una menor formación de radicales libres en la piel en las muestras tratadas con los sistemas lipídicos con y sin β-caroteno, siendo los bicosomas con antioxidante el sistema más efectivo.

Mediante la simulación de los espectros obtenidos se identificaron seis tipos de aductos de DMPO en la piel, aductos del grupo alcoxi (primarios/secundarios y terciarios), aductos de carbono, aductos de hidroxilo, hidrógeno y aductos aminoxilo. Los aductos más abundantes fueron los de carbono.

En base a publicaciones anteriores se sugiere que los diferentes radicales formados pueden proceder principalmente de la queratina, de los lípidos o del ADN de las células. También se sugiere que puedan proceder de otras moléculas como los

aminoácidos Trp o la vitamina B2 (riboflavina) que son susceptibles a formar radicales libres.

En resumen, se puede concluir que la medición de la concentración de radicales libres en la piel simultáneamente a la radiación UV-VIS, es una manera adecuada para estudiar la evolución de estas especies en la piel.

Por otro lado, queda demostrada la capacidad anti-radicalaria en la piel de las bicelas y los bicosomas, siendo los bicosomas con β-caroteno el sistema más efectivo. Por lo tanto, ambas nanoestructuras demuestran tener gran potencial de aplicabilidad en el campo de la protección solar.

RSC Advances

PAPER

View Article Online
View Journal | View Issue

Cite this: *RSC Adv.*, 2014, **4**, 53109

Bicelles and bicosomes as free radical scavengers in the skin

Estibalitz Fernández,*[a] Lluís Fajarí,[a] Gelen Rodríguez,[b] Carmen López-Iglesias,[c] Mercedes Cócera,[b] Lucyanna Barbosa-Barros,[b] Alfonso de la Maza[a] and Olga López[a]

In the present work, β-carotene antioxidant was incorporated in two different lipid nanoaggregates, bicelles and bicosomes, and its effectiveness against free radical formation in porcine skin *in vitro* was determined using 5,5-dimethyl-1-pyrroline-N-oxide (DMPO) spin trap and Electron Paramagnetic Resonance spectroscopy (EPR). Bicelles are discoidal nanostructures formed by self-assembly of phospholipids dispersed in aqueous solution. Bicosomes emerge as a strategy to stabilize and protect bicelles encapsulating these nanostructures in liposomes. Results from Dynamic Light Scattering (DLS) and cryo Transmission Electron Microscopy (cryo-TEM) demonstrated a slight modification in the size of both systems when β-carotene was incorporated. EPR revealed that after skin irradiation both systems presented free radical scavenging activity. This activity was statistically significant for bicosomes containing β-carotene. Differences regarding this scavenging activity between bicelles and bicosomes would probably be due to the different interaction of both systems with the skin. In this study, six different radicals were identified in skin spectra: two originated from oxygen centred radicals (primary/secondary and tertiary alkoxyl radicals) and another from carbon-centred radicals. Additionally, the presence of 5,5-dimethyl-2-oxo-pyrroline-1-hydroxyl (DMPO-OH), 5,5-dimethyl-2-oxo-pyrroline-1-hydrogen (DMPO-H) adducts and aminoxyl radicals (RR′NO•) were detected. Considering these results, bicelles and bicosomes could be useful lipid systems for future dermopharmaceutical applications.

Received 30th May 2014
Accepted 3rd October 2014

DOI: 10.1039/c4ra05157b

www.rsc.org/advances

Introduction

Exposure of skin to ultraviolet light (UV) leads to formation of free radicals. These radicals are in part responsible for erythema/edema, inflammation, and premature skin aging (photoaging).[1] Fortunately the skin has a wide range of coupled antioxidant defense systems to protect itself from the free radicals induced by UV radiation.[2] However, this defense system can be overwhelmed by excessive exposure to radiation. Supporting the cutaneous defence system with antioxidants could reduce the formation of free radicals in the skin.[3] Nevertheless, in some cases the chemical instability and poor solubility in water of exogenous antioxidants leads to a loss of their efficiency. In order to avoid this problem, the formulation of antioxidant derivates and their incorporation in liposomes and other vehicles have been developed in the last decade.[4,5] However, the large size of these vehicles as well as the inappropriate composition and elasticity of vesicles make difficult the incorporation of antioxidants inside the skin. This complex tissue specifically the outermost layer, the stratum corneum (SC), is responsible of the skin barrier function. The well-organized lipid assembly of SC, difficults the pass of vesicles and other nanostructures through the tissue.[6–8]

Bicelles are lipid discoidal nanostructures with sizes around 15–25 nm (Fig. 1A). They are composed by long and short alkyl chain phospholipids dispersed in aqueous solution forming a bilayer organization similar to the lipid bilayers of the skin stratum corneum (SC).[9,10] Bicosomes emerge as a strategy to stabilize bicelles and modulate their effect encapsulating these nanostructures in liposomes.[11] Thus, they are based on mixtures of spherical vesicles around 100–200 nm in diameter and discoidal structures (bicelles) (Fig. 1B).

The combination of lipid composition, small size and morphological versatility give high applicability to both structures for skin uses. Bicelles have the ability to penetrate through

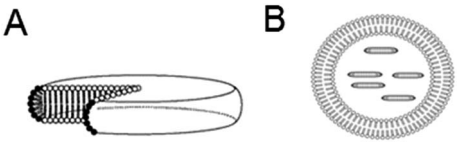

Fig. 1 (A) Bicelle structure and (B) bicosome structure.

[a]*Institute of Advanced Chemistry of Catalonia (IQAC-CSIC), Jordi Girona 18-26, 08034 Barcelona, Spain. E-mail: efptqt@cid.csic.es*

[b]*Bicosome S.L., Jordi Girona 18-26, 08034 Barcelona, Spain*

[c]*Centros Científicos y Tecnológicos de la Universidad de Barcelona, Baldiri Reixac, 4-8, Torre D, 08028 Barcelona, Spain*

the narrow intracellular spaces of the skin SC and to modulate the barrier function of this tissue and bicosomes can combine the advantages of disk and spherical vesicles.[12] Moreover, considering the nanostructure and composition of bicelle and bicosome systems and their possibility of encapsulating different molecules, they are good carriers for topical applications and as delivery systems.[11,13,14]

β-Carotene is one of the most studied carotenoids which can inactivate highly reactive oxygen species involved in UV radiation process.[15] Additionally, other authors documented the peroxyl radical scavenging properties of β-carotene that could act as a chain-breaking antioxidant especially effective at low partial oxygen pressures.[16] Also, it has been proposed that β-carotene scavenged peroxyl radicals by addition to double bond and producing carbon-centred conjugates.[17] This fact differentiates β-carotene from other antioxidants such as, vitamin C and E, which act by donating of hydrogen-atom. Because of these properties, this active has been used topically to inhibit oral carcinogenesis, and skin melasma.[18,19] Moreover, the antioxidant effect of β-carotene in homogeneous solutions and in lipid systems has been demonstrated in several studies.[17]

The objectives of this work have been to study the ability of bicelles and bicosomes as carries of β-carotene antioxidant and to evaluate the potential free radical scavenging effect on the skin of these colloidal systems. With this aim β-carotene has been included in bicelles and bicosomes and the potential of these systems as free radical scavengers in the skin has been evaluated. The lipid nanostructures were characterized by Dynamic Light Scattering (DLS) and by cryo Transmission Electron Microscopy (cryo-Tem). Both techniques have been used in previous studies for characterizing dimensional and morphological aspects of bicelles and bicosomes.[11–13] Besides, Electron Paramagnetic Resonance technique (EPR) was used to detect the free radicals formed in native skin and in skin treated with these systems. Free radicals in the skin have a short-life and are measured by EPR using a spin trapping method in which a diamagnetic spin trap, 5,5-dimethyl-1-pyrroline-N-oxide (DMPO), reacts with the short-lived radicals to form more stable radicals (DMPO adducts). EPR technique has been used in other studies to evaluate the oxidation of biological tissues such as skin and hair.[20,21] The identification and quantification of different free radical was performed using computer simulation.

Results

Characterization of different lipid systems

DLS and cryo-TEM techniques were used to characterize bicelles and bicosomes. The size distribution curves for bicelles and bicosomes with β-carotene at 25 °C are shown in Fig. 2A and B.

Size distribution curves of both systems show two peaks centred on populations of different sizes. In the distribution curve of bicelles incorporating β-carotene (Fig. 2A), small size population shows higher scattered intensity than large size population. Whereas in the distribution curve of bicosomes with β-carotene (Fig. 2B) the opposite effect in observed. The large size population shows the highest scattered intensity.

The sizes as HD of the different populations at the distribution curves of every lipid systems obtained by DLS at 25 °C are shown in Table 1. The HD corresponds to a hypothetical hard sphere that diffuses with the same speed as the particle under experiment and the percentage of intensity represents the proportion of scattered light corresponding to the size population obtained.

The size of bicellar systems not including β-carotene showed two populations with HD around 12 nm and 1400 nm. The corresponding proportion of light scattered for these populations were about for 60% and 40% respectively. The PI obtained for this system was 0.36. Incorporation of β-carotene in the bicellar systems led to a slight increase in the particle size with HD about 16 nm. The corresponding proportion of light scattered for this population was about for 76%. PI obtained for this system containing β-carotene was 0.30. After the application of Mazer equation (eqn (1)), the HD for bicelles resulted around 14 nm and for bicelles with β-carotene about 18 nm. These results are in the range with the diameters obtained in DLS (12.32 and 15.80 nm for bicelles and bicelles incorporating β-carotene respectively).

The size increase could be due to the location of β-carotene in the bilayer of bicelles. β-Carotene is highly lipophilic and has a very low solubility in water, then this active would be preferably included in lipid bilayers promoting a slight increase in the size of the nanostructure.

DLS results obtained for bicosomes with and without incorporation of β-carotene are also shown in Table 1. Two peaks around 200 nm and 27 nm were observed for bicosomes without β-carotene with 86% and 14% of light scattered respectively. The incorporation of β-carotene in bicosomes generated two peaks around 250 nm and 32 nm with a proportion of light scattered of about 84% and 16% respectively (Fig. 2B). For both bicosome systems the obtained PI was 0.99. The high PI values in both of the bicosome systems reflect the coexistence of these large and small populations.

The cryo-TEM technique allowed us to characterize the morphology of bicelles and bicosomes. A number of images were analyzed and some of them are visualized in Fig. 3A–E. Adobe Photoshop software was used to calculate directly from the images the diameters of the nanostructures.

Micrograph of bicellar systems without β-carotene (Fig. 3A) shows discoidal structures in edge-on (black open arrow) and face-on (white open arrow) dispositions with sizes between 15–25 nm. Bicellar systems containing β-carotene exhibited similar size and/or dimensional patterns with diameters around 24–30 nm as Fig. 3B shows. Neither, in bicellar systems with and without β-carotene, large aggregates were visualized. Fig. 3C–E imaging bicosome samples without (C) and with β-carotene (D and E). These micrographs show vesicles encapsulated in vesicles (dotted black arrow), free discoidal bicelles (black open arrow) and bicelles encapsulated in vesicles, *i.e.* bicosomes (white closed arrow). Vesicles are visualized as uni-, multi- and oligolamellar structures. The size of bicosome structures was around 150–250 nm (C–E). Non-encapsulated bicelles without the antioxidant (C) show sizes about 35–65 nm and non-

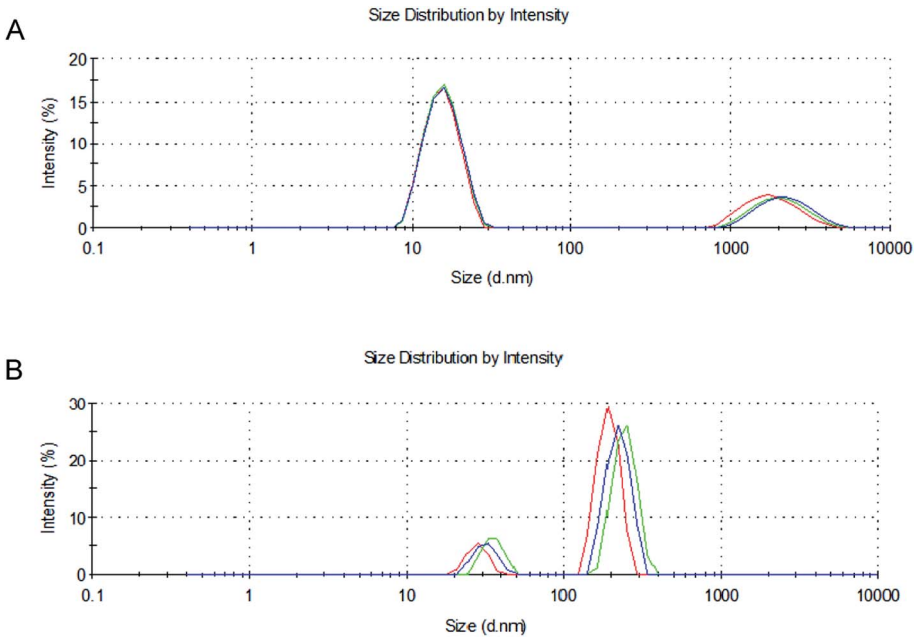

Fig. 2 Size distribution curves obtained from DLS at 25 °C for (A) bicellar systems incorporating β-carotene and (B) bicosomes incorporating β-carotene.

encapsulated bicelles with β-carotene (D and E) were about 50–85 nm in diameter. Additionally, a tendency of bicelles to form stacks was observed (black closed arrow), more noticeable with the incorporation of β-carotene.

The high variability in size of the different structures could explain the PI of 0.99 detected by DLS, which corroborates the very heterogeneous distribution of size in bicosome systems. The population with small size detected by DLS was probably due to the non-encapsulated bicelles.

The sizes of bicelles measured by cryo-TEM resulted larger than those obtained by DLS. The appropriate comparison between both techniques involves the transformation of sizes obtained in cryo-TEM to HD. This data treatment is presented in discussion section.

EPR and UV radiation

Spin-trap measurement. When DMPO is used to identify radicals generated by UV radiation in photochemical systems, it is important to consider the possible reactions that may occur in the spin-trap by effect of this radiation.[22] The typical process related with the decomposition of DMPO is the formation of aminoxyl radical (RR′NO•), which results in the formation of triplet spectrum.[23] In this section the possible decomposition of DMPO solution by irradiation was investigated following the procedure of the cellulose paper (smoking paper) detailed in the Experimental section.

Fig. 4 shows the EPR spectra obtained for DMPO solution in cellulose before (A) and after (B) UV radiation. Spectra of the DMPO solution in the native skin are superimposed in Fig. 4 for comparative purposes.

Before irradiation no signals of any radical–adducts were observed for DMPO in cellulose (Fig. 4A, black line). However, EPR spectrum of DMPO in the skin showed a signal with high intensity (Fig. 4A, green line). This indicates the formation of different DMPO adducts, suggesting the presence of free radicals in the skin even before irradiation. After UV radiation the intensity of the spectrum of DMPO in cellulose increases (Fig. 4B, black line). The spectral lines of Fig. 4B marked with (*) would correspond to the triplet of RR′NO• radicals and were simulated using the parameter $a(N) = 14.52$ G, which was reported previously in the literature.[23] Comparing this spectrum (DMPO absorbed in cellulose after irradiation) with the spectrum of DMPO in the skin after irradiation (Fig. 4B, green line),

Table 1 Mean value and standard deviation of HD and proportion of scattered intensity corresponding to different population at size distribution curves at 25 °C for each lipid system

Lipid system	HD (nm) (peak 1)	% Int (peak 1)	HD (nm) (peak 2)	% Int (peak 2)
Bicelles	12.32 ± 0.30	60	1393.00 ± 205.70	40
Bicelles + β-carotene	15.80 ± 0.18	76	2121.00 ± 219.00	24
Bicosomes	26.89 ± 9.40	14	202.30 ± 31.00	86
Bicosomes + β-carotene	31.91 ± 26.00	16	250.00 ± 26.00	84

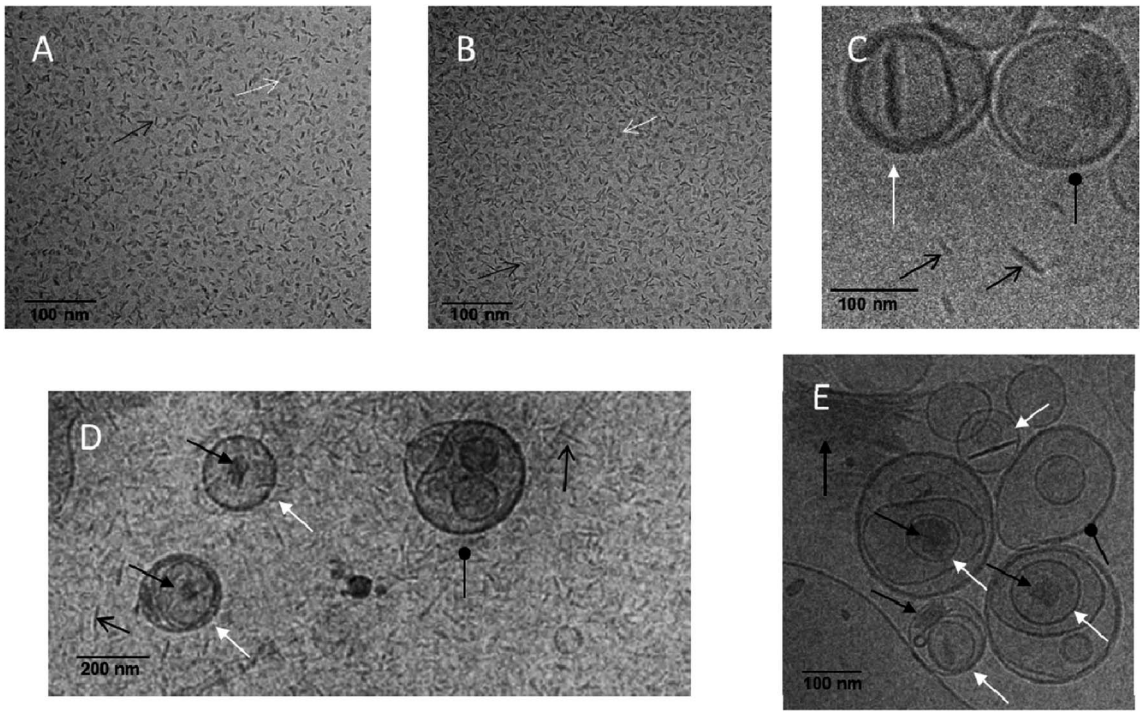

Fig. 3 Cryo-TEM micrographs of bicelles and bicosomes. (A) Discoidal structures (bicelles) are shown in all projections, face-on (white open arrow) and edge-on (black open arrow). (B) Bicelles with encapsulated β-carotene are shown in all projections, face-on (white open arrow) and edge-on (black open arrow). (C) Bicosomes without β-carotene show vesicles encapsulated in vesicles (dotted black arrow), bicosomes (white closed arrow) and non-encapsulated bicelles (black open arrow). (D) Bicosomes with β-carotene show vesicles encapsulated in vesicles (dotted black arrow), bicosomes (white closed arrow) and non-encapsulated bicelles (black open arrow) with β-carotene. A tendency of bicelles to form stacks was observed (black closed arrow). (E) Bicosomes with β-carotene show encapsulated bicelles (white closed arrow). A tendency of bicelles to form stacks was observed (black closed arrow).

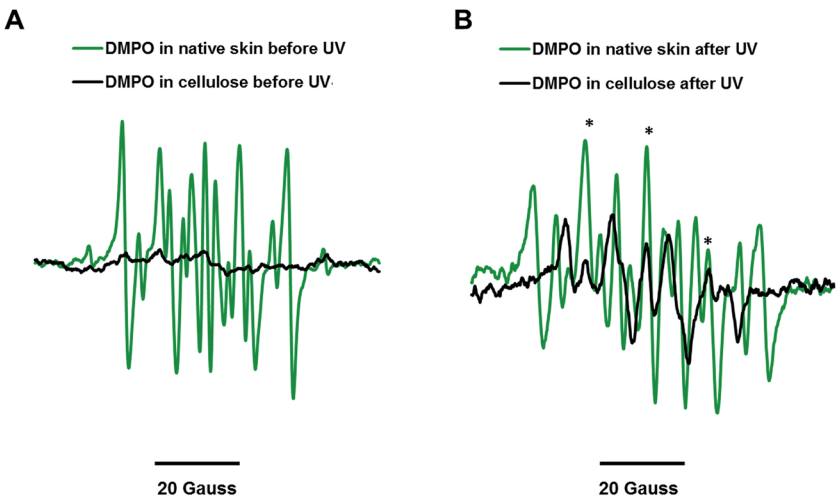

Fig. 4 EPR spectra for DMPO applied to native skin and to cellulose, (A) before UV radiation, (B) after UV radiation. The spectral lines marked with (*) correspond to the triplet of RR′NO˙ radicals.

we observe that the signal of the RR′NO˙ radicals generated by the decomposition of DMPO in cellulose was very low. Considering the height of the triplet peaks in both spectra, a notable difference was observed between them. From these results we can assume that the spectral lines of RR′NO˙ radicals due to the DMPO decomposition would contribute sparsely to the signals obtained when DMPO was applied to skin. As consequence, the skin spectra signals would derive from radicals formed in this tissue, and not from the spin-trap decomposition.

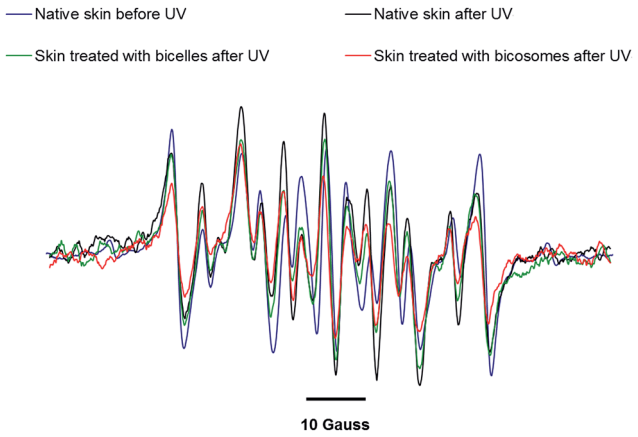

Fig. 5 EPR spectra of porcine skin samples untreated and treated with different lipid systems (as described in the text).

EPR experiments and computer simulation of the skin samples. With the aim to evaluate the scavenging effect of β-carotene in solution, a preliminary assay was performed. The antioxidant was dissolved in DMSO–H_2O (2 : 10) mixture, which was the most appropriate solvent in order to get solubilize the antioxidant without affecting skin permeability. The antiradical effect of this solution was compared with the scavenging effect of β-carotene incorporated in bicosomes. The results showed a reduction of 45.5% in the formation free radicals in the skin samples treated with bicosomes containing β-carotene comparing with those treated with the same amount of β-carotene in DMSO–H_2O (2 : 10) (38.6%).

Considering these data and to evaluate the benefits of each lipid system on skin properties, we decided focused our attention in the differences between bicelles and bicosomes in subsequent experiments.

The generation of free radicals in pig skin samples was determined by EPR measurements using the DMPO spin-trap, which traps the radicals formed in the tissue. All of the obtained spectra showed a symmetric spectral model. The symmetric characteristic indicates that the detected free radicals come only from DMPO-adducts. These DMPO-adducts have very similar constant *g* value around 2.0054.[24] Fig. 5 shows the spectra of native porcine skin before and after UV radiation. Besides, skin samples treated with bicelles and bicosomes without β-carotene and subsequently irradiated are also shown in this figure.

It is known that the concentration of free radicals is proportional to the second integral intensity of the EPR lines.[25] Then, for determination of trapped radicals after UV radiation, the integration values of the spectra were calculated and are shown in Fig. 6.

The lowest integration value was obtained for native skin before irradiation, while the highest integration value was achieved for native sample after irradiation. This high difference between native skin before and after irradiation was statistically significant. The skin samples treated with all the lipid systems showed lower integration values than the native skin after irradiation. Besides, a significant difference between integration values of native skin and skin treated with bicosomes with β-carotene was obtained. It is important to note that the integration value of skin samples treated with bicosomes containing β-carotene after irradiation showed a similar integration value as native skin sample before irradiation. This result indicates the considerable scavenging effect of this system. Therefore, the inclusion of β-carotene in bicosomes promoted a decrease in the integration value indicating a

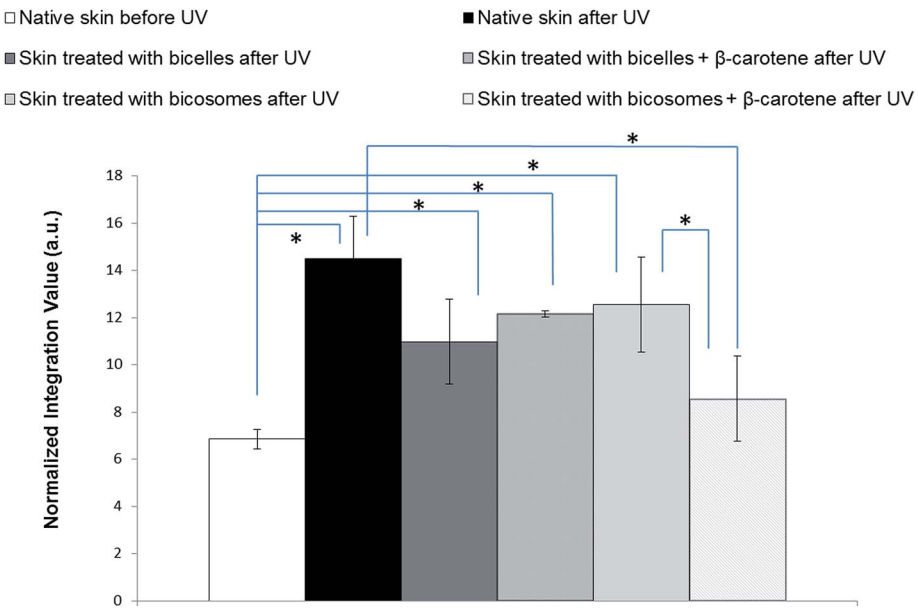

Fig. 6 Normalized second integration value of the obtained EPR spectra for skin samples treated with different systems (mean ± standard deviation (SD)). Significant differences are indicated with * ($p < 0.05$).

Table 2 Radical skin protection factor (RSF) and scavenging effectiveness (*E*) after UV radiation of different lipid systems applied in the skin

	Bicelles	Bicelles β-carotene	Bicosomes	Bicosomes β-carotene
RSF	1.32	1.19	1.16	1.69
E	0.24	0.16	0.13	0.41

significant difference between bicosomes with and without the antioxidant. This indicates an enhanced scavenging effect in bicosomes when the antioxidant was included in the system producing the lowest integration value after irradiation. In the case of bicelles, non-significant difference was observed with the inclusion of the antioxidant.

Additionally, the spectra of bicelles and bicosomes before irradiation were also registered. The integration value of these spectra was in the order of native skin before irradiation (data not shown).

The values of radical skin protection factor (SPF) and scavenging effectiveness (*E*) in Table 2 support data from Fig. 6.

In both parameters the best UV protection value was obtained for bicosomes with β-carotene, followed by bicelles, bicelles with β-carotene and bicosomes, indicating the best effectiveness for bicosomes with the antioxidant.

The obtained EPR spectra are the superimposition of signal from different DMPO adducts. In this work, experimental spectra were fitted by simulation as a combination of six different adducts signals using the Bruker WinEPR programs. The spectra of these DMPO adducts were reported by previous authors and are shown in Fig. 7.

Species (A) and (B) were originated from oxygen centred radicals, primary/secondary (a(N) = 15.90 G, a(H) = 12.40 G

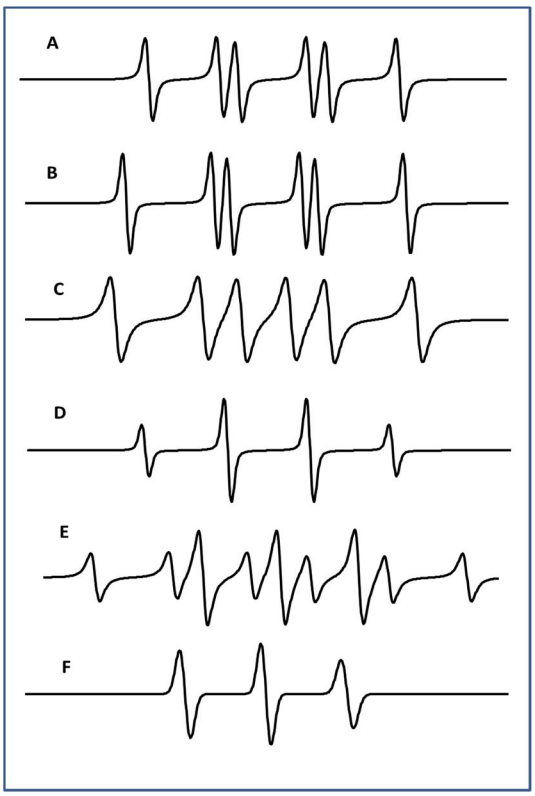

Fig. 7 EPR spectra of free radicals using, (A) a(N) = 15.90 G, a(H) = 12.40 G (primary/secondary alkoxyl radical-adduct), (B) a(N) = 15.79 G, a(H) = 18.63 G (tertiary alkoxyl radical-adduct), (C) a(N) = 15.58 G, a(H) = 22.57 G (carbon-centred radical-adduct), (D) a(N) = 14.90 G, a(H) = 14.90 G (hydroxyl radical-adduct), (E) a(N) = 14.83 G, a(H) = 24.35 G (hydrogen radical-adduct) and (F) a(N) = 14.52 G (RR′NO$^{\bullet}$ radical). g = 2.0054 in all spectra.

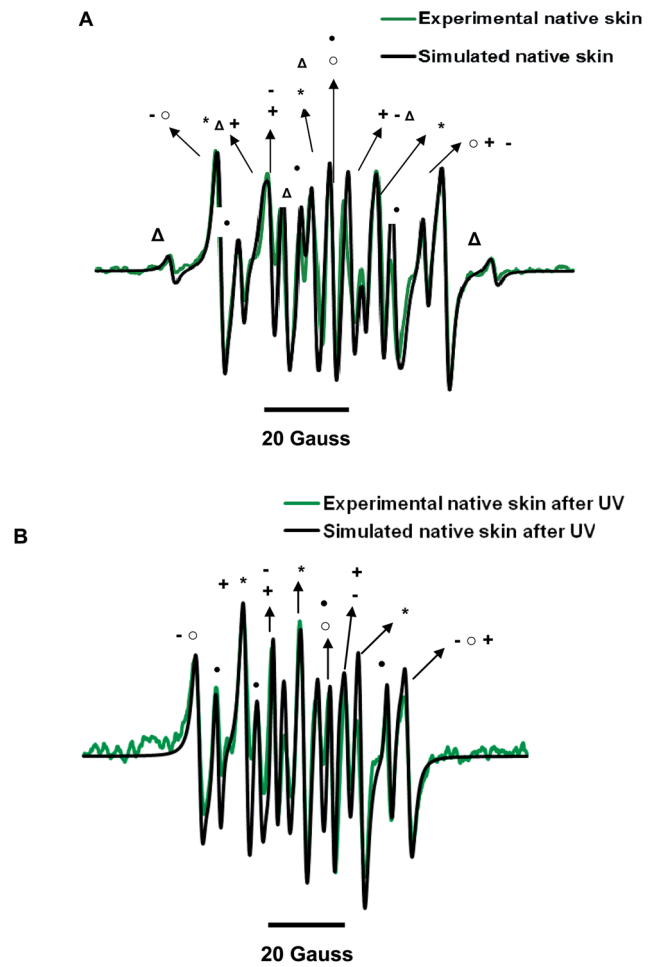

Fig. 8 Comparison of experimental spectrum (green) and simulated spectrum (black) (A) before UV radiation, (B) after UV radiation. Symbols: (+) primary/secondary alkoxyl radical–adducts, (0) tertiary alkoxyl radical–adducts, (–) carbon-centred radical–adducts, (●) DMPO-OH radical–adducts, (Δ) DMPO-H radical–adducts and (*) RR′NO$^{\bullet}$ radicals.

and $g = 2.00540$) and tertiary-alkoxyl adducts (a(N) = 15.79 G, a(H) = 18.63 G and $g = 2.00540$) respectively, while species (C) corresponded to carbon-centred radicals (a(N) = 15.58 G, a(H) = 22.57 G and $g = 2.00541$). The (D) and (E) species corresponded to hydroxyl (using a(N) = 14.91 G, a(H) = 14.91 G and $g = 2.00541$) and hydrogen (a(N) = 14.83 G, a(H) = 24.35 G and $g = 2.00541$) DMPO adducts respectively, and finally the (F) species were originated from RR′NO$^{\bullet}$ radicals (a(N) = 14.52 G and $g = 2.00540$).[23–26]

The simulated spectra obtained with the fitting of these different radical–adducts before and after UV radiation are shown in Fig. 8A and B, respectively.

The spectral lines of Fig. 8A and B marked with (+) were attributed to primary/secondary alkoxyl-adducts, which were observed previously in UV-A irradiated pork fat.[24] The lines marked with (0) were assigned to tertiary-alkoxyl and the most intense signals were originated to carbon-centred radical adducts (−). (●) and (Δ) symbols were attributed to DMPO-OH and DMPO-H radical–adducts respectively. Finally, the lines marked with (*) were assigned to RR′NO$^{\bullet}$ radicals. Similar spectral lines and type of adducts were detected before and after irradiation. The only differences between both spectra were the extinction of the hydrogen-adducts after irradiation and obviously, the higher intensity of the signals after irradiation.

From the simulation, the contribution of the different radical–adducts to the experimental signal were also obtained. Tables 3 and 4 show the relative proportion of the six different radical–adducts on the simulated spectra for skin samples submitted to different treatments before and after irradiation. It is important to consider that the different percentages were calculated with respect to the total integration value of every simulated spectrum.

Before irradiation (Table 3), the native pig skin displayed the highest contribution for carbon-centred species, followed by RR′NO$^{\bullet}$ radicals. The radicals that contributed in a minor extension to the experimental spectrum from the native skin were primary/secondary and tertiary-alkoxyl adducts. With the application of the lipid systems in the skin the relative proportion of carbon-centred adducts increased and the contribution of RR′NO$^{\bullet}$ radicals decrease drastically.

It is interesting to note the no-contribution of tertiary-alkoxyl adducts in skin sample treated with bicelles containing β-carotene. Additionally, EPR results from tissue treated with bicosomes with and without β-carotene exhibited a low contribution for the hydroxyl radical–adducts.

After irradiation (Table 4), the hydrogen radical adducts did not contribute to the experimental spectra in any case. As before irradiation, in native samples the higher contribution corresponded to the carbon-centred adducts followed by RR′NO$^{\bullet}$ radicals. Again, the radicals with a minor contribution were primary/secondary and tertiary-alkoxyl adducts. When the skin was treated with the lipid systems, the relative contribution of carbon-centred adduct increased and a drastic decrease in the RR′NO$^{\bullet}$ radicals was observed following the same tendency as before irradiation. It is important to emphasize the notable decrease in the contribution of hydroxyl species with the incorporation of β-carotene in both systems after radiation. Besides, a higher contribution of carbon-centred radicals was observed when β-carotene was included in both systems.

Table 3 Relative contribution (%) of the six radical adducts studied on the simulated spectra for different skin samples before UV radiation. (1) Native skin, (2) skin treated with bicelles, (3) skin treated with bicelles with β-carotene, (4) skin treated with bicosomes, (5) skin treated with bicosomes with β-carotene

Skin sample	Primary/secondary alkoxyl radical–adducts	Tertiary alkoxyl radical–adducts	Carbon-centred radical–adducts	Hydroxyl radical–adducts	Hydrogen radical-addcuts	RR′NO$^{\bullet}$ radical–adducts
1	1.3	1.3	58.9	3.6	12.3	22.6
2	0.9	1.2	71.5	4.3	15.0	7.1
3	1.0	0.0	73.0	2.8	15.2	8.0
4	1.6	1.5	78.3	1.4	9.6	7.6
5	0.7	1.2	75.9	1.5	13.2	7.5

Table 4 Relative contribution (%) of the six radical adducts studied on the simulated spectra for different skin samples after UV radiation. (1) Native skin, (2) skin treated with bicelles, (3) skin treated with bicelles with β-carotene, (4) skin treated with bicosomes, (5) skin treated with bicosomes with β-carotene

Skin sample	Primary/secondaryalkoxyl radical–adducts	Tertiary alkoxyl radical–adducts	Carbon-centred radical–adducts	Hydroxyl radical–adducts	Hydrogen radical-adducts	RR′NO$^{\bullet}$ radical–adducts
1	1.4	1.3	54.0	8.5	0.0	34.8
2	2.6	1.6	73.4	9.8	0.0	12.7
3	1.7	2.5	78.1	4.8	0.0	12.9
4	4.6	2.2	69.8	9.2	0.0	14.2
5	3.2	2.2	74.9	5.8	0.0	13.9

Discussion

Bicelle and bicosome characterization

DLS and cryo-TEM experiments indicate that the incorporation of β-carotene induces a slight increase in the size of bicellar systems and bicosomes. The observed increase could be caused by the location of this antioxidant inside the bilayer of the lipid systems. The precise location of β-carotene in other lipid carriers is not yet fully known. Some authors propose that this active is aligned parallel in the central hydrophobic region of the lipid bilayer,[17] and Yamamoto and Bangham propose that β-carotene is aggregated within the lipid bilayer in liposomes.[27] Considering the low solubility in water of β-carotene, the location of the antioxidant in the lipophilic bilayer is expected, promoting an increase in bicelle and bicosome size.

In the formation of bicosomes, the lipid film is hydrated with the initial solution of preformed bicelles. At this step, a portion of the lipids of the bicelles could be incorporated in the external membrane of bicosomes. Therefore, the incorporation of β-carotene at the external bilayer of bicosomes is also expected inducing an increase in bicosome size.

In the same sense, a slight modification in the composition of the initial bicelles during the formation of bicosomes is previsible. This slight modification would explain the increase in the size of bicelles in bicosome systems respect to initial bicelles that we observed by cryo-TEM. Moreover, the strong tendency of bicelles to stack inside the vesicles and free in the medium could be consequence of the mixture of lipids and of the increase in size of these bicelles during the formation of bicosomes. The incorporation of β-carotene could promote even more this effect due to its tendency to increase the size of the systems.

The analysis by DLS of bicellar systems showed a population of large size, which was not appreciable in cryo-TEM. This discrepancy between DLS and cryo-TEM could be associated with the different methodological approaches of both techniques.[28] DLS gives information about the Brownian movement and diffusion coefficient of particles and the size is reported as HD. Cryo-TEM offers a direct visualization of particles and dynamics are not considered.

In DLS measurement large and small particles contribute differently to the intensity of scattered light. Large particles scatter light at a higher intensity than small particles,[29] thus, an analysis by intensity inflates the proportion of large particles. In addition, the apparent population of larges sizes detected by DLS could be due to existence of strong interparticle interaction in the sample.

Some differences were appreciated between the size of discoidal structures measured by DLS and cryo-TEM. In order to appropriate comparison of results from both techniques, the HD of particles was calculated from the dimensions of the discoidal structures visualized by cryo-TEM. According to the literature, HD $\sim$ 0.95 DS where, DS is the diameter of the sphere with the equivalent volume to the disk and HD the hydrodynamic diameter. Obtaining the volume of the disks using the bilayer thickness (5.4 nm) obtained by SAXS in previous work[30] and disks radius measured from microscopy, we can calculate the HD of the particles to compare with the HD obtained in DLS and Mazer equation (eqn (1)). The HD obtained from cryo-TEM was about 14 nm for bicelles and about 17 nm for bicelles with the antioxidant, which agrees fairly well with the HD detected by DLS (12.32 nm for bicelles and 15.80 nm for bicelles with β-carotene). In the same sense, the HD calculated for non-encapsulated bicelles present in bicosomes without the antioxidant (Fig. 3C) was around 20–30 nm and for non-encapsulated bicelles present in bicosomes with β-carotene (Fig. 3D and E) was about 25–40 nm.

Then, we can consider both techniques as complementary studies in the sense that DLS reported average values for the HD and distribution curve and cryo-TEM provided a direct visualization of the sample depicting the structure of the individual aggregates.

In the case of bicosomes, the HD increase with the incorporation of β-carotene is corroborated with the images obtained by cryo-TEM. The great size variety of the aggregates in bicosome systems observed in the images of cryo-TEM agrees with the high PI obtained by DLS. The small size population detected in the sample by DLS could be attributed to the presence of not encapsulated bicelles visualized by cryo-TEM.

It is important to emphasize that bicelles and bicosomes allow the incorporation of the lipophilic molecule β-carotene in aqueous solution. This antioxidant is usually formulated in presence of organic solvents and or alcoholic mixtures that have potential harmful effects on the skin.[31] Then our systems allow the topical application of this antioxidant preventing the use of aggressive agents in skin.

EPR measurements

DMPO stability under UV radiation. DMPO is one of the most frequently employed spin traps in organic and biological chemistry. This fact is mainly due to its solubility in water and in most organic solvents and also to its superior ability to trap oxygen centred radicals compared with nitroso compounds or other nitrones such as, α-phenyl-N-*tert*-butylnitrone (PBN) and α-(4-pyridyl-1-oxide)-N-*tert*-butylnitrone (POBN). The significant advantages over other nitrone spin traps are related to the redox inactivity and to the possible identification of trapped radicals.[32] Nevertheless, DMPO spin trapping can in some instances be problematic due to the appearance of artificial signals derived from their decomposition.

The experiment using the cellulose paper (smoking paper) as support was useful to simulate the amount of DMPO absorbed in the skin, although considering the characteristics of both substrates (cellulose and skin) we assume higher absorption in cellulose than in the skin. Therefore, spectral lines corresponding to the possible decomposition of the spin-trap in the cellulose by UV would be higher than in the skin. The formation of radical–adducts from DMPO oxidation was ruled out considering the strong conditions required for that oxidation process, which are not present in our experiment conditions. These facts allow us to ensure the good stability of the spin-trap and confirming that DMPO-adducts detected in our

experiments derived from reaction of the skin components and not from oxidation or decomposition of DMPO.

Free radical scavenging effect of the lipid systems. Skin is a very susceptible organ to UV radiation. There are many potential targets in the skin layers that may serve as candidates for oxidative damage. These biological sites include lipids, proteins and cellular DNA.[33] Damage to any of these sites may lead to a severe interference with normal functions and might induce pathological processes. Strategies for reducing these processes are being recently developed to prevention of free radical formation instead of the neutralization of formed radicals.[34] This approach is focused by our current research in which lipid systems are used as scavengers of free radical formation in the skin. Both systems have different interaction with the skin, which could influence in the scavenging effect. Previous works have published the penetration mechanism of bicelles through the narrow interlamellar spaces of the SC lipid structure. Bicelles due to their small size are able to penetrate into skin and once there, these nanostructures self-assemble with SC lipids forming new structures inside the tissue that reinforce the barrier function.[12,35,36] Bicosomes exhibits a more complex structural variability than bicelles, thus, other mechanisms of interaction with the skin are considered. In bicosomes, vesicles and free and encapsulated bicelles coexist. Free bicelles of bicosome system would penetrate and exert the reinforcement effect described before. On the other side vesicles, with a size around 200 nm, would not able to penetrate through SC remaining on the skin surface, in a similar way as was described for other lipid vesicles.[37] This fact promotes the formation of a lipid film on the skin surface (visually observed) that could exert a screen-like effect reducing the pass of UV through inner layers and decreasing the formation of free radicals. This combined effect of discoidal structures and spherical vesicles present in bicosomes, could be responsible of the higher scavenging activity of bicosomes comparing with bicelles.

The improvement of the scavenging activity of bicosome systems by incorporation of β-carotene is expected due to the well-known antiradical effect of this antioxidant. This molecule has demonstrated to be efficient against lipid oxidation in different solutions, liposomes, microsomes and also in skin studies working as an inhibitor of peroxidation of these systems and tissues.[17] This fact would avoid or minimize not only the formation of free radicals in the skin, but also the oxidation of bicosome lipids producing an additional enhancement in the antiradical effect of this system.

Other factor that could explain the increased antiradical effect of bicosomes comparing with bicelles is related to the total amount of lipids in both systems. Bicosomes are more concentrated in lipids than bicelles and, if a possible antioxidant effect of lipids is regarding, a higher scavenging activity of bicosomes should be expected. However, the antioxidant effect has only been associated to chemically modified lipids, such as glycosylated lipids.[38] In our experiments standard phospholipids were used, for this reason we do not consider this possibility.

Identification and quantification of the different radicals formed in the skin. Studied pig skin resulted in the detection of at least six different radicals. The signals assigned to primary/secondary and tertiary alkoxyl-adducts could be originated from lipid radicals formed in the skin by oxidation of the lipids of this tissue.[25,26] Additionally, tertiary alkoxyl radicals can also come from low-molecular-weight proteins present in the skin.[26] The signals that we associated to alkoxyl radicals could also be related to sulphur-centred radicals because of the similar splitting of both radicals. Nevertheless, sulphur-centred radicals have a little stability (half-lives <20 ms (ref. 39)) and their detection is highly improbable. Thus, we attribute this signal to alkoxyl radicals. On the other hand, the primary/secondary alkoxyl radicals have splitting similar to peroxyl radicals. However, it has been demonstrated that peroxyl radicals act as intermediates of alkoxyl radicals, which finally are trapped by DMPO.[40] Consequently, we consider only the formation of primary/secondary alkoxyl radicals at this splitting.

Concerning carbon-centred adducts, it is interesting to note that these species have been previously detected in UV irradiated skin and have been ascribed to oxidation of phospholipids.[25,26] Additionally, the carbon-centred radicals have been also detected in irradiated DNA isolated from skin cells and in samples of tryptophan exposed to radiation.[26] This amino acid is present in keratin. Thus, carbon-centred adducts detected in our skin samples could be assigned to different trapped species derived from lipids, DNA, and keratin, all of them present in the skin.

The formation of the DMPO-OH and DMPO-H adducts have been also previously observed in the skin.[25,26] Those studies showed that the signal of both adducts could be ascribed to riboflavin (vitamin B2), DNA from skin cells and a variety of skin molecules. In the case of DMPO-H adducts the signals have been also detected in irradiated arginine amino acid, suggesting another origin for these radicals in the skin. The absence of the hydrogen adducts in our spectra after radiation, could be related with the instability of these adducts. Until 2005, the hydrogen radicals had not been detected successfully with DMPO because the low sensibility and stability of the formed adducts.[41] In that work Yoo *et al.* observed the decay of hydrogen radicals after irradiation, which agrees with our results. Therefore, this instability of DMPO-H adducts would explain the lack of this signal after irradiation in our experiments.

It is important to emphasize the contribution of RR′NO$^{\bullet}$ radicals for the fitting of the skin spectra. The RR′NO$^{\bullet}$ radicals exhibit a triplet spectrum only with the splitting for nitrogen atom of DMPO ($a(\mathrm{N}) = 14.52$ G). In general, the different DMPO-adducts formed, have nitrogen and hydrogen splitting. The hydrogen splitting comes from the hydrogen atom in the beta-position of DMPO adducts, (the same position where the radical is incorporated). Therefore, the lack of hydrogen splitting in RR′NO$^{\bullet}$ radicals indicates the absence of hydrogen atom in this position, suggesting a possible double substitution in the beta-position of DMPO. Likely, any of the detected species could incorporate in this second position, but considering the

steric effects between radicals, this double substitution would be restricted to voluminous radicals.

Usually, ascorbate radical derived from oxidation of endogen vitamin C is observed in human and mouse irradiated skin.[3,20] Given the similarity between skin from these species and porcine skin, the presence of this radical also could be expected in our experiments (two broad lines with g about 2.0052). However, the high symmetry of our spectra indicates that the signal of ascorbate radical is not differentiable in our experiments. The absence of this signal in our spectra could be due to the superimposition of the signals of identified radicals. These six different signals would dominate the spectra, thus, the signal of ascorbate radical would be hindered by the other radical signals.

The carbon-centred adducts display the highest contribution in simulated spectra of skin samples before and after irradiation. This fact would be related to the composition of this tissue that is constituted by organic molecules susceptible to form this radical such as was described before. In general, the application of bicelles and bicosomes led to an increase in the contribution of these carbon-centred radicals. It could believe that this increase is due to the alkyl composition of these systems that after irradiation could generate an extra amount of carbon-centred adducts with DMPO. However, this fact only would justify the increase in these adducts after irradiation. From our data we see that this increase is observed even before irradiation. Possibly, the treatment with lipid systems would modify skin permeability (fact demonstrated in previous works[5,12,35,36]) and the spin-trap could be distributed in a different way in treated and native samples. This fact could induce the different relative proportions of the radical–adducts formed before and after treatment.

The relative contribution of RR′NO$^{\bullet}$ radicals after treatments with the lipid systems decreases drastically in both cases before and after irradiation. Again a modification in the skin permeability after treatment could be associated with this fact. This decrease in the proportion of RR′NO$^{\bullet}$ is more noticeable before irradiation and would indicate a neutralization of these radicals present in the sample by effect of our systems. Given that after irradiation this decrease is also observed, a scavenging effect in the formation these radicals could be envisaged. The application of the lipid systems could inhibit the double substitution in DMPO. The inhibition of the double substitution in DMPO and the subsequent decrease in the contribution of RR′NO$^{\bullet}$ radicals entail an increase of free radicals in the medium, and therefore, the possibility of formation of other DMPO adducts. From our results, this increase in the free radicals in medium would induce the formation of additional carbon-centred adducts (the relative proportion of these adducts increases, Tables 3 and 4).

The presence of β-carotene in both systems also increases the contribution of the carbon-centred radicals after irradiation. Some authors propose that β-carotene acts by addition to double bond to give carbon-centred radicals. Moreover, in the study of its oxidation products, carbonyl compounds were found.[16,17] Thus, this fact would corroborate the higher contribution of carbon-centred radicals in presence of β-carotene after irradiation obtained in our results.

Experimental section

Materials

Bicelles were formed using 1,2-dipalmitoyl-*sn-glycero*-3-phosphocholine (DPPC) and 1,2-dihexanoyl-*sn-glycero*-3-phosphocholine (DHPC) purchased from Avanti Polar Lipids (Alabaster, USA). Bicosomes were formed using Cholesterol (CHO) obtained from Sigma-Aldrich (Sto Louis, MO, USA) and Lipoid S-100, whose main component (>94%) is phosphatidylcholine (PC). This lipid was obtained from Lipoid GmbH (Ludwigshafen, Germany). β-Carotene and DMPO spin-trap (>98%) were also purchased from Sigma-Aldrich (Sto Louis, MO, USA). Purified water was obtained by an ultra-pure system, Milli-Q plus 185 (Millipore, Bedford, USA). Finally, chloroform was purchased from Merck (Darmstadt, Germany).

Preparation of the lipid systems

Four systems were formed, including bicelles and bicosomes with and without β-carotene. Bicellar system with β-carotene was prepared by mixing appropriate amounts of DPPC, DHPC and β-carotene in chloroform solution to reach a molar ratio of DPPC/DHPC 3.5. After mixing the components, the chloroform was removed with a rotary evaporator, and the system was hydrated with water to reach 5% (w/v) of total lipid concentration and 1 μg ml^{-1} of β-carotene. Bicellar solution was prepared by subjecting the sample to several cycles of sonication and freezing until the sample became transparent.

Bicosomes with β-carotene were prepared mixing 80% of Lipoid S-100 and 20% of cholesterol in chloroform to reach 10% (w/v) of lipid concentration. The chloroform was evaporated with a rotary evaporator until a lipid film was obtained. After, the film was hydrated with the previously formed bicellar systems containing β-carotene. The total lipid concentration in bicosomes with β-carotene was 15% and the concentration of the antioxidant was 1 μg ml^{-1}.

Bicelles and bicosomes without β-carotene were prepared following the same procedure with the exception of the inclusion of the antioxidant.

Characterization of the lipid systems

Dynamic light scattering (DLS). The hydrodynamic diameter (HD) and polydispersity index (PI) were determined at 25 °C using a Zetasizer nano ZS90 (Malvern Instruments, UK). This instrument employs DLS technique to determine the particle size between 1 nm and 3 μm. DLS measures the diffusion coefficient of the particles, which depends on Brownian movement. From the diffusion coefficient the HD was obtained. The PI is a measure of the variability of mean particle size in the dispersion. This index ranges from 0.00 for an entirely monodisperse sample (homogeneous sample) up to 1.00 for a completely polydisperse sample (heterogeneous sample).

Considering that bicelles may display different particle sizes and mainly discoidal morphology, the values of the particle size obtained with this technique are considered an estimation of the dimensions of the structures. To more accuracy of results, we adopted a model for the discoidal morphology and converted the

apparent hydrodynamic radius into a disk radius (see equation below). This type of model was used in early studies about bile salt/lecithin systems[42] and has lately been adopted to interpret the structure of the bicelles.[43] In previous papers we also used this approximation in the study of bicellar systems by DLS.[9,11]

$$RH = \frac{3r}{2\left(\left[1+(t/2r)^2\right]^{1/2} + \left[2r/t\,\ln\left[1+(t/2r)^2\right]^{1/2}\right] - t/2r\right)} \quad (1)$$

In which RH is the hydrodynamic radius for spherical shape and r is de hydrodynamic radius for disk shape. For the thickness (t), a fixed value of 5.4 nm based on a previous SAXS work[30] was used.

DLS measurements of each lipid system were performed in triplicate and from each triplicate the mean size of the different populations in the distribution curves were obtained.

Cryo-transmission electron microscopy (cryo-TEM). Bicellar systems and bicosomes with and without β-carotene were visualized by cryo-TEM. Vitrified specimens were prepared using a Vitrobot (FEI Company, Eindhoven, Netherlands). 5–10 μl of sample were placed onto a glow-discharged holey carbon grid. After, the grid was blotted with filter paper, leaving thin sample films spanning the grid holes. The blotted samples were vitrified by plunging the grid into liquid ethane at its freezing point (−183 °C) and stored under liquid nitrogen (LN_2) prior to examination in the microscope. The vitreous sample films were transferred to a microscope Tecnai F20 (FEI Company, Eindhoven, Netherlands) using a Gatan cryotransfer (Barcelona, Spain) cooled with LN_2 to temperature between −170 and −175 °C. The visualization was taken at 200 kV and using low-dose imaging conditions.

For each sample, 10 overview and approximately 30–40 detail electron micrographs were taken.

Preparation of skin samples

Porcine skin from the back of Landrace large white pigs weighing around 60 kg was obtained from the Hospital Clinic of Barcelona (Spain); 2–3 h after the animal was sacrificed for medical experiments following the *Guide for the Care and Use of Laboratory Animals* published by the US National Institutes of Health (Eighth edition, 2011). The skin was washed with water and the dermis of excised skin was removed following the procedure described in literature.[35] Epidermis was cutting in pieces with an area of 25 mm^2 and then, 10 μl of each system were applied. All the skin pieces were from the same animal and have the same thickness. The systems applied were bicelles without β-carotene, bicelles with β-carotene, bicosomes without β-carotene and bicosomes with β-carotene. The treatment was carried out for 1 h incubation at room temperature using three skin pieces covered with aluminium paper for every lipid system. After the incubation time the skin pieces were cleaned with distilled water and then 20 μl of DMPO 5 M in phosphate buffer saline (PBS) were added to the surface of the skin for 20 min. Finally, the excess of DMPO was removed from the skin and samples were washed with distilled water.

EPR measurements

The skin samples untreated and treated with the different lipid systems were put into the quartz tissue cell of EPR spectrometer (EMX-Plus 10/12 Brucker BioSpin spectrometer), with a X-band microwave bridge (~9 GHz) (EMX Premium X), magnet of 10″ (ER073) with a 12 kW (ER083) power supply. Afterwards, skin samples were subjected to electromagnetic radiation for 30 min. The irradiation was performed with a 500 W high pressure Mercury lamp (Oriel) attached to EPR spectrometer at distance of 50 cm. The skin samples were exposed at power density of 147.9 W m^{-2} which corresponded to 12.1% of UV-A, 5.9% UV-B, 3.5% UV-C, 39.9% visible and 38.5% of infrared radiation. This latter was blocked with a water filter, thus, only UV and visible light arrived to skin samples. All measures were performed at room temperature. The temperature in the EPR cavity was measured using a laser thermometer T-637 (Crison Instruments, Alella, Barcelona) with probe Pt-100 immersion (Cat. no: 30.900.971). No temperature variations were detectable during all the experiments. The EPR spectra were obtained before and after irradiation at the measurement conditions showed in Table 5.

Changes in the skin properties during the experiment could disturb the EPR signal. Thus, to check the stability of the skin, a sample with DMPO was located for 1 h in the EPR cavity under conditions described in Table 5, and the EPR signal during this period was evaluated. Given that no changes in the structure and in the composition of the registered spectra were observed for 1 h, we assume the stability of the skin at the experimental conditions.

From the obtained spectra, the second integration of the signal was calculated. This integration value is directly correlated to the proportion of created free radicals in the skin.[19] In this work, the second integration value was used to compare the scavenging effect of the different lipid systems. Additionally, the integral values allowed us to calculated the radical skin protection factor (RSF, eqn (1)) and the scavenging effectiveness (E, eqn (2)).[3,44]

$$RSF = \frac{(\text{Second Integral value})_{\text{native skin}}}{(\text{Second Integral value})_{\text{treated skin}}} \quad (2)$$

$$\text{If } RSF > 1 = \text{UV protection}$$

Table 5 Spectrometer parameters

Magnetic field	3485 Gauss
Sweep width	100 Gauss
Microwave frequency	9.73 GHz
Microwave power	20.00 mW
Modulation frequency	100 kHz
Modulation amplitude	2 Gauss
Time constant	20.48 ms
Sweep time	41 s

$$E = \frac{(\text{Second Integral value})_{\text{native skin}} - (\text{Second Integral value})_{\text{treated skin}}}{(\text{Second Integral value})_{\text{native skin}}} \quad \text{If } E < 1 = \text{UV protection} \tag{3}$$

In order to check the stability of DMPO against UV radiation, an experiment using cellulose paper (smoking paper) as a support was carried out. The cellulose paper had the same area of the skin samples (25 mm^2). 20 μl of the spin-trap solution were deposited on cellulose paper and non-absorbed solution was removed. Then, the paper was put into the quartz tissue cell of EPR spectrometer. The spectra of the impregnated cellulose were also registered at the same experimental conditions before and after irradiation.

Computer simulation

Processing and computer simulation was carried out using Bruker WIN-EPR System (v 2.22 Rev. 12) and WIN-EPR SimFonia (v 1.26 beta) software. The identification and quantification of the radicals in the simulation are relative. Consequently, it is possible the presence of other radicals than the species proposed in the simulation.

Statistical analysis

Mean and standard deviations were calculated in DLS and EPR experiments. Analysis of variance (ANOVA) with a one-way layout was applied in EPR results to group comparisons. The software used was the STATGRAPHICS plus 5. Significant differences in the mean values were evaluated by the *F*-test. A p value below 0.05 (95% of confidence level) was considered significant.

Conclusions

The new self-assembled lipid nanostructures, bicelles and bicosomes are able to incorporate β-carotene in aqueous solution and are good carriers for skin applications due to they can combine the advantages of disks and vesicles. These nanostructures are promising vehicles to incorporate antioxidants inside the skin, thus, they could be useful to protect the skin against UV radiation. Bicosomes with β-carotene exhibit the best free radical scavenging effect, suggesting a new application of these systems in prevention of free radical formation. In this sense, it would be interesting the possibility to study the reduction of skin damage caused by radiation with the treatment of these lipid systems (in further studies *in vivo*). The use of these lipid systems could be considered as a good strategy for future dermatological formulations focussed on sun protection.

Abbreviations

UV	Ultraviolet radiation
SC	Stratum corneum
DLS	Dynamic light scattering
Cryo-TEM	Cryo transmission electron microscopy
EPR	Electron paramagnetic resonance spectroscopy
DMPO	5,5-Dimethyl-1-pyrroline-N-oxide
DPPC	1,2-Dipalmitoyl-*sn-glycero*-3-phosphocholine
DHPC	1,2-Dihexanoyl-*sn-glycero*-3-phosphocholine
CHO	Cholesterol
PC	Phosphatidylcholine
HD	Hydrodynamic diameter
PI	Polydispersity index
PBS	Phosphate buffer saline
RSF	Radical skin protection factor
E	Scavenging effectiveness
$RR'NO^{\bullet}$	Aminoxyl radicals
DMPO-OH	5,5-Dimethyl-2-oxo-pyrroline-1-hydroxyl
DMPO-H	5,5-Dimethyl-2-oxo-pyrroline-1-hydrogen

Acknowledgements

The authors wish to thank Avencia Díez for technical assistance. This work has supported by funds from CICYT (CQT 2010-16964) and Generalitat de Catalunya (2009 SGR 1212).

References

1 M. Ichihashi, M. Ueda, A. Budiyanto, T. Bito, M. Oka, M. Fukunaga, K. Tsuru and T. Horikawa, *Toxicology*, 2003, **189**, 21–39.
2 K. U. Schallreuter and J. M. Wood, *Free Radical Biol. Med.*, 1989, **6**, 519–532.
3 P. Jurkovic, M. Sentjurc, M. Gasperlin, J. Kristl and S. Pecar, *Eur. J. Pharm. Biopharm.*, 2003, **56**, 59–66.
4 D. A. Bricarello, M. J. Prada and N. Nitin, *Soft Matter*, 2012, **8**, 11144–11151.
5 Z. E. Suntres, *J. Toxicol.*, 2011, 152474–152489.
6 G. M. El Maghraby, A. C. Williams and B. W. Barry, *J. Pharm. Pharmacol.*, 2006, **58**, 415–429.
7 O. A. Ogunsola, M. E. Kraeling, S. Zhong, D. J. Pochan, R. L. Bronaugh and S. R. Raghavan, *Soft Matter*, 2012, **8**, 10226–10232.
8 M. Cocera, G. Rodrıguez, L. Rubio, L. Barbosa-Barros, N. Benseny-Cases, J. Cladera, M. Sabes, F. Fauth, A. de la Maza and O. Lopez, *Soft Matter*, 2011, **7**, 8605–8611.
9 G. Rodriguez, L. Rubio, M. Cocera, J. Estelrich, R. Pons, A. de la Maza and O. Lopez, *Langmuir*, 2010, **26**, 10578–10584.

10 J. Ramos, A. Imaz, J. Callejas-Fernandez, L. Barbosa-Barros, J. Estelrich, M. Quesada-Perez and J. Forcada, *Soft Matter*, 2011, **7**, 5067–5082.
11 G. Rodriguez, G. Soria, E. Coll, L. Rubio, L. Barbosa-Barros, C. Lopez-Iglesias, A. M. Planas, J. Estelrich, A. de la Maza and O. Lopez, *Biophys. J.*, 2010, **99**, 480–488.
12 L. Barbosa-Barros, G. Rodriguez, C. Barba, M. Cocera, L. Rubio, J. Estelrich, C. Lopez-Iglesias, A. de la Maza and O. Lopez, *Small*, 2012, **8**, 807–818.
13 L. Rubio, G. Rodriguez, L. Barbosa-Barros, C. Alonso, M. Cocera, A. de la Maza, J. L. Parra and O. Lopez, *Colloids Surf., B*, 2012, **92**, 322–326.
14 L. Rubio, G. Rodríguez, C. Alonso, C. López-Iglesias, M. Cócera, L. Coderch, A. de la Maza, J. L. Parra and O. Lopez, *Soft Matter*, 2011, **7**, 8488–8497.
15 C. S. Foote and R. W. Denny, *J. Am. Chem. Soc.*, 1968, **90**, 6233–6235.
16 M. N. Sarbolouki, P. Maghdooni Bagheri and V. Sanee, *Daru, J. Pharm. Sci.*, 2005, **13**(4), 148–154.
17 H. Tsuchihashi, M. Kigoshi, M. Iwatsuki and E. Niki, *Arch. Biochem. Biophys.*, 1995, **323**, 137–147.
18 D. Suda, J. Schwartz and G. Shklar, *Carcinogenesis*, 1986, **7**, 711–715.
19 H. K. Kar, *Indian J. Dermatol. Venereol.*, 2003, **69**, 92–94.
20 B. A. Jurkiewicz and G. R. Buettner, *Photochem. Photobiol.*, 1996, **64**, 918–922.
21 E. Fernandez, C. Barba, C. Alonso, M. Marti, J. L. Parra and L. Coderch, *J. Photochem. Photobiol., B*, 2012, **106**, 101–106.
22 P. Bilski, K. Reszka, M. Bilska and C. F. Chignell, *J. Am. Chem. Soc.*, 1996, **118**, 1330–1338.
23 M. Cano, J. Quintana, l. Juliá, F. Camps and J. Joglar, *J. Org. Chem.*, 1999, **64**, 5096–5099.
24 G. R. Buettner, *Free Radical Biol. Med.*, 1987, **3**, 259–303.
25 R. Haywood, F. Rogge and M. Lee, *Free Radical Biol. Med.*, 2008, **44**, 990–1000.
26 R. Haywood, C. Andrady, N. Kassouf and N. Sheppard, *Photochem. Photobiol.*, 2011, **87**, 117–130.
27 H. Y. Yamamoto and A. D. Bangham, *Biochim. Biophys. Acta*, 1978, **507**, 119–127.
28 K. S. Schmitz, *An introduction to dynamic light scattering by macromolecules*, Academic Press, San diego (CA), 1990.
29 H. G. Barth, *Modern methods of particle size analysis*, Wiley Interscience, New york, 1984.
30 L. Barbosa-Barros, A. de la Maza, J. Estelrich, A. M. Linares, M. Feliz, P. Walther, R. Pons and O. López, *Langmuir*, 2008, **24**, 5700–5706.
31 K. Abrams, J. D. Harvell, D. Shriner, P. Wertz, H. Maibach, H. I. Maibach and S. J. Rehfeld, *J. Invest. Dermatol.*, 1993, **101**, 609–613.
32 R. U. Rojas Wahl, L. Zeng, S. A. Madison, R. L. DePinto and B. J. Shay, *J. Chem. Soc., Perkin Trans. 2*, 1998, 2009–2018.
33 M. M. Koan and G. J. Blanchard, *J. Phys. Chem. B*, 2006, **110**, 16584–16590.
34 B. Poljsak, *Oxid. Med. Cell. Longevity*, 2011, **2011**, 194586.
35 G. Rodriguez, L. Barbosa-Barros, L. Rubio, M. Cocera, C. Lopez-Iglesias, A. de la Maza and O. Lopez, *Colloids Surf., B*, 2011, **84**, 390–394.
36 G. Rodriguez, L. Barbosa-Barros, L. Rubio, M. Cocera, A. Diez, J. Estelrich, R. Pons, J. Caelles, A. de la Maza and O. Lopez, *Langmuir*, 2009, **25**, 10595–10603.
37 R. H. Muller, R. D. Petersen, A. Hommoss and J. Pardeike, *Adv. Drug Delivery Rev.*, 2007, **59**, 522–530.
38 R. Zamora, M. M. León and F. J. Hidalgo, *Food Chem.*, 2011, **124**, 1490–1495.
39 M. J. Davies, L. G. Forni and S. L. Shuter, *Chem.-Biol. Interact.*, 1987, **61**, 177–188.
40 S. I. Dikalov and R. P. Mason, *Free Radical Biol. Med.*, 1999, **27**, 864–872.
41 D. H. Yoo, S. K. Han, M. J. Lee and J. W. Kang, *J. Ind. Eng. Chem.*, 2005, **2**, 215–221.
42 N. A. Mazer, G. B. Benedek and M. C. Carey, *Biochemistry*, 1980, **19**, 601–615.
43 K. J. Glover, J. A. Whiles, G. Wu, N. Yu, R. Deems, J. O. Struppe, R. E. Stark, E. A. Komives and R. R. Vold, *Biophys. J.*, 2001, **81**, 2163–2171.
44 T. Herrling and K. Jung, *Int. J. Cosmet. Sci.*, 2012, **34**, 285–290.

ARTÍCULO 4

Advanced lipid systems containing ß-carotene: stability under UV-VIS radiation and application on porcine skin *in vitro*

Physical Chemistry Chemical Physics, 2015*,* **17,** 18710-18721

En este artículo se estudia la estabilidad de las bicelas y los bicosomas con β-caroteno expuestos a radiación UV-VIS. Para ello, ambos sistemas se han caracterizado por DLS y Crio-TEM antes y después de la irradiación. También se ha evaluado la oxidación de los lípidos de las dos nanoestructuras y la oxidación del β-caroteno incluido en los sistemas expuestos a la misma dosis de irradiación. Las técnicas utilizadas para estos dos últimos ensayos son el ensayo del TBA y la espectroscopia de Raman, respectivamente. Por último, se ha aplicado el sistema de bicosomas con β-caroteno en piel normal y piel expuesta a radiación UV-VIS y se ha observado por FSTEM.
La irradiación se aplica mediante un simulador solar (Suntest CPS+) a una intensidad de 500 W/m^2 durante 30 minutos y 2 h (entre 310 y 800 nm).

Los resultados mostraron una conservación del diámetro y de la morfología de los sistemas bicelares con y sin antioxidante frente a radiación UV-VIS. Al contrario, los bicosomas con y sin antioxidante no conservaron su morfología, la vesícula exterior de los bicosomas se rompe agregándose y/o fusionándose con otras vesículas. Como consecuencia, las bicelas encapsuladas en los bicosomas, que mantienen su tamaño y morfología, son liberadas.
Los resultados de la espectroscopia de Raman mostraron que el β-caroteno incluido en ambos sistemas lipídicos se conservó un 95% en los bicosomas y un 10% en la bicelas, mientras que la conservación del antioxidante en liposomas fue del 70% y en solución de cloroformo del 0%. Asimismo, con la misma dosis de irradiación utilizada en los experimentos de Raman, el ensayo del TBA mostró que los lípidos de ambas nanoestructuras no sufren oxidación, por lo tanto, la conservación del β-caroteno en ambos sistemas lipídicos no fue a consecuencia de la oxidación de las moléculas de lípidos de las bicelas y los bicosomas.
Las fotos de microscopia mostraron la presencia de vesículas en el interior de la piel tratada con bicosomas incorporando β-caroteno demostrando la penetración de este

sistema lipídico en la piel. Asimismo, el β-caroteno queda retenido en la piel gracias al bicosoma. Por otro lado, la dosis aplicada de radiación UV-VIS no produjo cambios microestructurales en este tejido.

Por lo tanto, se concluye que la estructura de las bicelas es más resistente a la radiación UV-VIS que la de los bicosomas, mientras que la degradación del β-caroteno por irradiación se evita mejor en bicosomas que en las bicelas y en los liposomas. Por último, las imágenes de microscopia demuestran la capacidad de los bicosomas de penetrar en la piel, hecho que facilitaría la incorporación del β-caroteno en el tejido, lo que convierte a los bicosomas en vehículos prometedores para incorporar activos en la piel.

PCCP

PAPER

Cite this: *Phys. Chem. Chem. Phys.*, 2015, **17**, 18710

Advanced lipid systems containing β-carotene: stability under UV-vis radiation and application on porcine skin *in vitro*†

Estibalitz Fernández,*[a] Gelen Rodríguez,[b] Mercedes Cócera,[b] Lucyanna Barbosa-Barros,[b] Cristina Alonso,[a] Carmen López-Iglesias,[c] Tariq Jawhari,[c] Alfonso de la Maza[a] and Olga López[a]

Received 8th April 2015,
Accepted 10th June 2015

DOI: 10.1039/c5cp02052b

www.rsc.org/pccp

Phospholipid-based nanostructures, bicelles and bicosomes, are proposed as carriers of the antioxidant β-carotene. The stability of these nanostructures and their carotenoid cargo was evaluated in an oxidation environment induced by ultraviolet A, visible and infrared A radiation (UVA-VIS-IRA). Additionally, the effect of these nanoaggregates on non-irradiated and irradiated skin microstructure was studied. The characterization of the lipid systems was performed using dynamic light scattering (DLS) and cryo-transmission electron microscopy (Cryo-TEM) and lipid peroxidation of the systems was determined by thiobarbituric acid (TBARS) assay. Moreover, the stability of β-carotene in these lipid systems under this radiation was investigated using Raman spectroscopy. The results showed that the particle size of the bicelles did not change due to radiation. However, the size of the bicosomes increased slightly after irradiation. The TBARS assay showed the absence of peroxides in the bicelles and bicosomes, indicating the preservation of the lipid molecules under the radiation used. Raman experiments showed that bicosomes protected β-carotene from degradation induced by radiation better than liposomes or dissolution in chloroform. With respect to the skin microstructure, no changes after irradiation were observed *via* freeze substitution transmission electron microscopy (FSTEM). This technique also showed the presence of vesicular structures in the stratum corneum (SC) after treatment with bicosomes.

1. Introduction

Sunlight can severely damage biological structures of skin such as DNA, lipids and proteins.[1,2] It is known that ultraviolet radiation (UV) accelerates skin aging and can cause damage to the barrier function located in the superficial layer of the skin known as the stratum corneum (SC).[1,2] Additionally, visible light (VIS) and infrared radiation (IR) coming from sunlight can also affect the skin.[3,4] In this sense, the topical application of antioxidants or antioxidant mixtures has received much attention to protect skin under radiation.[5,6] However, the use of antioxidants is limited due to their poor solubility and chemical instability. To avoid premature oxidation, these molecules have been encapsulated in different lipid carriers,[7,8] *i.e.*, liposomes, emulsions, and solid lipid nanoparticles.

As a precursor of retinol and retinoic acid, β-carotene is the most extensively studied carotenoid and is an organic and lipophilic antioxidant chemically classified as a hydrocarbon and more specifically as a terpenoid (isoprenoid), with a chain of 40 carbons. This antioxidant has been used orally to treat photosensivity diseases and has proven to be an effective agent for the prevention of cancer when incorporated in diets.[9,10] Moreover, the topical use of β-carotene has been shown to inhibit oral carcinogenesis and skin melasma.[11,12]

Bicelles are described as discoidal nanostructures with diameters of approximately 15–25 nm and a thickness of 5.4 nm formed by long and short alkyl chain phospholipid molecules dispersed in aqueous solution (Fig. 1A).[13,14] Because of their small size and discoidal morphology, bicelles have the ability to

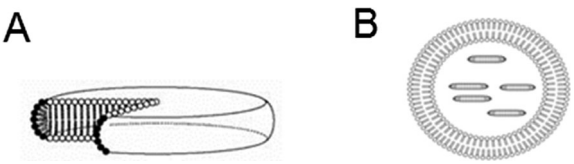

Fig. 1 (A) Bicelle structure and (B) bicosome structure.

[a] *Institute of Advanced Chemistry of Catalonia (IQAC-CSIC), Jordi Girona, Barcelona, 18-26, 08034, Spain. E-mail: efptgt@cid.csic.es; Fax: +34 932 045 904; Tel: +34 934 006 100*
[b] *Bicosome S.L., Barcelona, Spain*
[c] *CCiT Universitat de Barcelona, Barcelona, Spain*

† Electronic supplementary information (ESI) available. See DOI: 10.1039/c5cp02052b

penetrate through the narrow intercellular spaces of the SC (6–10 nm) and reinforce its lipid lamellar structure.[15,16] The bicelle structure also allows the encapsulation of different molecules that can be carried through the skin layers, thus forming a nanosystem with high potential for dermatological applications.[13,17]

However, these nanostructures display structural and morphological dependence on environmental conditions, *e.g.*, in environments with high water content. To maintain the bicelle morphology, these discoidal nanostructures have been encapsulated in liposomes to produce new structures with diameters of approximately around 100–200 nm referred to as ''bicosomes'' (Fig. 1B). Bicosomes protect bicelles from dilution and preserve the discoidal morphology until the target tissue is reached.[18]

The advantages of bicelles and bicosomes over two lipid nanostructures typically used for skin purposes, *i.e.*, liposomes or micelles, are based on the following aspects:

Compared with liposomes, bicelles exhibit diameters of approximately 200 nm, which are sufficiently small to pass through the intercellular space of the SC. Thus, the appropriate size of the bicelles allows better interaction with the skin.

Furthermore, bicosomes combine the advantages of bicelles described previously and a superficial effect on the skin produced by the external bilayer. The superficial effect includes (among other factors) improvement of drug delivery into the skin and fusion with the SC to restore possible injuries to this barrier.[15,19]

Compared with micelles, which usually contain surfactants, bicelles and bicosomes are formed exclusively from lipid molecules, thus avoiding skin irritation promoted by surfactant molecules.

The objective of this work is the evaluation of the stability under a range of UVA-VIS-IRA radiation of bicelles and bicosomes for studying their functionality as beta-carotene vehicles. In this way, the use of a well-known antioxidant such as beta-carotene helps us to determine specific data about stability under radiation and the potential of the lipid systems as stabilizers of this molecule. In addition, the study of the interaction of bicosomes with the skin was also carried out.

Characterization of the systems was performed before and after irradiation by combining dynamic light scattering (DLS) and cryo-transmission electron microscopy (Cryo-TEM). Raman spectroscopy was used to evaluate the oxidation of incorporated β-carotene and a thiobarbituric acid assay (TBARS) was performed to evaluate the possible oxidation of the lipid molecules due to the range of optical radiation used. Finally, the effect of bicosomes with β-carotene on the SC's microstructure of irradiated and non-irradiated skin was investigated using freeze substitution transmission electron microscopy (FSTEM).

2. Experimental

2.1. Materials

Bicellar systems were formed using 1,2-dipalmitoyl-*sn-glycero*-3-phosphocholine (DPPC) and 1,2-dihexanoyl-*sn-glycero*-3-phosphocholine (DHPC) purchased from Avanti Polar Lipids (Alabaster, USA). Bicosomes were formed using Cholesterol (CHO) obtained from Sigma-Aldrich (Sto Louis, MO, USA) and Lipoid S-100 (Ludwigshafen, Germany), whose main component (>94%) is phosphatidylcholine (PC). β-carotene was also purchased from Sigma-Aldrich (Sto Louis, MO, USA) and purified water was obtained from an ultra-pure system, Milli-Q plus 185 (Millipore, Bedford, USA). Chloroform was purchased from Merck.

2.2. Preparation of the lipid systems

Four systems were formed: bicelles with and without β-carotene and bicosomes with and without β-carotene. Moreover, for comparative purposes, a sample of liposomes with incorporated β-carotene was also prepared.

Bicelles with β-carotene were prepared by mixing appropriate amounts of DPPC, DHPC and β-carotene in a chloroform solution to reach a molar ratio of DPPC/DHPC of 3.5 (3.5 mol DPPC/1 mol DHPC). After the components were mixed, the chloroform was evaporated using a rotary evaporator, and the obtained lipid film was hydrated. The bicellar solution was subjected to several cycles of sonication and freezing until the sample became transparent.[14] The total lipid concentration in the bicelles was 5% w/v, and the concentration of β-carotene was 1 μg mL^{-1}, except in those samples prepared for Raman spectroscopy experiments; in these experiments, the concentration of β-carotene was 100 μg mL^{-1}.

Bicosomes with β-carotene were prepared by mixing 80% w/v of Lipoid S-100 and 20% w/v of cholesterol in chloroform. The chloroform was removed using a rotary evaporator until a lipid film was obtained. Afterwards, the film was hydrated using the previously formed bicelles with β-carotene.[17] The total lipid concentration in the bicosomes was 15% w/v, and the concentration of β-carotene was 1 μg mL^{-1}, except in those samples prepared for Raman spectroscopy experiments; in these experiments, the concentration of β-carotene was 100 μg mL^{-1}.

Bicelles and bicosomes without β-carotene were prepared following the same procedures with the exception of the included antioxidant.

The liposomes with incorporated β-carotene for Raman experiments were prepared by mixing appropriate amounts of antioxidant, Lipoid S-100 and cholesterol in chloroform. The chloroform was removed using a rotary evaporator until a lipid film was obtained. Afterwards, the film was hydrated with water. The total lipid concentration in the liposomes was 10% w/v and the concentration of β-carotene was 100 μg mL^{-1}.

2.3. Radiation exposure of skin and lipid systems

The lipid systems and the skin samples were subjected to electromagnetic radiation spectroscopy from 310 nm to 800 nm (UVA from 310–400 nm, VIS from 400–760 nm and a small region of IRA from 760 to 800 nm). The radiation was performed using a light source that simulated solar radiation (Suntest CPS+, Atlas, USA) at 500 W m^{-2} for 30 min and 2 h (90 and 360 J cm^2, respectively). This radiation intensity is equivalent to the radiation exposure for two days in June in Catalonia.[20]

2.4. Characterization of bicelles and bicosomes

2.4.1. Dynamic light scattering (DLS). The sizes of bicelles and bicosomes were measured at 25 °C before and after 30 min

and 2 h of irradiation using detection of the hydrodynamic diameter (HD) *via* a Zetasizer nano ZS90 (Malvern Instruments, UK). The DLS technique measures the diffusion coefficient (D) of the particles due to Brownian motion. The relationship between the size of a particle and its D due to Brownian motion is defined by the Stokes–Einstein equation:

$$\mathrm{HD} = Kt/3\pi\eta' D \quad (1)$$

where HD is the hydrodynamic diameter of a hypothetical hard sphere that diffuses with the same speed as the particle in the experiment, D is the translational diffusion coefficient ($m^2\ s^{-1}$), k is the Boltzmann constant ($1.3806503 \times 10^{-23}$ m kg s $^{-2}$ k^{-1}), t is the absolute temperature (298 K) and η' is the viscosity of the dispersant at 25 °C (water, 0.8872 mPa s).

Considering that bicelles might display different particle sizes and primarily discoidal morphology, the values of the particle size obtained from this technique are considered an estimation of the actual dimensions of these discoidal structures. For additional accuracy of these results, we adopted a model for the discoidal morphology and converted the apparent hydrodynamic radius into a disk radius (see the equation below). This type of model was used in early studies on bile salt/lecithin systems[21] and has been adopted recently to interpret the structure of bicelles.[22] In previous papers we also used this approximation in the study of bicellar systems *via* DLS.[13,18]

$$\mathrm{RH} = \frac{3r}{2\left(\left[1+(t/2r)^2\right]^{1/2} + \left[2r/t\ln\left[1+(t/2r)^2\right]^{1/2}\right] - t/2r\right)} \quad (2)$$

in which RH is the hydrodynamic radius for the spherical shape, and r is the hydrodynamic radius for a disk shape. For the thickness (t), a fixed value of 5.4 nm was used based on a previous SAXS study.[23]

The DLS measurements of each lipid system were performed in triplicate, and the mean size of different populations in the distribution curves was obtained for each triplicate.

2.4.2. Cryo-transmission electron microscopy (Cryo-TEM). The morphologies of bicelles and bicosomes with and without β-carotene were evaluated *via* cryo-TEM before and after 2 h of irradiation. A thin aqueous film was formed by dipping a bare specimen grid (glow-discharged holey carbon grid) in the suspension and withdrawing it from the suspension. After withdrawal from suspension, the grid was blotted against a filter paper, leaving thin sample films that spanned the grid holes. These films were vitrified by plunging the grid into ethane held at its melting point by liquid nitrogen using a Vitrobot (FEI-Company, Eindhoven, Netherlands). The temperature for vitrification was initiated at 20 °C. The vitreous sample films were transferred to a Tecnai F20 microscope (FEI Co., Eindhoven, Netherlands) using a Gatan cryotransfer (Barcelona, Spain). Visualization was carried out at 200 kV at a temperature between −170 °C and −175 °C under low-dose imaging conditions.

For each sample, 10 overviews and approximately 30–40 detailed electron micrographs were collected. The radii obtained from cryo-TEM were calculated using Adobe Photoshop software.

To quantify the data obtained by cryo-TEM, a test square (area = 4 cm^2) was applied to suitable regions of pictures with the same magnification, following the procedure described by Orci *et al.*[24] Using this method, the diameters of discoidal structures (bicelles) and vesicles present in the different systems were quantified from the squares in the cryo-TEM micrographs.

2.5. Lipid peroxidation of bicelles and bicosomes

The lipid peroxidation in the four lipid systems was determined before and after 30 min and 2 h of irradiation *via* thiobarbituric acid assay (TBARS). Malonaldehyde species (MDA), which form under lipid peroxidation, participate in a nucleophilic addition reaction with TBA to generate a red fluorescent malonaldehyde bis(dimethylacetal) adduct (1 : 2 MDA : TBA) at low pH and at high temperature. This adduct was quantified using spectrophotometry at 534 nm, and the obtained absorbance was expressed as MDA:TBA μM using a standard curve for the pure MDA:TBA complex. The calibration curve was obtained using MDA at different concentrations (0–30 μM). The obtained MDA:TBA concentration is proportional to the lipid peroxides present in the sample.

Lipid systems (0.5 mL) were added to aliquots (1 mL) of a solution consisting of 0.4% TBA and 15% trichloroacetic acid (TCA) in 100 mL of an HCl solution (0.25 M). Next, the mixture was incubated in a boiling water bath for 1 h. After the reaction was completed, the samples were filtered and measured using a spectrophotometer (Varian's Cary 300 Bio UV-Vis Spectrophotometer, USA).

The absorbance measurements at 534 nm were performed in triplicate for each lipid system, and an average was calculated from the three obtained absorbance values. The corresponding concentration of the MDA:TBA complex was calculated from the absorbance average at 534 nm.

2.6. Raman spectroscopy

Raman spectroscopy was used to evaluate the degradation of β-carotene under radiation. Raman spectra of the β-carotene incorporated in the bicelles and bicosomes were obtained at room temperature before and after 30 min and 2 h of irradiation using a micro-Raman spectrometer (Labram HR 800, Horiba-Jobin Yvon, France) with a 600 g mm^{-1} grating. For comparative purposes, the stability of the antioxidant against radiation was also measured in chloroform solution and after incorporation into the liposomes. The source used in this study was a solid-state laser emitting at 532 nm, and the power at the sample was fixed at 5 mW. All samples analyzed by Raman microscopy had the same concentration of β-carotene and measurements were obtained directly through the capillary using a long distance microscope objective (50×). All Raman measurements were obtained with an acquisition time of 5 s and an accumulation of 10 spectra, and the baseline correction was applied for all Raman spectra. This procedure was performed in triplicate for each of the samples.

For quantitative analysis, integration of the β-carotene characteristic peaks of Raman spectra (at 1156 and 1523 cm^{-1}) was performed for all samples before and after 30 min and 2 h

of irradiation. The integration value of these peaks is directly proportional to the concentration of β-carotene present in the evaluated sample. Thus, in this work, the integration values of the peaks are useful for comparison of the antioxidant degradation in all samples.

2.7. Skin preparation and treatment with bicosomes

Pig-skin from the backs of large Landrace white pigs weighing approximately 35 kg was obtained from the Universidad Autónoma of Barcelona, Spain. To separate the dermis and epidermis, the excised skin was placed in water at 65 °C for 4–5 min, and the epidermis was scraped off in sheets. The epidermal sheets were cut into pieces each with an area of 25 mm^2. Next, 10 μL of bicosomes containing β-carotene were applied to three skin pieces (only epidermis). After the treatment (18 h) the skin pieces were cleaned with water and prepared for visualization by FSTEM.

We assume that the heating process used to separate dermis and epidermis did not affect skin microstructure. It has been described that thermal treatments, above 80 °C for at least 30 min, are able to induce phase transitions in the SC lipid organization, but these transitions are reversible[25] and temperature and time conditions in our experiments are fairly soft. In addition, X-ray scattering patterns obtained for epidermis and reported by other authors show the preservation of the skin lipids when the epidermis is isolated by the same procedure used in our experiment.[26]

2.8. Freeze-substitution transmission electron microscopy (FSTEM)

The epidermis was cut into approximately 2 mm × 1 mm ribbons. The ribbons were fixed in 5% (w/v) glutaraldehyde in a 0.1 M sodium cacodylate buffer at pH 7.2. Next, the ribbons were post-fixed in 0.2% (w/v) RuO_4 in a sodium cacodylate buffer at pH 6.8 with 0.25% (w/v) potassium ferrocyanide ($K_4Fe(CN)_6$). After 1 h, the RuO_4 solution was replaced with fresh RuO_4 to establish optimal fixation. After rinsing in buffer, the tissue samples were cryofixed by rapid freezing on a liquid nitrogen-cooled metal mirror (Cryovacublock, Leica) at −196 °C prior to freeze-substitution, which was performed using an AFS (Automatic Freeze Substitution) system (Leica). The tissue samples were cryosubstituted at −90 °C for 48 h using 100% methanol containing 1.0% (w/v) osmium tetroxide (OsO_4), 0.5% (w/v) uranyl acetate and 3.0% (w/v) glutaraldehyde. After the 48 h substitution period, the temperature was increased to −50 °C, and the samples were washed three times in 100% methanol. Subsequently, the methanol solution was gradually replaced by the embedding medium of Lowicryl HM20 (100%). This resin was replaced after 24 h and 48 h with freshly prepared embedding medium. Finally, the samples were transferred to a mold containing Lowicryl and were incubated for 48 h at −50 °C under UVA radiation to facilitate polymerization. Ultra-thin sections were cut (Ultracut UCT, Leica), transferred to Formvar-coated grids, and examined using a Hitachi 600 transmission electron microscope.[27] Ten cryofixations and freeze-substitutions were carried out for each sample. Next, one native sample (incubated with Milli-Q water), one sample treated with bicosomes carrying β-carotene, one native sample irradiated for 30 min and one sample treated with bicosomes carrying β-carotene and then irradiated for 30 min were cryofixed and freeze substituted. On an average, 10 overviews and approximately 30–40 detailed electron micrographs for each freeze-substitution process were collected. These micrographs were evaluated by five independent investigators, of which three were blind to the sample treatment.

3. Results

3.1. Characterization of bicelles and bicosomes

The DLS technique was used to characterize the bicelles and bicosomes. The size distribution curves for every lipid system showed two populations with different HDs and light-scattering intensities. The HD corresponds to a hypothetical hard sphere that diffuses with the same speed as the particle under scrutiny, and the percentage intensity represents the proportion of scattered light corresponding to the population obtained.

The HDs for the two populations in samples of bicelles with and without β-carotene were approximately 16 nm and within the range of 1400–2100 nm. The distribution of intensity for the small-size population was approximately 80%, and the value for the large-size population was much lower. In the case of bicosomes with and without the antioxidant, the HDs were in the ranges of 25–50 nm (small size) and between 150–300 nm (large size). The distribution of intensity for the small-size population was approximately 15% and was approximately 85% for the large-size population. In this case, the distribution of intensity was much higher for the large-size population.

The size distribution curves detected in the bicelles and bicosomes are included in the ESI.†

The HD and the intensity of scattered light obtained at 25 °C for different systems before and after irradiation are shown in Table 1. In this table, the size populations of the upper 80% of light scattered are shown.

Before irradiation, the size of the bicellar system without β-carotene was approximately 16 nm with a distribution of intensity of approximately 80%. The incorporation of β-carotene did not promote changes in the size of the bicellar systems, which exhibited a HD of 16 nm and a distribution intensity of 80%. After the application of eqn (2), which allows the approximation of the discoidal dimensions from DLS, the HD for bicelles without and with β-carotene was calculated to be approximately 18 nm. These results are in the range of the diameters obtained from DLS.

The DLS results obtained for bicosomes with and without β-carotene are also shown in Table 1. One peak at approximately 170 nm was observed for bicosomes without β-carotene with a distribution of intensity of 85%. Bicosomes with β-carotene showed one peak at approximately 285 nm with a distribution of intensity of approximately 85%. Thus, the presence of β-carotene promoted an increase of the HD in bicosomes.

After 30 min and 2 h of irradiation, the size of bicelles with and without β-carotene did not show appreciable changes with

Table 1 Mean value and standard deviation of HD and percentage of scattered intensity corresponding to size population at 25 °C before and after irradiation for each lipid system (500 W m^{-2} for 30 min and 2 h). β-carotene concentration in bicelles and bicosomes was 1 μg mL^{-1}

	Before irradiation		After 30 min		After 2 h	
Lipid system	HD (nm)	%Int	HD (nm)	%Int	HD (nm)	%Int
Bicelles	16 ± 0.30	80	17 ± 0.28	87	16 ± 0.15	80
Bicelles + β-carotene	16 ± 0.16	80	17 ± 0.15	82	16 ± 0.23	80
Bicosomes	170 ± 31.00	85	215 ± 30.50	82	430 ± 29.84	80
Bicosomes + β-carotene	285 ± 26.00	85	310 ± 28.50	80	400 ± 27.63	80

respect to the non-irradiated samples. Therefore, we assume that the size of the bicellar systems was maintained regardless of irradiation or addition of β-carotene. A slight increase in size was detected in bicosomes with and without β-carotene after 30 min of irradiation compared with the sizes obtained for these nanostructures before irradiation. After 2 h of irradiation, one peak at approximately 430 nm was observed for bicosomes without β-carotene with a distribution intensity of 80%. Bicosomes with incorporated β-carotene showed one peak at approximately 400 nm with a distribution of intensity of about 80%. Comparing the sizes of these bicosomes before and after 2 h of irradiation, it is interesting to note that the increase in size after irradiation was slightly higher in systems without β-carotene.

In summary, the bicelles maintained their size under irradiation, and in contrast, the size of bicosomes changed in the oxidation environment.

The cryo-TEM technique allowed us to characterize the morphology of the bicelles and bicosomes. A number of images were analysed, and a subset is displayed in Fig. 2A–D. The micrograph of bicellar systems with β-carotene after 2 h of irradiation (Fig. 2A) shows discoidal structures in edge-on (black open arrow) and face-on (white open arrow) dispositions. This figure shows similar structural patterns to the non-irradiated and conventional bicelles published previously.[13,14,17] Thus, in the first examination, no changes were observed in this lipid system due to the incorporation of the antioxidant and due to irradiation.

Fig. 2B and C show bicosome samples without and with β-carotene before irradiation, respectively. In these micrographs, vesicles encapsulated in vesicles (black dotted arrow) and bicelles encapsulated in vesicles (white closed arrow) are observed. Vesicles are visualized as uni-, multi- and oligolamellar structures. The size of the encapsulated bicelles is between 50 nm and 70 nm in bicosomes with and without the antioxidant. Additionally, the tendency of bicelles to form stacks is observed and is more noticeable with the incorporation of β-carotene (black closed arrow).

Fig. 2D shows a micrograph of bicosomes with the antioxidant after 2 h of irradiation. In this image, empty vesicles, vesicles inside vesicles and large structures (black dotted arrow) are observed. Moreover, many free bicelles are observed (black open arrow), suggesting the break-up of the external bilayer of bicosomes that would deliver the internal bicelles. This process could facilitate the aggregation and/or fusion between broken external lipid bilayers, which could be responsible for the large structures detected in DLS.

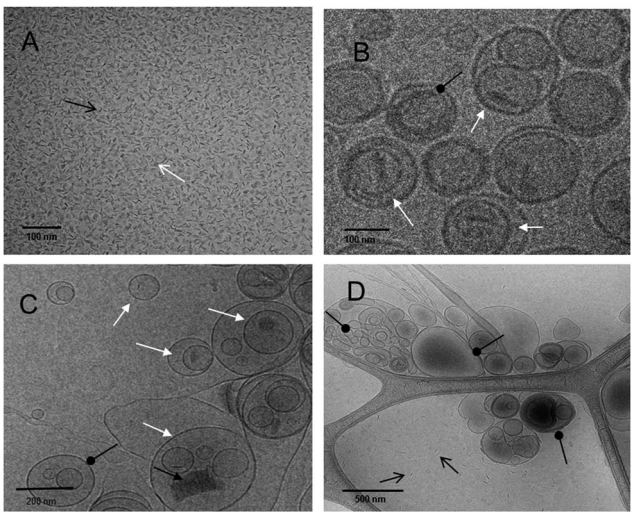

Fig. 2 Cryo-TEM micrographs of bicelles and bicosomes before and after irradiation (500 W m^{-2} for 2 h). (A) Bicelles + β-carotene after irradiation show bicelles face-on (white open arrow) and edge-on (black open arrow). (B) Bicosomes without β-carotene before irradiation show vesicles encapsulated in vesicles (dotted black arrow) and bicelles encapsulated in vesicles (white closed arrow). (C) Bicosomes + β-carotene before irradiation show vesicles encapsulated in vesicles (dotted black arrow), bicelles encapsulated in vesicles (white closed arrow) and bicelles forming stacks (black closed arrow). (D) Bicosomes + β-carotene after irradiation show large structures (black dotted arrow) and free bicelles (black open arrow). The concentration of β-carotene in bicelles and bicosomes was 1 μg mL^{-1}.

To obtain a more representative measure of the dimensions of structures from cryo-TEM, the analysis of micrographs based on a square test described by Orci *et al.* (see the Experimental section) was performed, and the diameters obtained for bicelles without and with β-carotene were 20 nm and 26 nm, respectively. From the analysis of micrographs, bicosomes with mean diameters of 178 nm and 309 nm were obtained for systems without and with the antioxidant, respectively. The analysis of micrographs for bicosomes with β-carotene after 2 h of irradiation showed a mean diameter of 406 nm.

In general, the increase in the size of the nanostructures with the incorporation of β-carotene was more noticeable in the case of bicosomes than in bicelles. Additionally, the irradiation also caused an increase in the size of the bicosomes.

Furthermore, the sizes of bicelles measured by cryo-TEM were larger than those obtained by DLS. In the case of bicosomes, the diameters shown in Fig. 2B–D are in agreement with the results obtained by DLS. An appropriate comparison between dimensions obtained from both techniques involves the

transformation of sizes obtained from cryo-TEM to HD. This data treatment is presented in the Discussion section.

Therefore, we conclude that the strong stability of bicellar systems was maintained under the experimental conditions (incorporation of the antioxidant and irradiation), whereas the bicosome system was unable to maintain its structure after 2 h of irradiation and also suffered an increase in size due to the incorporation of β-carotene.

3.2. Peroxidation of bicelles and bicosomes

Using the TBARS assay the peroxidation of lipids was measured in bicelles and bicosomes with and without β-carotene after 30 min and 2 h of irradiation. The absorbance values obtained at 534 nm are proportional to the MDA:TBA adduct concentration present in the systems, and consequently, these values are proportional to that of the lipid peroxides present in the samples. As a control, this procedure was also performed for non-irradiated bicelles and bicosomes. The lipid concentration in bicelles (5%) was lower than that in bicosomes (15%), and thus, a higher absorbance value is expected at 534 nm in bicosomes than in bicelles.

Fig. 3 shows the absorbance spectra of bicelles (Fig. 3A) and bicosomes (Fig. 3B) before and after 2 h of irradiation.

Bicellar systems without β-carotene showed similar absorbance values at 534 nm before and after irradiation, approximately 0.11 and 0.12, respectively (Fig. 3A). The MDA:TBA adduct concentration corresponding to these absorbance values was 0.05 nM and 0.13 nM before and after irradiation, respectively (Table 2). These two concentrations of the MDA:TBA adduct represent a value lower than 0.00% with respect to the total lipid concentration present in the system. Thus, we do not consider the peroxide formation of lipids from bicelles.

When β-carotene was incorporated into the bicelles, the absorbance values were approximately 0.03 before irradiation and 0.07 after irradiation (Fig. 3A), and the MDA:TBA adduct concentration associated with these absorbance values was 0.00 nM for both absorbance values (Table 2). This result indicated the absence of peroxide molecules in the system formed by bicelles with β-carotene, thus indicating the total preservation of the lipids.

Table 2 Mean and SD of lipid peroxides present in bicelles and bicosomes before and after irradiation (500 W m^{-2} for 2 h). β-carotene concentration in bicelles and bicosomes was 1 μg mL^{-1}

Samples	Before irradiation (nM MDA:TBA)	After 2 h (nM MDA:TBA)
Bicelles	0.05 ± 0.02	0.13 ± 0.02
Bicelles + β-carotene	0.00 ± 0.00	0,00 ± 0.00
Bicosomes	4.47 ± 0.30	5.86 ± 0.40
Bicosomes + β-carotene	3.71 ± 0.20	5.60 ± 0.20

In summary, we conclude that bicellar systems (with and without β-carotene) did not show any formation of peroxide species under the experimental conditions.

Bicosomes without β-carotene showed similar absorbance values of approximately 0.46 and 0.57 before and after irradiation, respectively (Fig. 3A). In addition, the MDA:TBA adduct concentrations were 4.47 nM and 5.86 nM before and after irradiation, respectively (Table 2). When the antioxidant was incorporated, the absorbance values were around 0.40 before irradiation and 0.55 after irradiation, and the MDA:TBA adduct concentrations were 3.71 nM and 5.60 nM before and after irradiation, respectively.

As in the case of bicelles, the obtained concentrations of the MDA:TBA adduct in the bicosomes represent values lower than 0.00% with respect to the total lipid concentration present in the system. Thus, we consider that this irradiation does not induce peroxidation of lipids from bicosomes.

3.3. Raman experiments in bicelles and bicosomes

The Raman spectra of β-carotene in chloroform solution and incorporated in bicelles, bicosomes and liposomes were registered before and after 30 min and 2 h of irradiation (Fig. 4A–D).

The typical Raman spectrum was obtained for β-carotene in chloroform solution and in the different lipid systems before irradiation (Fig. 4A–D, blue spectra).

The three Raman bands of β-carotene can be easily recognized. The Raman peak at 1005 cm^{-1} corresponds to rocking

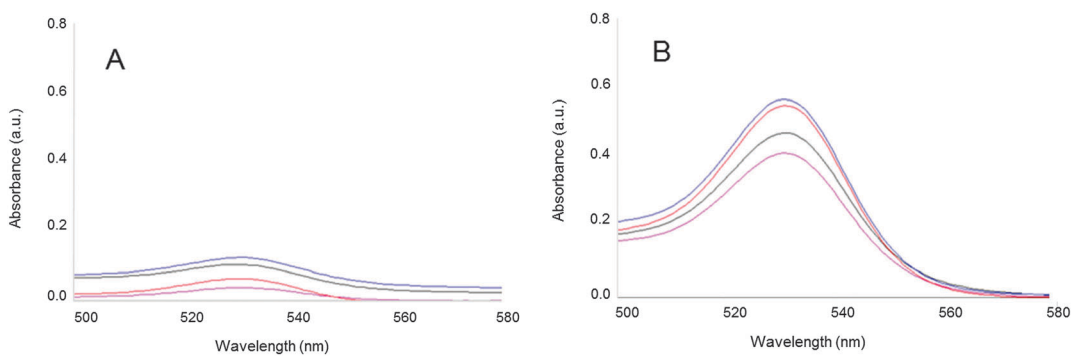

Fig. 3 Lipid peroxidation after irradiation of bicelles and bicosomes represented by the absorbance of the formed MDA-TBA adduct at 534 nm. (A) Non-irradiated bicelles (green line), bicelles after irradiation (blue line), non-irradiated bicelles with β-carotene (violet line) and bicelles with β-carotene after irradiation (red line). (B) Non-irradiated bicosomes (green line), bicosomes after irradiation (blue line), non-irradiated bicosomes with β-carotene (violet line) and bicosomes with β-carotene after irradiation (red line) (500 W m^{-2} for 2 h). All measures were performed at room temperature and at 1 μg mL^{-1} concentration of β-carotene.

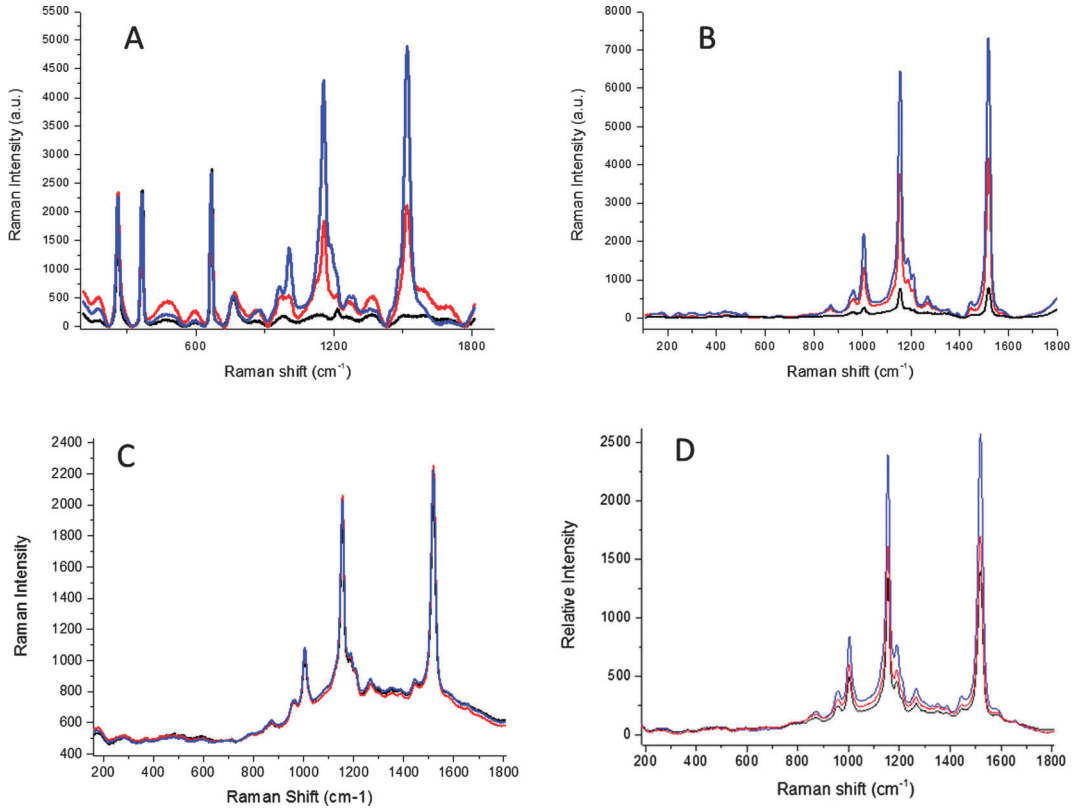

Fig. 4 Raman spectra of β-carotene in chloroform solution (A), incorporated into bicelles (B), incorporated into bicosomes (C) and incorporated into liposomes (D). Before irradiation (blue spectrum), after 30 min of irradiation (red spectrum) and after 2 h of irradiation (black spectrum). Radiation intensity: 500 W m^{-2}. All measures were performed at room temperature and at 100 μg mL^{-1} concentration of β-carotene.

motions of the methyl groups. The strong peaks at 1156 and 1523 cm^{-1} originate from the carbon–carbon single bond and from the double-bond stretch vibrations of the conjugated backbone, respectively.[28] In this section, the comparison between the spectra of the different samples is based on the study of the two strong peaks at 1156 and 1523 cm^{-1}. Additionally, the peaks corresponding to chloroform solvent are clearly observed in Fig. 4A (approximately 200–400 cm^{-1} (two peaks), 700 cm^{-1} (one peak) and 1200 cm^{-1} (one peak)).[29]

After 30 min of irradiation, the chloroform solution of β-carotene showed a decrease in the intensity values of the peaks at 1156 and 1523 cm^{-1} (Fig. 4A, red spectrum) compared with the intensity before irradiation.

Bicellar systems with β-carotene (Fig. 4B, red spectrum) also showed a decrease in the intensity values at 1156 and 1523 cm^{-1} with respect to those shown before irradiation, although the reduction observed in this lipid system was less that observed in the chloroform solution. This observation indicated greater preservation of the antioxidant in the bicelles than in chloroform solution.

In the spectrum obtained for bicosomes with β-carotene the intensity values of the peaks at 1156 and 1523 cm^{-1} were maintained after 30 min of irradiation (Fig. 4C, red spectrum). Nevertheless, the spectrum of liposomes with β-carotene after 30 min of irradiation (Fig. 4D, red spectrum) showed a decrease in the aforementioned intensity values. As in the case of bicellar systems, this decrease was less than that observed in the chloroform solution.

After 2 h of irradiation, the chloroform solution of β-carotene did not show any signal assigned to the antioxidant (Fig. 4A, black spectrum). Consequently, the total degradation of β-carotene under these experimental conditions is assumed.

In the spectrum of bicelles with the antioxidant, a noticeable decrease in the intensity values after 2 h of irradiation was observed with respect to those shown after 30 min of irradiation. However, the detection of the peaks at 1156 and 1523 cm^{-1} indicates the presence of this antioxidant in the system (Fig. 4B, black spectrum). This result indicated the partial preservation of β-carotene.

In the spectrum obtained for bicosomes and liposomes with β-carotene a decrease of the peaks at 1156 and 1523 cm^{-1} was observed with respect to the peaks after 30 min of irradiation (Fig. 4C and D, black spectrum). However, this decrease was lower in the case of bicosomes than that in the case of liposomes. Therefore, the conservation of β-carotene was greater in bicosomes than that in liposomes.

To quantify the degradation of the antioxidant, the integration of the β-carotene characteristic peaks from the Raman spectra (at 1156 and 1523 cm^{-1}) was performed in all samples before and after 30 min and 2 h of irradiation. Next, the percentage of antioxidant conservation was calculated and these values are shown in Table 3. In general, the degradation tendency

Table 3 Percentage of β-carotene preservation incorporated into different lipid systems and chloroform after radiation (500 W m^{-2} for 2 h). β-carotene concentration in bicelles and bicosomes was 100 μg mL^{-1}

Sample	Exposure time at 500 W m^{-2}	β-carotene preservation (%)
Chloroform + β-carotene	0 h	100.00
	30 min	49.63
	2 h	0.00
Bicelles + β-carotene	0 h	100.00
	30 min	57.94
	2 h	10.63
Bicosomes + β-carotene	0 h	100.00
	30 min	100.00
	2 h	94.90
Liposomes + β-carotene	0 h	100.00
	30 min	73.36
	2 h	69.94

obtained for both peaks was the same, and thus, only the data for the peak at 1523 cm^{-1} are shown in Table 3.

After 30 min of irradiation, the highest preservation of β-carotene was observed in the bicosome sample and in fact, the antioxidant was completely preserved. This preservation of the antioxidant was followed by that of the liposomes (approximately 73%) and bicelles (approximately 58%). Additionally, the lowest preservation of the antioxidant was detected in the chloroform solution, where 50% of β-carotene was degraded after 30 min of irradiation.

The same trend was observed after 2 h of irradiation, where 95% of β-carotene was preserved in bicosomes, approximately 70% was preserved in liposomes, and approximately 11% was preserved in bicelles. The antioxidant was completely degraded in chloroform solution after 2 h of irradiation. These results confirm the qualitative analyses obtained from the spectra.

To determine if the reference light of the Raman laser used (532/534 nm) could potentially induce oxidative stress conditions in β-carotene in a similar way to the radiation applied using the solar simulator, a preliminary study was performed. A number of measures were carried out in the same chloroform sample and at the same place of the sample. The results showed similar intensity in characteristic peaks of the β-carotene in the first three measurements, which indicated that the radiation induced by the reference light used in Raman spectroscopy did not produce any damage in the sample. In any case in order to avoid erroneous measurements our final experiments were performed in three different solutions for each sample.

In conclusion, all of the lipids are better able to protect β-carotene under these irradiation conditions than the chloroform solution, and the bicosomes were the most effective vehicle for protecting the antioxidant.

3.4. Effect of bicosomes on the skin microstructure

Micrographs of skin SC under different conditions are shown in Fig. 5A–E.

Panel A shows the native skin. In this micrograph, skin corneocytes (C) with the typical absence of cell organelles were observed. In the space between the corneocytes, lipid bilayers (L) are located, forming the typical lamellar organization of SC

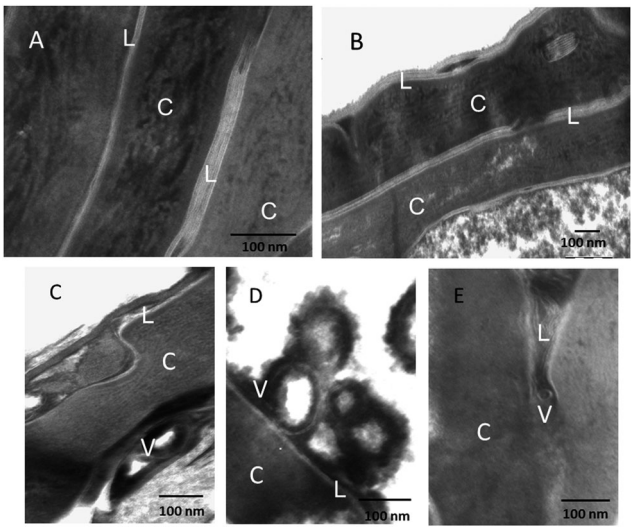

Fig. 5 FSTEM micrographs of (A) native skin, (B) irradiated native skin, (C) and (D) skin treated with bicosomes with β-carotene and (E) irradiated skin treated with bicosomes incorporating β-carotene (500 W m^{-2} for 30 min). The β-carotene concentration in bicosomes was 1 μg mL^{-1}. L: Lipids, C: Corneocyte, and V: Vesicle.

lipids from healthy skin. A sample of irradiated native skin is shown in Fig. 5B, and corneocytes (C) and lipid bilayers (L) were also visualized. This image was quite similar to that of Fig. 5A for native skin. Thus, no microstructural changes were observed after irradiation.

Fig. 5C and D show a SC sample after treatment with bicosomes containing β-carotene. In this image, corneocytes and the intercellular lipid structure are also observed. Additionally, vesicular structures are observed (V) within the lipid lamellae and on the surface of the skin. These vesicles were not observed in Fig. 5A and B, and therefore, these new nanostructures were deemed as a consequence of the treatment with bicosomes.

The micrograph of the skin sample treated with bicosomes carrying β-carotene and after subsequent irradiation is shown in Fig. 5E. No differences in corneocytes (C) or in lipid organization (L) were observed. The presence of vesicles (V) in the skin was also observed as shown in Fig. 5C and D, indicating the possible interaction of the bicosome systems with the skin to form new vesicular structures inside the tissue.

4. Discussion

4.1. Incorporation of β-carotene in bicelles and bicosomes

For the level of incorporation of β-carotene into bicelles and bicosomes, it is important to consider the lipophilic character of β-carotene and that these lipid systems are formed by lipids dispersed in water. Consequently, the incorporation of this molecule into bicelle and bicosome aqueous systems would be possible only if the total amount of β-carotene is incorporated into the lipid fraction of these structures. If any fraction of this antioxidant was not incorporated into the bicelles and bicosomes, amounts of non-dissolved beta-carotene would be present in the solution of both lipid systems.

The β-carotene was completely dispersed in our systems. The solutions were homogeneous and without precipitates, and thus, we assume that the total concentration of β-carotene added to the bicelles and bicosomes was incorporated into these nanoaggregates.

4.2. Effect of β-carotene and irradiation on bicelle and bicosome size

The precise location of β-carotene in lipid bilayers is not yet fully known. Certain studies suggest the location of β-carotene inside the lipophilic region of the lipid bilayer and perpendicular to the alkyl chains of phospholipids.[30] According to these studies and the low solubility in water of β-carotene, the location of this antioxidant in the lipophilic region of the bilayer of bicelles and bicosomes is expected.

The incorporation of β-carotene perpendicular to the alkyl chains of phospholipids, *i.e.*, parallel to the membrane surface, would explain the different effects on the size of bicelles and bicosomes when this antioxidant is included in these systems. Following this hypothesis, β-carotene would be incorporated into a flat membrane of the bicelles and into a curved membrane of the bicosomes. The inclusion in the flat bilayer of bicelles between the two layers of the bilayer (parallel to the membrane surface) should not severely affect the diameter of the discoidal structure of bicelles. However, the same type of inclusion in a curved membrane, *i.e.*, in the external membrane of bicosomes, could flatten this bilayer, which would decrease the curvature radius of bicosomes, and the diameter of the spherical vesicle would increase,[31] as our DLS and cryo-TEM results have shown.

Certain differences were noted between the size of discoidal structures measured by DLS and by cryo-TEM. To appropriately compare the results from both techniques, the HD of the particles was calculated from the dimensions of the discoidal structures visualized by cryo-TEM. According to the literature, HD $\sim$ 0.95 DS,[32] where DS is the diameter of the sphere with an equivalent volume to the disk, and HD is the hydrodynamic diameter. By obtaining the volume of disks using the bilayer thickness (5.4 nm) from SAXS in a previous study[23] and the disk radius measured from microscopy, we can calculate the HD of the particles for comparison with the HD obtained from DLS and eqn (2). The HD obtained from cryo-TEM measurements was approximately 15 nm for the bicelles and approximately 17 nm for the bicelles with β-carotene, values that agree fairly well with the HD detected by DLS (18 nm for bicelles with and without β-carotene and after the application of eqn (1)).

In the case of spherical structures (bicosomes), the diameter obtained from cryo-TEM can be approximated by the dynamic diameter, and it is not necessary to convert the diameter obtained from cryo-TEM to HD.

Next, we consider both techniques as complementary studies in the sense that the DLS reported average values for the HD and distribution curve, and cryo-TEM provided a direct visualization of the sample by depicting the structure of the individual aggregates.

After irradiation, many changes are observed depending on the type of lipid system. According to our DLS and cryo-TEM results, bicelles maintain their dimensions with and without β-carotene after irradiation with higher efficacy than bicosomes.

In general, the lipid bilayer is stabilized by different forces, one of which is the Van der Waals (VDW) interaction, which acts among the lipid chains of adjacent lipid molecules.[33] Saturated lipids have greater tendency to aggregate and form more stable VDW interactions than unsaturated lipids. Hence, saturated lipids form more rigid bilayers.[34] Factors such as application of electromagnetic radiation could destabilize these VDW forces. Given that the proportion of saturated lipids in bicelles is much higher than that in bicosomes (100% in bicelles and 33% in bicosomes) a stronger VDW interaction is expected between the lipids that form bicelles. This observation could be related to the significantly higher resistance of bicelles against these irradiation conditions with respect to bicosomes.

Bicosomes with and without β-carotene exhibited an increase in size after irradiation indicating that the structure of the external bilayer could be affected. This external bilayer is formed from a mixture of different PC molecules enriched in unsaturated lipids. Thus, the VDW forces among the lipid molecules of bicosomes could be weaker than the VDW forces presented in bicelles. As a result, irradiation could generate bilayer breakage, and aggregations or fusions between broken lipid bilayers might form larger structures. This observation would explain the large sizes obtained in bicosomes with and without β-carotene *via* DLS (Table 1) and cryo-TEM after irradiation (Fig. 2D).

4.3. Peroxidation of lipids in bicelles and bicosomes

The Raman experiments show that after 30 min and 2 h of irradiation, the beta-carotene antioxidant is better preserved in bicosomes than in chloroform and liposomes. This preservation could be associated with peroxide formation in the lipids. For this reason, we evaluated the formation of these peroxide species under the same irradiation conditions.

In other words, the objective of this section of the study was to evaluate the relationship between the preservation of beta-carotene and the peroxidation of the lipids.

The TBARS assay is an excellent marker of lipid peroxidation and is commonly used to evaluate the oxidation degree of many lipid systems.[35,36] The oxidation of lipids plays an important role in the preparation and preservation of the lipid-based formulations and can be induced by electromagnetic radiation, among other factors.[33]

The resistance to peroxide formation in bicelles and bicosomes after irradiation could be related to the lipid composition of these systems as well as the experimental conditions used in this study.

Unsaturated lipids are generally more susceptible to oxidation than saturated lipids.[37–39]

Some authors have attributed this observation to the presence of π–π^* electronic transitions arising in molecules that contain C=C bonds (unsaturated lipids), which facilitates the oxidation of these molecules.[37–39] This process would explain the absence of peroxides in bicellar systems. As mentioned previously, bicelles are formed by DPPC and DHPC (both saturated lipids), which are more resistant to oxidative modification due to the absence of double bonds in their alkyl chains.

In the case of bicosomes, the external spherical vesicles are formed primarily by PC and CHOL mixtures. The unsaturated alkyl chains present in PC and CHOL are susceptible to oxidation.[34,37–39] However, under the experimental conditions we did not detect peroxide formation in the bicosomes. It is likely that the irradiation applied was not sufficient to induce peroxide formation. The absence of peroxide formation under these irradiation conditions demonstrates that the preservation of beta-carotene is not due to the peroxidation of the lipid systems.

4.4. Degradation of β-carotene under radiation

The oxidation of β-carotene involves the addition of its double bonds to other molecules. This oxidation mechanism can be avoided *via* biochemical or biophysical processes. A biochemical process would entail that the oxidation of the lipid molecules is present in both lipid systems and would consequently avoid the degradation of β-carotene. However, our results did not show peroxide formation; thus, the preservation of the antioxidant is not a consequence of lipid peroxide species formation.

The preservation of β-carotene could also be attributed to a biophysical process. Recent studies have attributed scattering properties to lipid nanoparticles.[40,41] The scattering of the lipid matrix could play an important role in the photo-protection of incorporated active substances and could prevent the degradation of these active molecules under irradiation. This process would support our results on the preservation of β-carotene incorporated into lipid systems such as bicelles, bicosomes or liposomes. Additionally, the more effective preservation of β-carotene in bicosomes and liposomes than that in bicelles could be due to the higher lipid concentration present in this lipid system.

The location of β-carotene in the lipophilic region of the lipid bilayer could facilitate the conservation of the antioxidant. In this manner, the irradiation that arrives at β-carotene (incorporated in lipid lamellae) would be diminished due to the scattering properties of the lipid systems.

For these reasons, bicosomes have become useful vehicles for preserving antioxidants or other active molecules against radiation.

4.5. Skin microstructure: effect of radiation and interaction with bicosomes

The interaction mechanism between bicosomes and the skin could be understood by considering the different nanostructures present in the system. The bicosomes include spherical vesicles and encapsulated disks (bicelles). The vesicles, with a size of approximately 200 nm, would not be able to penetrate through the SC and would remain on the skin surface in a manner similar to that described for other lipid vesicles with similar sizes.[42] However, the presence of vesicles inside this tissue is observed in the micrographs of our experiments.

Previous studies have shown that bicelles are able to penetrate through the narrow interlamellar spaces of the SC lipid structure. Once incorporated into the SC, bicelles undergo an increase in size due to a dilution effect inside the SC and form a mixture with SC lipids.[13,14] This increase involves a transition from bicelles to vesicles inside the tissue and the detection of new vesicular and lamellar structures inside the SC.[13,14] Once in contact with the skin surface, the external bilayer of the bicosomes could burst and the encapsulated bicelles would be released from inside, acting as free bicelles in the mechanism explained previously. The stacks of bicelles could be separated and would be able to penetrate inside the SC spaces. Therefore, the vesicular structures detected inside the SC tissue visualized in Fig. 4C and E could originate from the bicelles delivered from the external vesicle. Additionally, this penetration mechanism of bicelles would retain the β-carotene molecules inside the tissue.

In conclusion, the advantage of the application of bicosomes instead of bicelles could be related to the presence of a superficial interaction stemming from the external vesicles of bicosomes, which are not able to pass through the SC due to a size of approximately 200–300 nm.

The electromagnetic radiation used in our experiments is based on UVA, VIS and IRA. The negative effect induced by radiation in this range is mainly associated with UV exposure, however, VIS and IR can also affect the skin.[3,4] The damage caused by IRA has been mainly associated with an increase in the temperature, which can reach 43–45 °C. In our experiments the irradiation procedure was performed using a ventilation system, and the skin temperature was maintained at 35 °C avoiding the possible damage produced by IRA radiation.

Concerning the visible light, some authors have demonstrated the reversible damage induced by blue light (380–495 nm) *in vivo* after 100 J cm^{-2}.[3] Other authors showed the formation of free radicals with a combination of UV and VIS light *ex vivo*, and that the influence of UV radiation always dominated this process.

About UV radiation, different studies have described that exposure of skin to this radiation leads to changes in the structure of this tissue depending on the UV range used.[1,43–46] Some authors demonstrated that UVB radiation increases the SC thickness to produce changes in corneocytes and SC lipids. These authors also showed that intercellular lipid cohesion decreased with UVB exposure and reduced the barrier function of SC *in vivo*.[43] The harmful effects of UVA radiation are much fewer than those of UVB radiation.[1] Although UVA can also alter the protein and lipid structure of SC, it is not strongly absorbed by the proteins and lipids and this radiation does not produce structural changes upon moderate exposure. Our results (in which mainly the UVA and VIS source was used) support these facts. No structural changes are observed in SC lipids and proteins from irradiated skin samples regardless of treatment with bicosomes. This outcome is expected considering that UVA radiation-induced damage is mostly located within the dermal compartment,[46] and only epidermis and SC are evaluated in our experiments.

Therefore, the application of UVA (less harmful than UVB) and VIS radiation in our experiments does not modify the skin microstructure. Moreover, it is necessary to note that our experiments were carried out *in vitro*. Obviously, the interaction

of UVA-VIS radiation with skin *in vivo* is highly complex, and many additional factors must be analysed to assess skin damage induced by this radiation. According to our results, the damage associated with microstructural changes could be discarded.

5. Conclusions

The characterization results demonstrate the strong morphological stability of bicelles under UVA-VIS-IRA radiation, whereas bicosome systems undergo changes in structure under the same irradiation conditions. Furthermore, the absence of peroxide formation corroborates the high stability against this radiation of both systems.

The preservation of β-carotene under radiation was reduced by the incorporation of this molecule into lipid systems such as bicelles, bicosomes and liposomes compared with that dissolved in chloroform, likely due to the scattering properties of lipid molecules. The highest preservation of the antioxidant was observed when incorporated into bicosomes.

The images obtained by FSTEM show that bicosome systems are able to penetrate inside the skin following a mechanism similar to that described for bicelles. This ability could entail the retention of β-carotene between lipid layers inside this tissue.

In summary, bicelles and bicosomes have demonstrated utility as lipid carriers and as nanoaggregates that are able to stabilize the antioxidant under irradiation. These nanostructures are promising vehicles in future studies for the incorporation of active molecules into the skin, which would be interesting in future studies with human skin in order to reinforce the antioxidant barrier of this tissue.

Acknowledgements

This work was supported by funds from CTQ 2013-44998-P.

References

1 M. Ichihashi, M. Ueda, A. Budiyanto, T. Bito, M. Oka, K. Ysuru and T. Horikawa, *Toxicology*, 2012, **189**, 21–39.
2 Y. Matsumura and H. N. Ananthaswamy, *Expert Rev. Mol. Med.*, 2002, **4**, 1–22.
3 S. Vandersee, M. Lademann and M. E. Darvin, *Oxid. Med. Cell. Longevity*, 2015, **2015**, 579675.
4 M. Y. Akhalaya, G. V. Maksimov, A. B. Rubin, J. Lademann and M. E. Darvin, *Ageing Res. Rev.*, 2014, **16**, 1–11.
5 J. Lademann, A. Patzelt, S. Schanzer, H. Richter, M. C. Meinke, W. Sterry, L. Zastrow, O. Doucet, T. vergou and M. E. Darvin, *Skin Pharmacol. Physiol.*, 2011, **24**, 269–273.
6 G. Bellemere, G. N. Stamatas, V. Bruere, C. Beertin, N. Isschar and T. Oddos, *Skin Pharmacol. Physiol.*, 2009, **22**, 200–209.
7 S. H. Han, J. S. Lee, Y. J. Kin, J. Kim, I. S. Chang, D. J. Chung, K. D. Suh and J. W. Kim, *Talanta*, 2007, **71**, 2129–2133.
8 Z. E. Suntre, *J. Toxicol.*, 2011, **2011**, 152474.
9 S. T. Mayne, *FASEB J.*, 1996, **10**, 690–701.
10 T. Byers and G. Perry, *Annu. Rev. Nutr.*, 1992, **12**, 139–159.
11 D. Suda, J. Schwartz and G. Shklar, *Carcinogenesis*, 1986, **7**, 711–715.
12 H. K. Kar, *Indian J. Dermatol. Venereol.*, 2003, **69**, 92–94.
13 G. Rodríguez, M. Cócera, L. Rubio, C. Alonso, R. Pons, C. Sandt, P. Dumas, C. López-Iglesias, J. Estelrich, A. de la Maza and O. López, *Phys. Chem. Chem. Phys.*, 2012, **14**, 14523–14533.
14 G. Rodríguez, L. Barbosa-Barros, L. Rubio, M. Cócera, F. Fernández-Campos, A. Calpena, E. Fernández, A. de la Maza and O. López, *J. Biomed. Nanotechnol.*, 2015, **11**, 282–290.
15 G. M. El Maghraby, A. C. Williams and B. W. Barry, *J. Pharm. Pharmacol.*, 2006, **58**, 415–429.
16 D. D. Verma, S. Verma, G. Blume and A. Fahr, *Eur. J. Pharm. Biopharm.*, 2003, **55**, 271–277.
17 L. Rubio, G. Rodríguez, L. Barbosa-Barros, C. Alonso, M. Cócera, A. de la Maza, J. L. Parra and O. López, *Colloids Surf., B*, 2012, **92**, 322–326.
18 G. Rodríguez, G. Soria, E. Coll, L. Rubio, L. Barbosa-Barros, C. López-Iglesias, A. M. Planas, J. Estelrich, A. de la Maza and O. López, *Biophys. J.*, 2010, **99**, 480–488.
19 G. M. El Maghraby, B. W. Barry and A. C. Williams, *Eur. J. Pharm. Sci.*, 2008, **34**, 203–222.
20 J. M. Baldasano, C. Soriano, H. Flores and J. Esteve, in *Atlas de Radiació solar a Catalunya*, ed. A. Press, Institut Català d' Energia, Academic Press, Barcelona, Spain, 2001.
21 N. A. Mazer, G. B. Benedek and M. C. Carey, *Biochemistry*, 1980, **19**, 601–615.
22 K. J. Glover, J. A. Whiles, G. Wu, N. Yu, R. Deems, J. O. Struppe, R. E. Stark, E. A. Komives and R. R. Vold, *Biophys. J.*, 2001, **81**, 2163–2171.
23 L. Barbosa-Barros, A. de la Maza, J. Estelrich, A. M Linares, M. Feliz, P. Walther, R. Pons and O. López, *Langmuir*, 2008, **24**, 5700–5706.
24 L. Orci, A. Perrelet and J. E. Rothman, *Proc. Natl. Acad. Sci. U. S. A.*, 1998, **95**, 2279–2283.
25 C. Ribaud, J. C. Garson, J. Doucet and J. L. Lévêque, *Pharm. Res.*, 1994, **11**, 1414–1418.
26 M. Cócera, G. Rodríguez, L. Rubio, L. Barbosa-Barros, N. Benseny-Cases, J. Cladera, M. Sabés, F. Fauth, A. de la Maza and O. López, *Soft Matter*, 2011, **7**, 8605–8611.
27 B. Van den Bergh, J. Bouwstra, H. Junginger and P. Wertz, *J. Controlled Release*, 1999, **62**, 367–379.
28 M. E. Darvin, I. Gersonde, H. Albrecht, S. A. Gonchukov, W. Sterry and J. Lademann, *Laser Phys.*, 2005, **15**, 295–299.
29 D. Bermejo, R. Escribano and J. M. Orza, *J. Raman Spectrosc.*, 1977, **6**, 151–154.
30 H. P. McNulty, J. Byun, S. M. Lockwood, R. F. Jacob and R. P. Mason, *Biochim. Biophys. Acta*, 2007, **1768**, 167–174.
31 H. J. Risselada and S. J. Marrink, *Phys. Chem. Chem. Phys.*, 2009, **11**, 2056–2067.
32 K. S. Schmitz, *An introduction to dynamic light scattering by macromolecules*, San Diego, CA, 1990, p. 50.
33 B. Maherani, E. Arab-Tehrany, M. R. Mozafari, C. Gainai and M. Linder, *Curr. Nanosci.*, 2011, **7**, 436–452.
34 B. Alberts, A. Johnson, J. Lewis, M. Raff, K. Roberts and P. Walter, *Mol. Biol. Cell*, New York, 2002, ch. 10.

35 T. H. Clark, C. Faustman, W. K. M. Chan, H. C. Furr and J. W. Riesen, *J. Food Sci.*, 1999, **64**, 982–986.
36 V. Paromov, S. Kumari, M. Brannon, N. S. Kanaparthy, H. Yang, M. G. Smith and W. L. Stone, *J. Toxicol.*, 2011, **2011**, 109516.
37 M. H. Brodnitz, *J. Agric. Food Chem.*, 1968, **16**, 994–999.
38 A. Reis and C. M. Spicket, *Biochim. Biophys. Acta*, 2012, **1818**, 2374–2387.
39 T. P. A. Devasagayam, K. K. Boloor and T. Ramasarma, *Indian J. Biochem. Biophys.*, 2003, **40**, 300–308.
40 I. Lacatusu, N. Badea, A. Murariu, D. Bojin and A. Meghea, *Mol. Cryst. Liq. Cryst.*, 2010, **523**, 247–258.
41 G. Niculae, I. Lacatusu, N. Badea, O. Oprea and A. Meghea, *U.P.B. Sci. Bull.*, 2013, **75**, 79–92.
42 R. H. Muller, R. D. Petersen, A. Hommos and J. Pardeike, *Adv. Drug Delivery Rev.*, 2007, **59**, 522–530.
43 S. J. Jiang, J. Y. Chen, Z. F. Lu, J. Yao, D. F. Che and X. J. Zhou, *J. Dermatol. Sci.*, 2006, **44**, 29.
44 D. J. McAuliffe and I. H. Blank, *J. Invest. Dermatol.*, 1991, **96**, 758–762.
45 K. Biniek, K. Levi and R. H. Dauskardt, *Proc. Natl. Acad. Sci. U. S. A.*, 2012, **109**, 17111–17116.
46 F. Bernerd, C. Marionnet and C. Duval, *Indian J. Dermatol. Venereol.*, 2012, **78**(suppl 1), 15–23.

ARTÍCULO 5

A rhenium tris-carbonyl derivative as a model molecule for incorporation into phospholipid assemblies for skin applications

Colloid and Surfaces B: Biointerfaces, 2015, **131**, 102-107

El EC, es el responsable de la función barrera de la piel, y hace muy difícil la penetración de substancias en este tejido. En este trabajo se evalúa la capacidad de los bicosomas para promover la penetración de activos en la piel mediante FTIR usando radiación sincrotrón. Para ello, se escoge una molécula que se pueda distinguir en la piel mediante microscopia IR para incorporarla en los bicosomas. La molécula escogida es un derivado tricarbonílico de Re acoplado a una cadena de 12 carbonos ($C_{12}Re(CO)_3$ deriv.), que muestra vibraciones en la región infrarroja a 1920 y 2020 cm^{-1} y que no interfiere con las vibraciones de IR de la piel.

Además, la penetración del derivado de Re en solución también es estudiada. Para poder evaluar la capacidad de los bicosomas de promover la penetración del derivado de Re y compararlo con un solvente común. Finalmente, el diámetro medio de los bicosomas con y sin el derivado de Re es medido por DLS para evaluar las posibles modificaciones en la estructura del bicosoma al incorporar esta molécula.

La caracterización por DLS mostró un ligero incremento en el diámetro de los bicosomas con la incorporación del derivado de Re. Probablemente la inclusión del derivado de Re en la bicapa de los bicosomas fue la responsable del incremento en el tamaño de este sistema.

Los resultados de FTIR mostraron que un 60% del derivado de Re fue retenido en el EC y que un 40% alcanzó la epidermis (Epi) por medio de los bicosomas. En cambio, cuando el derivado de Re se aplicó a la piel mediante un solvente que potencia la permeabilidad de la piel como el DMSO, un 95% de esta molécula lipofílica quedó retenida en el EC y sólo el 5% alcanzó la Epi.

Por lo tanto, se puede concluir que el derivado del Re utilizado es una molécula útil para estudios de piel mediante FTIR ya que se puede distinguir de las vibraciones de este tejido. Queda demostrado que los bicosomas son vehículos efectivos que

promueven la penetración del derivado de Re, incluso más que un disolvente que potencia la penetración de moléculas en la piel. Además, los resultados obtenidos en este trabajo con el derivado de Re, pueden predecir el comportamiento de otros activos con características físico-químicas similares a esta molécula, al ser aplicados en la piel por medio de los bicosomas.

Colloids and Surfaces B: Biointerfaces 131 (2015) 102–107

Contents lists available at ScienceDirect

Colloids and Surfaces B: Biointerfaces

journal homepage: www.elsevier.com/locate/colsurfb

A rhenium tris-carbonyl derivative as a model molecule for incorporation into phospholipid assemblies for skin applications

Estibalitz Fernández[a,*], Gelen Rodríguez[b], Sarah Hostachy[c], Sylvain Clède[c], Mercedes Cócera[b], Christophe Sandt[d], François Lambert[c], Alfonso de la Maza[a], Clotilde Policar[c], Olga López[a]

[a] Institute of Advanced Chemistry of Catalonia (IQAC-CSIC), Jordi Girona 18-26, 08034 Barcelona, Spain
[b] Bicosome S.L., Jordi Girona 18-26, 08034 Barcelona, Spain
[c] Ecole Normale Supérieure, Rue Lhomond, 75005 Paris, France
[d] Synchrotron SOLEIL, SMIS Beamline, L'Orme des Merisiers, 91190 Saint-Aubin, France

ARTICLE INFO

Article history:
Received 4 March 2015
Received in revised form 7 April 2015
Accepted 20 April 2015
Available online 28 April 2015

Keywords:
Bicosomes
Skin
Fourier-transform infrared spectroscopy
Synchrotron radiation
Rhenium tris-carbonyl complexes

ABSTRACT

A rhenium tris-carbonyl derivative (fac-[$Re(CO)_3Cl$(2-(1-dodecyl-1H-1,2,3,triazol-4-yl)-pyridine)]) was incorporated into phospholipid assemblies, called bicosomes, and the penetration of this molecule into skin was monitored using Fourier-transform infrared microspectroscopy (FTIR). To evaluate the capacity of bicosomes to promote the penetration of this derivative, the skin penetration of the $Re(CO)_3$ derivative dissolved in dimethyl sulfoxide (DMSO), a typical enhancer, was also studied.

Dynamic light scattering results (DLS) showed an increase in the size of the bicosomes with the incorporation of the $Re(CO)_3$ derivative, and the FTIR microspectroscopy showed that the $Re(CO)_3$ derivative incorporated in bicosomes penetrated deeper into the skin than when dissolved in DMSO. When this molecule was applied on the skin using the bicosomes, 60% of the $Re(CO)_3$ derivative was retained in the stratum corneum (SC) and 40% reached the epidermis (Epi). Otherwise, the application of this molecule via DMSO resulted in 95% of the $Re(CO)_3$ derivative being in the SC and only 5% reaching the Epi.

Using a $Re(CO)_3$ derivative with a dodecyl-chain as a model molecule, it was possible to determine the distribution of molecules with similar physicochemical characteristics in the skin using bicosomes. This fact makes these nanostructures promising vehicles for the application of lipophilic molecules inside the skin.

1. Introduction

The topical application of different drugs and active compounds has received significant interest in the medical and pharmaceutical fields. However, the incorporation of molecules in the skin is difficult due to the barrier function of the superficial layer of this tissue, the stratum corneum (SC) [1]. The incorporation of lipophilic molecules is facilitated by their dissolution into intercellular lipids around the cells of the SC [2]. Additionally, lipid vehicles are frequently used to facilitate the incorporation of different active compounds in the skin [2,3].

Bicosomes are phospholipid assemblies based on mixtures of spherical vesicles with diameters of approximately 100–200 nm and discoidal structures with sizes of approximately 15–25 nm in diameter and 5.4 nm in thickness (Fig. 1). In this sense, bicosomes combine the advantages of disks and spherical vesicles [4]. Lipid vesicles have been used in dermatological applications for decades as delivery systems with different active compounds in the skin [5], and discoidal lipid structures have recently demonstrated a significant potential as carriers and modifiers of skin permeability [6,7]. The combination of discoidal and vesicular assemblies forming bicosomes could potentiate the effects of both nanostructures on the cutaneous tissue.

Fourier-transform infrared spectroscopy (FTIR) has been used to evaluate skin composition as well as penetration of different substances in this tissue [8,9]. This technique is employed to investigate the weak energies involved in vibrational levels. The IR spectrum of the skin shows at least three bands associated with different molecules from polypeptides and proteins, as follows: amide A (NH vibration, approximately 3300 cm^{-1}), amide I (CO vibration, approximately 1650 cm^{-1}), and amide II (CN vibration, approximately 1550 cm^{-1}). The bands associated with the alkyl chains

* Corresponding author. Tel.: +34 934 006 100; fax: +34 932 045 904.
E-mail address: efptqt@cid.csic.es (E. Fernández).

http://dx.doi.org/10.1016/j.colsurfb.2015.04.045
0927-7765/

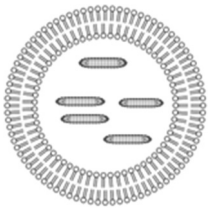

Fig. 1. Bicosome structure.

of skin lipids through the CH_3 and CH_2 stretching vibration are also present (approximately 2920 and 2850 cm^{-1} for asymmetric and symmetric, respectively) [8,9]. Due to the chemical similarity between lipids from different vehicles and skin lipids (both have CH_3 and CH_2 stretching), their characteristic vibrational features cannot be separated. Consequently, in a previous work, the deuteration of lipids from different vehicles was performed to differentiate the vibrations of endogenous (skin lipids) and exogenous lipids [8,9]. This method allowed for the detection of lipids from vehicles in the skin but not the study of the penetration of other active compounds in these lipid systems. An IR active probe with vibrational levels that do not interfere with those from the skin and carrier is needed for this evaluation.

In this work, the use of another type of lipid tagging metal–CO probes that are appropriate for IR imaging is proposed [10–12]. Our research group recently showed that $Re(CO)_3$ is a useful probe for IR and luminescent imaging. These compounds can be used for tagging different molecules, including alkyl chains of various lengths, tamoxifen-like derivatives, oestrogen, or peptides, to image them in cells or tissue using both IR microscopy and fluorescence imaging [13–19]. Interestingly, these $Re(CO)_3$ probes, which are very stable in biological environments, show a very intense signal in the region of 1900–2000 cm^{-1}, that does not interfere with the IR signals from the skin and can be easily quantified [13]. For these reasons, they are the probes of choice for detection and quantification in the IR and have been considered for tagging bicosomes and monitoring their penetrations.

A $Re(CO)_3$ derivative can be attached to several different molecules and provides a way to mark and follow these molecules for skin penetration studies. Recently, a nona-arginine was conjugated with a $Re(CO)_3$ derivative and imaged in skin after permeation [16]. Moreover, the synthesis, sub-cellular imaging and quantification in cells of a $Re(CO)_3$ derivative appended with a $C_{12}N_3$ chain were previously described. In this study, this lipophilic molecule was simultaneously detected using FTIR and fluorescence spectroscopy [13–16,18].

From a spectroscopic point of view, $C_{12}Re(CO)_3$ (Fig. 2) shows a specific vibrational signature with two bands at 1920 cm^{-1} and 2020 cm^{-1}, where no absorption from skin constituents occurs. The first band (E-band at 1920 cm^{-1}) corresponds to asymmetric stretching vibrations, and the second (A_1-band at 2020 cm^{-1}) comes from symmetric stretching vibrations [16,18]. Therefore, this lipophilic molecule can be detected without interference in the skin using FTIR.

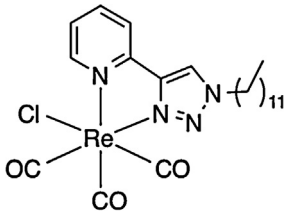

Fig. 2. $C_{12}Re(CO)_3$: (fac-[$Re(CO)_3Cl$(2-(1-dodecyl-1H-1,2,3,triazol-4-yl)-pyridine)]). See synthesis in [10].

In the present study, the lipophilic $C_{12}Re(CO)_3$, which is composed of a $Re(CO)_3$ derivative attached to a dodecyl chain, was used. This lipophilic derivative can be inserted into the bicosome membrane. This strategy enables the study of the penetration and location of this molecule inside the skin and, at the same time, the evaluation of bicosome systems as carriers for the incorporation of lipophilic molecules in the skin.

2. Experimental

2.1. Chemicals

Bicosome systems were formed using 1,2-dipalmitoyl-*sn*-glycero-3-phosphocholine (DPPC) and 1,2-dihexanoyl-*sn*-glycero-3-phosphocholine (DHPC) purchased from Avanti Polar Lipids (Alabaster, Alabama, USA). Cholesterol (CHO) was obtained from Sigma–Aldrich (St. Louis, MO, USA), and Lipoid S-100, whose main component (>94%) is phosphatidylcholine (PC), was obtained from Lipoid GmbH (Ludwigshafen, Germany). The $C_{12}Re(CO)_3$ was synthesized and obtained from the Ecole Normale Supérieure (Paris, France) [13,18]. Chloroform and dimethyl sulfoxide 99% (v/v) (DMSO) were purchased from Merck, and purified water was obtained using an ultra-pure system, Milli-Q plus 185 (Millipore, Bedford, MA, USA).

2.2. Preparation of bicosomes incorporating $C_{12}Re(CO)_3$

Bicosomes incorporating $C_{12}Re(CO)_3$ were prepared by mixing an appropriate amount of DPPC, DHPC and the $Re(CO)_3$ derivative in a chloroform solution to reach a molar ratio of DPPC/DHPC of 3.5. After the components were mixed, the chloroform was evaporated with a rotary evaporator, and the resulting lipid film was hydrated. The resulting solution was subjected to several cycles of sonication and freezing until the sample became transparent.

After that, 80% (w/v) Lipoid S-100 and 20% (w/v) cholesterol in chloroform were mixed and the solvent was removed with a rotary evaporator. The resulting film was hydrated with the previously formed solution [4].

The total lipid concentration in the bicosomes was 15% (w/v) and the concentration of $C_{12}Re(CO)_3$ was 1% (w/v).

The solution in DMSO was prepared by dissolving the appropriate amount of $C_{12}Re(CO)_3$ in DMSO to reach the same concentration as the bicosomes (1%, w/v).

2.3. Dynamic light scattering (DLS)

The sizes of the bicosomes incorporating $C_{12}Re(CO)_3$ were measured by detecting the hydrodynamic diameter (HD) using a Zetasizer nano ZS90 (Malvern Instruments, Malvern, Worcestershire, UK). For comparative purposes, the size of the bicosomes without any incorporated molecule was also measured.

DLS measures the Brownian motion of the particles and correlates this to the particle size. The relationship between the size of a particle and its speed due to Brownian motion is defined by the Stokes–Einstein equation:

$$\mathrm{HD} = \frac{k_B T}{3\pi\eta D}$$

where HD is the hydrodynamic diameter of a hypothetical hard sphere that diffuses with the same speed as the particle in the experiment, D is the translational diffusion coefficient (m^2/s), k_B is the Boltzmann's constant ($1.3806503 \times 10^{-23}$ $J\,K^{-1}$), T is the absolute temperature (K) and η is the viscosity (mPa s) [20].

DLS measurements were performed in triplicate and the mean size and standard deviation (SD) of the different populations in the distribution curves were obtained.

2.4. Preparation of skin samples

Pig skin from the back of a Landrace large white pig weighing around 35 kg was obtained at the Autonomous University of Barcelona (Spain). The skin was removed from the back of the pig minutes after the animal was sacrificed. The animal was sacrificed for medical experimentation in the veterinary faculty of Autonomous University of Barcelona (Spain). The protocols used for these medical studies were approved by the Ethical Commission of Animal and Human Experimentation (Spanish Government) under the auspices of the Ethical Commission of the Autonomous University of Barcelona.

The removed skin was dermatomed to 500 ± 50 μm thick (Dermatome GA630, Aesculap, Tuttlingen, Germany), vacuum packed and stored in a refrigerator. After 18 h, 10 μL of bicosome systems (15%, w/v phospholipids; 85%, w/v water and 1%, w/v $C_{12}Re(CO)_3$) containing $C_{12}Re(CO)_3$ was applied on the skin for 24 h at room temperature (20–25 °C). For comparative purposes and to evaluate the capacity of the bicosomes to promote the penetration capacity of $C_{12}Re(CO)_3$, 10 μL of DMSO solution of this lipophilic molecule was also applied on the skin under the same conditions.

The treatment was performed using three skin pieces for each $C_{12}Re(CO)_3$ solution (bicosomes and DMSO).

The incubation of the skin pieces was performed at room temperature (20–25 °C) on a Petri plate on wet filter paper. Then, the plate was covered with paraffin. Under these conditions, drying of the skin and evaporation of the solvent (DMSO/bicosomes) were avoided. The relative humidity inside the Petri plate was approximately 90%. During the treatment, the hydration and temperature of the skin samples remained constant.

Finally, all skin samples were covered with optimal cutting temperature compound (OCT) and frozen in liquid N_2 before cutting into transverse 6-μm thick sections. The cuts were performed using a Cryostat CM3050 (Leica Biosystems Nussloch, Germany). The different skin sections were placed on CaF_2 circular windows (1 cm in diameter).

Considering that a small fraction of the bicosome/DMSO could flow over the edges of the skin, the slices from the edges of the tissue were removed. Only skin slices from the middles of the pieces were used in the FTIR microspectroscopy.

2.5. FTIR experiments

IR microspectroscopy was performed using synchrotron radiation at the SMIS beamline in synchrotron SOLEIL. Synchrotron radiation was employed because it provides a high spectral quality and produces high contrast chemical imaging. A Thermo Continuum XL IR microscope coupled to an FTIR Nicolet Nexus 5700 spectrometer (Thermo electron corporation, Madison, WI, USA) was employed in these experiments. The microscope is equipped with a 32X/NA 0.65 Schwarzschild objective and matching condenser, a mercury-cadmium-telluride (MCT) type A narrow band detector cooled by liquid nitrogen and an X-Y-Z motorized stage.

Optical micrographs were produced from the microscope in the visible image mode to define the sampling positions. The spectra were acquired at room temperature in transmission mode, in the 3600–1000 cm^{-1} range, and 128 scans were averaged at 4 cm^{-1} resolution. Spectral maps were recorded with an aperture of 10 μm × 10 μm and steps of 10 μm in X and Y.

2.6. Data treatment

To quantify the amount of $C_{12}Re(CO)_3$ in the skin using the FTIR maps, the ratio between the areas under the curves (AUC) of the $C_{12}Re(CO)_3$ vibrations (A_1 and E) and the Amide II skin vibration was calculated. This calculation was performed in all of the maps obtained for skin treated with bicosomes and DMSO solution (approximately 7–9). The mean values and SDs of the ratios were calculated and are presented with error bars. Analysis of variance (ANOVA) was used to determine the significant differences between the ratios obtained from different treatments of $C_{12}Re(CO)_3$ (bicosomes and DMSO) using the Statgraphics plus 5 programme. A *p*-value below 0.05 was considered significant.

Table 1
Mean value of hydrodynamic diameter (HD) and standard deviation (SD) of different bicosomes and proportion of the particle populations analyzed by intensity of light scattered at 25 °C (*N* = 3).

Lipid system	HD ± SD (nm)	%Int
Bicosomes	185 ± 15	85
Bicosomes + $C_{12}Re(CO)_3$	290 ± 10	85

3. Results

3.1. Characterization of bicosomes using DLS

The HDs obtained using DLS at 25 °C for bicosomes incorporating $C_{12}Re(CO)_3$ are shown in Table 1. The HD corresponds to a hypothetical hard sphere that diffuses with the same speed as the particle in the experiment. For comparative purposes, the size of the bicosomes without any incorporated molecules is also shown.

The size of the bicosomes without $C_{12}Re(CO)_3$ was approximately 185 nm with a proportion of light scattered approximately 85%. Incorporation of $C_{12}Re(CO)_3$ led to an increase in the particle size with an HD of approximately 290 nm and 85% light scattered.

The size increase of the bicosomes with the incorporation of $C_{12}Re(CO)_3$ could be due to the location of this lipophilic molecule in the bicosome structure. Considering the low solubility in water of $C_{12}Re(CO)_3$, the location of this molecule in the lipophilic region of the bilayer of the bicosomes is expected. Then, the incorporation of this lipophilic molecule inside the lipid bilayer of the bicosomes would promote a slight increase in the sizes of the nanostructures.

3.2. Distribution of $C_{12}Re(CO)_3$ through the skin

3.2.1. Qualitative analysis

IR spectra of skin samples were recorded in transmission mode in the 3600–1000 cm^{-1} range (Fig. 3). The spectrum for skin samples treated with $C_{12}Re(CO)_3$ incorporated in bicosomes shows bands that are characteristic of skin amides at approximately 3300 cm^{-1} corresponding to NH vibrations (1); at 1660 cm^{-1}, corresponding to CO vibrations (2); and at 1550 cm^{-1} (3). The characteristic CH_3 and CH_2 stretching vibration of lipids is at approximately 2920 cm^{-1} (4) (Fig. 3) [7]. A_1 and E vibration bands of the lipophilic $C_{12}Re(CO)_3$ are detected in the gap between the amide and the CH_3 and CH_2 stretching, which are at 2020 and 1920 cm^{-1} (5, 6), respectively (Fig. 3) [16,18]. In general, the spectra obtained for skin samples treated with $C_{12}Re(CO)_3$ in DMSO

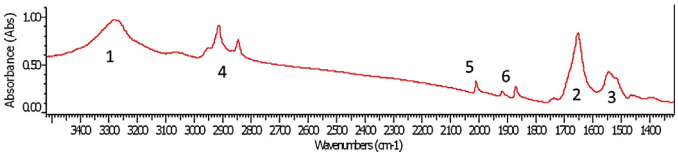

Fig. 3. IR spectra of skin sample treated with bicosomes incorporating $C_{12}Re(CO)_3$ at 1% for 24 h and at room temperature. (1) NH vibration of polypeptides and proteins of the skin, (2) CO vibration of proteins, (3) CN vibration of proteins, (4) CH_3 and CH_2 stretching vibration of skin and bicosome lipids and (5, 6) symmetric and asymmetric stretching vibrations of $C_{12}Re(CO)_3$ (A_1 and E respectively).

showed similar patterns to the spectra obtained for skin samples treated with bicosomes including the lipophilic molecule. These results demonstrate the possibility of detecting this molecule without any interference when it is applied on the skin.

The maps obtained for skin samples treated with $C_{12}Re(CO)_3$ incorporated in bicosomes or dissolved in DMSO are shown in Fig. 4A–D. The micrograph sections show the skin surface, SC and epidermis (Epi). These figures show the distribution of the lipophilic molecule (A_1 and E bands) among the different regions of the skin. The colour scale from blue to red represents the localization of the molecule. The red areas have the highest concentration of $C_{12}Re(CO)_3$, while the lipophilic molecule is not detected in the blue areas. Yellow and green represent areas with intermediate amounts of $C_{12}Re(CO)_3$.

The maps obtained from skin treated with bicosomes tagged with $C_{12}Re(CO)_3$ (Fig. 4A, B) shows the largest fraction of this lipophilic molecule in the SC. Moreover, $C_{12}Re(CO)_3$ is also observed in the Epi, that is, deeper than the SC. Therefore, the incorporation of this lipophilic molecule in bicosomes leads to deeper penetration into the skin. Considering the enhancing properties of DMSO, a significant penetration of $C_{12}Re(CO)_3$ in the skin would be expected when it was incorporated in this solvent [21]. However, the maps obtained for skin treated with the DMSO solution indicate that the largest fraction of the lipophilic molecule did not penetrate into the skin (Fig. 4C, D). $C_{12}Re(CO)_3$ is often localized outside and on the surface of skin slices, indicating poor penetration of this lipophilic molecule into the tissue. Some $C_{12}Re(CO)_3$ was also detected in the Epi, but the overall amount of $C_{12}Re(CO)_3$ in the skin was less in the case of the DMSO solution than in the case of the penetration using the bicosomes.

3.2.2. Quantitative analysis

To quantify the distribution of $C_{12}Re(CO)_3$ throughout the different layers of the skin and to confirm the qualitative evaluation of the results visualized in the maps, the ratios between the AUC of the $C_{12}Re(CO)_3$ bands (A_1 and E) and the Amide II vibration (skin signal) were calculated and compared. Thus, two parameters were obtained: the $AUC_{C_{12}Re(CO)_3,\ A_1}/AUC_{Amide\ II}$ ratio and the $AUC_{C_{12}Re(CO)_3,\ E}/AUC_{Amide\ II}$ ratio. This quantification was performed for all the maps obtained using FTIR (approximately 7–9, including the skin slices shown in Fig. 4A–D), and the mean values and standard deviations (SD) were calculated for each ratio. The Amide II vibration was used as an internal reference (skin reference). Generally, this vibration is constant at different skin depths. Therefore, the ratio between the $C_{12}Re(CO)_3$ and Amide II vibrations enables the estimation of amounts of $C_{12}Re(CO)_3$ retained in the different skin layers after the application of this molecule incorporated in the bicosomes or DMSO.

Fig. 5 shows the $AUC_{C_{12}Re(CO)_3,\ A_1}/AUC_{Amide\ II}$ (A) and $AUC_{C_{12}Re(CO)_3,\ E}/AUC_{Amide\ II}$ (B) ratios obtained for the skin samples treated with $C_{12}Re(CO)_3$ included in the bicosomes or dissolved in DMSO. The total detected amount of $C_{12}Re(CO)_3$ was smaller in the DMSO experiments. The lipophilic molecule dissolved in DMSO was detected outside of the SC and we did not include these values in the quantitative results. Considering the total values of the ratios (ratio in SC + ratio in Epi) the $C_{12}Re(CO)_3$ incorporated

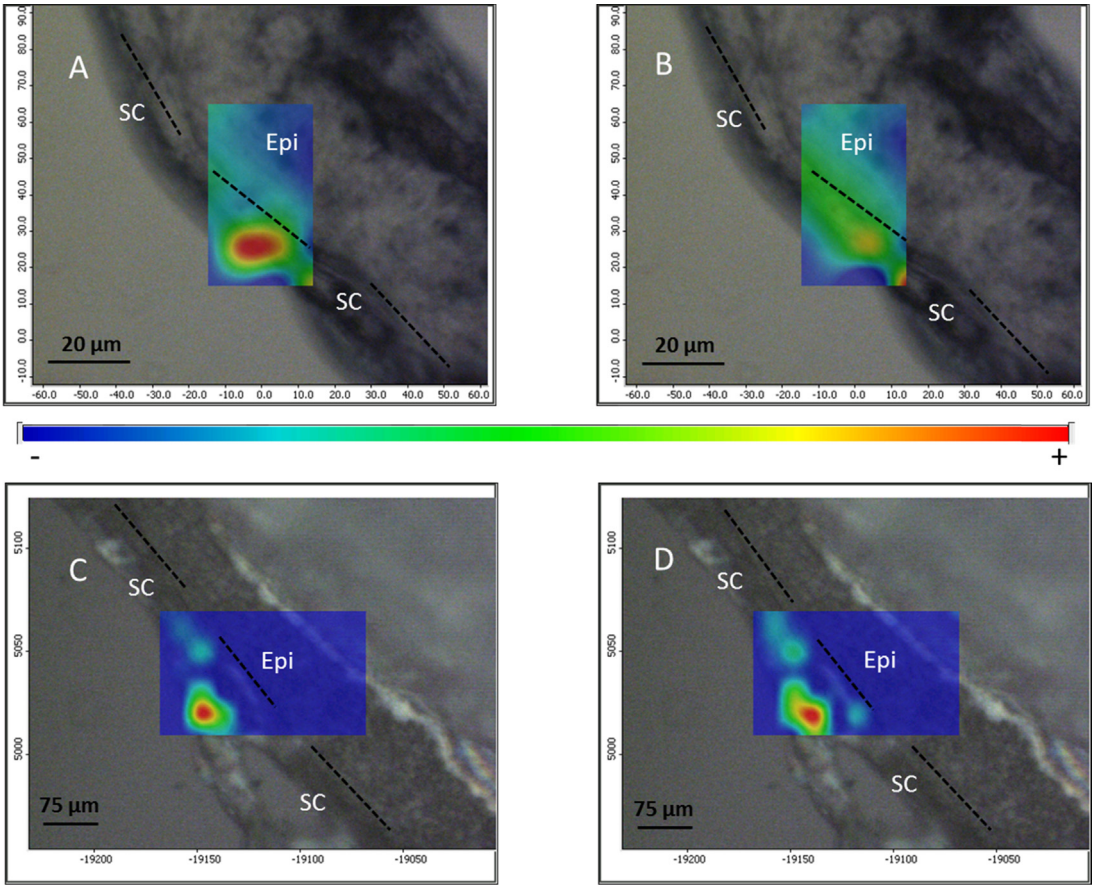

Fig. 4. IR maps obtained from skin samples treated with $C_{12}Re(CO)_3$ incorporated in bicosomes and dissolved in DMSO. (A) $C_{12}Re(CO)_3$ distribution (A_1-band) included in bicosomes, (B) $C_{12}Re(CO)_3$ distribution (E-band) included in bicosomes, (C) $C_{12}Re(CO)_3$ distribution (A_1-band) dissolved in DMSO and (D) $C_{12}Re(CO)_3$ distribution (E-band) dissolved in DMSO. The $C_{12}Re(CO)_3$ scale goes to blue from red, indicating no amount in blue colour and high amount in red colour. The concentration of $C_{12}Re(CO)_3$ is 1% (w/v) in both vehicles.

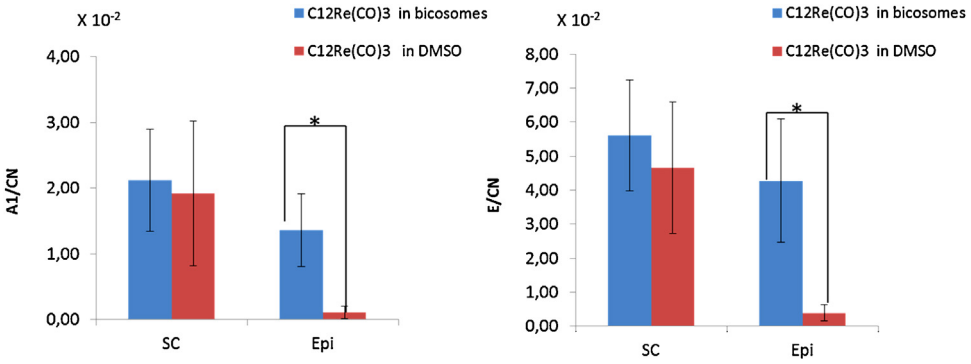

Fig. 5. Mean values and standard deviation (SD) of $AUC_{C_{12}Re(CO)_3,\ A_1}/AUC_{Amide\ II}$ ratio (A) and $AUC_{C_{12}Re(CO)_3,\ E}/AUC_{Amide\ II}$ ratio (B) as a function of penetration depth through the skin (SC and Epi) for $C_{12}Re(CO)_3$ incorporated in bicosomes or dissolved in DMSO ($N = 9$).

in the skin by the bicosomes was approximately twice the amount dissolved in DMSO.

The $AUC_{C_{12}Re(CO)_3,\ A_1}/AUC_{Amide\ II}$ ratios obtained in SC were similar for skin samples treated with the lipophilic molecule incorporated in the bicosomes and dissolved in DMSO (Fig. 5A, SC). In the Epi (Fig. 5A, Epi), the ratio calculated for the skin samples treated with bicosomes was higher that the treated with DMSO. This difference was statistically significant. From the values plotted in Fig. 5A, $C_{12}Re(CO)_3$ is incorporated in the bicosomes, 61% of this lipophilic molecule was retained in the SC and 39% reached the Epi. However, when $C_{12}Re(CO)_3$ was dissolved in DMSO, 95% was retained in the SC and only 5% reached the Epi.

The same trend was observed for the $AUC_{C_{12}Re(CO)_3,\ E}/AUC_{Amide\ II}$ ratios obtained in the SC and the Epi (Fig. 5B). In this case, when $C_{12}Re(CO)_3$ is incorporated in the bicosomes, 57% of this lipophilic molecule was retained in the SC and 43% reached the Epi. When $C_{12}Re(CO)_3$ was dissolved in DMSO, 92% was retained in the SC, and only 8% reached the Epi.

Therefore, we can conclude that only a small amount of the $C_{12}Re(CO)_3$ reached the Epi when it was applied on the skin dissolved in DMSO (approximately 5–8% of the total concentration). However, approximately 40% of this lipophilic molecule reached the Epi when it was applied in the bicosomes. These results are in agreement with the information show in the maps in Fig. 4A, B and clearly indicate the penetration capacity of the lipid system compared with the DMSO solution.

4. Discussion

Although skin has a large surface area, delivery of molecules into this tissue is difficult because the skin acts as a formidable barrier [22]. One of the investigated strategies to enhance drug delivery through skin is the introduction of structural alterations within the skin via the addition of chemical enhancers, such as DMSO, surfactants, fatty acids, alcohols, peptides and other molecules [23–26]. However, the use of chemical enhancers is restricted because these molecules can produce skin irritation and alter skin properties [23].

Liposomes and micellar systems have often been used for skin treatment [5]. Nevertheless, the large size of liposomes (with diameters ranging from 25 nm to several micrometres) as well as the inappropriate composition and elasticity of vesicles make the incorporation of molecules inside the skin using these lipids systems difficult [27]. In addition, the presence of surfactants in micelles usually promotes skin irritation [28].

Bicosomes exhibits a more complex structural variability than liposomes and micelles. In bicosomes, vesicles and free and encapsulated discoidal structures coexist. Spherical vesicles, with a size of approximately 200 nm, would not be able to penetrate through the SC, remaining on the skin surface, in a similar way as described for other lipid vesicles [29]. When in contact with the skin, the bilayer of the external vesicle of the bicosomes bursts, and the encapsulated disks release from the inside. Previous works have published the penetration mechanism of these discoidal structures, called bicelles, through the narrow interlamellar spaces of the SC [7,8]. Due to their small size and thickness, bicelles are able to penetrate into skin. Once incorporated into the SC, they have the ability to increase in size due to a dilution effect inside the SC mixing with SC lipids [7,8]. This increase involves a transition from bicelles to vesicles [4] and promotes the retention of the bicelle components in the skin [7]. This mechanism of penetration-retention would explain the presence of the $C_{12}Re(CO)_3$ in the skin when it was applied in bicosomes. These facts show that bicosome systems are promising vehicles for the incorporation of different molecules inside the skin, including bioactive derivatives [4]. The use of bicosomes facilitates the penetration and retention of bioactive molecules inside the skin. Moreover, the application of this lipid system on skin does not produce any harmful effects on the tissue [5–7]. In this way, these nanoaggregates can be useful carriers for the incorporation of different active compounds inside this tissue to reinforce the skin barrier or treat the tissue.

When $C_{12}Re(CO)_3$ was dissolved in DMSO, this molecule did not penetrate through the spaces of the SC and remained on the skin surface. DMSO is a known enhancer that interacts with skin proteins and lipids to facilitate the transport of hydrophilic and lipophilic molecules [21,23]. The effects of DMSO are concentration dependent. Concentrations of approximately 60% (v/v) are required in the formulation to achieve significant skin penetration enhancement [23]. In our work pure DMSO was used; thus, an enhanced effect of this solvent on the skin should be expected. However, the penetration of $C_{12}Re(CO)_3$ in DMSO was very weak. The incorporation of molecules in the skin depends on their molecular weights and shapes [30]. DMSO has demonstrated its ability to facilitate the penetration of many drugs, such as steroids or antibiotics among others [31–35]. All of them had weights below the molecular weight of $C_{12}Re(CO)_3$ (620 g/mol). This difference in molecular weight could be responsible for the poor penetration of this lipophilic molecule in our skin samples when dissolved in DMSO. In contrast, the differences in our experimental conditions (temperature, pH, application time, type of skin) with respect to the conditions used in other studies could also be responsible for the low penetration of $C_{12}Re(CO)_3$ inside the skin [31–35]. Under these experimental conditions, this lipophilic molecule penetrates at higher concentrations when incorporated in bicosomes than dissolved in DMSO. Therefore, it is important to emphasize the increasing penetration capacity of this lipid system, which is more effective than a typical enhancer molecule, such as DMSO.

5. Conclusions

This work reports the monitoring of the penetration of a model lipophilic molecule into skin in solution and in bicosomes using FTIR. $C_{12}Re(CO)_3$ is a good tag for use in skin because it can be differentiated from the skin vibrations. This fact makes the use of this derivative interesting for skin applications.

The penetration of this lipophilic molecule into the skin is more efficient when incorporated into bicosomes than dissolved in DMSO. The specific interactions between the bicosomes and the skin seem to be responsible for this effect.

The results of the incorporation of $C_{12}Re(CO)_3$ into bicosomes are promising. We suggest the use of bicosomes to promote the penetration of other molecules with similar physicochemical characteristics into skin.

We can conclude that bicosomes are promising vehicles for the incorporation of lipophilic molecules inside skin.

Acknowledgements

The authors wish to thank the Veterinary Faculty of the Universidad Autónoma de Barcelona which was the provider of the pig skin. This work has supported by funds from CTQ 2013-44998-P.

References

[1] P.W. Wertz, Adv. Drug Deliv. Rev. 18 (1996) 283.
[2] P. Desai, R.R. Patlolla, M. Sinngh, Mol. Membr. Biol. 27 (2010) 247.
[3] Z.E. Suntre, J. Toxicol. 2011 (2011) 152474.
[4] G. Rodriguez, G. Soria, E. Coll, L. Rubio, L. Barbosa-Barros, C. Lopez-Iglesias, A.M. Planas, J. Estelrich, A. de la Maza, O. Lopez, Biophys. J. 99 (2010) 480.
[5] B. Maherani, E. Arab-Tehrany, M.R. Mozafari, C. Gaiani, M. Linder, Curr. Nanosci. 7 (2011) 436.
[6] L. Rubio, G. Rodríguez, C. Alonso, C. López-Iglesias, M. Cócera, L. Coderch, A. de la Maza, J.L. Parra, O. López, Soft Matter 78 (2011) 8488.
[7] G. Rodríguez, L. Barbosa-Barros, L. Rubio, M. Cócera, C. López-Iglesias, A. de la Maza, O. López, Colloids Surf. B: Biointerfaces 84 (2011) 390.
[8] G. Rodríguez, M. Cócera, L. Rubio, C. Alonso, R. Pons, C. Sandt, P. Dumas, C. López-Iglesias, A. de la Maza, O. López, Phys. Chem. Chem. Phys. 17 (2012) 14523.
[9] M. Cotte, P. Dumas, M. Besnard, P. Tchoreloff, P. Walter, J. Control. Release 97 (2004) 269.
[10] S. Clède, C. Policar, Chem. Eur. J. 21 (2015) 942.
[11] K.V. Kong, W. Chew, L.H.K. Lim, W.Y. Fan, W.K. Leong, Bioconjug. Chem. 18 (2007) 1370.
[12] K. Meister, J. Niesel, U. Schatzschneider, N. Metzler-Nolte, D.A. Schmidt, Angew. Chem. Int. Ed. 49 (2010) 3310.
[13] S. Clède, F. Lambert, R. Saint-Fort, M.A. Plamont, H. Bertrand, A. Vessières, C. Policar, Chem. Eur. J. 20 (2014) 8714.
[14] C. Policar, J.B. Waern, M.A. Plamont, S. Clède, C. Mayet, R. Prazeres, J.M. Ortega, A. Vessières, A. Dazzi, Angew. Chem. Int. Ed. 50 (2011) 860.
[15] S. Clède, F. Lambert, C. Sandt, S. Kascakova, M. Unger, E. Harté, M.-A. Plamont, R. Saint-Fort, A. Deniset-Besseau, Z. Gueroui, C.J. Hirschmugl, A. Vessières, C. Policar, Analyst 138 (2013) 5627.
[16] S. Clède, N. Delsuc, C. Laugel, F. Lambert, C. Sandt, A. Baillet-Guffroy, C. Policar, Chem. Commun. 51 (2015) 2687.
[17] S. Clède, C. Policar, C. Sandt, Appl. Spectrosc. 68 (2014) 113.
[18] S. Clède, F. Lambert, C. Sandt, Z. Gueroui, M. Réfrégiers, M.A. Plamont, P. Dumas, A. Vessières, C. Policar, Chem. Commun. 48 (2012) 7729.
[19] H.C. Bertrand, S. Clède, R. Guillot, F. Lambert, C. Policar, Inorg. Chem. 53 (2014) 6204.
[20] K.S. Schmitz, An Introduction to Dynamic Light Scattering by Macromolecules, Academic Press, San Diego, CA, 1990.
[21] Z. Yu, P.J. Quinn, Mol. Membr. Biol. 15 (15) (1998) 59.
[22] K.C. Madison, J. Invest. Dermatol. 121 (2003) 231.
[23] A.C. Williams, B.W. Barry, Adv. Drug Deliv. Rev. 56 (2004) 603.
[24] L.B. Lopes, E. Furnish, P. Komalavilas, B.L. Seal, A. Panitch, M.V.L. Bentley, C.M. Brophy, Eur. J. Pharm. Biopharm. 68 (2008) 441.
[25] S. Wang, D. Zeng, J. Niu, H. Wang, L. Wang, Q. Li, C. Li, H. Song, J. Chang, L. Zhang, J. Mater. Chem. B 2 (2014) 877.
[26] J.B. Rothbard, S. Garlington, Q. Lin, T. Kirschberg, E. Kreider, L.P. McGrane, P.A. Wender, P.A. Khavari, Nat. Med. 6 (2000) 1253.
[27] G.M. El Maghraby, A.C. Williams, B.W. Barry, J. Pharm. Pharmacol. 58 (2006) 415.
[28] E. Berardesca, G.P. Vignoli, F. Distante, P. Brizzi, G. Rabbiosi, Contact Dermat. 32 (1995) 83.
[29] R.H. Muller, R.D. Petersen, A. Hommos, J. Pardeike, Adv. Drug Deliv. Rev. 59 (2007) 522.
[30] D. Cobb, J. Orthomol. Med. 25 (2010) 214.
[31] R.B. Stoughton, Arch. Dermatol. 91 (1965) 657.
[32] S.G. Elfbaum, K. Laden, J. Soc. Cosmet. Chem. 19 (1967) 119.
[33] B.M. Tashtoush, S.A. Al-Safi, K.J. Al-Fanek, Pharmazie 59 (2004) 143.
[34] L.H. Reddy, B. Ghosh, Indian J. Exp. Biol. 39 (2001) 47.
[35] B. Kumar, S.K. Jain, S.K. Prajapati, Int. J. Drug Deliv. 3 (2011) 83.

ARTÍCULO 6

Conditional factors in skin permeation of antioxidants using bicosomes

Expert Opinion on Drug Delivery- en revisión

La incorporación de antioxidantes en la piel puede ser beneficiosa para reforzar el sistema antioxidante de este tejido. Sin embargo, para asegurar la eficacia de los antioxidantes en la piel, es necesario que el activo quede incorporado dentro del tejido. En este trabajo se evalúa la penetración en la piel de dos sistemas de bicosomas con antioxidante mediante FTIR usando fuente de radiación sincrotrón. Los antioxidantes utilizados son el β-caroteno y un complejo de Mn. Este complejo de Mn está sintetizado mediante la unión de un ligando (*N-(2-hydroxy-benzyl)-N'-hexadecyl-N,N'-bis-(2-(N-methylimidazolyl)methyl)ethane-1,2-diamine*) a una cadena alquílica de 16 carbonos y ha demostrado su capacidad antioxidante en células.

Para detectar el sistema de bicosoma en la piel mediante FTIR, se incluye un derivado de Re en el sistema lipídico como marcador. Esta molécula es detectable en el espectro IR y sus vibraciones no interfieren con las vibraciones de la piel (tal como se demostró en el artículo 5). Adicionalmente, se estudia la penetración de ambos bicosomas en piel sometida a radiación UV-VIS para poder evaluar la influencia de la irradiación en la permeabilidad de este tejido. La irradiación es aplicada mediante un simulador solar (Suntest CPS+) a una intensidad de irradiación de 500 W/m^2 durante 30 minutos (rango entre 310 y 800 nm).

Los resultados de FTIR mostraron una mayor y más profunda penetración de los bicosomas con complejo de Mn que con los sistemas de β-caroteno. Probablemente las diferentes propiedades físico-químicas de ambos antioxidantes pudieron ser la causa de la diferencia de penetración en la piel. El carácter lipófilo del β-caroteno puede potenciar la retención del sistema en las capas más superficiales de la piel con más contenido lipídico como el EC. Por otro lado, la estructura del complejo de Mn puede darle al bicosoma una parcial hidrofilia que puede arrastrar al bicosoma a capas más profundas de la piel con más contenido de agua, como la Epi.

La penetración de ambos bicosomas en piel irradiada fue notablemente más baja que en piel normal, siendo más afectada la penetración de los bicosomas con el complejo

de Mn. La alteración del transporte de agua producida en la piel por la irradiación pudo ser la causante de que la dispersión acuosa de ambos bicosomas penetre en menor cantidad que en piel normal.

CONDITIONAL FACTORS IN SKIN PERMEATION OF ANTIOXIDANTS USING BICOSOMES

Estibalitz Fernández[*1], Sarah Hostachy[2], Gelen Rodríguez[3], Helene C Bertrand[2], Sylvain Clède[2], Mercedes Cócera[3], Christophe Sandt[4], Alfonso de la Maza[1], François Lambert[2], Clotilde Policar[2] & Olga López[1].

[1]Institute of Advanced Chemistry of Catalonia (IQAC-CSIC), Jordi Girona 18-26, 08034 Barcelona, Spain.

[2]École Normale Supérieure – PSL Research University, Département de Chimie Soborne Universités – UPMC UNIV Paris 06, CNRS UMR 7203 LBM, 24 rue Lhomond, 75005 Paris, France.

[3]Bicosome S.L., Jordi Girona 18-26, 08034, Barcelona, Spain.

[4]Synchrotron SOLEIL, SMIS beamline, L'Orme des Merisiers, 91190 Saint-Aubin, France.

*Corresponding author: Address: IQAC-CSIC, Jordi Girona 18-26, 08034 Barcelona, Spain. Tel.: (34) 934 006 100; fax: (34) 932 045 904.

E-mail address: *efptqt@cid.csic.es* (E. Fernández)

Keywords: Bicosomes, skin, synchrotron radiation, Fourier-Transform Infrared microspectroscopy, β-carotene, Mn complexes.

Abstract

This study evaluates the penetration of bicosome systems incorporating two different antioxidants into normal skin and skin exposed to ultraviolet-visible radiation (UV-VIS) by Fourier-Transform Infrared microspectroscopy (FT-IR) using synchrotron radiation.

Bicosomes are phospholipid assemblies based on mixtures of discoidal lipid structures protected by spherical lipid vesicles able to incorporate different molecules. In the current work, the antioxidants incorporated in these systems were β-carotene and a Mn complex. Additionally, a rhenium tri-carbonyl derivative was incorporated in the bicosome systems in order to map their penetration following the tag specific carbonyl signal by FT-IR microspectroscopy.

The characterization of bicosome systems using dynamic light scattering technique (DLS) showed a decrease in size of the system containing β-carotene (Bcβ). However, the size of the bicosomes containing the Mn^{II} complex (BcMn) increased with the incorporation of this antioxidant.

After skin permeation, FT-IR results indicated a higher and deeper penetration of BcMn system than Bcβ system into the skin. Likely, the different physico-chemical properties of both antioxidants could be responsible of this effect. Moreover, the penetration of both bicosome systems in irradiated skin was lower in comparison with the normal skin. This fact could be a consequence of the alteration of water transport in the skin during the irradiation process.

In conclusion, these results indicated the effectiveness of bicosome systems as skin carriers, and provide information to protect skin under radiation using antioxidants.

ABBREVIATIONS

AUC, area under the curve

Bcβ, bicosomes containing β-carotene

BcMn, bicosomes containing the C_{16}-enPI$_2$-Mn

BcRe, bicosomes containing the $C_{12}ReCO_3$

C_{16}-enPI$_2$-Mn Manganese(II) N-(2-hydroxy-benzyl)-N'-hexadecyl-N,N'-bis-(2-(N methylimidazolyl) methyl) ethane-1,2-diamine

CHO, cholesterol

$C_{12}ReCO_3$, fac-[Re(CO)$_3$Cl(2-(1-dodecyl-1H-1,2,3,triazol-4-yl)-pyridine))]

DCM, dichloromethane

DHPC, 1,2- dihexanoyl-*sn*-glycero-3-phosphocholine

DLS, dynamic light scattering

DPPC, 1,2- dipalmitoyl-*sn*-glycero-3-phosphocholine

Epi, epidermis

FT-IR, Fourier-transform infrared microspectroscopy

HD, hydrodynamic diameter

HEPES, 2-[4-(2-hydroxyethyl)piperazin-1-yl]ethanesulfonic acid

IR, infrared light

PC, phosphatidylcholine

SC, stratum corneum

SD, standard deviation

UV, ultraviolet light

VIS, visible light

1. INTRODUCTION

The absorption of different active compounds into skin can be an efficient strategy to protect normal skin and to treat impaired skin [1]. However, the efficacy of topically applied active compounds on the skin mainly depends on their incorporation in this tissue. Factors such as, the strong barrier function of the skin or the solar exposure can affect the absorption of these actives in this tissue [2, 3]. The use of lipid vehicles to facilitate the incorporation of active compounds in the skin is frequently used to address this problem [4].

Bicosomes are phospholipid assemblies based on mixtures of discoidal lipid structures with diameters of approximately 10-20 nm and a thickness of 5.4 nm (bicelles) protected by spherical lipid vesicles with diameters of approximately 150-250 nm [5]. The bilamellar structure of both aggregates forming bicosomes has been studied in previous works and is represented in Figure 1 [5, 6].

Bicelles are bilayer aggregates with a discoidal shape composed by long and short chain phospholipids, in general 1,2- dipalmitoyl-*sn*-glycero-3-phosphocholine (DPPC) and 1,2- dihexanoyl-*sn*-glycero-3-phosphocholine (DHPC), respectively. The long chain phospholipids form a bilayer section that is surrounded by short-chained phospholipids. Bicelles have recently demonstrated a great potential as carriers and as modifiers of skin permeability, and lipid vesicles have been used in dermatological applications for decades as delivery systems of different actives [4, 7]. The combination of discoidal and vesicular assemblies forming bicosomes potentiates the effects of both nanostructures on the cutaneous tissue, and allows a two-step process of interaction with the skin difficult to achieve with other nanostructures [8].

The purpose of this work was to study the penetration of bicosomes incorporating β-carotene (Figure 2A) and a Mn^{II} complex C_{16}-enPI_2-Mn (Figure 2B) into pig skin by Fourier-Transform Infrared microspectroscopy (FT-IR) using synchrotron radiation

source. The β-carotene has demonstrated antioxidant activity in previous works [9]. Moreover, the Mn^{II} moiety ($enPI_2$-Mn) was shown to be a mimic of superoxide dismutase (or SOD mimics), with an anti-superoxide activity characterized both out of any cellular context and in cells [10]. In the present work, this moiety was conjugated to a lipophilic C_{16} alkyl chain to form the complex C_{16}-$enPI_2$-Mn.

The β-carotene is a lipophilic molecule, while the C_{16}-$enPI_2$-Mn has hydrophilic and lipophilic sites in its structure. The hydrophilic character of the C_{16}-$enPI_2$-Mn comes from the $enPI_2$-Mn moiety, and the lipophilic property comes from the C_{16} alkyl chain. Thus, these two antioxidants could provide to bicosomes different character; lipophilic character incorporating β-carotene and amphiphilic character in the case of C_{16}-$enPI_2$-Mn. They also show a different reactivity, the SOD mimics being active on reactive oxygen species such as superoxide, whereas the β-carotene is known to quench peroxyl radicals. In the present study the penetration of bicosomes incorporating β-carotene (Bcβ system) and bicosomes incorporating the C_{16}-$enPI_2$-Mn (BcMn system) was also studied in irradiated skin in order to evaluate the influence of the radiation in the permeation of both bicosome systems.

The distribution of bicosome systems through the different layers of normal and irradiated skin was evaluated by monitoring the IR signal of a rhenium tri-carbonyl derivative $C_{12}ReCO_3$ (fac-[$Re(CO)_3Cl$(2-(1-dodecyl-1H-1,2,3,triazol-4-yl)-pyridine))]) attached to this lipid system (Fig. 3). Indeed, this probe displays two IR bands around 1920 cm^{-1} and 2020 cm^{-1} for the E vibration and A_1 vibration respectively, and it was used for FT-IR microspectroscopy bio-imaging in cells and tissues. [11-15]. This lipophilic derivative has also demonstrated to be a good probe for skin penetration studies by FT-IR microspectroscopy [16] and it has been used in previous works for evaluating the penetration of bicosome systems [17]. In one of these studies, the penetration of bicosomes tagged by $C_{12}ReCO_3$ was compared to the penetration of this derivative dissolved in a solution of the classical permeation enhancer dimethyl

sulfoxide (DMSO). The results showed a higher penetration of the $C_{12}ReCO_3$ incorporated in the bicosomes. This fact demonstrated the properties of our bicosome systems as penetration enhancer and vector for skin delivery.

2. MATERIALS AND METHODS

2.1. Chemicals

Bicosome systems were formed using 1,2- dipalmitoyl-*sn*-glycero-3-phosphocholine (DPPC) and 1,2- dihexanoyl-*sn*-glycero-3-phosphocholine (DHPC) purchased from Avanti Polar Lipids (Alabaster, USA), cholesterol (CHOL) obtained from Sigma-Aldrich (Sto Louis, MO, USA) and Lipoid S-100, whose main component (>94%) is phosphatidylcholine (PC), purchased from Lipoid GmbH (Ludwigshafen, Germany). Chloroform was purchased from Merck and purified water was obtained by an ultra-pure system, Milli-Q plus 185 (Millipore, Bedford, USA). β-carotene was purchased by Sigma-Aldrich (St. Louis, MO, USA).

The $C_{12}Re(CO)_3$ derivative was synthesized by the École Normale Supérieure (Paris, France) as described previously [11].

The C_{16}-enPI$_2$-Mn was synthetized for this study and we have to include the description of this synthesis in the section 2.1.1. Reagents and chemicals for the synthesis of the C_{16}-enPI$_2$-Mn were purchased from Sigma-Aldrich unless otherwise stated.

2.1.1. Synthesis of the Mn^{II}-SODmimic (C_{16}-enPI$_2$-Mn)

Synthesis of C_{16}-enPI$_2$ ligand (N-(2-hydroxy-benzyl)-N'-hexadecyl-N,N'-bis-(2-(N-methylimidazolyl)methyl)ethane-1,2-diamine) :

enPI$_2$ (73.8 mg, 0.21 mmol, 1.0 equiv.) and hexadecanal (50.0 mg, 0.21 mmol, 1.0 equiv.) were dissolved in EtOH (absolute, 3 mL) and the solution was stirred at room temperature for 2 h. $NaBH_3CN$ (19.7 mg, 0.31 mmol, 1.5 equiv.) and trifluoroacetic acid (TFA) (32.0 mL, 0.42 mmol, 2.0 equiv.) were added and the solution was stirred at room temperature for 2 h. A 1 M aqueous solution of NaOH (3.0 mL) was added, EtOH

was evaporated and dichloromethane (DCM) was added. The pH was adjusted to pH 9 by addition of a 1 M aqueous HCl solution. The aqueous phase was extracted three times with DCM; the organic phase was dried over Na_2SO_4, filtered and evaporated. The residue was purified by column chromatography on silica gel (gradient DCM/MeOH 95:5 to 5:5) to afford C_{16}-enPI$_2$ as a colourless oil (79.0 mg, 66%). enPI$_2$ ligand and hexadecanal were synthesized as previously described [18, 19].

C_{16}-enPI$_2$-Mn was prepared by combining a stock solution of the C_{16}-enPI$_2$ ligand (1 mL at 20 mM in H_2O/ACN 1:1) with an aqueous stock solution of $MnCl_2$ (1 mL at 20 mM, 1.0 equiv.) and 1 mL of 2-[4-(2-hydroxyethyl)piperazin-1-yl]ethanesulfonic acid (HEPES) buffer (100 mM, pH 7.5). The resulting solution was lyophilised to give a powder, which was re-dissolved in 2 mL of H_2O to afford a 10 mM [C_{16}-enPI$_2$-Mn]Cl in a 50 mM HEPES solution.

2.2. Preparation of bicosomes

Two different bicosome systems tagged with the $C_{12}Re(CO)_3$ derivative were formed: Bcβ system and BcMn system.

Bicelles with β-carotene were prepared by mixing appropriate amount of DPPC, DHPC, $C_{12}Re(CO)_3$ derivative and β-carotene in a chloroform solution. Once the components were mixed, the chloroform was evaporated with a rotary evaporator and the obtained lipid film was hydrated. The obtained water dispersion was subjected to several cycles of sonication and freezing until the sample became transparent.

Bicelles with the C_{16}-enPI$_2$-Mn were prepared following the same procedure, but this complex was added in a water solution.

To prepare the bicosome systems appropriate amounts of PC and CHOL were mixed in chloroform. The chloroform was removed with a rotary evaporator until a lipid film

was obtained. Finally, the film was hydrated with the previously prepared bicelle dispersions.

The concentration of each ingredient in the bicosome systems was the following (w/v%): DPPC 4.25%, DHPC 0.75%, $C_{12}Re(CO)_3$ derivative 1%, β-carotene/C_{16}-enPI$_2$-Mn 0.01%, PC: 8% and CHOL 2%.

2.3. Size measurement of bicosomes by dynamic light scattering (DLS)

The hydrodynamic diameter (HD) was determined by means of DLS using a Zetasizer nano ZS90 (Malvern Instruments, UK). The particle sizes were determined by detection and analysis of the scattered light from the 632 nm He/Ne laser beam. Non-invasive back-scatter technology was used to minimize multiple scattering effects. The detection of the scattered light was performed at an angle of 173º. Measurements were carried out at 25 ºC in triplicate for each bicosome system. Values presented in table 1 are the mean values of HD and the standard deviations (SD) from the triplicate. The intensity percentages of the proportion of scattered light are also presented.

2.4. Skin preparation and irradiation procedure

The skin from the back of Landrace large white pigs weighing around 40 kg was obtained from the Veterinary Faculty of the *Universitat Autònoma of Barcelona*, Spain. The skin was washed with tap water and dermatomed to 500 ± 50 µm thicknesses (Dermatome GA630, Aesculap, Tuttlingen, Germany). Then, the skin was cut into two pieces and one of them was subjected to irradiation. The exposure was performed using a light source simulating solar radiation (Suntest CPS+, Atlas, USA) at 500 W/m^2 for 30 min (90 J/cm^2). The radiation range was from 310 nm to 800 nm (2% Ultraviolet B, 18% Ultraviolet A, 72% Visible light and 8% Infrared A). This irradiation intensity (500 W/cm^2) is the equivalent to the solar exposure for two days in June in Catalonia. The irradiation was performed with a ventilation system. The maximum temperature reached in the simulator was 35 ºC.

2.5. Skin treatment with bicosomes

The normal and irradiated skin samples were cut into pieces of an area of 25 mm^2 and then were treated with 10 µl of Bcβ and BcMn systems. The treatment was performed overnight at room temperature (20-25°C) on a Petri plate on wet filter paper. Then, the plate was covered with paraffin. Under these conditions, the drying of the skin was avoided. The relative humidity inside the Petri plate was approximately 90%. During the treatment, the hydration and temperature of the skin samples remained constant. After the treatment, the skin pieces were cleaned with water. The treatment was performed using three skin pieces for each lipid system.

Finally, all skin samples were covered firstly with aluminium paper and then with Optimal Cutting Temperature compound (OCT). The aluminum paper was used to avoid the direct contact between the skin and the OCT. Next, skin samples were frozen in liquid N_2 before cutting into transverse 6-µm thick sections. The cuts were performed using a Cryostat CM3050 (Leica Biosystems Nussloch, Germany). The different skin sections were placed on CaF_2 circular windows (1 cm in diameter).

Considering that a small fraction of the bicosome systems could flow over the edges of the skin during the treatment, the slices from the edges of the tissue were removed. Only skin slices from the central part of the pieces were used in the FT-IR microspectroscopy.

2.6. FT-IR experiments

IR microspectroscopy was performed using synchrotron radiation at the SMIS beamline in synchrotron SOLEIL. Synchrotron radiation was employed because it provides a high spectral quality and produces high contrast chemical imaging. A Thermo Scientific Continuum XL IR microscope coupled to a Thermo Scientific FT-IR Nicolet 5700 spectrometer (Thermo electron corporation, Madison, Wisconsin, USA) was employed in these experiments. The microscope is equipped with a 32X/NA 0.65 Schwarzschild

objective and matching condenser, a mercury-cadmium-telluride (MCT) type A narrow band detector cooled by liquid nitrogen and an X-Y-Z motorised stage.

Optical micrographs were produced from the microscope in the visible image mode to define the sampling positions. The spectra were acquired at room temperature in transmission mode, in the 3600-1000 cm $^{-1}$ range, and 128 scans were averaged at 4 cm^{-1} resolution. Spectral maps were recorded with an aperture of 10x10 µm² and steps of 10 µm in X and Y.

The spectra and mappings obtained by FT-IR technique generated information about the penetration of the $C_{12}Re(CO)_3$ derivative attached to bicosomes. Thus, the presence of the $C_{12}Re(CO)_3$ derivative in the skin allowed to predict the location and distribution of bicosome systems inside the tissue.

2.7. Data processing

To calculate the relative concentration of the $C_{12}Re(CO)_3$ derivative in the skin from FT-IR maps, the ratio between the areas under the curves (AUC) of A_1 vibration of the $C_{12}Re(CO)_3$ and amide II skin vibration were calculated [17]. Amide II vibration was used as internal reference (skin reference) since this vibration is generally constant at the different depths of the skin.

The ratio $AUC_{Re(CO)3,\ A1}/AUC_{Amide\ II}$ was calculated in each step of the map (spectral maps were recorded with steps of 10 µm) and then, the mean value of all the ratios was calculated. Thus, from each map a mean value of the ratio $AUC_{Re(CO)3,\ A1}/AUC_{Amide\ II}$ in SC and in Epi was obtained. This procedure was performed in all the maps obtained for skin treated with Bcβ and BcMn systems using Omnic-Atlus software. Finally, from all the means obtained in SC and Epi in each bicosome system, the median value was calculated for each skin layer. These median values of the ratios $AUC_{Re(CO)3,\ A1}/AUC_{Amide\ II}$ are presented in table 2.

The quantification of the $C_{12}Re(CO)_3$ derivative in the skin allows monitoring accurately the localization and distribution of bicosomes inside the skin.

3. RESULTS

3.1. Characterization of bicosome systems

The sizes as HD of the different bicosome systems obtained by DLS at 25 ºC are shown in Table 1. For comparative purposes the size of bicosomes only with the $C_{12}Re(CO)_3$ derivative was also measured.

In all cases, two populations with different HDs and light scattered intensities were found. As commented in the introduction section, bicosomes are formed by discoidal nanostructures, bicelles, encapsulated in spherical vesicles. Some non-encapsulated bicelles could be found in this dispersion. Thus, in the bicosome systems the small size population (peak 1) detected by DLS corresponds to non-encapsulated discoidal structures (free bicelles) and the large population (peak 2) corresponds to the external vesicle encapsulating discoidal bicelles [20].

The HDs for free bicelles with the $C_{12}Re(CO)_3$ derivative and for the corresponding external vesicle (BcRe) were approximately 16 nm and 253 nm, and their intensity percentages were 25% and 71%, respectively.The Bcβ system showed HDs of approximately 15 nm (18%) and approximately 154 nm (76%). Finally, the HDs for the BcMn system were approximately 9 nm for free bicelles and 371 nm for external vesicle, and the intensity percentages were 17% and 82%, respectively.

3.2. Penetration of bicosomes inside the skin

IR spectra of normal and irradiated skin samples were recordered in the 3600-1000 cm^{-1} range. Figure 4 shows the spectrum for normal skin treated with bicosomes tagged with the $C_{12}Re(CO)_3$ derivative. The spectra obtained for irradiated skin treated with bicosome systems displayed similar patterns to the spectra obtained for normal skin treated with these systems (data not shown). The spectrum shows bands characteristics of skin amides about 3300 cm^{-1} corresponding to NH vibrations (Amide A), at 1660 cm^{-1} corresponding to CO vibration (Amide I) and at 1550 cm^{-1} corresponding to CN vibrations (Amide II). The characteristic vibrations of CH_3, CH_2

stretching of lipids are around 2960 and 2920 cm^{-1} respectively [21]. From a spectroscopic point of view the $C_{12}Re(CO)_3$ derivative shows a specific vibrational signature with two characteristic bands. The first one (E-band at 1920 cm^{-1}) corresponds to asymmetric stretching vibrations and the second (A_1-band at 2020 cm^{-1}) comes from symmetric stretching vibrations [11]. These vibrations do not interfere with the IR signals from the skin and consequently, the $C_{12}Re(CO)_3$ derivative can be detected in the skin by FT-IR without any interferences[16, 17] .

The FT-IR maps obtained for normal and irradiated skin samples treated with the Bcβ and BcMn systems are shown in figure 5 A-D. The sections of the micrographs display the skin surface including, the SC and the Epidermis (Epi). These figures reflect the distribution of the band A_1 of the $C_{12}Re(CO)_3$ derivative across the different regions of the skin. The colour scale, from blue to red, represents the location of the $C_{12}Re(CO)_3$ derivative attached to bicosomes. Red areas concentrate the highest amount of the $C_{12}Re(CO)_3$ derivative (hotspots) while in blue areas no amount of this molecule is detected. Yellow and green represent areas with intermediate amounts. Hence, the detection of the $C_{12}Re(CO)_3$ derivative in the skin brings the distribution of bicosome systems through the tissue. The use of the $C_{12}Re(CO)_3$ derivative as a probe to follow bicosome systems into the skin has been well established in a previous work [17]. This lipophilic molecule allows estimating the penetration and distribution of the systems incorporating the studied antioxidants.

The image of normal skin treated with the Bcβ system shows the main signal intensity of the $C_{12}Re(CO)_3$ derivative located in the SC, the superficial layer of the skin (Fig. 5A). The map obtained for normal skin treated with the BcMn system shows the main signal intensity in the SC and in the Epi (Fig. 5B).

The maps obtained for irradiated skin treated with the bicosome systems are also shown in figure 5C, D. As in the case of normal skin, the irradiated skin treated with the

Bcβ system shows the main signal intensity of the $C_{12}Re(CO)_3$ derivative located in the SC (Fig. 5C). In the case of the BcMn system (Fig. 5D), the main intensity of the BcMn system is localized in the SC. This result contrasts with the result obtained in normal skin treated with the BcMn system (Fig. 5B), where a high signal intensity of this lipid system is also observed in the Epi.

Semi-quantitative analysis was performed by calculating the median of the AUC $_{Re(CO)3, A1}$ / AUC $_{Amide\ II}$ ratio in the SC and the Epi (see experimental section) and these results are shown in table 2. To overcome problems that could be associated with different thickness of the skin, and considering that amides are homogeneously distributed, amide II vibration was used to normalize the AUC obtained from the $C_{12}Re(CO)_3$ derivative. This quantification was performed in all the maps obtained by FT-IR for each bicosome system (between 4-8 maps for each bicosome system).

The relative concentrations of the $C_{12}Re(CO)_3$ derivative in SC and Epi in normal skin treated with the BcMn system were higher than the relative concentrations of this molecule detected in normal skin treated with the Bcβ system. Thus, the penetration of the BcMn system was higher than penetration of the Bcβ system.

Otherwise, the relative amounts of the $C_{12}Re(CO)_3$ derivative in both skin compartments were lower in irradiated skin with respect to those obtained for non-irradiated skin in both bicosome systems. In this case these relative concentrations were similar for bicosome system.

4. DISCUSSION

4.1. Size of bicosome systems

4.1.1. Comparison of the sizes of the free bicelles (Small size population)

The smallest size was observed for the bicelles containing the $C_{12}Re(CO)_3$ derivative and the C_{16}-enPI$_2$-Mn. Considering that the C_{16}-enPI$_2$-Mn is soluble in water, the location of this complex out of bicelle structure could be expected. However, the

significant different size between the bicosome systems with the $C_{12}Re(CO)_3$ derivative and bicosomes containing the C_{16}-enPI$_2$-Mn together with this derivative (Table 1) suggests an interaction between the Mn^{II} complex and bicelle membrane. Probably the C_{16}-enPI$_2$-Mn complex is partitioned between aqueous phase and the lipid structures. The unique alkyl chain present in the C_{16}-enPI$_2$-Mn could give to this molecule an amphiphilic character similar as DHPC. Consequently, the location of the Mn^{II} complex would be more favoured in the edges of bicelles, following similar behaviour as DHPC [6, 7]. This fact would entail an increase in the amount of molecules to locate in the edge of bicelles surrounding the flat bilayer (DHPC and the C_{16}-enPI$_2$-Mn), and consequently, the ratio between the molecules located in the flat side and the molecules located in the edges would decrease. This distribution involves a decrease in the diameter of the discs in order to increase edge areas in which DHPC and C_{16}-enPI$_2$-Mn molecules would be accommodated. This fact is in agreement with our results, where the bicelles containing the C_{16}-enPI$_2$-Mn have the smallest size due to the location of this antioxidant in the edges of this nanostructure. Moreover, this behaviour was also observed for other amphiphilic molecules incorporated in bicellar systems [22].

4.1.2. Comparison of the sizes of the external vesicles encapsulating bicelles (Large size population)

The incorporation of β-carotene in bicosomes promoted a decrease in the size of the external vesicle of bicosome systems, while, the incorporation of the C_{16}-enPI$_2$-Mn entailed an increase in the HD of the large size (Table 1). This fact could be related to the partial location of both antioxidants in the external bilayer of bicosome systems. The C_{16}-enPI$_2$-Mn is an amphiphilic molecule and the incorporation of this antioxidant could happen between the hydrophilic and lipophilic region of the bilayer, that is, between polar heads and lipophilic chains of phospholipids. Thus, the C_{16}-enPI$_2$-Mn should be located parallel with respect to the alkyl chain of lipids. This fact would entail

the separation between the lipid molecules promoting an increase in the diameter of the external vesicle.

Further, considering the planar geometry and the low solubility in water of β-carotene, the location of this antioxidant in the lipophilic region of the bilayer is expected. This fact agrees with some works that suggest the incorporation of β-carotene inside the lipophilic region of lipid bilayer. This location, perpendicular to the alkyl chains of phospholipids deep into the lipid bilayer [23, 24], could be responsible of the decrease of external vesicle of the Bcβ system in the current study.

4.2. Distribution of Bcβ and BcMn systems in normal and irradiated skin

In a previous work we demonstrated the interaction of the $C_{12}Re(CO)_3$ derivative with bicosomes and the penetration of this molecule in the skin [17]. Those results allowed us to assume that the $C_{12}Re(CO)_3$ derivative remains linked to lipid aggregates. Consequently, this molecule was proposed as a useful tag for the bicosome systems incorporating new actives.

The most common route for delivery of molecules in the skin is the intercellular route. To understand the penetration of bicosome systems into the skin by this route, the structure of the SC and the structure of these systems should be considered. As previous papers describe the penetration mechanism using bicosome systems involve a multi-step process of the interaction with the skin. The dimensions of the intercellular spaces of the SC, where transcellular penetration occurs, are approximately 6-10 nm, thus, only systems with dimensions around or smaller than 6-10, nm would be able to pass through these spaces. Considering the morphology of this lipid system, the external spherical vesicles with a size of approximately 200 nm are not be able to penetrate through the SC by a intercellular route, and they remain on the skin surface in a similar way as described for other lipid vesicles [25]. However, in contact with the skin, these external vesicles burst and the encapsulated bicelles are released from

inside and due to their small dimensions are able to penetrate through the narrow interlamellar spaces of the SC [6]. Once incorporated into the SC, bicelles could mix with SC lipids or could reach the Epi. Next, bicelles increase in size, all together due to the natural hydration gradient of the skin [8, 26]. This increase involves a transition from bicelles to vesicles and promotes the retention of bicelle components into the skin [8]. Besides, the non-encapsulated bicelles would also penetrate with the same mechanism. Therefore, the bicelles are the responsible of the penetration of the $C_{12}Re(CO)_3$ derivative into the skin, and the external vesicle provides a superficial treatment to this tissue.

The penetration of BcMn is higher and deeper than the penetration of Bcβ (Table 2). The different physical-chemical properties of the antioxidants could be also involved in the different penetration behaviour of both bicosome systems. β-carotene is a lipophilic molecule and the C_{16}-enPI_2-Mn is an amphiphilic molecule. This fact could lead not only to different size but also different properties of the structures presenting in the systems and consequently different interaction with the skin. The intercellular route of the skin provides hydrophilic and lipophilic sites through the SC [27]. Therefore, while the Bcβ system preferably passes through the lipophilic areas inside the skin, the BcMn system could be located in the hydrophilic and lipophilic pathways of this tissue. Considering these possibilities of interaction with the skin, a higher distribution and overall concentration of the BcMn system seems reasonable. Moreover, the amphiphilic character of the BcMn system would facilitate the distribution of this system to deeper areas of the skin with high water environments, that is, the Epi.

The different sizes observed for the bicelles forming the Bcβ and BcMn systems (15 and 10 nm respectively), could be another reason to explain the higher penetration of BcMn system. Nevertheless, considering that both bicelles have the same thickness (5 nm) and that SC is an adaptable structure, the penetration of both nanostructures could

be favoured and not much difference could be expected in the interaction of both systems with the skin concerning size. Probably, this reason would be negligible to explain our results we consider the different physical-chemical properties of both antioxidants is the main reason of the higher penetration of BcMn system into the skin.

The penetration of both bicosome systems was lower in irradiated skin than in normal skin. The electromagnetic radiation (310-800 nm) used in our experiments is based on ultraviolet (UV), visible light (VIS) and infrared A (IR-A). The negative effect induced by radiation in this range is mainly associated to UV exposure, however, VIS and IR can also affect the skin [28, 29]. The damage caused by IR-A has been mainly associated to an increase in the temperature in the range of 40-45 ºC [29, 30]. In our experiments the irradiation procedure was performed with a ventilation system, and the skin temperature was maintained at 35 ºC to avoid the possible damage produced by IR-A radiation.

Concerning the visible light, some authors have demonstrated the reversible damage induced by blue light (380-495 nm) *in vivo* after 100 J/cm^2 [28]. Previous works showed the formation of free radicals with a combination of UV and VIS light *ex vivo*, and the influence of UV radiation always dominated this process [31].

Therefore, we assume that the main damage produced to the skin samples come from the radiations in the UV range and that the possible heat damage coming from VIS light would be negligible with respect the UV radiation.

It is know that UV radiation can modify skin structure, which can affect the skin permeation [32, 33]. The irradiation does not necessarily increase the permeation of substances in this tissue [3, 34]. In fact, our results demonstrated the opposite effect. Some studies have demonstrated that UVA radiation can alter the skin barrier characteristics causing the loss of endogenous water, and consequently, the alteration of water transport inside the skin [32, 35]. This fact can alter the passage of hydrophilic molecules or aqueous systems. Thus, although bicosome systems are formed by

lipids, these structures are dispersing in 85% water, and consequently, the penetration of these lipid systems could be restricted.

Other studies suggest the creation of new polar sites, such as, -COOH and $–NH_2$ under UV radiation improving the permeation of aqueous systems [32]. Nevertheless, considering the smaller penetration in irradiated skin of our results, this effect would be negligible to explain our results. Therefore, we consider the alteration of water transport as the main reason of the low penetration of both bicosome systems in irradiated skin.

5. CONCLUSIONS

Our results suggested the following conclusions:

- Bicosomes are able to incorporate both antioxidants and are useful carriers for skin applications.
- The physical-chemical properties of the actives incorporated in bicosome systems are an important factor to estimate its penetration in the skin. The hydrophilic actives would be more favoured to penetrate in the skin than the lipophilic actives.

  Therefore, the modification of the hydrophilicity or lipophilicity of the actives and of the bicosome should be considered to obtain the required distribution of these actives into the skin.
- The radiation applied makes skin more impermeable (*in vitro experiments*). Therefore, in order to achieve the required concentration of these antioxidants into the skin, the application of these actives before the solar exposition should be considered.

Acknowledgements

This work has supported by funds from CTQ 2013-44998-P.

References

1. Rubio L, Alonso C, Lopez O, et al. Barrier function of intact and impaired skin: percutaneous penetration of caffeine and salicylic acid. Int J Dermatol 2012;50(7):881-9.

2. Norlén L. Skin barrier structure and function: the single gel phase model. J Invest Dermatol 2001;117(4):830-36.

3. Duracher L, Blasco L, Abdel Jaoued A, et al. Irradiation of skin and contrasting effects on absorption of hydrophilic and lipophilic compounds. Photochem Photobiol 2009;85(6):1459-67.

4. Suntres ZE. Liposomal Antioxidants for Protection against Oxidant-Induced Damage. J Toxicol 2011:152474-89.

5. Rodriguez G, Soria G, Coll E, et al. Bicosomes: bicelles in dilute systems. Biophys J 2010;99(2):480-88.

6. Rodríguez G, Barbosa-Barros L, Rubio L, et al. Bicelles: New Lipid Nanosystems for Dermatological Applications. J Biomed Nanotech 2015;11(2):282-90.

7. Barbosa-Barros L, Rodriguez G, Barba C, et al. Bicelles: Lipid Nanostructured Platforms with Potential Dermal Applications. Small 2011;8(6):807-18.

8. Fernández E, Rodríguez G, Cócera M, et al. Advanced lipid systems containing β-carotene: stability under UV-vis radiation and application on porcine skin in vitro. Phys Chem Chem Phys 2015;17(28):18710-21.

9. Stahl W, Sies H. Carotenoids and protection against solar UV radiation. Skin Pharmacol Appl Skin Physiol 2002;15(5):291-6.

10. Bernard AS, Giroud C, Ching HY, et al. Evaluation of the anti-oxidant properties of a SOD-mimic Mn-complex in activated macrophages. Dalton Trans 2012;41(21):6399-403.

11. Clede S, Lambert F, Sandt C, et al. A rhenium tris-carbonyl derivative as a single core multimodal probe for imaging (SCoMPI) combining infrared and luminescent properties. Chem Commun 2012;48(62):7729-31.

12. Clede S, Lambert F, Sandt C, et al. Synchrotron radiation FTIR detection of a metal-carbonyl tamoxifen analog. Correlation with luminescence microscopy to study its subcellular distribution. Biotechnol Adv 2013;31(3):393-5.

13. Clede S, Lambert F, Sandt C, et al. Detection of an estrogen derivative in two breast cancer cell lines using a single core multimodal probe for imaging (SCoMPI) imaged by a panel of luminescent and vibrational techniques. Analyst 2013;138(19):5627-38.

14. Clède S, Policar C. Metal–Carbonyl Units for Vibrational and Luminescence Imaging: Towards Multimodality. Chemistry-A European Journal 2015;21(3):942-58.

15. Policar C, Waern JB, Plamont MA, et al. Subcellular IR imaging of a metal–carbonyl moiety using photothermally induced resonance. Angewandte Chemie 2011;123(4):890-94.

16. Clède S, Delsuc N, Laugel C, et al. An easy-to-detect nona-arginine peptide for epidermal targeting. Chem Comm 2015;51(13):2687-89.

17. Fernández E, Rodríguez G, Hostachy S, et al. A rhenium tris-carbonyl derivative as a model molecule for incorporation into phospholipid assemblies for skin applications. Colloids Surf B: Biointerfaces 2015;131:102-07.

18. Lankalapalli RS, Eckelkamp JT, Sircar D, et al. Synthesis and antioxidant properties of an unnatural plasmalogen analogue bearing a trans O-vinyl ether linkage. Org Lett 2009;11(13):2784-87.

19. Cisnetti F, Lefèvre AS., Guillot R, et al. A new pentadentate ligand forms both a Di- and a mononuclear Mn-II complex: Electrochemical, spectroscopic and superoxide dismutase activity studies. Eur J Inorg Chem 2007:4472-80.

20. Fernández E, Fajarí L, Rodríguez G, et al. Bicelles and bicosomes as free radical scavengers in the skin. RSC Advances 2014;4(95):53109-21.

21. Rodriguez G, Barbosa-Barros L, Rubio L, et al. Conformational changes in stratum corneum lipids by effect of bicellar systems. Langmuir 2009;25(18):10595-603.

22. Rubio L, Alonso C, Rodriguez G, et al. Bicellar systems for in vitro percutaneous absorption of diclofenac. Int J Pharm 2010;386(1-2):108-13.

23. Liebler DC, Stratton SP, Kaysen KL. Antioxidant actions of beta-carotene in liposomal and microsomal membranes: role of carotenoid-membrane incorporation and alpha-tocopherol. Arch Biochem Biophys 1997;338(2):244-50.

24. Tsuchihashi H, Kigoshi M, Iwatsuki M, et al. Action of beta-carotene as an antioxidant against lipid peroxidation. Arch Biochem Biophys 1995;323(1):137-47.

25. Muller RH, Petersen RD, Hommoss A, et al. Nanostructured lipid carriers (NLC) in cosmetic dermal products. Adv Drug Deliv Rev 2007;59(6):522-30.

26. Rodriguez G, Barbosa-Barros L, Rubio L, et al. Bicellar systems as modifiers of skin lipid structure. Colloids Surf B Biointerfaces 2011;84(2):390-4.

27. Benson HA. Transdermal drug delivery: penetration enhancement techniques. Curr Drug Deliv 2005;2(1):23-33.

28. Vandersee S, Beyer M, Lademann J, et al. Blue-Violet Light Irradiation Dose Dependently Decreases Carotenoids in Human Skin, Which Indicates the Generation of Free Radicals. Oxid Med Cell Long 2015;2015:579675-81.

29. Akhalaya MY, Maksimov G, Rubin A, et al. Molecular action mechanisms of solar infrared radiation and heat on human skin. Ageing Res Rev 2014;16(1):1-11.

30. Darvin M, Haag S, Meinke M, et al. Radical production by infrared A irradiation in human tissue. Skin Pharmacol Physiol 2010;23(1):40-46.

31. Haywood R. Relevance of Sunscreen Application Method, Visible Light and Sunlight Intensity to Free-radical Protection: A Study of ex vivo Human Skin. Photochem Photobiol 2006;82(4):1123-31.

32. McAuliffe DJ, Blank IH. Effects of UVA (320-400 nm) on the barrier characteristics of the skin. J Invest Dermatol 1991;96(5):758-62.

33. Wefers H, Melnik BC, Flur M, et al. Influence of UV irradiation on the composition of human stratum corneum lipids. J Invest Dermatol 1991;96(6):959-62.

34. Hung C-F, Fang C-L, Al-Suwayeh SA, et al. Evaluation of drug and sunscreen permeation via skin irradiated with UVA and UVB: Comparisons of normal skin and chronologically aged skin. J Dermatol Sci 2012;68(3):135-48.

35. Jacques SL, McAulife DJ, Blank IH, et al. Low dose ultraviolet radiation alters human stratum corneum Photochem Photobiol 1987;45S:94S.

Table 1: Mean values and standard deviation (SD) of hydrodynamic diameters (HD) of the different bicosome systems. Proportions of the scattered intensity corresponding to the different populations in the size distribution curves at 25ºC for each lipid system are also shown.

BICOSOME SYSTEM	HD (nm) ± SD (Peak 1)	% Int ± SD (Peak 1)	HD (nm) ± SD (Peak 2)	% Int ± SD (Peak 2)
BcRe	16 ± 6	25 ± 6	253 ± 78	71 ± 2
Bcβ	15 ± 4	18 ± 4	154 ± 39	76 ± 4
BcMn	10 ± 1	17 ± 4	371 ± 21	82 ± 2

Table 2. The median value of the $AUC_{Re(CO)3\ A1}/AUC_{Amide\ II}$ ratio in SC and Epi for normal and irradiated skin treated with different bicosome systems.

SKIN SAMPLE	SC ratio ($X10^{-2}$)	Epi ratio ($X10^{-2}$)
Normal skin + Bcβ	1.72	0.35
Normal skin + BcMn	2.57	1.85
Irradiated skin + Bcβ	0. 83	0.24
Irradiated skin + BcMn	0.77	0.37

Figure 1

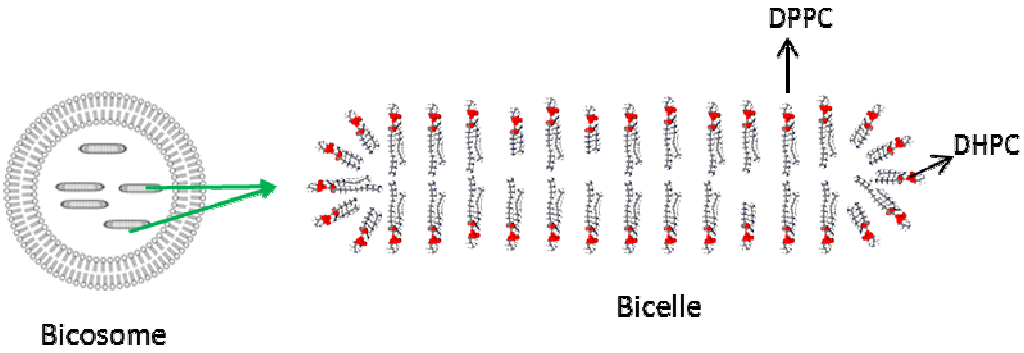

Figure 2

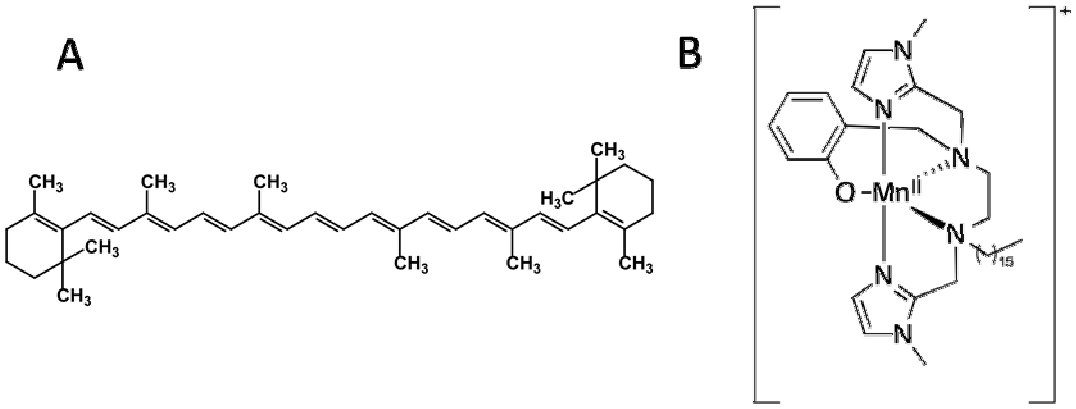

Figure 3

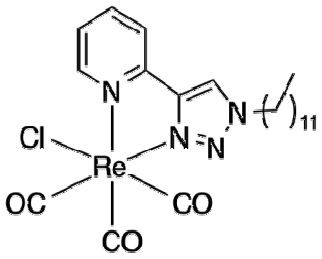

Figure 4

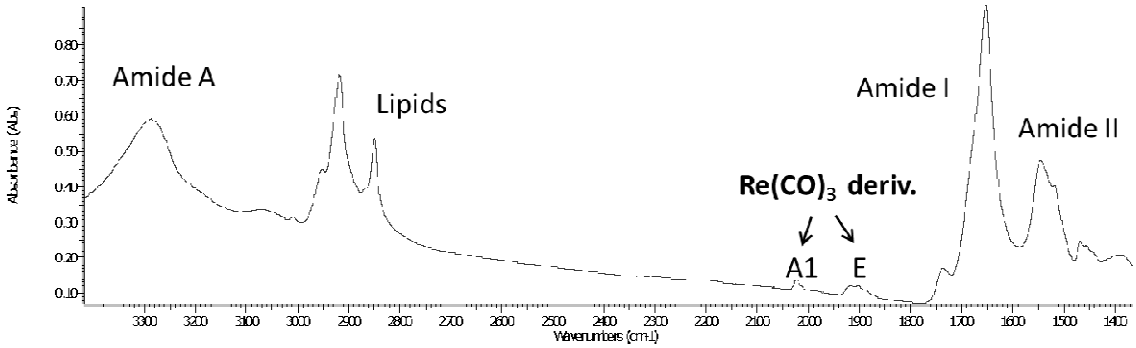

Figure 5

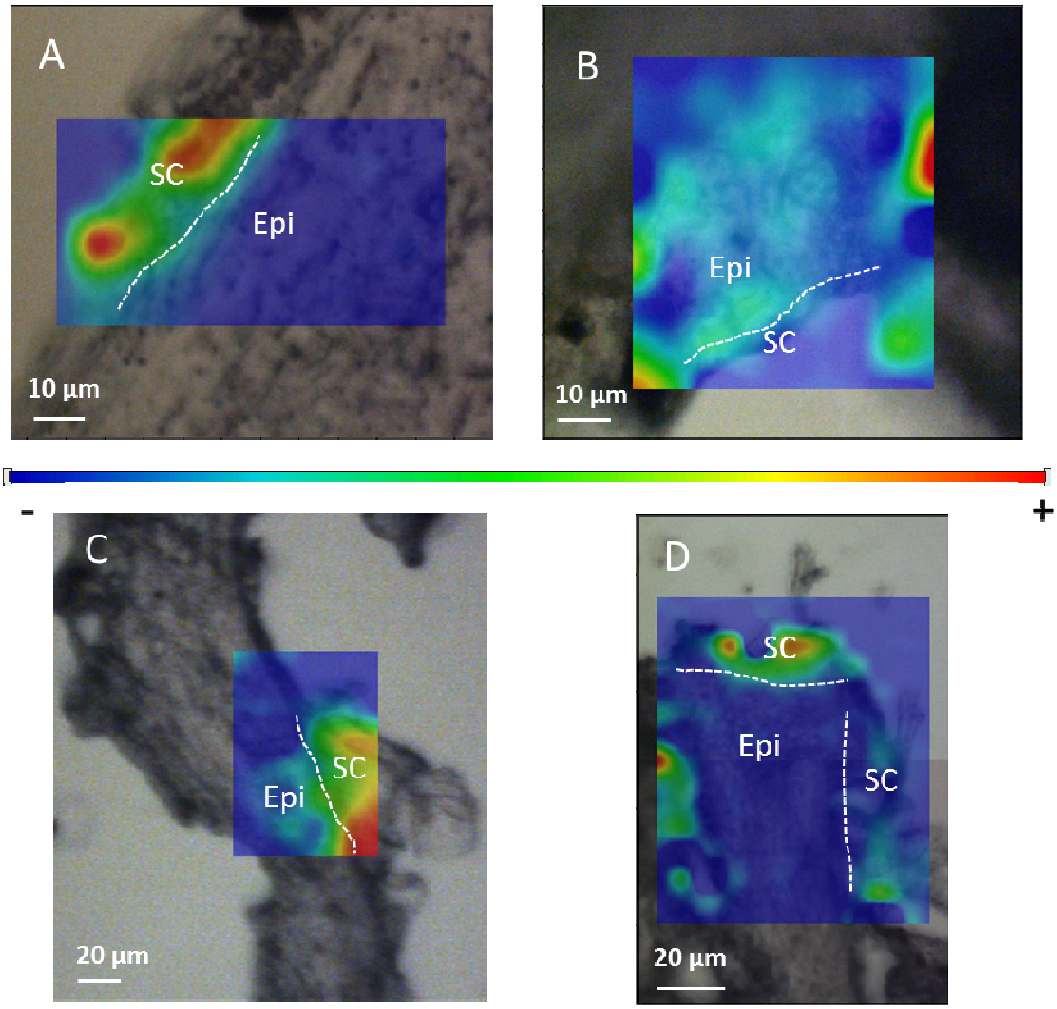

Fig. 1 Bicosome structure: discoidal bicelles encapsulated in spherical vesicles.

Fig. 2: (A) β-carotene and (B) C_{16}-enPI$_2$-Mn complex.

Fig. 3 $C_{12}Re(CO)_3$ derivative (fac-[$Re(CO)_3Cl$(2-(1-dodecyl-1H-1,2,3,triazol-4-yl)-pyridine)]).

Fig. 4 IR spectra of normal skin treated with bicosomes tagged with $C_{12}Re(CO)_3$. From left to right; NH vibration of polypeptides and proteins of skin (Amide A), CH_3 and CH_2 stretching vibration of skin and bicosome lipids, symmetric and asymmetric stretching vibrations of CO from $C_{12}Re(CO)_3$ molecule (A1 at 2020 cm^{-1} and E at 1920 cm^{-1}), CO vibration of proteins of skin (Amide I) and CN vibration of proteins of skin (Amide II) [17].

Fig. 5 IR maps of A1 vibration obtained for normal and irradiated skin treated with different bicosomes. A) Normal skin treated with Bcβ system, B) normal skin treated with BcMn system, C) irradiated skin treated with Bcβ system and D) irradiated skin treated with BcMn system. The scale goes from blue to red, indicating no amount of $C_{12}Re(CO)_3$ derivative in blue colour and high amount of this molecule in red colour. SC: Stratum corneum, Epi: Epidermis.

ARTÍCULO 7

Reducing the harmful effects of IR radiation in the skin using bicosomes

Journal of Dermatological Science- en revisión

La radiación IR supone un 50% de la radiación del sol recibida en la tierra, que dependiendo de la dosis aplicada puede producir efectos terapéuticos o patológicos en la piel. Hasta hoy, el efecto de la radiación IR se ha asociado principalmente al calor producido por esta radiación, sin embargo, trabajos recientes empiezan a considerar que la luz IR pueda causar daños de una forma más directa debido a su energía, independientemente del aumento de temperatura.

En este trabajo se evalúa el efecto de la radiación IR en la piel. Por un lado, se determina la formación de radicales libres en la piel a temperatura fisiológica mediante EPR usando el "spin-trap" DMPO. La irradiación IR se lleva a cabo mediante un accesorio acoplado al equipo de EPR que permite disipar el calor producido por la radiación IR (descripción del accesorio en el apartado 1.4.4.1.). De esta manera, se puede evaluar si la formación de radicales libres por exposición al IR es independiente del aumento de temperatura causado por esta radiación.

Por otro lado, también se evalúa el efecto de la radiación IR sobre el colágeno de la dermis mediante SAXS con fuente sincrotrón. Adicionalmente, la piel se trata con bicosomas incorporando β-caroteno y se evalúa el posible efecto preventivo de estos sistemas en la formación de radicales libres y en la degradación del colágeno.

Los resultados mostraron un incremento de radicales libres en la piel por efecto de la exposición a la luz IR incluso cuando la temperatura se mantuvo a 25-30ºC, lo que supone que no sólo el calor producido por la radiación IR es el causante de la formación de radicales libres, sino que la energía de la propia radiación también es influyente, algo que no se había observado hasta el momento.

El estudio de SAXS mostró la degradación del colágeno cutáneo alrededor de los 65ºC aunque no se pudo concluir si la degradación del colágeno fue debida al choque térmico o a la energía producida por la radiación IR.

La piel tratada con bicosomas incorporando β-caroteno mostró un descenso de radicales libres y una mejor conservación del colágeno frente a radiación IR en

comparación con la piel no tratada. Por lo tanto, los bicosomas con β-caroteno demuestran ser un sistema efectivo para prevenir los radicales libres y la degradación del colágeno producidos por radiación IR.

REDUCING THE HARMFUL EFFECTS OF IR RADIATION ON THE SKIN USING BICOSOMES

Estibalitz Fernández[*a], Lluís Fajari[a], Gelen Rodríguez[b], Mercedes Cócera[b], Verónica Moner[a], Lucyanna Barbosa-Barros[b], Christina Kamma-Lorger[c], Alfonso de la Maza[a] and Olga López[a].

[a] Institute of Advanced Chemistry of Catalonia (IQAC-CSIC), Barcelona, Spain.
[b] Bicosome S.L., Barcelona, Spain.
[c] ALBA Synchrotron, Cerdanyola, Spain.

*Corresponding author: Address: IQAC-CSIC, Jordi Girona 18-26, 08034 Barcelona, Spain. Tel.: (34) 934 006 100; fax: (34) 932 045 904.
E-mail address: *efptqt@cid.csic.es* (E. Fernández)

Keywords: Skin, bicosomes, IR radiation, collagen, EPR, SAXS, free radicals.

Abstract

The measurement of free radicals (FR) that are induced by infrared radiation (IR) while maintaining the sample at physiological temperature (30 to 33 ºC) could report interesting information about the direct action of IR exposure avoiding temperature effect. In addition, other indicators such as evaluation of the skin collagen organization after IR radiation could help to determine the potential therapeutic or pathological effects of IR exposure.

In this work the formation of FR in the skin under IR exposure near physiological temperatures was evaluated using 5,5-Dimethyl-1-Pyrroline-N-Oxide (DMPO) spin trap and Electron Paramagnetic Resonance spectroscopy (EPR) coupled with a homemade device. This device is formed by an IR lamp and a ventilator that maintains the skin temperature within the range of 25-30ºC. The study of collagen structure was performed by Small Angle X-ray Scattering (SAXS) using Synchrotron radiation.

Additionally, different skin treatments were carried out with phospholipid nanostructures (bicosomes) incorporating β-carotene (Bcb) to evaluate their protective effect on the skin against IR exposure.

EPR results showed an increase in hydroxyl radical (●OH) in the irradiated skin near physiological temperatures compared to the native skin, suggesting that the formation of FR by IR does not depend on the increase of skin temperature.

The skin collagen was degraded by IR exposure and high temperatures of approximately 65ºC are needed to degrade this protein.

The treatment of skin samples with Bcb reduces the formation of FR and keeps the structure of collagen intact. This fact could suggest evidence the decrease of FR and hence the preservation of collagen fibres in the skin treated with this system indicating the potential of bicosomes to protect the skin under IR exposure.

1. INTRODUCTION

The skin is designed to protect the organism against injuries and works as a physical barrier against the external environment. Sunlight damages human skin, resulting in formation of free radicals (FR), which are in part responsible of erythema/edema, inflammation, photoaging and skin disorders [1-4]. The negative effect of solar radiation on skin is usually associated with exposure to ultraviolet radiation (UV) [1-3]. However, skin is also exposed to infrared radiation (IR) [5, 6]. IR radiation can generate FR in the skin, which depending on doses are able to initiate a cascade of different signaling pathways inducing therapeutic or pathological effects [4]. Some studies relate FR formation to the increase in the temperature subsequent to IR radiation [5, 6]. The question of whether the IR induces directly the formation of FR, or it is a result of IR-induced heat shock is still open. This question is relevant due to the skin is daily exposed to IR from sunlight at physiological skin temperatures. The accurate measurement of FR induced during IR exposure maintaining the sample near physiological temperature, could report interesting information about the direct action of this radiation avoiding the temperature effect.

Moreover IR radiation penetrates the epidermal and dermal layers of skin and reaches deeper than UV and consequently, it can damage both skin compartments. The epidermis contains the stratum corneum (SC), which is a physical barrier for the body [7]. Dermis is the second innermost layer and contains structural proteins such as collagen and elastin. Collagen accounts around 75% of total dry weight of skin and provides strength and integrity to the tissue [8]. Changes in the structure or organization of collagen are responsible of alterations in the skin morphology such as, discoloration, loss of elasticity, wrinkles or impairment of barrier function [8-10]. The regularly staggered structure of collagen induces periodic variations of electron density visible by X-ray scattering as sharp Bragg peaks. The X-ray profile in healthy skin shows a characteristic d-spacing of around 65 nm and several reflections associated to this distance [8, 10]. Position, intensity and number of reflections of the typical axial

periodicity of skin collagen change by effect of tissue physiology or physical conditions. These changes indicate a macromolecular disorganization of collagen, and consequently can indicate the degradation of the protein. Therefore, the study of organization of the skin collagen after IR radiation also can help to determine the potential effects of IR exposure to the skin.

In the current work the formation of FR in the skin under IR exposure near physiological temperatures was evaluated using 5,5-Dimethyl-1-Pyrroline-N-Oxide (DMPO) spin trap and Electron Paramagnetic Resonance spectroscopy (EPR). The maximum skin temperature reached during the experiment was 30ºC. Therefore, the formation of FR only by exposure to IR and without raising the temperature was investigated.

Skin structural changes before and after IR exposure were also studied by Small Angle X-ray Scattering (SAXS) using Synchrotron radiation.

Additionally, different skin treatments were carried out with bicosomes incorporating β-carotene (Bcb) to evaluate their protective effect on FR formation and on skin collagen structure against IR exposure.

Bicosomes are phospholipid assemblies formed by spherical vesicles of approximately 150-250 nm and discoidal structures between 15-25 nm (Fig. 1) [11, 12]. The combination of lipid composition and small size as well as their morphological versatility make them very useful for various skin treatments as carriers [12, 13].

2. MATERIALS AND METHODS

2.1. Chemicals

Bicosome systems were formed using 1,2- dipalmitoyl-*sn*-glycero-3-phosphocholine (DPPC) and 1,2- dihexanoyl-*sn*-glycero-3-phosphocholine (DHPC) purchased from Avanti Polar Lipids (Alabaster, USA). Cholesterol (CHO) obtained from Sigma-Aldrich (Sto Louis, MO, USA) and Lipoid S-100, whose main component (>94%) is

phosphatidylcholine (PC) was obtained from Lipoid GmbH (Ludwigshafen, Germany). β-carotene was purchased by Sigma-Aldrich and DMPO (>99%) was purchased by Dojindo (Tokyo, Japan) and purified water was obtained by an ultra-pure system, Milli-Q plus 185 (Millipore, Bedford, USA). Chloroform was purchased from Merck.

2.2. Preparation of bicosomes incorporating β-carotene

Bicosomes with β-carotene (Bcb) were prepared by mixing appropriate amount of DPPC, DHPC and β-carotene in a chloroform solution. Once the components were mixed, the chloroform was evaporated with a rotary evaporator and the obtained lipid film was hydrated. The obtained water dispersion was subjected to several cycles of sonication and freezing until the sample became transparent.

Next, another lipid film was prepared by mixing appropriate amounts of PC and CHOL in chloroform. The chloroform was removed with a rotary evaporator until a lipid film was obtained. Finally, the film was hydrated with the first prepared dispersion.

The concentration of each ingredient in the bicosomes was the following (w/v%):

DPPC 4.25%, DHPC 0.75%, β-carotene 0.01%, PC: 8% and CHOL 2%.

2.3. Dynamyc light scattering (DLS)

The hydrodynamic diameter (HD) of Bcb were determined by Dynamic light scattering (DLS) using a Zetasizer nano ZS90 (Malvern Instruments, UK). The particle sizes were determined by detection and analysis of the scattered light from the 632 nm He/Ne laser beam. Non-invasive back scatter technology was used in order to minimize multiple scattering effects. The detection of the light scattered was performed at an angle of 173º.

The relationship between the size of a particle and its speed due to Brownian motion is defined by the Stokes-Einstein equation (eq 1):

$$HD = k_B T / 3\pi\eta D \quad \text{(eq 1)}$$

where *HD* is the hydrodynamic diameter of a hypothetical hard sphere that diffuses with the same speed as the particle in the experiment, *D* is the translational diffusion coefficient (m^2/s), k_B is the Boltzmann`s constant (1.3806503 x 10^{-23} J K^{-1}), *T* is the absolute temperature (K) and η is the viscosity (mPa•s) [14].

DLS measurements were performed in triplicate and the mean size and standard deviation (SD) of the different populations in the distribution curves were obtained.

2.4. Skin treatment with bicosomes

The skin obtained from the back of Landrace large white pigs was provided from the Hospital Vall Hebron, Barcelona, Spain. The skin was removed from the back of the pig minutes after the animal was sacrificed. The removed skin was cleaned with water and dermatomed to 500 ± 50 µm thick pieces (Dermatome GA630, Aesculap, Tuttlingen, Germany), vacuum packed and stored at 4ºC. After 18 h the skin was cut into 25 mm^2 pieces. Then, 10 µL of Bcb were applied on skin pieces for 24 h at room temperature (20-25℃). The incubation of the skin pieces was performed on a Petri plate on wet filter paper. Then, the plate was covered with paraffin. Under these conditions, drying of the skin and evaporation of the solvent were avoided. The relative humidity inside the Petri plate was approximately 90%. During the treatment, the hydration and temperature of the skin samples remained constant. The bicosome treatment was performed in triplicate.

2.5. Small Angle X-ray Scattering (SAXS)

The SAXS profile of each skin sample was analysed to characterise the organisation of collagen in the skin. The diffraction experiments were performed at NACD beamline, ALBA Synchrotron Light Source (Cerdanyola del Valles, Barcelona, Spain), with a monochromatic beam of 12.4 keV. The scattering patterns were recordered with a SAXS 2D detector ADSC 210r (ADSC, Poway, CA, USA) with single exposed times of

about 3 seconds. The sample to detector distance was 6.4 m. The typical axial periodicity of collagen is the result of the displacement of each molecule with respect to the adjacent molecules in a particular direction. The scattered intensity I (in arbitrary units) was measured as a function of the scattering vector Q (in reciprocal Å). The latter is defined as the following (eq 2):

$$Q=(4\pi\sin\theta)/\lambda \quad (2)$$

where θ is the scattering angle, and λ is the wavelength of the radiation (in this case 1 Å). The position of the scattering peaks is directly related to the repeat distance of the molecular structure, as described by Bragg´s law [15] (eq 3):

$$2d= \sin\theta = n\lambda \quad (3)$$

Where n and d represent the order of the diffraction peak and repeat distance, respectively. In a lamellar structure, the various n peaks are located at equidistant positions (eq 4),

$$Qn = 2\pi n/\lambda \quad (4)$$

and Qn represents the position of the n^{th} order reflection.

2.6. Electron Paramagentic Resonance (EPR)

Native and Bcb treated skin samples were put into the quartz tissue cell of EPR spectrometer (EMX-Plus 10/12 Brucker BioSpin spectrometer), with a X-band microwave bridge (~9 GHz) (EMX Premium X), magnet of 10" (ER073) with a 12 kW (ER083) power supply. The EPR spectra were registered before and during the IR radiation at the following measurement conditions: magnetic field 3485 G; sweep width

100 G; microwave frequency 9.73 GHz; microwave power 20 mW; modulation amplitude 2 G; modulation frequency 100 kHz and time constant 20.48 mn.

Changes in the skin properties during the experiment would affect the EPR signal. Thus, in order to check the stability of the skin structure, a sample with DMPO spin-trap was placed in the EPR cavity under aforementioned conditions for 1 h. The EPR signal was evaluated during this period. Given that no changes in the structure and in the composition of the registered spectra were observed for 2 h, we assume that the stability of the skin is not disturbed with the conditions of the experiment.

Each spectrum was acquired at intervals of 2-3 minutes accumulating ten scans. The second integration of the signal was calculated from the obtained spectra at different irradiation times. This integration value is directly correlated to the FR concentration in the skin[16]. In the current work, the second integration value was used to compare the FR formation in the different skin samples.

2.7. IR exposure

EPR experiments

The skin samples were irradiated with IR light *in situ* in the EPR equipment using a homemade coupled device (Fig. 2). This device consists of an IR lamp of 250 W (Philips Infrared BR I 25), which is isolated from the external environment and ambient light with an aluminum block (A). In this way, the whole IR radiation that is emitted by the lamp hits the sample within the EPR cavity (B). The distance between the lamp and skin samples was 38 cm and IR exposure time was 120 min. At these conditions the irradiation intensity from the lamp was 0.11 W/cm^2 and the dose applied was 777.60 J/cm^2. The temperature in the EPR cavity and in the sample was maintained stable with a ventilator (C). The temperature in the EPR cavity was measured using a probe Pt-100 immersion (Cat. nº: 30.900.971). The maximum skin temperature reached during the experiment was 30ºC. Using this device the IR radiation and the EPR measurements were performed simultaneously in the spectrometer. In this way, the

formation of FR by IR radiation with independency of the temperature could be evaluated.

SAXS experiments

Skin samples were exposed to IR radiation using an IR lamp of 250 W (Philips Infrared BR I 25). In order to determine a dose of IR radiation able to damage the skin collagen, the skin-lamp distance and the exposition time were optimised. First, different skin-lamp distances were used for the same period of irradiation time (30 min). The distances between the lamp and skin were 10, 15 and 30 cm, and the irradiation intensities corresponding to these distances were 0.91, 0.48 and 0.16 W/cm^2, respectively. From the results of this experiment the optimum distance between the skin and the lamp was determined at 10 cm (0.91 W/cm^2). Consequently, different irradiation times were applied to the skin at this distance. The tested irradiation times were 5, 10 and 15 min, and the doses corresponding to these irradiation times were 273, 546 and 819 J/cm^2, respectively. From this experiment the optimum irradiation time was set at 10 min. Therefore, the optimized conditions for the determination of the possible effect of Bcb in protecting the collagen were 10 cm of distance and 10 min of irradiation (546 J/cm^2).

3. RESULTS

3.1. Bicosome size

The HDs obtained using DLS at 25°C for Bcb are shown in Table 1. For comparative purposes, the original size of the bicosomes without any incorporated molecule is also shown.

Table 1: Mean value and standard deviation of HD of the different bicosome systems and proportion of the particle population analysed by intensity of light scattering at 25ºC.

LIPID SYSTEM	HD (nm)	%Int
Bicosomes	**180 ± 20**	**85**
Bicosomes + β-carotene (Bcb)	**250 ± 30**	**85**

The size of the bicosomes without β-carotene was approximately 180 nm with a proportion of light scattered approximately 85%. Incorporation of β-carotene led to an increase in the particle size to approximately 250 nm and 85% of light scattered.

The increase in size of the Bcb could be due to the location of this lipophilic molecule in the bicosome structure [13]. Considering the low solubility in water of this antioxidant, this molecule is expected to be located in the lipophilic region of the bilayer of the bicosomes. Therefore, the incorporation of this lipophilic molecule inside the lipid bilayer of the bicosomes would promote a slight increase in the size of the nanostructures.

3.2. Free radical formation under IR exposure

The generation of FR in pig skin samples was investigated by EPR using the DMPO probe, as it traps the FR formed in the tissue.

Fig. 3 shows the spectra of native porcine skin before and after 120 min of IR radiation. Both spectra represents the symmetric spectral model of DMPO hydroxyl spin adduct (DMPO-OH), and in general, in the current work the spectra that were obtained from all the skin samples showed similar patterns of DMPO-OH adduct [17, 18].

The spectrum intensity of the skin after IR exposure was higher than the spectrum intensity before IR radiation (Fig. 3). This fact was a consequence of FR formation in the skin due to IR exposure, and demonstrated the formation of FR at physiological temperatures.

It is known that the second integral value of the EPR spectrum is proportional to the FR concentration [16, 19]. Hence, for quantitative determination of the FR in the skin after IR radiation, the second integration values of the spectra at different irradiation times were calculated (Fig. 4). This figure represents the kinetic evolution of FR

concentration of native and irradiated skin at physiological temperatures under IR exposure.

The native skin showed a decrease in the FR concentration along the time. This decay is a typical trend of these species and it is a consequence of the destruction of the radicals [20, 21]. The FR concentration in irradiated skin was constant during the first minutes, but approximately 50 min later the FR concentration increased, leading to the conclusion that new FRs are formed. Finally, with approximately 80 min of irradiation the FR concentration was maintained. This fact demonstrated the capacity of IR radiation to form FR in the skin when the skin temperature is around 25-30ºC.

Additionally, different skin treatments were carried out with Bcb to evaluate their protective effect reducing the formation of FR (Fig. 5).

Overall, the FR concentration was lower in skin treated with Bcb. In fact, the FR concentration in skin treated with Bcb was maintained during the 120 min. After 75-80 min of IR radiation a clear difference in the FR concentration was observed between the irradiated skin and skin treated with Bcb indicating a FR scavenging effect on the skin. Moreover, it is important to note that before irradiation (time 0 min) the FR concentration was also lower in skin treated with Bcb indicating the neutralization of FR even in absence of irradiation.

3.3. Collagen degradation under IR exposure

3.3.1. Establishing the required dose to cause skin collagen degradation

It is known that the IR radiation degrades the skin collagen, but up to date it is not clearly determined the required IR dose that causes this degradation. Therefore, to evaluate the possible effect of Bcb protecting or repairing the negative effects on the skin collagen caused by IR radiation, it is necessary to establish the IR conditions to degrade the protein (see experimental section).

The regular staggered structure of collagen induces periodic variations of electron density visible by X-ray scattering as sharp Bragg peaks [8, 10]. The study of these peaks can be used to evaluate the organization of the skin collagen.

Fig. 6 shows the resulting SAXS profile of collagen when samples were irradiated adjusting the IR lamp at various distances from the sample (i.e. 10, 15 and 30 cm) and irradiated for 30 minutes each time. The irradiation intensities for each distance correspond at 0.91, 0.48 and 0.16 W/cm^2, respectively.

When skin is irradiated at a skin-lamp distance of 30 and 15 cm, the collagen peaks are clearly present, while, at 10 cm, the loss of the characteristic peaks of collagen indicated the disruption of the molecular disorganization of the protein. The skin temperature was 44ºC when the skin-lamp distance was set at 30 cm, 68ºC when the skin-lamp distance was 15 cm and 75ºC when the skin-lamp distance was 10 cm. Therefore, in order to evaluate the possible protecting effect of Bcb on the skin, the skin-lamp distance was fixed at 10 cm. Then, while keeping the distance between the IR lamp and the sample fixed at 10 cm, different irradiation times were applied to the skin while SAXS profiles were registered.

Fig. 7 shows the gradual degradation of collagen of native skin exposed to IR at a fix distance skin-lamp (10 cm) over different periods of time.

At this distance, the irradiation intensity delivered to the skin was 0.91 W/cm^2, and the doses corresponding to these irradiation times were 273, 546 and 819 J/cm^2, respectively. After 5 and 10 min of irradiation the collagen peaks were still observed, but these peaks were shorter when compared to the ones obtained from native skin. This fact could be due to the disorganization of collagen, which was consequence of the degradation of the protein at this irradiation time. The skin temperature with the application of these doses was in the range of 60-65 ºC. After 15 min of IR exposure the collagen peaks were not observed indicating the total degradation of the protein. The skin temperature at this dose was approximately 70ºC.

With these results and in order to evaluate the possible effect of Bcb to protect the skin collagen, the skin-lamp distance was fixed at 10 cm and the irradiation time was fixed at 10 min.

3.3.2. Collagen protection with bicosomes incorporating β-carotene

Various skin treatments were carried out with bicosomes incorporating β-carotene in order to evaluate their protective effect on skin collagen against IR exposure. Fig. 8 shows the gradual degradation of collagen of native skin and skin treated with bicosomes incorporating β-carotene exposed to IR at a fix distance skin-lamp (10 cm) for 10 min. The characteristic collagen peaks in the X-ray profiles indicated an alteration in the molecular organization of collagen in the skin samples exposed to IR light in comparison with native skin, which demonstrated the damage produced in this protein at this irradiation time. The skin samples previously treated with Bcb and subjected to IR kept the X-ray profile with the characteristic features of collagen. This fact would evidence the preservation of collagen fibres of the skin treated with this system under IR exposure, indicating the potent efficacy on collagen preservation of Bcb. The skin temperature at this dose was approximately 60-65ºC.

4. DISCUSSION

4.1. Influence of IR radiation forming free radicals in the skin

Nowadays, small data are available demonstrating that IR radiation could produce FR in the skin. Some studies claim that these FR can induce therapeutic or pathological effects on the skin depending of the irradiation dose applied. At low doses (1-10 J/cm^2), IR radiation stimulates therapeutics effects, and at high doses (> 120 J/cm^2) stimulates pathological effects [4]. The most known pathological effect of IR radiation on the skin (especially IR-A) is the overexpression of matrix metalloproteinases (MMP) molecules that have a degrading effect on skin collagen [4, 22]. In general, the FR formation is attributed to the increase in the skin temperature that causes the exposure to IR

radiation [6]. The IR radiation could increase the temperature of the skin surface to 43ºC. However, whether the IR induces directly FR formation in the skin, or it is a result of IR-induced heat shock is not clear up to date. A recent study has showed that a direct heat action to the skin does not increase the expression of MMP in the same manner to the observed with IR radiation [4]. This study demonstrates that the effect of heat produced by water bath does not induce the same process as the IR radiation[4]. Therefore, it is important to evaluate the effect of the IR radiation independently of the heat produced by this type of radiation and consequently, the potential of this effect to initiate therapeutic or pathological effects on the skin.

The homemade device used in this study provides the optimal conditions to measure *in situ* the FR formation near physiological temperatures. The ventilator was able to remove the heat coming from IR lamp, and therefore, the temperature of the skin was maintained between 25-30ºC, allowing us to evaluate the effect of IR exposure on skin.

Previous work has demonstrated that doses up to 120 J/cm^2 could initiate pathologic effects on human skin [4] (approximately 1.5 h during direct sun exposure in summer time in Munich, Germany). In our experiments the irradiation intensity was 0.108 W/cm^2, thus, to achieve the dose of 120 J/cm^2 it is necessary 18 min of IR exposure. As it is shows in this study, the FR concentration near physiological temperatures is similar as the FR concentration before IR exposure at this irradiation time (red line Figs. 4 and 5). Therefore, the possibility of this FR concentration to cause pathological effects could be disregarded. Likely, the dose that was used maintaining the temperatures between 25 and 30 ºC the IR energy is not enough to initiate negative effects on the skin. The increase of FR concentration near physiological temperatures is achieved around 50 min of IR exposure, that is, when the dose is about 324 J/cm^2. Hence, the possibility to initiate pathological effects on the skin could be considered.

Further, it is important to consider that the minimum dose to increase the FR concentration is higher using IR radiation than using UV radiation. Previous works have shown FR formation in the skin exposed to UV radiation at doses around 25-30 J/cm^2 [12]. This dose is noticeably lower than the dose of IR radiation used in this work. This fact is related to the difference in energy values between IR and UV radiation. The energy of UV radiation is higher than the energy of IR radiation, thus, high doses of IR radiation could be necessary to increase FR concentration in the skin.

In summary, the FR formation is possible near physiological temperatures during IR exposure and it does not necessarily occur at high temperatures. Consequently, the initiation of different signaling pathways inducing therapeutic or pathological effects at physiological temperature could be considered.

4.2. Stability of skin collagen under IR radiation

The skin collagen accounts 75% of the dry weight of the tissue. This protein provides the elasticity to the skin and is responsible of the integrity of the tissue[8]. Collagen molecules are formed by three α-polypeptide chains folded together forming a triple helical structure. The assembly between these triple helix molecules forms fibrillar groups in skin collagen and the assembly once again between these fibrillar groups form collagen fibers (Fig. 9) [8]. Abnormalities of collagen molecular structure affect the packing of collagen fibers in different tissues (bone, breast, or tendon), which is linked to the pathological state of the tissue [8]. Therefore, the state of collagen of the skin could be evaluated by studying the high of Bragg peaks obtained using SAXS technique.

The degradation of skin collagen occurs at a minimum dose of 273 J/cm^2, when the skin temperature is around 65ºC. The total degradation occurs at a dose of 820 J/cm^2 while the skin temperature reaches up until 70ºC. Therefore, in order to cause

degradation of skin collagen hard environmental conditions are necessary that are not normally part of everyday life. Nevertheless, the optimization of the conditions to degrade skin collagen helps to evaluate the effectiveness of various agents that aim to protect the protein structure.

The possible degradation of skin collagen that is exposed to IR radiation near physiological temperatures could be considered for further investigations. The EPR results showed an increase of FRs at doses up to 324 J/cm^2 and at near physiological temperatures. Induced FR formation could increase the expression of MMPs, and consequently cause the degradation of collagen. Thus, the degradation of skin collagen at physiological temperature and under IR radiation would be an interesting study in the future.

4.3. Skin protection under IR radiation by bicosomes incorporating β-carotene

The application of Bcb on skin reduces FR formation and collagen degradation that can be caused by IR radiation. This protection effect provided by Bcb could be associated to the properties of the β-carotene and to the characteristic of bicosome system.

β-carotene has demonstrated to be an efficient antioxidant in lipid environments by trapping FR or by quenching singlet oxygen radical [23, 24]. Hence, this antioxidant could act as a reducing agent of FR formation caused by IR radiation, and hence, the degradation of the collagen could be avoided. Nevertheless, this antioxidant is degraded at temperatures up to 50ºC, and the collagen degradation process required temperatures in the range of 65-70ºC.Therefore, the antioxidant ability of β-carotene in the collagen degradation process could be restricted at temperatures above 50ºC.

In the bicosomes, the lipid molecules that form this system are responsible of the reduction of FRs in the skin. Lipid molecules absorb the IR light at different wavelengths [25], and bicosomes are formed exclusively by lipids. Thus, the different structures of the bicosomes (bicelles and spherical vesicles) absorb IR radiation.

Consequently, the IR radiation intensity that penetrates into the skin would be diminished due to the absorption properties of bicosomes, and consequently the FR formation would be reduced. Additionally, the radiation that arrives to the dermis would also be reduced, which could contribute to the preservation of the skin collagen.

To understand the protective effect of bicosomes, it is important to understand the structure of this lipid system. The spherical vesicles, with a size of approximately 200 nm, would not be able to penetrate through the superficial layer of the skin, the SC, hence they remain on the skin surface in a similar way as described for other lipid vesicles [26]. Upon contact with the skin, the bilayer of the external vesicle of the bicosomes bursts, and the encapsulated bicelles are released. Due to their small size and thickness, bicelles are able to penetrate into the skin. Once incorporated into the SC, they have the ability to increase in size due to a dilution effect inside the SC [27]. This increase involves a transition from bicelles to vesicles and promotes the retention of the bicelle components (i.e. β-carotene) in the skin. Thus, the bicosome system has a double therapeutic effect as it treats the skin on the surface as well as inside the tissue.

5. CONCLUSIONS

In conclusion, the IR device attached to EPR spectrometer provides adequate conditions to perform FR measurements in the skin samples. The FR formation under IR exposure does not necessarily occur at high skin temperatures, it is also produced near physiological temperatures. Consequently, the initiation of different signaling pathways inducing therapeutic or pathological effects at physiological temperature could be further investigated. High temperatures of approximately 65ºC are needed to degrade skin collagen, which are not normally part of everyday life.

The treatment with Bcb reduces the FR formation in the skin subjected to IR and preserves the structure of collagen. This fact demonstrated the potent efficiency of bicosome systems in protecting the skin under IR exposure.

Acknowledgements

This work has supported by funds from CTQ 2013-44998-P.

References

[1] K. Biniek, K. Levi, R.H. Dauskardt, Solar UV radiation reduces the barrier function of human skin, Proc Natl Acad Sci USA 109 (2012) 17111-17116.

[2] M.F. Holick: Sunlight, UV-radiation, vitamin D and skin cancer: how much sunlight do we need?, In Sunlight, Vitamin D and Skin Cancer, Springer, 2008, pp. 1-15.

[3] M. Ichihashi, M. Ueda, A. Budiyanto, T. Bito, M. Oka, M. Fukunaga, et al., UV-induced skin damage, Toxicol 189 (2003) 21-39.

[4] M.Y. Akhalaya, G. Maksimov, A. Rubin, J. Lademann, M. Darvin, Molecular action mechanisms of solar infrared radiation and heat on human skin, Ageing Res Rev 16 (2014) 1-11.

[5] M. Darvin, S. Haag, M. Meinke, L. Zastrow, W. Sterry, J. Lademann, Radical production by infrared A irradiation in human tissue, Skin Pharmacol Physiol 23 (2010) 40-46.

[6] M.E. Darvin, S.F. Haag, J. Lademann, L. Zastrow, W. Sterry, M.C. Meinke, Formation of free radicals in human skin during irradiation with infrared light, J Invest Dermatol 130 (2010) 629-631.

[7] P.M. Elias, K.R. Feingold, Skin Barrier, Taylor and Francis group, New York (2006)

[8] M. Costa, N. Benseny-Cases, M. Cócera, C.V. Teixeira, M. Alsina, J. Cladera, et al.: Diagnosis Applications of Non-Crystalline Diffraction of Collagen Fibres: Breast Cancer

and Skin Diseases, In Applications of Synchrotron Light to Scattering and Diffraction in Materials and Life Sciences, Springer, 2009, pp. 265-280.

[9] J.J. Nam, K.E. Lee, Y.J. Kim, Metal oxide-coating PMMA or Talc as a new IR blocker inhibits IR-induced decrease of collagens in human dermal fibroblasts, Int J Cosmet Sci 37 (2015) 433-437.

[10] M. Cocera, G. Rodrıguez, L. Rubio, L. Barbosa-Barros, N. Benseny-Cases, J. Cladera, et al., Characterisation of skin states by non-crystalline diffraction, Soft Matter 7 (2011) 8605–8611.

[11] G. Rodriguez, L. Rubio, M. Cocera, J. Estelrich, R. Pons, A. de la Maza, et al., Application of bicellar systems on skin: diffusion and molecular organization effects, Langmuir 26 (2010) 10578-10584.

[12] E. Fernández, L. Fajarí, G. Rodríguez, C. López-Iglesias, M. Cócera, L. Barbosa-Barros, et al., Bicelles and bicosomes as free radical scavengers in the skin, RSC Advances 4 (2014) 53109-53121.

[13] E. Fernández, G. Rodríguez, M. Cócera, L. Barbosa-Barros, C. Alonso, C. López-Iglesias, et al., Advanced lipid systems containing β-carotene: stability under UV-vis radiation and application on porcine skin in vitro, Phys Chem Chem Phys 17 (2015) 18710-18721.

[14] K.S. Schmitz, An introduction to dynamic light scattering by macromolecules, Academic Press, San diego (CA), 1990.

[15] J.A. Bouwstra, G.S. Gooris, W. Bras, H. Talsma, Small angle X-ray scattering: possibilities and limitations in characterization of vesicles, Chem Phys Lipids 64 (1993) 83-98.

[16] J. Stankowski, W. Hilczer, Introduction to magnetic resonance spectroscopy, Warszawa: Wydawnictwo Naukowe PWN, 2005.

[17] G.R. Buettner, Spin trapping: ESR parameters of spin adducts, Free Radic Biol Med 3 (1987) 259-303.

[18] R. Haywood, F. Rogge, M. Lee, Protein, lipid, and DNA radicals to measure skin UVA damage and modulation by melanin, Free Radic Biol Med 44 (2008) 990-1000.

[19] G.R. Eaton, S.S. Eaton, D.P. Barr, R.T. Weber, Quantitative Epr, Springer Science & Business Media, 2010.

[20] T. Herrling, K. Jung, J. Fuchs, The role of melanin as protector against free radicals in skin and its role as free radical indicator in hair, Spectrochim Acta A: Mol Biomol Spectrosc 69 (2008) 1429-1435.

[21] P.M. Plonka, Electron paramagnetic resonance as a unique tool for skin and hair research, Exp Dermatol 18 (2009) 472-484.

[22] S. Cho, M.J. Lee, M.S. Kim, S. Lee, Y.K. Kim, D.H. Lee, et al., Infrared plus visible light and heat from natural sunlight participate in the expression of MMPs and type I procollagen as well as infiltration of inflammatory cell in human skin in vivo, J Dermatol Sci 50 (2008) 123-133.

[23] H. Tsuchihashi, M. Kigoshi, M. Iwatsuki, E. Niki, Action of beta-carotene as an antioxidant against lipid peroxidation, Arch Biochem Biophys 323 (1995) 137-147.

[24] L. Mueller, V. Boehm, Antioxidant activity of beta-carotene compounds in different in vitro assays, Molecules 16 (2011) 1055-1069.

[25] L.K. Tamm, S.A. Tatulian, Infrared spectroscopy of proteins and peptides in lipid bilayers, Quart Rev Biophys 30 (1997) 365-429.

[26] R.H. Muller, R.D. Petersen, A. Hommoss, J. Pardeike, Nanostructured lipid carriers (NLC) in cosmetic dermal products, Adv Drug Deliv Rev 59 (2007) 522-530.

[27] G. Rodríguez, L. Barbosa-Barros, L. Rubio, M. Cócera, F. Fernández-Campos, A. Calpena, et al., Bicelles: New Lipid Nanosystems for Dermatological Applications, J Biomed Nanotech 11 (2015) 282-290.

Figure 1

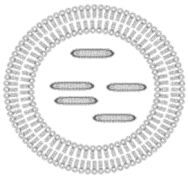

Figure 2

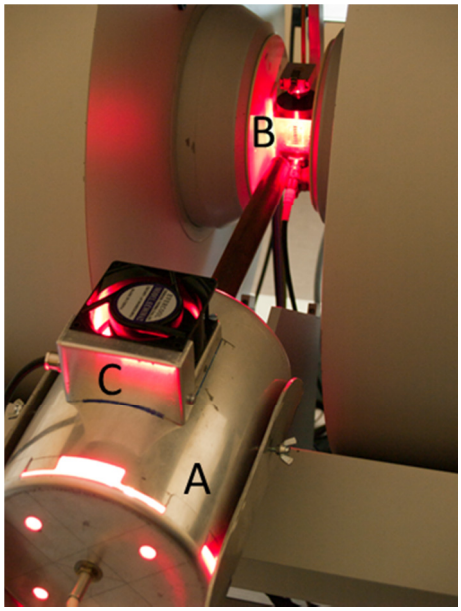

Figure 3

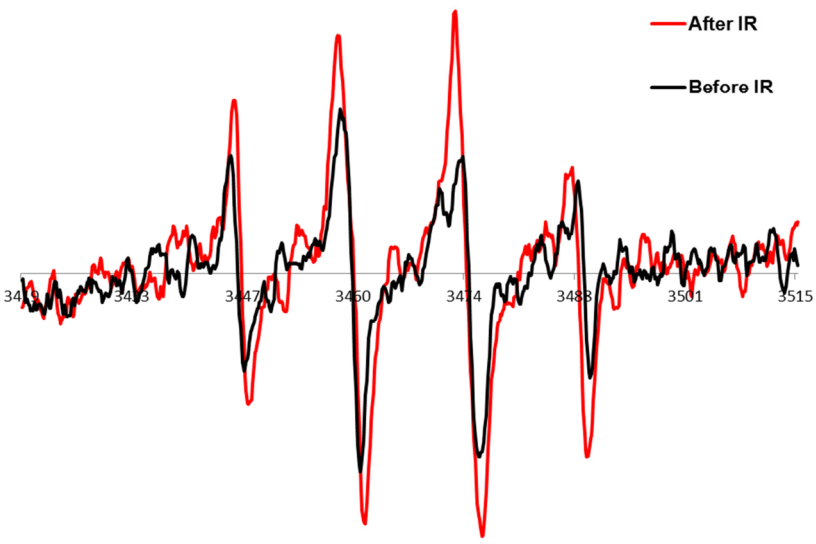

Figure 4

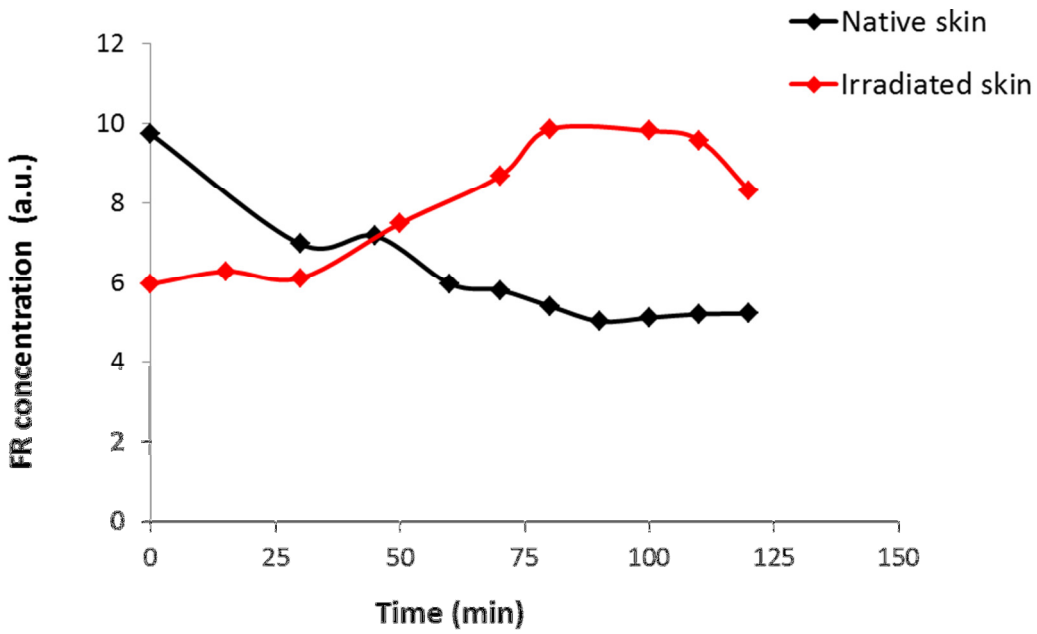

Figure 5

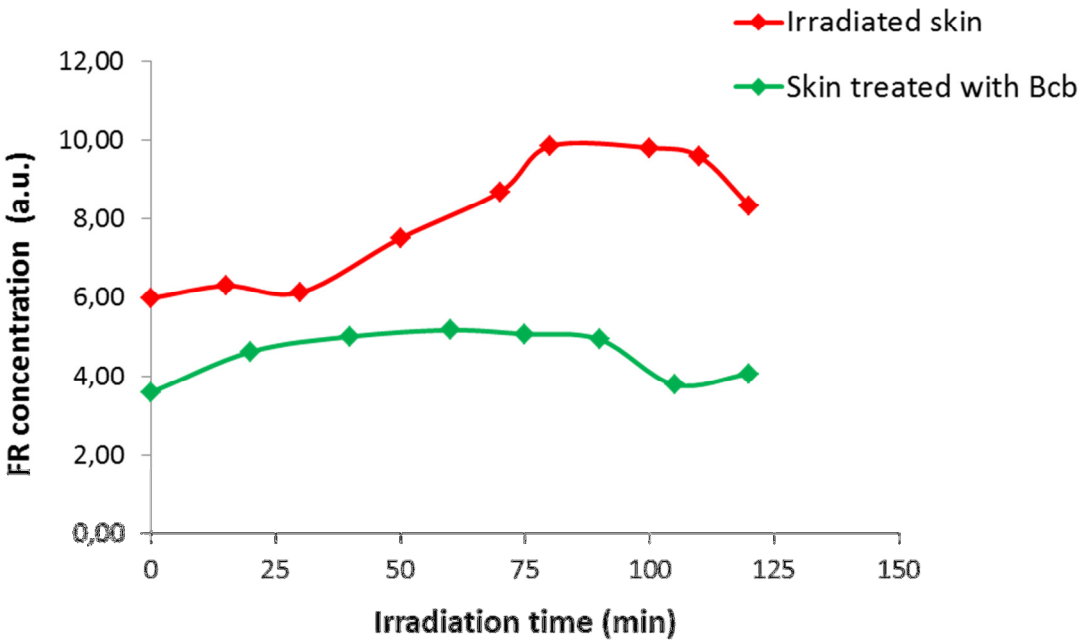

Figure 6

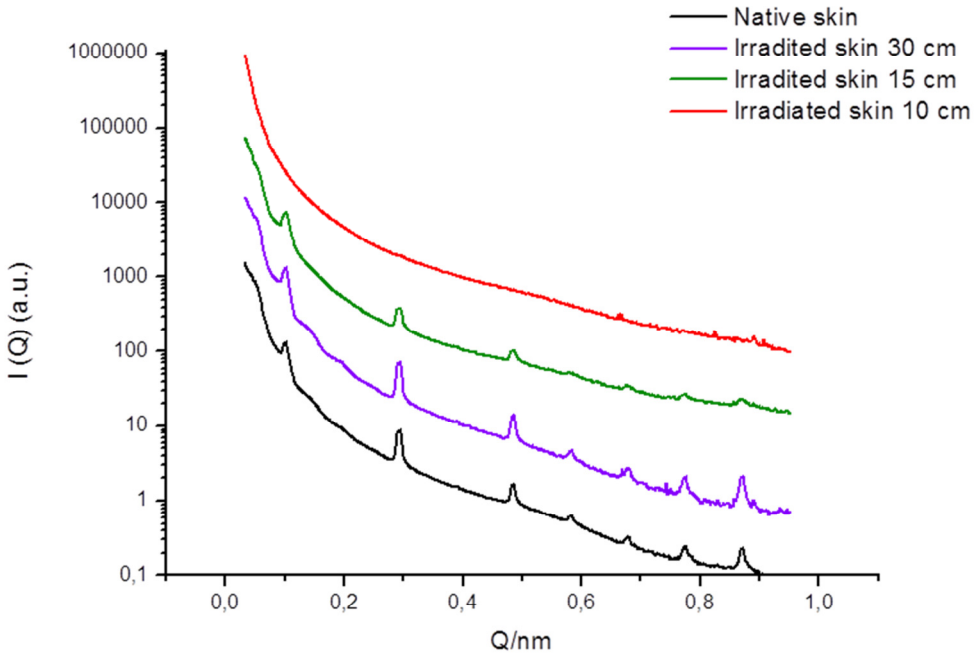

Figure 7

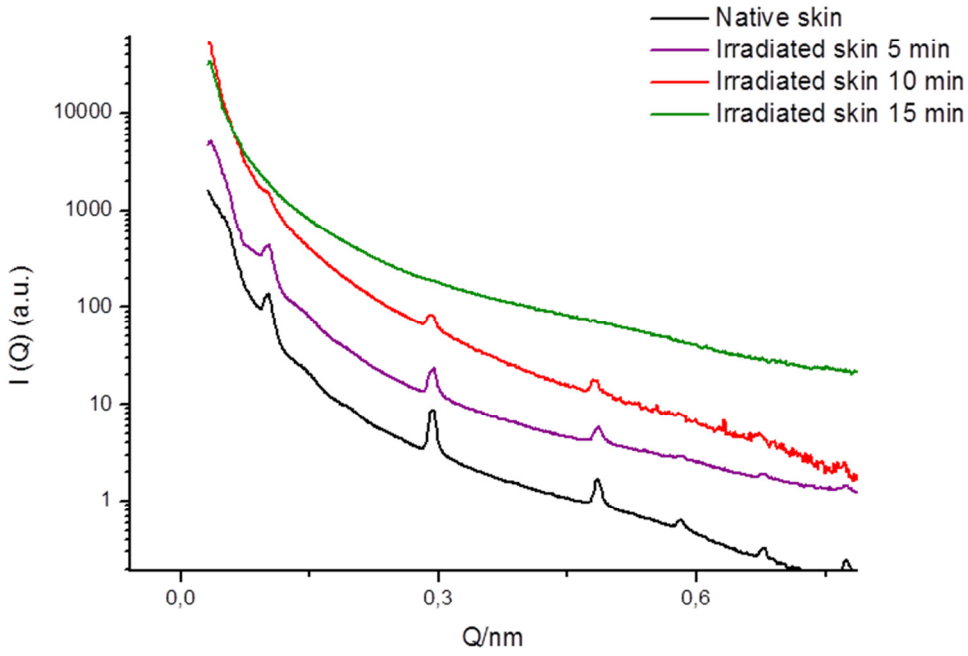

Figure 8

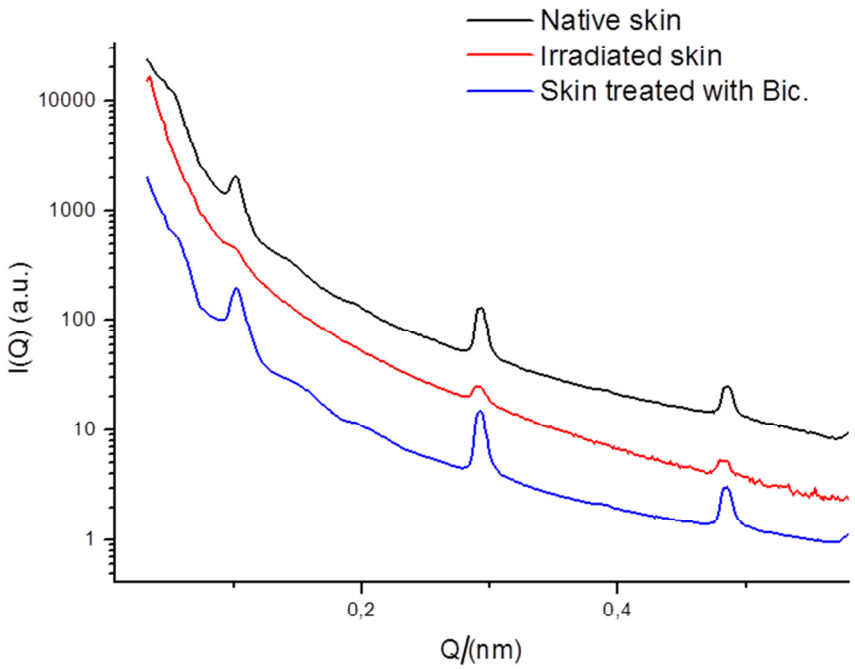

Figure 9

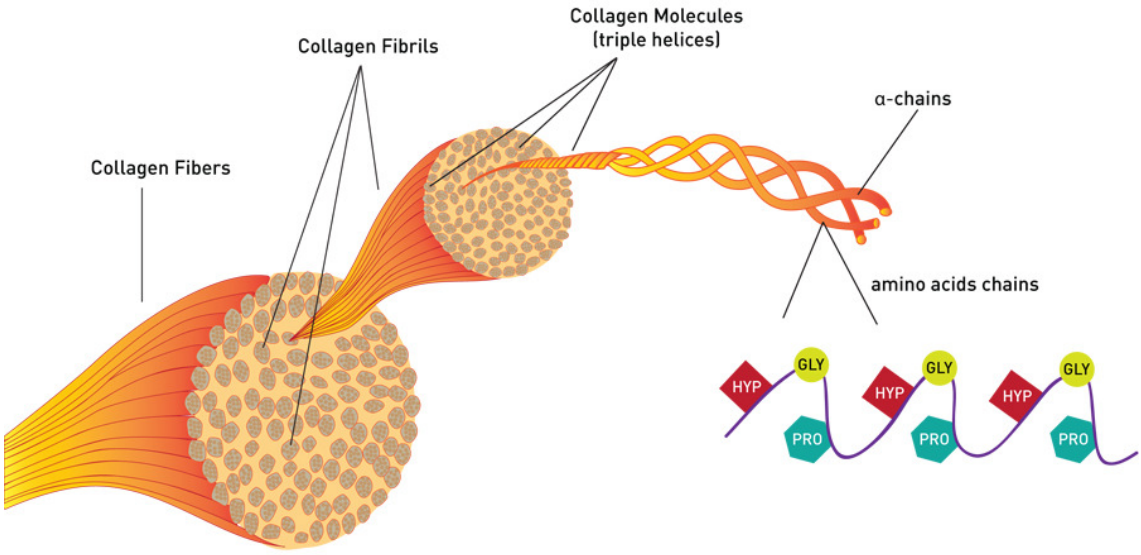

Figure Captions

Fig. 1. Bicosome structure.

Fig. 2. Homemade IR device attached to EPR equipment: A) Aluminium block isolating the IR lamp, B) EPR cavity and C) ventilator.

Fig. 3. EPR spectra of skin before and after IR exposure. Dose: 777.6 J/ cm^2.

Fig. 4. FR concetration for native and irradiated skin at different times. Irradiation intesity: 0.108 W/cm^2.

Fig. 5. FR cocentration at different irradiation times for irradiated skin and for skin tretaed with bicosomes incorporating β-carotene. Irradiation intensity: 0.108 W/cm^2.

Fig. 6. SAXS profiles of native skin and irradiated skin for 30 min at 30 cm (violet line), 15 cm (green line) and 10 cm (red line) from the source. The spectra were shifted on the vertical axis to allow visual comparison.

Fig. 7. SAXS profile of native skin and irradiated skin at 10 cm skin-lamp distance for 5 min (violet line), 10 min (red line) and 15 min (red line) showing the gradual collagen degradation. The spectra were shifted on the vertical axis to allow visual comparison.

Fig. 8. SAXS profiles of different skin samples with the correspondent reflections of collagen. Native skin (black), irradiated skin (red) and skin treated with bicosomes incorporating β-carotene (blue). The spectra were shifted on the vertical axis to allow visual comparison.

Fig. 9. Schematic drawing of the collagen structure in tissues.

4. DISCUSIÓN

4. DISCUSIÓN

4.1. EFECTO DE LA RADIACIÓN SOLAR EN EL CABELLO

La radiación solar causa la oxidación del cabello. Este proceso comienza por la degradación de la melanina formando radicales libres [33]. Las diferentes consecuencias de la oxidación del cabello son la ruptura de los enlaces disulfuro de la fibra, la oxidación de proteínas y aminoácidos como el Trp, la formación de peróxidos de los lípidos y la alteración de características físicas como el color, el brillo, la hidratación, la impermeabilidad o la resistencia mecánica [75-79]

La radiación UV es la principal responsable del daño causado en el cabello. Mientras la luz UVA es responsable del cambio de color, la luz UVB participa en la ruptura de enlaces de disulfuro en el interior y en la superficie de la fibra. En general, el daño producido por los rayos UVB es mayor que el producido por la luz UVA.
La radiación IR está presente en herramientas para el cuidado y acondicionamiento del cabello, y actualmente no existen estudios sobre los efectos de esta radiación en las fibras de cabello. Por lo tanto, dado que estas fibras están sometidas diariamente a luz IR, sería importante determinar si esta radiación es capaz de generar algún efecto negativo sobre el cabello.

Para poder evaluar los efectos de la radiación solar en el cabello, primero es necesario optimizar metodologías que puedan cuantificar las consecuencias mencionadas anteriormente. Este fue el objetivo del artículo 1, donde el cabello se sometió a radiación UV-VIS y se evaluaron diferentes propiedades físicas y químicas antes y después de la irradiación. Una vez optimizadas las metodologías que determinan la oxidación del cabello, se determinó la eficacia de dos formulaciones de antioxidantes derivadas de las hojas de alcachofa y del arroz. Además, con el fin de poder determinar si la luz IR puede tener efectos negativos en el cabello, se estudió la formación de radicales libres en esta fibra exponiéndola a esta radiación. Los resultados de este último estudio se han añadido en el apartado 4.1.3. de la discusión ya que aún no han sido publicados.

4.1.1. Alteraciones físicas del cabello causadas por la radiación UV-VIS

La técnica de SEM permite evaluar los cambios de la superficie del cabello (la cutícula) causados por radiación UV-VIS.

Las fotografías de los cabellos irradiados mostraron las cutículas levantadas, lo que indicó un daño superficial (artículo 2). Además, el estado de la cutícula también está relacionado con el brillo del cabello. Una cutícula dañada conlleva una pérdida de brillo [80], consecuencia que se observó claramente en los valores de brillo de los cabellos irradiados (artículo 2).

Igual que el brillo, el color es otra característica que se ve afectada por la radiación UV-VIS. La melanina, responsable del color de la fibra, proporciona protección solar al cabello filtrando y disipando en forma de calor la radiación solar. Sin embargo, con una excesiva dosis de irradiación, este pigmento se degrada, y los cabellos sufren una pérdida de color [33]. Esta pérdida de color se reflejó claramente en los resultados colorimétricos de las fibras irradiadas (artículo 2).

Por último, los resultados de trabajo de ruptura dan información sobre la integridad del cabello. Valores elevados de este parámetro señalan una mayor presencia de puentes de disulfuro en la estructura de la fibra indicando una gran resistencia mecánica [81]. Los resultados obtenidos en la medición de este parámetro no mostraron diferencias entre una fibra normal e irradiada. Probablemente, en este caso la dosis de irradiación no fue suficiente para modificar el trabajo de ruptura del cabello.

4.1.2. Alteraciones químicas del cabello causadas por la radiación UV-VIS

Un radical libre tiene un tiempo de vida media muy corta, por lo que reacciona rápidamente con otras espéciese, para generar otros radicales u otras moléculas neutras. En un tejido celular, en ausencia de irradiación u otra alteración externa, existe un equilibrio entre los radicales formados naturalmente y los destruidos por los antioxidantes. Sin embargo, mediante la exposición UV se altera este equilibrio y la cantidad de radicales formados es mayor que la cantidad de radicales destruidos, y como consecuencia la concentración total de radicales libres incrementa [33]. Cuando se deja de irradiar, se interrumpe la generación de radicales libres, observándose una

rápida disminución en la concentración de radicales, correspondiente al decaimiento de estas especies (decay) [10].

Los resultados de EPR del artículo 1 mostraron un incremento en la concentración de radicales libres al irradiar las fibras a 283 W/m^2 durante 45 y 90 min (Dosis: 76 y 152 J/cm^2 respectivamente), y una vez interrumpida la irradiación, la concentración de radicales libres descendió. Por el contrario, el cabello irradiado a 500 W/m^2 no mostró el típico descenso de radicales libres al interrumpir el proceso. Estas fibras se irradiaron durante 24 h, por lo que posiblemente este exceso de irradiación oxidó demasiado las fibras desequilibrando su comportamiento normal. Así pues, para evaluar la concentración de radicales libres en el cabello mediante EPR, se decidió establecer la intensidad de irradiación en 283 W/m^2 y los tiempos de exposición entre 30 y 90 min.

La oxidación de la fracción proteica del cabello conlleva cambios estructurales en esta fibra, y hace las proteínas más fáciles de ser extraídas del cabello [35]. Por lo tanto, una mayor concentración de proteínas extraídas indica una mayor oxidación de las mismas. Las condiciones para una óptima extracción se establecieron en una masa mínima de cabello de 100 mg, una temperatura de 45ºC y un tiempo de 5 h. Estas condiciones fueron las adecuadas para obtener resultados coherentes en el ensayo de Bradford, donde se observó como la cantidad de proteína extraída fue mayor a medida que aumenta el tiempo de irradiación (artículo 1).
Respecto al aminoácido Trp, la descomposición de 50 mg de cabello con una solución de NaOH 2M demostró ser útil para poder cuantificar la concentración de este aminoácido en el cabello mediante fluorescencia. Asimismo, también se observó una degradación del Trp a medida que se aumentaba el tiempo de exposición a la luz UV-VIS (artículo 1).

El cabello humano contiene entre 1.9 y 5 % de lípidos, una cantidad que aunque sea pequeña, juega un papel importante en la estructura del cabello [82]. La radiación solar también puede oxidar los lípidos del cabello formando especies de peróxido. Estas especies dañan principalmente el CMC. Para poder evaluar la oxidación de los

lípidos del cabello, es necesario encontrar unas condiciones óptimas de extracción de los peróxidos formados en esta fibra. Teniendo en cuenta que la cantidad de lípidos en el cabello es menor que la cantidad de proteína, la masa para una extracción optima se estableció en 500 mg, una cantidad mayor que la que se necesitó para extraer las proteínas. Esta cantidad de cabello es suficiente para obtener unos resultados coherentes en el ensayo del TBA, donde se observó que la concentración de peróxidos incrementaba a medida que aumentaba el tiempo de irradiación (artículo 1).

4.1.3. Efecto de la radiación IR en el cabello: Formación de radicales libres a temperatura ambiente

Actualmente no hay estudios que demuestren el efecto oxidativo de la radiación IR en el cabello a pesar de que esta fibra está sometida diariamente a la luz IR tanto procedente del sol como debido a diferente tratamientos capilares. Por lo tanto, es interesante evaluar si esta radiación también es capaz de crear alguna modificación en esta fibra.

Debido a que la oxidación del cabello comienza por la formación de radicales libres (explicado en el apartado 1.2.4.), se realizó un estudio para evaluar la capacidad de la radiación IR formando estas especies.

La radiación IR genera un aumento de temperatura que hace complicado detectar radicales libres por EPR en las condiciones experimentales propuestas. Para solucionar este problema se diseñó un accesorio que pudiese disipar el calor producido por la luz IR sin interrumpir la irradiación. La descripción del accesorio está incluida en el apartado 1.2.4. Dicho accesorio consta de una lámpara de luz IR aislada con un bloque de aluminio. A este bloque se le acopló un ventilador que permitía disipar el calor producido por la radiación IR manteniendo el cabello a temperaturas entre 25 y 30ºC. De esta manera se pudieron obtener y medir los radicales libres del cabello simultáneamente a la irradiación.

Se utilizaron tres muestras de cabello de 32 mg y se sometieron a una intensidad de irradiación de 0.10W/cm^2 durante 30 min (Dosis: 180 J/cm^2). A continuación, en la figura 32 se muestran los resultados obtenidos, donde se representa la concentración

de radicales libres formados en el cabello a diferentes tiempos de exposición a la luz IR (resultados sin publicar).

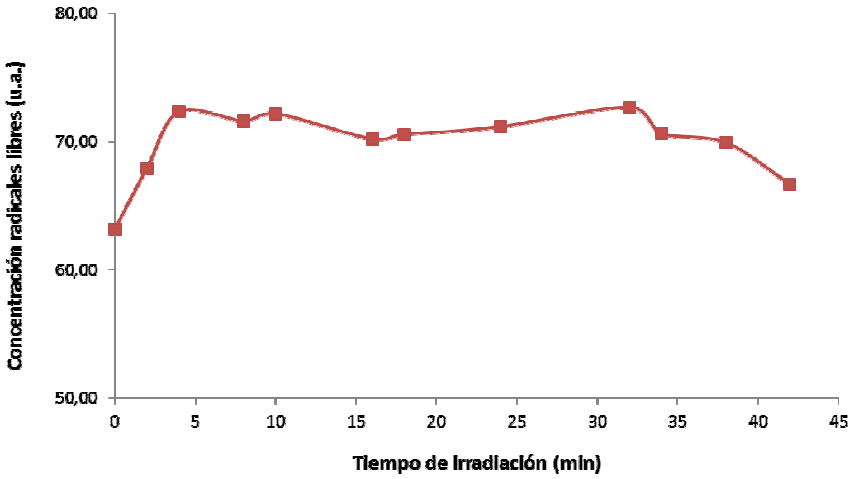

Figura 31: Concentración de radicales libres en el cabello a diferentes tiempos de exposición IR a temperaturas entre 25 y 30ºC (interrupción de la irradiación a los 30 min).

Los resultados muestran un incremento de radicales libres en los primeros 5 min de exposición. A continuación, la concentración de radicales libres se mantiene constante hasta que la irradiación se interrumpe a los 30 min. A partir de este momento, la cantidad de radicales tiende a descender.

El incremento de radicales libres fue alrededor de un 10 %, por lo que se puede concluir que radiación IR también es capaz de crear radicales libres en el cabello a temperaturas entre 25 y 30ºC. A partir de estos resultados, sería interesante evaluar en trabajos futuros si este incremento conlleva algún efecto negativo sobre el cabello.

Resumen

- Alteraciones físicas causadas por la radiación UV-VIS en el cabello
  - Daño cuticular observado por SEM.
  - Pérdida de brillo y color.
- Alteraciones químicas causadas por la radiación UV-VIS en el cabello
  - Incremento de radicales libres determinado por EPR.
  - Aumento de la degradación proteica determinada por el ensayo de Bradford.
  - Aumento de la degradación del aminoácido Trp determinada por espectroscopia de fluorescencia.
  - Aumento de la formación de peróxidos de lípidos determinada por el ensayo del TBA.
- Efectos de la radiación IR en el cabello
  - Incremento de radicales libres en un 10% a temperaturas entre 25 y 30ºC.

4.1.4. Uso de antioxidantes

Las metodologías optimizadas para cuantificar la oxidación del cabello descritas en el apartado anterior, resultaron muy útiles para evaluar la eficacia de productos antioxidantes sobre la fibra. El uso de antioxidantes para prevenir la oxidación del cabello es objeto de estudio de muchas publicaciones, y fue el objetivo del artículo 2 enfocándose en dos formulaciones concentras, KERACYN tm y KERARICE tm (suministradas por la empresa Provital). Estos productos fueron formulados a partir de dos extractos, uno obtenido de hojas de alcachofa (*Cynara scolymus L.*) y otro del arroz (*Oryza sativa L.*).

Los activos principales del **extracto de las hojas de alcachofa** fueron los ácidos hidroxicinámicos. Estos ácidos son un grupo de compuestos cuyos principales representantes son el ácido ferúlico, p-cumárico, cafeico y sinápico, de los cuales el ácido ferúlico y p-cumárico son los de mayor abundancia en la naturaleza. Están formados básicamente por un anillo aromático, un grupo alifático y un ácido carboxílico en el extremo. Son denominados hidroxicinámicos por la sustitución del grupo -OH (hidroxilo) en el anillo aromático (Figura 32), y han demostrado en trabajos previos su actividad antioxidante [83].

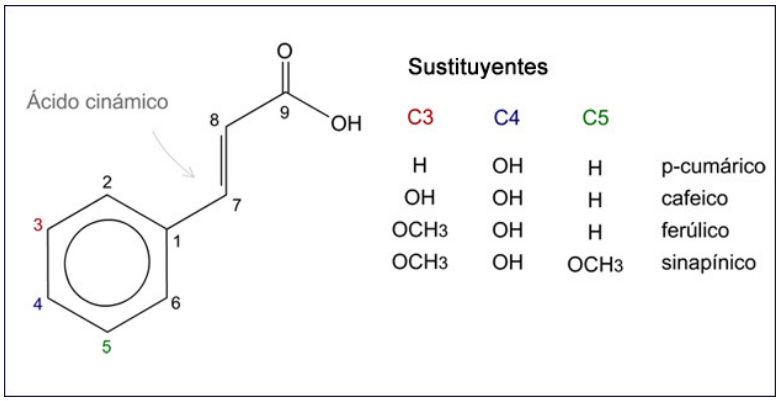

Figura 32: Estructura química del grupo de los ácidos hIdroxicinámicos.

Los flavonoides fueron otros ingredientes también presentes en el extracto de hojas de alcachofa. Estos antioxidantes han demostrado su eficacia como inhibidores de radicales libres [84].

Los principales ingredientes del **extracto de arroz** fueron un grupo de péptidos y aminoácidos biofuncionales, polisacáridos y el ácido fítico. Entre los péptidos presentes se encontraban en gran concentración el ácido glutámico (17%), acido aspártico, y los aminoácidos arginina, leucina, fenilalanina, serina, valina y tirosina (por encima del 10%). Aproximadamente el 80% de los péptidos del extracto de arroz, fueron clasificados de bajo y medio peso molecular. Los péptidos de bajo peso molecular (<1000 Da) son capaces de penetrar en el cabello y reparar la cutícula desde el interior (desde el cortex), y los péptidos de medio peso molecular reparan la fibra desde el exterior del cabello, es decir, desde la cutícula (1000-3000 Da) [85].

Entre los polisacáridos del extracto de arroz, se encontraba principalmente la amilopectina. Su estructura ramificada, le confiere una configuración con capacidad para contener entre 100.000-200.000 moléculas de glucosa, y permite que el producto se mantenga en la superficie del cabello.

Finalmente estaba presente el ácido fítico que ha demostrado ser un inhibidor de radicales libres e inhibidor de la oxidación de lípidos (Figura 33) [86].

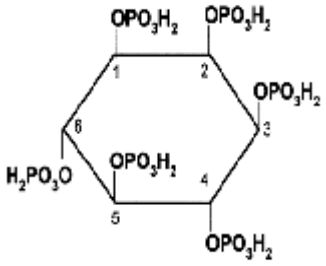

Figura 33: Estructura química del ácido fítico.

Ambas formulaciones se aplicaron en el cabello y posteriormente las fibras tratadas fueron sometidas a radiación UV-VIS. Por último, se evaluó la oxidación de las fibras utilizando las metodologías descritas en el artículo 1.

Los valores de trabajo de ruptura obtenidos para muestras de cabello tratadas con ambas formulaciones y posteriormente sometidas a irradiación, mostraron un aumento de este parámetro en comparación con las fibras no tratadas. Este hecho implicó un aumento de la resistencia mecánica de las fibras tratadas con antioxidantes. En este caso, la formulación más efectiva fue la del extracto de arroz.
Existen varios trabajos que indican que el cortex es el responsable de las propiedades mecánicas del cabello, por lo tanto, un cambio en las propiedades mecánicas de esta fibra es un indicativo de una modificación en el cortex [87]. Probablemente el grupo de péptidos y aminoácidos de bajo peso molecular presentes en el extracto de arroz, fue el responsable del aumento en los valores del trabajo de ruptura. Como se ha comentado anteriormente, los péptidos de tamaños inferiores a 1000 Da son capaces de penetrar hasta el cortex, por lo que seguramente reforzaron las fibras tratadas con esta formulación.

En el caso de las proteínas, el aminoácido Trp y los lípidos, los resultados mostraron que ambas formulaciones previenen su oxidación. La formulación más efectiva para evitar la oxidación de las proteínas y los lípidos fue la del extracto de alcachofa. En este caso, los derivados del ácido hidroxicinámico y los flavonoides presentes podrían haber sido los responsables de este efecto protector. Sin embargo, en el caso de la

protección del aminoácido Trp, la mezcla de antioxidantes presente en la formulación de arroz fue la más efectiva.

Las imágenes de SEM de la superficie del cabello, mostraron las cutículas de las fibras tratadas con antioxidantes completamente cerradas, al contrario que las cutículas de cabello sin formulación antioxidante. Estas últimas se encontraron levantadas, lo que indicó un daño cortical causado por la radiación UV-VIS. Por lo tanto, el recubrimiento del cabello con las formulaciones fue responsable de la protección de la superficie del cabello.

Por último, el brillo y el color se conservaron significativamente mejor en las fibras tratadas con ambas formulaciones (cabello normal y teñido). Para ambas propiedades la formulación de extracto de arroz fue la más efectiva, por lo que la formulación a base de péptidos, polisacáridos y antioxidantes pareció ser la mejor opción para conservar estas dos propiedades físicas del cabello.

En la siguiente tabla se muestra un resumen de resultados indicando cuál de las dos formulaciones fue más eficaz en cada estudio.

Formulación / Estudio	**Extracto de hojas de alcachofa**	**Extracto de arroz**
Trabajo de ruptura		X
Oxidación proteica	X	
Degradación Trp		X
Peroxidación lipídica	X	
Superficie (cutícula)	X	X
Brillo		X
Color		X

4.2. EFECTO DE LA RADIACIÓN SOLAR EN LA PIEL

La radiación solar ayuda a mejorar determinados problemas cutáneos y hace posible la producción de la vitamina D [88, 89]. Sin embargo, exposiciones prolongadas a la radiación solar pueden provocar un exceso de radicales libres en la piel. El desequilibrio de estas especies es entre otros factores, responsable del envejecimiento prematuro de la piel, la despigmentación, el eritema/edema, la inflamación o incluso el cáncer [90].

La luz UVA causa variaciones inmediatas en la pigmentación de la piel. Además puede provocar enrojecimiento y envejecimiento cutáneo. Esta radiación penetra en la piel más profundamente que la radiación UVB pudiendo alcanzar la dermis [91]. Debido a esto, los rayos UVA pueden dañar al sistema inmunológico y ocasionar enfermedades como el melanoma [91].

Los rayos UVB tienen rangos de energía superiores a los rayos UVA. La radiación UVB puede dañar directamente las proteínas, los lípidos y el ADN de las células de la piel, y es la principal responsable de las quemaduras solares. Asimismo, se ha descrito que causa la mayoría de los cánceres de piel [92, 93]. Igual que en el cabello, en la piel la radiación UVB se considera más perjudicial que la luz UVA [90].

Las radiaciones VIS e IR también son capaces de formar radicales libres en la piel. Se ha demostrado que en ciertas condiciones la luz azul puede incrementar la concentración de radicales libres en este tejido [14]. La radiación IR alcanza las capas más profundas de la piel y causa la pérdida de firmeza y elasticidad que son responsables del envejecimiento cutáneo [94]. Esta radiación provoca un incremento de temperatura que se denomina “estrés térmico” elevando la concentración de radicales libres en la piel. Además, se ha demostrado que la exposición a la luz IR provoca una respuesta mitocondrial que conduce a un incremento en la expresión de la metaloproteasa de matriz-1 (MMP-1), enzima responsable de la descomposición del colágeno en la piel [11].

El tratamiento con antioxidantes podría ser una posibilidad para reducir las consecuencias citadas anteriormente. Sin embargo, la incorporación de antioxidantes

en la piel puede resultar muy complicada debido a la función barrera que ejerce el EC [41]. El uso de vehículos lipídicos para facilitar la incorporación de activos en la piel es una estrategia muy utilizada [95]. En esta tesis se han utilizado dos sistemas lipídicos de escala nanométrica para llevar a cabo los tratamientos con antioxidantes, las bicelas y los bicosomas. Para poder evaluar si el tratamiento con antioxidantes incluidos en las bicelas y los bicosomas tiene un efecto protector frente a radiación solar, el primer paso es estudiar la interacción que tienen estos sistemas lipídicos con la piel. Dado que la interacción de las bicelas con la piel se ha estudiado en previos trabajos [96], en esta tesis se estudia principalmente la interacción de los bicosomas con este tejido.

4.3. OPTIMIZACIÓN DE LA TÉCNICA DE EPR PARA DETECCIÓN DE RADICALES LIBRES EN TEJIDOS LIPOQUERATINICOS

Para determinar la concentración de radicales libres en el cabello y la piel mediante la técnica de EPR, fue necesario optimizar condiciones tales como, el tiempo de irradiación o la concentración de "spin-trap" a aplicar.

La determinación de la cantidad de radicales libres de la piel implica un proceso más complicado que en el cabello. Los radicales libres formados en la piel son más inestables que los del cabello, y no son detectados por EPR. Para solucionar este problema, es necesario la utilización de una molécula (un "spin-trap") que se encarga de capturar los radicales libres formados en la piel para hacerlos más estables, y así, poder detectarlos por EPR [72]. El funcionamiento de un "spin-trap" está incluido en el apartado 1.4.4.1.

El hecho de que los radicales libres de la piel sean más inestables que los del cabello, está relacionado con la movilidad que tienen estas especies dentro de cada tejido. El cabello es una estructura sólida, en cambio, la piel es un tejido más fluido debido al agua que se encuentra en su interior. Los radicales libres formados en el cabello, tienen menos movilidad que los formados en la piel, por lo que la posibilidad de neutralizarse o reaccionar formando nuevas especies es más difícil en el cabello que en la piel. La vida de los radicales libres del cabello puede extenderse días, mientras que los radicales libres de la piel pueden desaparecer en cuestión de segundos.

4.3.1. Aspectos del "spin-trap" a tener en cuenta

El "spin-trap" es una molécula muy reactiva, por lo que su manipulación y conservación debe ser muy cuidadosa. Se debe evitar su exposición a luz solar, y es necesario que se conserve a -20 ºC para evitar que se descomponga. Su utilización no se puede alargar más de unos 2-3 días ya que pierde efectividad.

La elección y la concentración del "spin-trap" son dos de los puntos más importantes a tener en cuenta a la hora de diseñar un procedimiento para determinar la cantidad de radicales libres en la piel. El "spin-trap" más común es el DMPO, por lo que ésta molécula fue la elegida para los experimentos de esta tesis, aunque también se valoraron otras posibilidades (5-diethoxyphosphoryl-5-methyl-1-pyrroline-n-oxide (DEPMPO) o 2,2,6,6-Tetrameil-piperidin-1-yl) oxyl (TEMPO)).

La concentración de "spin-trap" aplicada a la piel debe ser capaz de capturar una cantidad suficiente de estas especies dentro del límite de detección del equipo.

Una vez tratada la piel con el DMPO, es necesario realizar un lavado con agua para quitar el exceso de esta molécula, ya que un exceso de esta molécula podría inducir a resultados erróneos. El lavado con agua de la piel debe ser suficiente para retirar el exceso de DMPO evitando diluirlo demasiado, ya que una dilución excesiva del "spin-trap" conlleva a alejarse del límite de detección del equipo.

Por último, el volumen de DMPO aplicado en la piel también es muy importante ya que debe de penetrar una cantidad suficiente de molécula en este tejido. En esta tesis se aplicó un volumen de 10 µl de solución de DMPO por cada 25 mm^2 de piel.

4.3.2. Radiación UV-VIS vs Radiación IR

La radiación IR genera un aumento de temperatura que hace complicada la detección de radicales libres por EPR en las condiciones experimentales propuestas. Para solucionar este problema se diseñó un accesorio que pudiese disipar el calor producido por la luz IR sin interrumpir la irradiación. La descripción del accesorio está incluida en el apartado 1.2.4. De esta manera, se consiguió evaluar la influencia que tiene la energía de la luz IR en tejidos y fibras como la piel y el cabello, algo que no se había estudiado hasta entonces.

Los parámetros de medición del equipo utilizados tanto en cabello como en piel fueron las mismas con radiación UV-VIS y radiación IR. Sin embargo, tanto en cabello como en piel, la dosis necesaria para observar un incremento de radicales libres, fue menor utilizando radiación UV-VIS que luz IR. La dosis necesaria para observar un incremento de radicales libres en el cabello fue de 76 J/cm^2 por radiación UV-VIS y de 180 J/cm^2 por exposición a la luz IR. En el caso de la piel, la dosis necesaria para observar un incremento de radicales libres fue de 27 J/cm^2 por radiación UV-VIS y de 778 J/cm^2 por exposición a la luz IR. Este hecho es lógico teniendo en cuenta que la radiación IR es mucho menos energética que la radiación UV-VIS. Por lo tanto, para tener un incremento de radicales libres causado por radiación IR, es necesario aplicar una dosis mayor que la aplicada por radiación UV-VIS.

En los experimentos con radiación IR, fue necesario utilizar más sección de piel que en las mediciones con radiación UV-VIS, y por lo tanto se utilizó más volumen de DMPO. Probablemente, los radicales libres formados por radiación IR en una sección de 25 mm^2 (igual que con radiación UV-VIS), no fueron suficientes para ser detectados por el equipo de EPR, es decir, la cantidad de estas especies capturadas por el DMPO estaba fuera del límite de detección del equipo. Por lo tanto, aumentando la sección de piel, la cantidad de radicales libres formados en este tejido incrementa, y consecuentemente esa cantidad puede ser detectada por EPR.

RESUMEN

- Para la determinación de radicales libres en la piel se requiere el uso de una molécula "spin-trap" debido a que los radicales libres formados en este tejido son muy inestables y no se pueden detectar directamente por EPR.
- Es importante optimizar la concentración de "spin-trap" necesaria para capturar los radicales formados en el tejido antes de realizar una serie de experimentos.
- La formación de radicales libres en el cabello y en la piel por radiación IR necesita dosis más elevadas que por luz UV-VIS.

4.4. INTERACCIÓN DE LOS BICOSOMAS CON LA PIEL

A continuación, se discuten aspectos relacionados con la interacción de los bicosomas con la piel. Se describe el mecanismo de penetración de estos sistemas, la influencia de las condiciones de la piel y la influencia de la naturaleza de los activos incorporados en los bicosomas.

4.4.1. Mecanismo de penetración de los bicosomas

El análisis microestructural por FSTEM de piel tratada con bicosomas incorporando β-caroteno mostró estructuras adheridas a la superficie de la piel y estructuras dentro del EC, entre los corneocitos (artículo 4). Este hecho indicó dos niveles de interacción de los bicosomas con el tejido cutáneo.

Para entender la interacción entre los bicosomas y la piel, hay que considerar las diferentes nanoestructuras presentes en este sistema lipídico. Los bicosomas son vesículas esféricas que encapsulan estructuras discoidales (bicelas) [66]. Las vesículas exteriores del bicosoma tienen tamaños alrededor de los 200 nm, por lo tanto, no son capaces de penetrar entre los espacios intercelulares del EC (con dimensiones entre 6 y 10 nm), y permanecen sobre la piel pudiendo proporcionar un tratamiento superficial del tejido.

Una vez que la vesícula esférica exterior se abre al contacto con la piel con la piel, las bicelas encapsuladas son liberadas al exterior. Las bicelas tienen diámetros entre los 6 y 20 nm y un espesor de 5 nm, por lo que son capaces de penetrar entre los espacios del EC [63].

La cantidad de agua del EC exhibe un gradiente de hidratación que aumenta desde las capas más exteriores a las más internas [97, 98]. Por lo tanto, a mayores profundidades del EC, el contenido de agua es mayor. Así pues, una vez las bicelas están dentro del EC, estas estructuras discoidales van pasando entre los espacios intercelulares hasta que debido al gradiente de agua, se transforman de discos a vesículas. Esta transición de la forma discoidal a la forma esférica que sufren las bicelas en ambientes diluidos, está relacionada con aspectos físico-químicos de esta estructura, y se ha explicado en el apartado 1.4.1.2.[65, 66].

De esta manera, después de esta transformación las estructuras lipídicas quedan retenidas entre los espacios intercelulares de la piel, y asimismo también queda

retenido el activo que se haya podido incorporar en el bicosoma (artículo 5). Además, considerando que los bicosomas también contienen bicelas que no se han encapsulado durante el proceso de formación, estas bicelas también pueden penetrar mediante el mismo mecanismo.

Por lo tanto, las vesículas que se observaron en las imágenes de FSTEM dentro del tejido proceden de las bicelas presentes en los bicosomas (encapsuladas o no encapsuladas), ya que las vesículas exteriores (de alrededor de 200 nm) son incapaces de penetrar en el EC y solo interaccionarían a nivel superficial. Así pues, la interacción de los bicosomas con la piel ocurre siguiendo un mecanismo de dos pasos; una primera interacción con la superficie de la piel seguida de otra dentro del tejido.

La técnica de FTIR combinada con la radiación sincrotrón permitió evaluar la capacidad de los bicosomas para incorporar activos en la piel. El activo que se incluyó en los bicosomas fue un derivado de Re. Esta molécula es visible en IR y no interfiere con las señales de luz IR del tejido cutáneo. Por lo tanto, es posible distinguir esta molécula en las diferentes capas de la piel mediante FTIR (ver apartado 1.4.4.3.). Además, el comportamiento de este derivado de Re puede servir para predecir el comportamiento de otras moléculas con similitud fisicoquímica al aplicarse en la piel mediante bicosomas.

Para poder evaluar la capacidad de los bicosomas de promover la penetración del derivado de Re, esta molécula también se aplicó en la piel mediante una solución de dimetilsulfoxido (DMSO) 99% V/V que es un solvente típicamente usado para promover la penetración de moléculas en la piel.

Los resultados mostraron una mayor y más profunda penetración del derivado de Re en la piel por medio de los bicosomas. En este caso, el derivado de Re penetró principalmente en el EC y cierta cantidad llegó hasta la Epi. Sin embargo, por medio del DMSO el derivado de Re se quedó retenido en la superficie y en el EC de la piel.

Teniendo en cuenta que el DMSO es un potenciador de la permeabilidad de la piel [99, 100], era de esperar que el derivado de Re hubiese penetrado en la piel de una manera significativa por medio de este solvente. Sin embargo, nuestros resultados indicaron lo contrario. La concentración mínima para que el DMSO se pueda utilizar como

potenciador de la permeabilidad es del 60% V/V [99], y en nuestros experimentos se utilizó una concentración de 99% V/V, por lo que la poca penetración del derivado de Re por medio del DMSO no fue debida a una baja concentración del solvente. La penetración de moléculas en la piel también depende del tamaño y peso molecular de las mismas. Varios estudios han demostrado el poder del DMSO incorporando moléculas como esteroides y antibióticos entre otras [100-104], todos ellos de menor peso molecular que el derivado de Re. Así pues, este hecho podría haber sido una de las razones por las que el derivado de Re penetró en menor cantidad por medio del DMSO.

Por lo tanto, aunque el DMSO es un conocido potenciador de la permeabilidad de la piel, en este estudio el derivado de Re penetró mucho más en la piel por medio de los bicosomas. Así pues, la interacción especifica que poseen los bicosomas con la piel, parece facilitar la penetración de esta molécula en el tejido cutáneo. Se podría esperar que otras moléculas con características parecidas tuvieran un comportamiento de penetración similar por medio de este sistema lipídico.

4.4.2. Efecto de la condiciones de la piel en la penetración de los bicosomas

Teniendo en cuenta que la piel está expuesta a la radiación solar diariamente, es interesante estudiar cómo puede influir esta radiación en la permeabilidad de este tejido. Para ello, se estudió la microestructura de la piel antes y después de la irradiación, y se monitorizó la penetración de los bicosomas en piel expuesta a radiación UV-VIS. La dosis aplicada fue de 90 J/cm^2.

Las micrografías de FSTEM de piel irradiada no mostraron diferencias microestructurales en comparación con la piel no irradiada (artículo 4). En ambas imágenes se observó claramente la estructura laminar lipídica y los corneocitos en buen estado. La irradiación se llevó a cabo con un simulador solar (Suntest CPS+), utilizando un rango entre 310 y 800 nm. En este rango se encuentran la radiación UVB (310-320), la radiación UVA (320-400 nm), la luz VIS (400-760 nm) y la radiación IR-A (760-800).

Se ha descrito que la radiación UVB puede incrementar el espesor del EC y puede dañar la estructura y composición de los corneocitos y de los lípidos, lo que conlleva alteraciones en la función barrera [92, 105]. La radiación UVA también puede modificar la estructura de los lípidos y corneocitos de la piel, aunque de una manera menos agresiva que la luz UVB [91]. Por lo tanto, los rayos UVA se consideran menos perjudiciales que los rayos UVB [90].

La radiación VIS también ha demostrado que puede generar alteraciones en la piel, aunque aplicada en conjunto con luz UV, su efecto en la piel es despreciable [14].

Por último, la radiación IR-A también ocupa un rango dentro de la radiación aplicada (760-800 nm). Esta radiación causa alteraciones principalmente en la dermis, capa cutánea que no fue utilizada en estos experimentos debido a que la función barrera de la piel se establece principalmente en le EC y en la Epi. Por lo tanto, los posibles efectos de esta radiación se despreciaron desde el principio.

La preservación de la microestructura de la piel podría ser debido a que el 90% de la radiación aplicada fue luz UVA y VIS, potencialmente menos dañina que la luz UVB. Además, la radiación UVA se considera más dañina en la capa dérmica (al igual que la radiación IR), capa cutánea que no fue utilizada en los experimentos. Este hecho podría haber sido otra razón por la que no se han observaron cambios microestructurales, aunque probablemente, la causa más influyente fue que la dosis de irradiación aplicada fue insuficiente para modificar la microestructura de la piel.

Las fotografías obtenidas por FSTEM de piel sometida a UV-VIS y tratada con bicosomas, mostraron vesículas en el interior del tejido. Por lo tanto, la radiación UV-VIS tampoco pareció afectar al mecanismo de penetración de estos sistemas lipídicos (mecanismo explicado en el apartado 4.3.1.).

Los espectros de FTIR de la piel no mostraron modificaciones antes y después de la irradiación en cuanto a desplazamiento ni intensidad de vibración de los componentes de la piel (artículo 6). Sin embargo, la penetración de los bicosomas fue menor en piel sometida a radiación UV-VIS que en muestras no irradiadas. Varios trabajos han demostrado que la radiación UV modifica la permeabilidad de la piel, aunque esta modificación no necesariamente tiene que hacer este tejido más permeable. La radiación UVA puede causar la deshidratación de la piel, y como consecuencia, el

transporte de agua dentro de este tejido puede verse afectado [91, 106]. De esta manera, el paso de sustancias acuosas a través de la piel puede quedar restringido. Teniendo en cuenta que los bicosomas son dispersiones acuosas, esta alteración del transporte de agua podría haber afectado a la penetración de estos sistemas lipídicos en la piel irradiada.

Por lo tanto, aunque la radiación UV-VIS no causó modificaciones en la microestructura de la piel, la penetración de los bicosomas se vio alterada posiblemente debido a la alteración de la permeabilidad cutánea.

4.4.3. Influencia de las características de los activos incorporados en el mecanismo de penetración de los bicosomas

Las características del activo incorporado en los bicosomas son un aspecto importante que puede influir en la penetración del sistema lipídico. Los resultados del artículo 6 mostraron como la incorporación de dos antioxidantes con diferentes características físico-químicas modificó la penetración de este sistema lipídico. Los antioxidantes incorporados fueron el β-caroteno y un complejo de Mn. El β-caroteno es insoluble en agua y es altamente lipofílico. El complejo de Mn fue sintetizado mediante la unión de un ligando (*N-(2-hydroxy-benzyl)-N'-hexadecyl-N,N'-bis-(2-(N-methylimidazolyl)methyl)ethane-1,2-diamine*) a una cadena alquílica de 16 carbonos. Este complejo posee una carga positiva y es soluble en agua. Además, tiene una cadena de 16 carbonos que aporta lipofília al compuesto. Por lo tanto, el complejo de Mn posee un cierto carácter anfifílico.

La incorporación del β-caroteno en los bicosomas incrementó el diámetro de las estructuras (artículo 4 y 6). Considerando que el β-caroteno es insoluble en agua, varios estudios sugirieren que el β-caroteno se sitúa dentro de la zona lipofílica de una bicapa [24, 107]. Esta localización conlleva que el β-caroteno esté en contacto con las cadenas lipofílicas de los fosfolípidos y perpendicular a éstas [107]. Por lo tanto, la localización de este antioxidante en la membrana exterior de los bicosomas podría aplanar la bicapa lipídica disminuyendo su radio de curvatura y consecuentemente incrementando el diámetro de este sistema lipídico. Sin embargo, la localización de

este antioxidante en las bicelas no conlleva un notable aumento de diámetro. Al colocarse perpendicular a las cadenas alquílicas, se incorporaría en la zona plana de la bicelas, lo que no conlleva un incremento significativo en el diámetro de los discos (artículo 4).

La incorporación del complejo de Mn junto con el derivado de Re en los bicosomas también incrementó en el diámetro de los bicosomas (artículo 6). Por un lado, el derivado de Re tiene un carácter lipofílico, lo que probablemente favorezca la incorporación de esta molécula en la bicapa lipídica. Por otro lado, el complejo de Mn posee un carácter anfifílico. Su estructura principal es soluble en agua, por lo que su localización se espera en las zonas hidrofílicas de la bicapa. Por otro lado, la cadena de 16 carbonos tiene tendencia a colocarse en la zona lipofílica de la bicapa. Por lo tanto, este complejo se colocará entre las zonas hidrofílicas y lipofílicas de la bicapa de los bicosomas, es decir, paralelo a las cadenas lipofílicas de los fosfolípidos. Esta localización del complejo de Mn en la bicapa de los bicosomas, conllevaría la separación de las cadenas alquílicas de los fosfolípidos aumentando el diámetro del bicosoma. Sin embargo, las bicelas que incorporaban el complejo de Mn fueron menores que las bicelas tradicionales (artículo 6). El complejo de Mn con carácter anfifílico pudo haberse incorporado en los laterales de las bicelas de la misma manera que lo hace el DHPC. Por lo tanto, al haber más moléculas colocadas en los laterales de las bicelas, el diámetro de estas estructuras se reduciría.

Para poder determinar la penetración de los bicosomas que contenían los diferentes antioxidantes mediante FTIR, se incorporó de nuevo el derivado de Re a los sistemas. La localización del derivado de Re en la piel, permitió obtener información sobre la distribución de los bicosomas con los dos antioxidantes en este tejido.

Los resultados mostraron una mayor y más profunda penetración de los bicosomas con complejo de Mn. Este hecho puede entenderse considerando que el mecanismo de penetración de los bicosomas esta guiado por la penetración de las bicelas y por la diferencia de tamaño de estas bicelas al incorporar el activo. Las bicelas del complejo de Mn registraron un diámetro menor que las bicelas de β-caroteno (9-11 nm para las bicelas de complejo de Mn y 11-19 nm para las bicelas de β-caroteno). De esta

manera, las bicelas con complejo de Mn pudieron tener más facilidad para pasar por los espacios intercelulares del EC (6-10 nm) que las bicelas de β-caroteno.

Las diferentes características de los antioxidantes mencionadas anteriormente también pudieron haber tenido influencia en la penetración de los bicosomas. Los bicosomas con β-caroteno tendrían más tendencia a distribuirse en las regiones lipofílicas de la piel, como por ejemplo el EC. Al contrario, los bicosomas con complejo de Mn debido a su carácter anfifílico podrían distribuirse tanto en regiones lipofílicas como hidrofílicas de la piel, es decir, dentro del EC o de la Epi, ya que la Epi contiene un mayor contenido de agua.

RESUMEN

- Los bicosomas interaccionan a nivel superficial y en el interior del tejido cutáneo: la vesícula exterior se funde con la superficie de la piel y las bicelas penetran el EC.
- Una dosis de 90 J/cm^2 (UV-VIS) no modifica la microestructura de la piel *in vitro*, pero incrementa la impermeabilidad de este tejido.
- La incorporación de un activo lipofílico en los bicosomas limita la penetración de este sistema lipídico a las capas más superficiales de la piel. Mientras, la incorporación de un activo con carácter más hidrófilo en los bicosomas, facilita que este sistema lipídico alcance capas más profundas, con mayor contenido de agua.

4.5. ESTABILIDAD DE BICELAS Y BICOSOMAS FRENTE A LA RADIACIÓN UV-VIS

Una vez estudiada la interacción de ambos sistemas lipídicos con la piel y teniendo en cuenta que las bicelas y los bicosomas se aplican en la piel expuesta a radiación solar, es importante saber que comportamiento tendrán estas nanoestructuras al someterlas a irradiación. La estabilidad de ambos sistemas se evaluó mediante estudios físicos y químicos. La estabilidad física se estudió por monitorización de los diámetros y de la morfología de las estructuras (mediante DLS y Crio-TEM, respectivamente).

La estabilidad química se llevó a cabo evaluando la oxidación de los lípidos que forman ambas estructuras. Adicionalmente, se estudió la capacidad de ambos sistemas lipídicos como protectores del antioxidante β-caroteno evitando su oxidación frente a

la radiación UV-VIS. En estos estudios se aplicaron dos dosis diferentes; 90 J/cm^2 y 360 J/cm^2.

4.5.1. Estabilidad física

Para estudiar la morfología de las bicelas y los bicosomas se determinó su tamaño y su estructura antes y después de la irradiación (90 y 360 J/cm^2, artículo 4). Los resultados mostraron que en el caso de las bicelas con y sin el antioxidante β-caroteno, la radiación solar no modificó la estructura ni su tamaño. El tamaño se conservó alrededor de los 14 nm y en las imágenes de microscopia se observó como la estructura discoidal de las bicelas se mantuvo intacta tras la irradiación. Por el contrario, los resultados de DLS mostraron que el tamaño de los bicosomas aumentó tras la exposición a la luz UV-VIS a la dosis de irradiación de 360 J/cm^2. Las imágenes de Crio-TEM de los bicosomas presentaron agregaciones de vesículas, grandes estructuras laminares y bicelas. Probablemente, la vesícula exterior de los bicosomas se rompió agregándose y/o fusionándose con otras vesículas, siendo estas nuevas estructuras los tamaños grandes detectados por DLS.

En general, una bicapa lipídica está estabilizada por diferentes fuerzas, una de ellas es la fuerza de Van der Waals (VDW) [108]. Los lípidos saturados forman interacciones de VDW más fuertes que los lípidos insaturados, por lo que los lípidos saturados forman bicapas mucho más estables que los lípidos insaturados [109-111]. Teniendo en cuenta que las bicelas están formadas por lípidos saturados, y que la vesícula exterior de los bicosomas está formada por lípidos insaturados, las bicelas formarían una estructura más estable que la vesícula exterior de los bicosomas. Este hecho podría ser el responsable de la mayor estabilidad morfológica de las bicelas frente a la irradiación.

4.5.2. Estabilidad química

Los resultados del artículo 4 mostraron que las moléculas de lípido que forman las bicelas y los bicosomas no formaron peróxidos después de la exposición a la radiación UV-VIS (90 y 360 J/cm^2). Probablemente las condiciones de irradiación no fueron suficientes para llegar a oxidar las moléculas de lípido.

El antioxidante β-caroteno se conservó un 100 % en bicosomas, un 58% en las bicelas y un 50% en una solución de cloroformo frente a una dosis de irradiación de 90 J/cm^2. Frente a una dosis de 360 J/cm^2 el β-caroteno se conservó un 95 % en bicosomas, un 10% en las bicelas y un 0% en una solución de cloroformo.

La oxidación del β-caroteno conlleva la adición de su doble enlace a otras moléculas [24, 112]. Este mecanismo de oxidación puede evitarse mediante procesos químicos o físicos. Un mecanismo químico de protección del β-caroteno dentro de las bicelas y los bicosomas conllevaría que otras moléculas tengan que oxidarse en lugar del antioxidante. En los sistemas de bicelas y bicosomas las moléculas presentes a parte del β-caroteno son los lípidos, por lo que un proceso químico para evitar la oxidación de β-caroteno sería la oxidación de los lípidos que forman estas estructuras. Sin embargo, no se observó oxidación lipídica en ninguna de las estructuras, por lo que la conservación del β-caroteno no se debió a que las moléculas de lípido se oxidaron evitando la degradación de este antioxidante.

La conservación de β-caroteno en nuestros estudios podría relacionarse con un fenómeno físico inducido por las moléculas de lípido de los sistemas. Ciertos estudios han demostrado que las propiedades de dispersión de los lípidos pueden reforzar un sistema antioxidante [113, 114]. Por lo tanto, este efecto de dispersión de la radiación que ejercen los lípidos de las bicelas y los bicosomas, pudo ser el responsable del efecto protector de ambos sistemas lipídicos conservando el β-caroteno.

Además, teniendo en cuenta la colocación del β-caroteno en la bicapa lipídica, la protección del antioxidante estaría aún más favorecida. El β-caroteno está totalmente dentro de la bicapa lipídica (perpendicular a las cadenas alquílicas de los fosfolípidos), por lo tanto, el primer contacto de la radiación con las bicelas y los bicosomas se produciría con las moléculas de lípido, que dispersarían la radiación y por lo tanto la intensidad que penetra hasta el interior de la bicapa (donde el β-caroteno está incorporado) sería menor.

Este razonamiento también podría explicar que los bicosomas sean más efectivos conservando el β-caroteno que las bicelas y que una solución de cloroformo de este antioxidante. Los bicosomas con un 15% de concentración de lípidos y una mayor proporción de bicapa tendrían mayor capacidad para dispersar la radiación, mientras

que las bicelas con un 5% de lípidos y la solución de cloroformo con un 0% de lípidos protegerían el β-caroteno con menor efectividad.

RESUMEN

•Una dosis de 360 J/cm^2 (UV-VIS) no modifica la forma ni el tamaño de las bicelas con y sin β-caroteno.

• Una dosis de 360 J/cm^2 (UV-VIS) modifica la estructura de los bicosomas. La vesícula exterior se rompe agregándose y/o fusionándose con otras vesículas y formando estructuras lipídicas más grandes y de diversa morfología.

• Una dosis de 360 J/cm^2 (UV-VIS) no oxida las moléculas de lípido que forman las bicelas y los bicosomas .

• A una dosis de 360 J/cm^2 (UV-VIS) el β-caroteno se conserva un 95% si está incluido en los bicosomas y un 10% si está incluido en la bicelas, mientras que la conservación del antioxidante en liposomas es del 70% y en solución de cloroformo del 0%.

4.6. BICOSOMAS Y BICELAS COMO SISTEMAS ANTI-RADICALARIOS EN LA PIEL

A continuación, se discute la capacidad anti-radicalaria que poseen las bicelas y los bicosomas en una piel expuesta a radiación solar mediante EPR, y se evalúa el efecto causado por la incorporación de β-caroteno en la capacidad anti-radicalaria de ambos sistemas lipídicos. Además, mediante la simulación de los espectros obtenidos por EPR, se analizan los diferentes tipos de radicales libres formados en la piel por radiación UV-VIS.

4.6.1. Radicales libres en piel nativa antes y después de la exposición a radiación UV-VIS

La piel nativa sin exponerla expresamente a la radiación contiene una concentración de radicales libres detectables por EPR, que incrementa cuando se le aplica una fuente de radiación. La radiación UV-VIS provocó un incremento en la concentración de radicales libres en una piel nativa (Dosis: 27 J/cm^2).

Mediante la simulación de los espectros obtenidos se identificaron seis tipos de aductos de DMPO en la piel, aductos del grupo alcoxi (primarios/secundarios y

terciarios), aductos de carbono, aductos de hidroxilo (DMPO-OH), de hidrógeno (DMPO-H) y aductos aminoxil (RR`NO). Los aductos de carbono fueron los más abundantes en la piel.

En base a publicaciones anteriores, se sugirió que los aductos del grupo alcoxi (primarios y secundarios) eran inducidos por las moléculas de lípidos de la piel, mientras que los aductos alcoxi terciaros podrían proceder de las proteínas de bajo peso molecular presentes en este tejido [115, 116]. Las señales de los aductos del grupo alcoxi primarios y secundarios también pueden asociarse a aductos de azufre, sin embargo, los aductos de azufre tienen una vida media más pequeña que los aductos del grupo alcoxi [117], por lo que esta señal se atribuyó a los alcoxilos. Por otro lado, los aductos del grupo alcoxi también forman espectros similares a los aductos de peróxido, aunque se ha demostrado que los aductos de peróxido son especies intermediarias de la formación de los aductos del grupo alcoxi [118]. Por lo tanto, se descartó la presencia de aductos de peróxido.

La formación de aductos de carbono se asoció principalmente a la oxidación de los fosfolípidos de la piel, al Trp de la queratina o al ADN de las células [115, 116]. Estos aductos fueron los más abundantes tanto antes como después de la irradiación. Este hecho es bastante lógico teniendo en cuenta que la piel es un tejido compuesto principalmente por moléculas orgánicas.

Respecto a los aductos DMPO-OH y DMPO-H varios trabajos han atribuido su presencia a la vitamina B2 (rivoflabina) y al ADN [115, 116]. Además, el radical DMPO-H se ha asociado a aminoácidos como la arginina [115]. En el caso del aducto DMPO-H, este fue el único aducto que no se encontró después a la irradiación. La inestabilidad de este radical podría haber sido la razón por la que desapareciese después de la irradiación [119].

Por último, se identificaron los aductos aminoxil. Este tipo de aducto deriva de una doble sustitución en el “spin-trap” DMPO. En general los aductos de DMPO detectados por EPR, están formados por un radical libre acoplado a la molécula de DMPO (ver Figura 24). Sin embargo, una vez que el DMPO forma un aducto con un radical, este aducto posee otra posición disponible donde otro radical puede colocarse. Si un segundo radical se coloca en la posición libre, el DMPO pasaría a estar unido a dos

radicales libres, es decir, pasaría a esta doblemente sustituido. Por lo tanto, la incorporación de dos radicales libres en el DMPO forma el aducto aminoxil.

4.6.1.1. Influencia de la estructura lipídica en la capacidad anti-radicalaria de las bicelas y los bicosomas

Tanto las bicelas como los bicosomas demostraron ejercer una acción anti-radicalaria en la piel expuesta a radiación UV-VIS. Este hecho podría relacionarse con el fenómeno de dispersión que ejercen las moléculas de lípido y que se ha explicado en el apartado 4.4.2.. La piel tratada con los sistemas lipídicos tendría una matriz lipídica reforzada, por lo que el efecto dispersivo de los lípidos seria mayor minimizando la intensidad de irradiación que penetra el tejido. Este hecho haría disminuir la formación de radicales libres en la piel por efecto de la irradiación. Este razonamiento también podría explicar que los bicosomas tengan una mayor capacidad anti-radicalaria que las bicelas. Los bicosomas con un 15% de concentración de lípidos tienen más moléculas lipídicas para dispersar la radiación, mientras que las bicelas con un 5% de lípidos protegerían la piel con menor efectividad.

Otra razón que explica la diferencia de la capacidad anti-radicalaria observada en las bicelas y los bicosomas podría ser la distinta interacción que tiene cada sistema con la piel. Debido a que las bicelas son capaces de penetrar en el EC, el efecto causado por este sistema podría ser principalmente en el interior de este tejido. Dado que los bicosomas están formados por bicelas encapsuladas en vesículas, estos sistemas lipídicos proporcionarían una interacción muy específica con la piel, aportando un efecto tanto en el interior como en la superficie del tejido (ver apartado 4.3.1.). En conclusión, el efecto superficial añadido en este sistema lipídico podría también ser el responsable del mayor efecto anti-radicalario en la piel, lo que convierte a los bicosomas en un sistema más completo para proteger la piel de la radiación UV-VIS.

La piel tratada con bicelas y bicosomas presentó una mayor contribución de aductos de carbono que la piel nativa. Teniendo en cuenta que las bicelas y los bicosomas están formados por fosfolípidos que presentan cadenas alquílicas, estas cadenas también

podrían formar radicales de carbono incrementando la contribución de estos aductos de DMPO.

La contribución del aducto aminoxil también fue más elevada en la piel tratada con las bicelas y los bicosomas tanto antes como después de la irradiación. El hecho de que el DMPO capture un tipo de radical u otro, está relacionado con la distribución de este "spin-trap" en la piel. Cada región de la piel tiene una específica composición molecular, por lo que los radicales libres formados en cada área de este tejido dependerán de su composición. El tratamiento de la piel con las bicelas y los bicosomas pudo haber modificado la distribución del DMPO en este tejido, lo que conllevaría la formación de especies diferentes, que a su vez modificaría la contribución de los aductos formados.

4.6.1.2. Influencia de la incorporación de β-caroteno en la capacidad anti-radicalaria de las bicelas y los bicosomas

Los resultados de EPR mostraron que la incorporación de β-caroteno en los bicosomas mejoró la capacidad anti-radicalaria de este sistema lipídico. Este antioxidante ha demostrado desde hace años su capacidad de neutralizar radicales libres y su poder antioxidante tanto en soluciones como en sistemas lipídicos [23, 24] . Por lo tanto, su ya conocido efecto antioxidante podría haber sido la causa de la mejora observada en actividad anti-radicalaria de los bicosomas.

La incorporación del β-caroteno en ambos sistemas lipídicos también aumentó la contribución de los aductos de carbono formados en la piel. La oxidación de este antioxidante conlleva la adición de su doble enlace a otras moléculas formando radicales de carbono, lo que podría explicar el incremento de aductos de carbono observado en la piel tratada con los sistemas de β-caroteno [24, 112].

4.6.2. Radicales libres inducidos por exposición IR

Más de la mitad de la energía solar que atraviesa la superficie terrestre nos llega en forma de radiación IR, siendo la porción IR-A la más importante. Además la radiación IR-A es la que tiene más capacidad de penetrar en nuestra piel, pudiendo llegar hasta la hipodermis [11, 94]. El hecho de que sea la radiación más abundante y la que

penetra hasta las capas más profundas de la piel, es la razón por las que debemos prestar una especial atención a la luz IR.

Aún son pocos los trabajos que demuestran la capacidad de la radiación IR de formar radicales libres, aunque sí existe un consenso en cuanto a la dependencia entre la dosis de irradiación y los potenciales efectos terapéuticos o patológicos que puede causar este tipo de radiación. A bajas dosis (1-10 J/cm^2), la radiación IR estimula efectos terapéuticos, mientras que a dosis mayores de 120 J/cm^2 desencadena procesos patológicos [11]. Uno de los efectos patológicos de la radiación IR en la piel, es el incremento de la expresión de la MMP que influye en la degradación del colágeno [11]. En general, la formación de radicales libres en la piel debido a la exposición a la luz IR se ha asociado al shock térmico causado por esta radiación[11]. El hecho de que la radiación IR pueda generar radicales libres directamente debido a su energía y sin necesidad de aumentar la temperatura, está en debate. Un estudio ha demostrado que la inducción de calor en la piel mediante un baño de agua, induce menos procesos patológicos que la radiación IR directa [11]. Dado que la piel no está sometida de manera habitual a temperaturas extremadamente superiores a la temperatura fisiológica, sería interesante evaluar el efecto de la energía de la radiación IR en la piel a temperaturas fisiológicas. Realizar este tipo de ensayos *in vitro* es difícil debido a que es necesario eliminar el calor producido por la radiación IR. Para solucionar este problema en el marco de esta tesis, se diseñó un accesorio que permitió disipar el calor producido por radiación IR y que se acopló al equipo de EPR (descrito en los apartados 1.4.4.1. y 4.1.3.). De esta manera se pudieron obtener y medir los radicales libres formados en la piel simultáneamente a la irradiación.

Estudios previos han establecido que los radicales libres formados a una dosis de luz IR de 120 J/cm^2 son capaces de activar procesos patológicos en la piel (esta dosis es equivalente a una exposición al sol durante 1.5 h en Múnich en verano, [11]).

Teniendo en cuenta que en nuestros experimentos la intensidad de irradiación fue de 0.108 W/cm^2, el tiempo necesario para lograr una dosis de 120 J/cm^2 se estimó alrededor de los 20 min. Sin embargo, a los 20 min de irradiación, la concentración de radicales libres en la piel fue similar a la concentración de estas especies antes de irradiar. Por lo tanto, no hubo formación de radicales libres causado por esta dosis.

Este hecho podría sugerir que una dosis de 120 J/cm^2 de luz IR no es capaz de desencadenar efectos negativos en la piel a temperatura fisiológica al menos debido a la producción de radicales libres.

El incremento de radicales libres respecto a la piel no irradiada se observó alrededor de los 50 min, a una dosis de 324 J/cm^2. En este caso, sería importante considerar la posibilidad de que la radiación IR pueda iniciar procesos perjudiciales para la piel como podría ser la degradación del colágeno mediante la expresión de MMP.

Así pues, la formación de radicales libres por exposición IR ocurre a temperaturas fisiológicas. Sin embargo, para inducir esta formación de radicales libres en la piel a temperatura fisiológica, es necesaria una dosis mayor que a temperaturas elevadas.

La aplicación de bicosomas incorporando β-caroteno minimizó la formación de radicales libres en piel expuesta a la radiación IR (artículo 7). Esta reducción de radicales libres podría estar asociada a las características del sistema. Por una parte, la presencia del antioxidante podría actuar neutralizando los radicales libres que se formen, ya que los bicosomas fomentan la penetración de este antioxidante. Por otra parte, el sistema de bicosoma podría reducir la formación de radicales libres debido a que las moléculas de lípido tienen capacidad de absorber la luz IR [120]. Los bicosomas están formados por estructuras laminares lipídicas que penetran el tejido cutáneo [96]. Estos lípidos ejercerían un efecto protector absorbiendo la radiación y bloqueando el paso de la misma. Por lo tanto, la intensidad de radiación que penetrase en la piel disminuiría minimizando la formación de radicales libres en la piel.

RESUMEN

• Una dosis de 27 J/cm^2 (UV-VIS) aumenta la concentración de radicales libres en la piel nativa.

• Mediante la simulación de espectros se encuentran seis tipos diferentes de aductos de DMPO, siendo los más abundantes los aductos de carbono.

• El tratamiento de bicelas y bicosomas con y sin β-caroteno en la piel reduce la formación de radicales libres a una dosis de 27 J/cm^2 (UV-VIS).

• Los bicosomas poseen mayor efectividad anti-radicalaria que las bicelas. La aplicación de estos sistemas en la piel eleva la contribución de radicales libres de carbono en la piel.

• La incorporación de β-caroteno mejora la capacidad anti-radicalaria de los bicosomas, y aumenta la contribución de radicales libres de carbono en la piel.

• La formación de radicales libres por exposición IR ocurre a temperaturas fisiológicas. Sin embargo, para inducir esta formación de radicales libres en la piel a temperatura fisiológica, es necesaria una dosis mayor que a temperaturas elevadas.

• La aplicación de bicosomas incorporando β-caroteno minimiza la formación de radicales libres en piel expuesta a la radiación IR.

4.7. EFECTO DE LA RADIACIÓN IR EN LA DEGRADACIÓN DEL COLÁGENO CUTÁNEO

La degradación del colágeno comienza por la formación de radicales libres, que son capaces de incrementar la expresión de la MMP. La MMP es responsable de la degeneración de esta proteína, por lo que su sobre-expresión conlleva una degradación prematura del colágeno.

La técnica de SAXS acoplada a una fuente de sincrotrón permitió evaluar la estructura del colágeno cutáneo y como esta estructura se modifica por diferentes factores [47]. El perfil de rayos X característico de esta proteína muestra reflexiones periódicas (picos de Bragg), que están relacionadas con su organización estructural. Por lo que evaluando la intensidad de los picos observados por SAXS es posible determinar el estado de esta proteína.

La degradación del colágeno se observó a partir de dosis de 273 J/cm^2 y a una temperatura de 65ºC, y su total degradación se observó a una dosis de 820 J/cm^2 y una temperatura de 70ºC. Por lo tanto, se necesitaron unas condiciones bastante extremas para poder degradar esta proteína. Obviamente el colágeno cutáneo no está expuesto a estas condiciones tan extremas en la vida diaria, pero la optimización de las condiciones necesarias para degradar el colágeno puede ser útil para poder evaluar

formulaciones protectoras de esta proteína. El hecho de utilizar estas condiciones se basa en la necesidad de establecer un diseño experimental que sea capaz de degradar, al menos parcialmente el colágeno, con el fin de poder evaluar el potencial efecto protector que ejercen los tratamientos con los sistemas lipídicos.

A partir de los resultados presentados en la tesis, no se pudo concluir si la degradación del colágeno fue debida al choque térmico o a la energía producida por la radiación IR, por lo que el estudio de la degradación del colágeno a temperaturas fisiológicas sería un punto importante a evaluar en futuros trabajos.

4.7.1. Efecto de los bicosomas como protectores de la degradación del colágeno

La aplicación de bicosomas incorporando β-caroteno en muestras de piel evitó la degradación del colágeno cutáneo tras la exposición a la luz IR (artículo 7). Este hecho podría ser debido a la reducción de radicales libres que se observó tras el tratamiento con este sistema lipídico y que se ha explicado en el apartado 4.5.2. Teniendo en cuenta que la degradación del colágeno comienza con la formación de radicales libres, una disminución de estas especies conllevaría una menor degradación de esta proteína.

Este efecto bloqueador de radicales de los bicosomas está relacionado con la absorbancia de los lípidos y la capacidad antioxidante del β-caroteno. Sin embargo, la acción protectora del β-caroteno a estas temperaturas estaría limitada. El β-caroteno se descompone a temperaturas por encima de los 50ºC [121], y la degradación del colágeno requiere temperaturas hasta 70ºC. Por lo tanto en las condiciones experimentales empleadas, a partir de los 50ºC la protección del colágeno se asociaría principalmente a la estructura lipídica de los bicosomas.

RESUMEN

- La degradación del colágeno es posible a partir de dosis de 273 J/cm^2 y a una temperatura de 65ºC. Su total degradación se observa a una dosis de 820 J/cm^2 y una temperatura de 70ºC.

- La aplicación de bicosomas incorporando β-caroteno en muestras de piel evita la degradación del colágeno cutáneo tras la exposición a la luz IR.

5. CONCLUSIONES

5. CONCLUSIONES

- Se han determinado los efectos producidos por la radiación solar en tejidos lipoqueratínicos como el cabello y la piel.

Efectos sobre el cabello

- La radiación UV-VIS genera un incremento de radicales libres, la oxidación de la fracción proteica, la peroxidación de los lípidos, la descomposición del aminoácido Trp, y la pérdida de brillo y color.
- La aplicación de antioxidantes derivados de alcachofa y de arroz sobre el cabello reduce los efectos negativos de la radiación UV-VIS.
- La radiación IR aumenta la cantidad de radicales libres a temperaturas entre 25 30ºC.
- La formación de radicales libres en el cabello por radiación IR requiere dosis mayores de exposición que la luz UV-VIS.

Efectos sobre la piel

- La radiación UV-VIS aumenta la concentración de radicales libres en la piel.
- A las condiciones experimentales empleadas, no se modifica la microestructura de la piel mediante radiación UV-VIS.
- La radiación IR genera un incremento de radicales libres a temperatura fisiológica.
- La formación de radicales libres en la piel por radiación IR requiere dosis mayores de exposición que la luz UV-VIS.
- Es posible degradar el colágeno cutáneo mediante radiación IR y a temperaturas superiores a 65ºC.

- La interacción de los bicosomas con la piel se establece en un mecanismo de dos pasos; la vesícula exterior se funde con la superficie de la piel y las bicelas penetran el interior del tejido.

- Las condiciones de la piel y los activos incorporados en los bicosomas influyen en la penetración de estos sistemas en el tejido cutáneo.

- La penetración de los bicosomas en piel expuesta a radiación UV-VIS es menor debido al incremento de la impermeabilidad del tejido.
- La incorporación de un activo lipofílico en los bicosomas limita la penetración de este sistema lipídico a las capas más superficiales del tejido cutáneo. Mientras, la incorporación de un activo con carácter más hidrófilo en los bicosomas, facilita que este sistema lipídico alcance capas más profundas con mayor contenido de agua.

- La estabilidad morfológica de las bicelas y los bicosomas frente a radiación UV-VIS depende de su composición química.

- Los sistemas bicelares formados de lípidos saturados no experimentan modificaciones ni en su tamaño ni en su estructura.
- La morfología de los bicosomas formados de lípidos saturados e insaturados se modifica frente a radiación UV-VIS. La vesícula exterior de los bicosomas se rompe agregándose y/o fusionándose con otras vesículas y formando estructuras lipídicas grandes de diversa morfología.

- Las bicelas y los bicosomas preservan la estabilidad del β-caroteno frente a radiación UV-VIS. Este hecho es posiblemente debido al fenómeno de dispersión de luz UV que ejercen las moléculas de lípido de ambas nanoestructuras, proceso que esta inducido por la estructuración de los sistemas.

- Queda demostrada la capacidad antioxidante de las bicelas y los bicosomas en la piel frente a radiación solar.

- El tratamiento de bicelas y bicosomas con y sin β-caroteno reduce la formación de radicales libres en piel expuesta a radiación UV-VIS. Los bicosomas poseen mayor efectividad anti-radicalaria que las bicelas debido a que poseen mayor concentración de lípidos estructurados.
- La incorporación de β-caroteno mejora la capacidad anti-radicalaria de los bicosomas.

- Los bicosomas incorporando β-caroteno reducen la formación de radicales libres y la degradación del colágeno cutáneo mediante luz IR.

En definitiva se han determinado los efectos de la luz UV, VIS e IR en el cabello y la piel y se han diseñado formulaciones y nanoestructuras con antioxidantes para prevenir el daño causado por estas radiaciones. Asimismo, se ha demostrado que el bicosoma es un sistema eficaz incorporando activos en el tejido cutáneo y reduciendo los efectos tanto de la radiación UV-VIS como los de la luz IR. Por lo tanto, el bicosoma resulta ser un vehículo prometedor para el uso cosmético o farmacológico.

6. ANEXOS

ANEXO I

Cálculo del radio del disco

La técnica de DLS nos permite medir el tamaño de partícula mediante el movimiento Browniano de ésta en solución. El Zetasizer Nano ZS analiza la fluctuación temporal de la intensidad dispersada por las partículas permitiendo obtener una función de autocorrelación [122, 123]. Para un sistema monodisperso, la función de autocorrelación, *g(t)* es una función exponencial dependiente del tiempo según la siguiente expresión:

$$g(t) = A\exp\left(-\frac{2t}{t_R}\right) + B \qquad \text{(Ec.1)}$$

donde *B* es la línea base y A es una constante instrumental, t_R es el tiempo de relajación, el cual tiene asociado un coeficiente de difusión (*D*)

$$t_R = \frac{1}{Dq^2} \qquad \text{(Ec. 2)}$$

donde *q* es el ángulo de dispersión. Aplicando la ecuación de Stokes-Einstein, a cada coeficiente de difusión se puede asociar un radio hidrodinámico R_h *[124]*

$$D = \frac{k_B T}{6\pi\eta R_h} \qquad \text{(Ec. 3)}$$

Donde k_B es la constante de Boltzmann, *T* es la temperatura absoluta y η es la viscosidad del sistema. Este R_h obtenido es el radio hipotético de una esfera que tiene el mismo coeficiente de difusión que la partícula a medir.

Dado que las bicelas son estructuras discoidales, la relación del R_h y del radio del disco no es del todo correcta, para realizar un cálculo más real del tamaño del disco utilizamos la siguiente ecuación [69], que relaciona ambos radios:

$$RH = \frac{3r}{2(\,[1+(t/2r)^2]^{1/2} + [2r/t \ln\,[1+(t/2r)^2]^{1/2}] - t/2r)} \qquad \text{(Ec. 4)}$$

donde t el grosor de la bicapa, y r el radio del disco.

7. BIBLIOGRAFÍA

7. BIBLIOGRAFÍA

1. Mitjavila, M., D. López, and M. Saiz, *Los radicales libres y su implicación en procesos fisiológicos y patológicos.* NCP Documenta, 2001. **258**: p. 5-11.
2. Sen, C.K., *Cellular thiols and redox-regulated signal transduction.* Current topics in cellular regulation, 1999. **36**: p. 1-30.
3. Wolin, M.S., *Interactions of oxidants with vascular signaling systems.* Arteriosclerosis, thrombosis, and vascular biology, 2000. **20**(6): p. 1430-1442.
4. Valko, M., et al., *Free radicals and antioxidants in normal physiological functions and human disease.* The international journal of biochemistry & cell biology, 2007. **39**(1): p. 44-84.
5. Ames, B.N., M.K. Shigenaga, and T.M. Hagen, *Oxidants, antioxidants, and the degenerative diseases of aging.* Proceedings of the National Academy of Sciences, 1993. **90**(17): p. 7915-7922.
6. Forman, H.J. and M. Torres, *Redox signaling in macrophages.* Molecular aspects of medicine, 2001. **22**(4): p. 189-216.
7. Kasai, H., et al., *Formation of 8-hydroxydeoxyguanosine in liver DNA of rats following long-term exposure to a peroxisome proliferator.* Cancer research, 1989. **49**(10): p. 2603-2605.
8. Eiserich, J.P., et al., *Dietary antioxidants and cigarette smoke-induced biomolecular damage: a complex interaction.* The American journal of clinical nutrition, 1995. **62**(6): p. 1490S-1500S.
9. Ames, B.N., M. Profet, and L.S. Gold, *Dietary pesticides (99.99% all natural).* Proceedings of the National Academy of Sciences, 1990. **87**(19): p. 7777-7781.
10. Herrling, T., K. Jung, and J. Fuchs, *Measurements of UV-generated free radicals/reactive oxygen species (ROS) in skin.* Spectrochim Acta A Mol Biomol Spectrosc, 2006. **63**(4): p. 840-5.
11. Akhalaya, M.Y., et al., *Molecular action mechanisms of solar infrared radiation and heat on human skin.* Ageing research reviews, 2014. **16**: p. 1-11.
12. Jurkiewicz, B.A. and G.R. Buettner, *EPR detection of free radicals in UV-irradiated skin: mouse versus human.* Photochem. Photobiol., 1996. **64**(6): p. 918-22.
13. Masatsuji-Kato, E., T. Tsuzuki, and S. Kobayashi, *Reduction of UVB/A generated free radicals by sodium L-ascorbyl-2-phosphate in cultured mouse skin.* Journal of Health Science, 2005. **51**: p. 122-129.
14. Vandersee, S., et al., *Blue-Violet Light Irradiation Dose Dependently Decreases Carotenoids in Human Skin, Which Indicates the Generation of Free Radicals.* Oxidative medicine and cellular longevity, 2015. **2015**.
15. Halliwell, B., *Reactive species and antioxidants. Redox biology is a fundamental theme of aerobic life.* Plant physiology, 2006. **141**(2): p. 312-322.
16. Ames, B.N., *Dietary carcinogens and anticarcinogens oxygen radicals and degenerative diseases.* Science, 1983. **221**(4617): p. 1256-1264.
17. Gey, K., *The antioxidant hypothesis of cardiovascular disease: epidemiology and mechanisms.* Biochemical Society Transactions, 1990. **18**(6): p. 1041-1045.
18. Sies, H., *Biochemistry of oxidative stress.* Angewandte Chemie International Edition in English, 1986. **25**(12): p. 1058-1071.
19. Diplock, A., et al., *Functional food science and defence against reactive oxidative species.* British Journal of Nutrition, 1998. **80**(S1): p. S77-S112.
20. Kohen, R. and A. Nyska, *Oxidation of biological systems: oxidative stress phenomena, antioxidants, redox reactions, and methods of their quantification. 2002; 30 (6): 620-50*. PMID.

21. Kohen, R., *Skin antioxidants: their role in aging and in oxidative stress--new approaches for their evaluation.* Biomed Pharmacother, 1999. **53**(4): p. 181-92.
22. Tyler, V.E., *Herbal medicine: from the past to the future.* Public health nutrition, 2000. **3**(4a): p. 447-452.
23. Mueller, L. and V. Boehm, *Antioxidant activity of beta-carotene compounds in different in vitro assays.* Molecules, 2011. **16**(2): p. 1055-69.
24. Tsuchihashi, H., et al., *Action of beta-carotene as an antioxidant against lipid peroxidation.* Arch. Biochem. Biophys., 1995. **323**(1): p. 137-47.
25. Stahl, W. and H. Sies, *Carotenoids and protection against solar UV radiation.* Skin Pharmacol Appl Skin Physiol, 2002. **15**(5): p. 291-6.
26. Bernard, A.S., et al., *Evaluation of the anti-oxidant properties of a SOD-mimic Mn-complex in activated macrophages.* Dalton Trans, 2012. **41**(21): p. 6399-403.
27. Parra, J.L. and L. Pons, *Ciencia Cosmética: Bases fisiológicas y criterios prácticos*, ed. C.G.d.C.O.d. Farmacéuticos. 1995, Madrid: Heliotopia artística.
28. Jones, L.N., *Hair structure anatomy and comparative anatomy.* Clinics in dermatology, 2001. **19**(2): p. 95-103.
29. Masukawa, Y., H. Narita, and G. Imokawa, *Characterization of the lipid composition at the proximal root regions of human hair.* International Journal of Cosmetic Science, 2005. **27**(3): p. 191-191.
30. Braida, D., et al., *Ceramide: a new approach to hair protection and conditioning.* Cosmetics and toiletries, 1994. **109**(12): p. 49-57.
31. Philippe, M., et al., *Synthesis of 2-N-oleoylamino-octadecane-1, 3-diol: a new ceramide highly effective for the treatment of skin and hair.* International journal of cosmetic science, 1995. **17**(4): p. 133-146.
32. Zviak, C., *The science of hair care*. 1986: Informa Health Care.
33. Herrling, T., K. Jung, and J. Fuchs, *The role of melanin as protector against free radicals in skin and its role as free radical indicator in hair.* Spectrochim Acta A Mol Biomol Spectrosc, 2008. **69**(5): p. 1429-35.
34. Buettner, G.R. and B.A. Jurkiewicz, *Ascorbate free radical as a marker of oxidative stress: an EPR study.* Free Radic Biol Med, 1993. **14**(1): p. 49-55.
35. Yuen, C., C. Kan, and S. Cheng, *Evaluation of keratin fibre damages.* Fibers and Polymers, 2007. **8**(4): p. 414-420.
36. Nogueira, A., et al., *Photo yellowing of human hair.* Journal of Photochemistry and Photobiology B: Biology, 2007. **88**(2): p. 119-125.
37. Alonso, C., et al., *An ex vivo methodology to assess the lipid peroxidation in stratum corneum.* J Photochem Photobiol B, 2009. **97**(2): p. 71-6.
38. Barba, C., et al., *New anionic surface-active agent derived from wool proteins for hair treatment.* Journal of applied polymer science, 2010. **115**(3): p. 1461-1467.
39. Schaefer, H. and T.E. Redelmeier, *Skin barrier: Principles in percutaneous penetration*. 1996, Basel, Switzerland: Karger.
40. Elias, P.M., *Epidermal barrier function: intercellular lamellar lipid structures, origin, composition and metabolism.* J. Control. Release, 1991. **15**: p. 199-208.
41. Elias, P.M., *Structure and function of the stratum corneum permeability barrier.* Drug Develop. Res., 1988. **13**: p. 97-105.
42. Potts, R.O. and M.L. Francoeur, *Lipid biophysics of water loss through the skin.* Proc. Natl. Acad. Sci. U.S.A, 1990. **87**: p. 3871-3873.
43. Quevedo, W., et al., *Biology of melanocytes.* Dermatology in general medicine, 1987. **1**: p. 224-251.
44. Stingl, G., et al., *The epidermis: an immunological microenvironment*. 1993.
45. Kim, D.-K. and K.A. Holbrook, *The appearance, density, and distribution of Merkel cells in human embryonic and fetal skin: their relation to sweat gland and hair follicle development.* Journal of investigative dermatology, 1995. **104**(3): p. 411-416.

46. Maynes, R., *Structure and function of collagen types*. 2012: Elsevier.
47. Costa, M., et al., *Diagnosis Applications of Non-Crystalline Diffraction of Collagen Fibres: Breast Cancer and Skin Diseases*, in *Applications of Synchrotron Light to Scattering and Diffraction in Materials and Life Sciences*. 2009, Springer. p. 265-280.
48. Thiele, J.J., F. Dreher, and L. Packer, *Antioxidant defense systems in skin.* Journal of Toxicology: Cutaneous and Ocular Toxicology, 2002. **21**(1-2): p. 119-160.
49. Afaq, F. and H. Mukhtar, *Botanical antioxidants in the prevention of photocarcinogenesis and photoaging.* Experimental dermatology, 2006. **15**(9): p. 678-684.
50. Goebel, C., et al., *Skin metabolism of aminophenols: Human keratinocytes as a suitable in vitro model to qualitatively predict the dermal transformation of 4-amino-2-hydroxytoluene in vivo.* Toxicol. Appl. Pharmacol. , 2009. **235**: p. 114-123.
51. Fartasch, M., E. Schnetz, and T.L. Diepgen, *Characterization of detergent-induced barrier alterations -- effect of barrier cream on irritation.* J Investig Dermatol Symp Proc, 1998. **3**(2): p. 121-7.
52. Triba, M.N., P.F. Devaux, and D.E. Warschawski, *Effects of lipid chain length and unsaturation on bicelles stability. A phosphorus NMR study.* Biophys. J., 2006. **91**(4): p. 1357-67.
53. Sanders, C.R. and J.P. Schwonek, *Characterization of magnetically orientable bilayers in mixtures of dihexanoylphosphatidylcholine and dimyristoylphosphatidylcholine by solid-state NMR.* Biochemistry, 1992. **31**(37): p. 8898-905.
54. Van Dam, L., G. Karlsson, and K. Edwards, *Morphology of magnetically aligning DMPC/DHPC aggregates-perforated sheets, not disks.* Langmuir, 2006. **28**: p. 3280-3285.
55. Struppe, J. and R.R. Vold, *Dilute bicellar solutions for structural NMR work.* J. Magn. Reson., 1998. **135**(2): p. 541-6.
56. Sanders, C.R., et al., *Magnetically oriented phospholipid micelles as a tool for the study of membrane associated molecules.* Prog. NMR Spectroscopy, 1994. **26**: p. 421-444.
57. Marcotte, I. and M. Auger, *Bicelles as model membranes for solid and solution-state NMR studies of membrane peptides and proteins.* Concept. Magn. Res. , 2005. **24**: p. 17-37.
58. Barbosa-Barros, L., et al., *Bicelles: lipid nanostructured platforms with potential dermal applications.* Small, 2012. **8**(6): p. 807-18.
59. Rubio, L., et al., *Structural effects of flufenamic acid in DPPC/DHPC bicellar systems.* Soft Matter, 2011. **7**: p. 8488-8497.
60. Rubio, L., et al., *Bicellar systems as a new colloidal delivery strategy for skin.* Colloid. Surface B, 2012. **92**: p. 322-326.
61. Barbosa-Barros, L., et al., *Ceramide effects in the bicelle structure.* Colloids Surf. A., 2008. **317**: p. 576-584.
62. Rodriguez, G., et al., *Conformational changes in stratum corneum lipids by effect of bicellar systems.* Langmuir, 2009. **25**(18): p. 10595-603.
63. Rodriguez, G., et al., *Application of bicellar systems on skin: diffusion and molecular organization effects.* Langmuir, 2010. **26**(13): p. 10578-84.
64. Rodriguez, G., et al., *A unique bicellar nanosystem combining two effects on stratum corneum lipids.* Mol. Pharm., 2012. **9**(3): p. 482-91.
65. Rodriguez, G., et al., *Bicellar systems to modify the phase behaviour of skin stratum corneum lipids.* Phys. Chem. Chem. Phys., 2012. **14**(42): p. 14523-33.
66. Rodriguez, G., et al., *Bicosomes: bicelles in dilute systems.* Biophys. J., 2010. **99**(2): p. 480-8.
67. Barbosa-Barros, L., et al., *Penetration and growth of DPPC/DHPC bicelles inside the stratum corneum of the skin.* Langmuir, 2008. **24**: p. 5700-5706.

68. Losonczi, J.A. and J.H. Prestegard, *Improved dilute bicelle solutions for high-resolution NMR of biological macromolecules.* J. Biomol. NMR, 1998. **12**: p. 447-451.
69. Mazer, N.A., G.B. Benedek, and M.C. Carey, *Quasielastic light-scattering studies of aqueous biliary lipid systems. Mixed micelle formation in bile salt-lecithin solutions.* Biochemistry, 1980. **19**(4): p. 601-15.
70. Almgren, M., K. Edwards, and G. Karlsson, *Cryo transmission electron microscopy of liposomes and related structures.* Colloids Surf. A, 2000. **174**(3-21).
71. Darvin, M.E., et al., *Determination of beta carotenen and lycopene concentrations in human skin using resonance raman spectroscopy.* Laser Physiscs, 2005. **15**(2): p. 295-299.
72. Buettner, G.R., *Spin trapping: ESR parameters of spin adducts.* Free Radic. Biol. Med., 1987. **3**(4): p. 259-303.
73. Clede, S., et al., *A rhenium tris-carbonyl derivative as a single core multimodal probe for imaging (SCoMPI) combining infrared and luminescent properties.* Chem Commun (Camb), 2012. **48**(62): p. 7729-31.
74. Cocera, M., et al., *Characterisation of skin states by non-crystalline diffraction.* Soft Matter, 2011. **7**: p. 8605–8611.
75. Signori, V., *Review of the current understanding of the effect of ultraviolet and visible radiation on hair structure and options for photoprotection.* Journal of cosmetic science, 2003. **55**(1): p. 95-113.
76. Hoting, E., M. Zimmermann, and S. Hilterhaus-Bong, *Photochemical alterations in human hair. I: Artificial irradiation and investigations of hair proteins.* Journal of the Society of Cosmetic Chemists, 1995. **46**(2): p. 85-99.
77. Hoting, E., M. Zimmermann, and H. Höcker, *Photochemical alterations in human hair. II: Analysis of melanin.* Journal of the Society of Cosmetic Chemists, 1995. **46**(4): p. 181-190.
78. Hoting, E. and M. Zimmermann, *Photochemical alterations in human hair. Part III: investigations of internal lipids.* Journal of the Society of Cosmetic Chemists, 1996. **47**(4): p. 201-211.
79. Nogueira, A.C.S. and I. Joekes, *Hair color changes and protein damage caused by ultraviolet radiation.* Journal of photochemistry and photobiology B: Biology, 2004. **74**(2): p. 109-117.
80. Zoe Diana Draelos, M., *Shine-protecting haircare products smooth cuticle, increase light reflection.* 2011.
81. Robbins, C. and R. Crawford, *Cuticle damage and the tensile properties of human hair.* J Soc Cosmet Chem, 1991. **42**: p. 59-67.
82. Juez, J.L.P. and L.P. Gimier, *Ciencia cosmética: bases fisiológicas y criterios prácticos*. 1995: Consejo General de Colegios Oficiales de Farmacéuticos.
83. Chen, J.H. and C.-T. Ho, *Antioxidant activities of caffeic acid and its related hydroxycinnamic acid compounds.* Journal of Agricultural and Food Chemistry, 1997. **45**(7): p. 2374-2378.
84. Bonina, F., et al., *Flavonoids as potential protective agents against photo-oxidative skin damage.* International Journal of Pharmaceutics, 1996. **145**(1): p. 87-94.
85. Stern, E.S. and V.L. Johnsen, *Studies on the molecular weight distribution of cosmetic protein hydrolysates.* J. Soc. Cosmet. Chem, 1977. **28**: p. 447-455.
86. Graf, E., K.L. Empson, and J.W. Eaton, *Phytic acid. A natural antioxidant.* Journal of Biological Chemistry, 1987. **262**(24): p. 11647-11650.
87. Robbins, C.R. and C.R. Robbins, *Chemical and physical behavior of human hair*. Vol. 4. 2002: Springer.
88. Ruzicka, T., et al., *Efficiency of acitretin in combination with UV-B in the treatment of severe psoriasis.* Archives of dermatology, 1990. **126**(4): p. 482-486.

89. Holick, M.F., *Sunlight, UV-radiation, vitamin D and skin cancer: how much sunlight do we need?*, in *Sunlight, Vitamin D and Skin Cancer*. 2008, Springer. p. 1-15.
90. Ichihashi, M., et al., *UV-induced skin damage.* Toxicology, 2003. **189**(1-2): p. 21-39.
91. McAuliffe, D.J. and I.H. Blank, *Effects of UVA (320-400 nm) on the barrier characteristics of the skin.* J Invest Dermatol, 1991. **96**(5): p. 758-62.
92. Jiang, S.J., et al., *Biophysical and morphological changes in the stratum corneum lipids induced by UVB irradiation.* J Dermatol Sci, 2006. **44**(1): p. 29-36.
93. Biniek, K., K. Levi, and R.H. Dauskardt, *Solar UV radiation reduces the barrier function of human skin.* Proc Natl Acad Sci U S A, 2012. **109**(42): p. 17111-6.
94. Darvin, M.E., et al., *Formation of free radicals in human skin during irradiation with infrared light.* Journal of Investigative Dermatology, 2010. **130**(2): p. 629-631.
95. Suntres, Z.E., *Liposomal Antioxidants for Protection against Oxidant-Induced Damage.* J. Toxicol., 2011: p. 152474-152489.
96. Rodríguez, G., et al., *Bicelles: New Lipid Nanosystems for Dermatological Applications.* Journal of Biomedical Nanotechnology, 2015. **11**(2): p. 282-290.
97. Elias, P.M. and K.R. Feingold, *Skin Barrier.* Taylor and Francis group, New York,2006.
98. Elias, P.M. and K.R. Feingold, *Lipids and the epidermal water barrier: metabolism, regulation, and pathophysiology.* Semin. Dermatol., 1992. **11**(2): p. 176-82.
99. Williams, A.C. and B.W. Barry, *Penetration enhancers.* Adv Drug Deliv Rev, 2004. **56**(5): p. 603-18.
100. Kumar, B., S.K. Jain, and S.K. Prajapati, *Effect of penetration enhancer DMSO on in - vitro skin permeation of acyclovir transdermal microemulsion formulation.* International Journal of Drug Delivery, 2011. **3**: p. 83-94.
101. Stoughton, R.B., *Dimethylsulfoxide (DMSO) induction of a steroid reservoir in human skin.* Archives of dermatology, 1965. **91**(6): p. 657-660.
102. Elfbaum, S.G. and K. Laden, *The effect of dimethyl sulfoxide on percutaneous absorption: a mechanistic study, part I.* J Soc Cosmet Chem, 1968. **19**: p. 119-27.
103. Tashtoush, B., S. Al-Safi, and K. Al-Fanek, *Azathioprine transport through rat skin and its immunosuppressive effect.* Die Pharmazie-An International Journal of Pharmaceutical Sciences, 2004. **59**(2): p. 143-146.
104. Reddy, L.H. and B. Ghosh, *Enhancer aided in vitro permeation of atenolol and prazosin hydrochloride through mice skin.* Indian journal of experimental biology, 2001. **39**(1): p. 47-51.
105. Halliday, G.M., *Inflammation, gene mutation and photoimmunosuppression in response to UVR-induced oxidative damage contributes to photocarcinogenesis.* Mutat Res, 2005. **571**(1-2): p. 107-20.
106. Jacques, S.L., et al., *Low dose ultraviolet radiation alters human stratum corneum* Photochemistry and photobiology, 1987. **45S**: p. 94S.
107. Yamamoto, H.Y. and A.D. Bangham, *Carotenoid organization in membranes. Thermal transition and spectral properties of carotenoid-containing liposomes.* Biochim Biophys Acta, 1978. **507**(1): p. 119-27.
108. Maherani, B., et al., *Liposomes: A review of manufacturing techniques and targeting strategies.* Current Nanoscience, 2011. **7**: p. 436-452.
109. Brodnitz, M.H., *Autoxidation of Saturated Fatty Acids. A review.* Journal of Agricultural Food Chemistry, 1968. **16**: p. 994-999.
110. Reis, A. and C.M. Spickett, *Chemistry of phospholipid oxidation.* Biochim Biophys Acta, 2012. **1818**(10): p. 2374-87.
111. Devasagayam, T.P., K.K. Boloor, and T. Ramasarma, *Methods for estimating lipid peroxidation: an analysis of merits and demerits.* Indian J Biochem Biophys, 2003. **40**(5): p. 300-8.

112. Sarbolouki, M.N., P. Maghdooni Bagheri, and V. Sanee, *The influence of lipid composition and ?-carotene on lipid peroxidation in liposomes.* DARU J. Pharm. Sci. , 2005. **13(4)**: p. 148-154.

113. Niculae, G., et al., *Optimization of lipid nanoparticles composition for sunscream encapsulation.* U.P.B. Science Bulletin Series B, 2013. **75**.
114. Lacatusu, I., et al., *Effect of UV sunscreens loaded in solid lipid nanoparticles: A combinated SPF assay and photostability.* Molecular Crystalography and Liquid Crystalography, 2010. **523**: p. 247-259.
115. Haywood, R., F. Rogge, and M. Lee, *Protein, lipid, and DNA radicals to measure skin UVA damage and modulation by melanin.* Free Radic. Biol. Med., 2008. **44**(6): p. 990-1000.
116. Haywood, R., et al., *Intensity-dependent direct solar radiation- and UVA-induced radical damage to human skin and DNA, lipids and proteins.* Photochem. Photobiol., 2011. **87**(1): p. 117-30.
117. Davies, M.J., L.G. Forni, and S.L. Shuter, *Electron spin resonance and pulse radiolysis studies on the spin trapping of sulphur-centered radicals.* Chem Biol Interact, 1987. **61**(2): p. 177-88.
118. Dikalov, S.I. and R.P. Mason, *Reassignment of organic peroxyl radical adducts.* Free Rad. Biol. Med., 1999. **27**(7-8): p. 864-72.
119. Yoo, D.H., et al., *Spin Trapping EPR Method for Simultaneous Monitoring of Hydroxyl Radicals and Hydrogen Atoms in gamma-Irradiation Process* J. Ind. Eng. Chem., 2005. **2**: p. 215-221.
120. Tamm, L.K. and S.A. Tatulian, *Infrared spectroscopy of proteins and peptides in lipid bilayers.* Quarterly reviews of biophysics, 1997. **30**(04): p. 365-429.
121. Boon, C.S., et al., *Factors influencing the chemical stability of carotenoids in foods.* Critical Reviews in Food Science and Nutrition, 2010. **50**(6): p. 515-532.
122. Pusey, P. and J. Vaughan, *Dielectric and related molecular processes*. Vol. 48. 1975, London: the chemical society.
123. Berne, B. and R. Pecora, *Dynamic Light Scattering* ed. W. Sons. 1996, NY.
124. Hofer, N., *Neutron X-ray and light scattering*, ed. N.-H. Delta. Vol. 301. 1991: P. Linder, Th. Zemb.